

Investigation On The Structure And Dynamics Of Water Molecules Around Electrolytes And Biologically Important Molecules

A thesis submitted for the award of the degree of

Doctor of Philosophy (Science)

In

Physics (Experimental)

by

Debasish Das Mahanta

Department of Physics

University of Calcutta

June 2018

Dedicated to

My beloved Parents & My Supervisor

“Education is the manifestation of the perfection already in man.”

- **Swami Vivekananda**

“Education is the most powerful weapon which you can use to change the world.”

- **Nelson Mandela**

DECLARATION

I hereby declare that the works manifested in thesis "*Investigation On The Structure And Dynamics Of Water Molecules Around Electrolytes And Biologically Important Molecules*", are original. The experimental works, instrumental setup and the molecular dynamics simulations are carried out by me with the assistance of my lab mates, my collaborators and my supervisor Dr. Rajib Kumar Mitra at Satyendra Nath Bose National Centre for Basic Sciences, Saltlake, Kolkata. I further declare that these results have not used for the award of any degree diploma from any university or institute.

.....

Debasish Das Mahanta (Email: *snbdebasish@gmail.com*)
Senior Research Fellow
S. N. Bose National Centre for Basic Sciences
Block-JD, Sector - III, Saltlake, Kolkata - 700106

Abstract

This thesis is focused on understanding the nature of the perturbations on the structure and dynamics of water as induced by electrolytes (chlorides of alkali metals), amphiphilic molecules (DME, DMSO, alcohols etc.) and by hydrophobic ions (cations that contain hydrophobic moieties: alkylammonium chlorides). Most of the bio-physical processes in real cellular environments are governed by electrostatic and/or hydrophobic interactions. We investigate the individual as well as simultaneous effects of electrolytes and hydrophobic molecules on water network and dynamics. We have experimentally investigated the local H-bonded structure (using FTIR spectroscopy) and dynamics (using optical pump-probe spectroscopy) as well as the collective water networks along with the cooperative hydration dynamics (using GHz-THz spectroscopy). We have also implemented molecular dynamics simulation technique to get a microscopic view of water structure and dynamics in presence of DME molecules. From MD simulation study, we capture non-monotonic character in the single molecule water reorientation times. We found that there exist quite stable H-bonded water clusters in all simulated water concentration mixtures (even in very low water concentration). Water reorientations are found to occur via a combination of large amplitude angular jumps and diffusive motions. With the understanding of the perturbations on water networks, we studied the structure and hydration of a model protein bovine serum albumin (BSA) in presence of co-solutes and co-solvents. The change in the protein native structure has been determined using dynamic light scattering (DLS) and circular dichroism (CD) spectroscopy techniques while the associated hydration dynamics is investigated with THz spectroscopy. We aim to mimic the real cellular environment as it contains hydrophilic, hydrophobic and ionic charged species simultaneously. We found that while the alkali metal cations do accelerate the collective dynamics of water, it hardly affects the protein structure and its hydration dynamics; salt hydration and the BSA hydration act independently of each other. On the other hand, alcohols and alkylammonium cations do perturb the protein structure significantly indicating that direct preferential hydrophobic interactions of these molecules accelerate protein denaturation processes. We found that there exist a delicate balance between direct and indirect interactions, where electrolytes prefer to interact indirectly and amphiphilic molecules perturbed with preferential hydrophobic interactions.

List of Publications

This thesis is based upon the following publications and manuscripts:

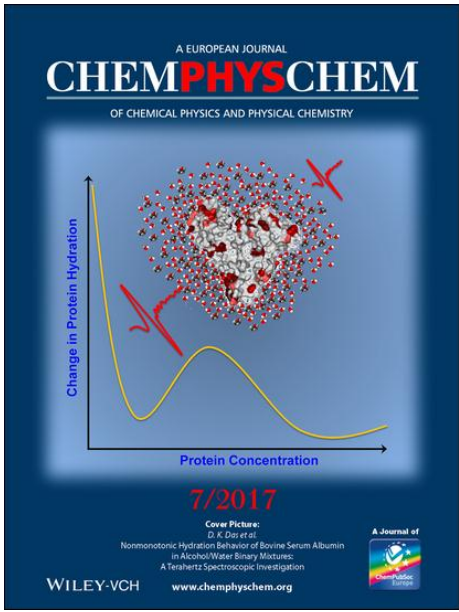
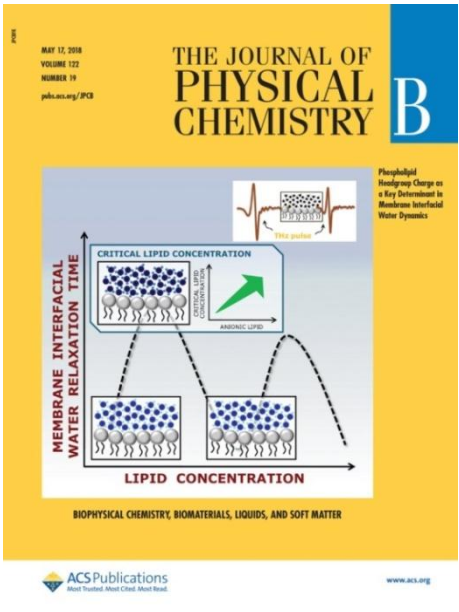
1. Das Mahanta, D., Islam, S. I., Das, D. K., Choudhury, S., Barman, A., and Mitra, R. K. (2018) "Contrasting hydration dynamics in DME and DMSO: A combine optical pump-probe and GHz-THz dielectric relaxation investigation", (*Manuscript communicated*).
2. Das Mahanta, D., Mukherjee, B., and Mitra, R. K. (2018) "Reorientational relaxation of water via large amplitude angular jumps and its connections to the dynamic heterogeneity in binary mixtures", (*Manuscript to be submitted*).
3. Das Mahanta, D., Rana, D., Patra A., Mukherjee, B., and Mitra, R. K. (2018) "Heterogenous structure and solvation dynamics of DME/water binary mixtures: A combined experimental and computer simulation study", *Chemical Physics Letters*, 700, 50-56.
4. Das Mahanta, D., Samanta, N., and Mitra, R. K. (2017) "The Decisive Role of Hydrophobicity on the Effect of Alkylammonium Chlorides on Protein Stability: A Terahertz Spectroscopic Finding", *Journal of Physical Chemistry B*, 121, 7777-7785.
5. Das, D. K., Das Mahanta, D., and Mitra, R. K. (2017) "Nonmonotonic Hydration Behavior of Bovine Serum Albumin in Alcohol/Water Binary Mixtures: A Terahertz Spectroscopic Investigation", *ChemPhysChem*, 18, 749-754.
6. Das Mahanta, D., Patra, A., Samanta, N., Luong, T. Q., Mukherjee, B., and Mitra, R. K. (2016) "Non-monotonic dynamics of water in its binary mixture with 1,2-dimethoxyethane: A combined THz spectroscopic and MD simulation study", *The Journal of Chemical Physics* 145, 164501-164512.
7. Das Mahanta, D., Samanta, N., and Mitra, R. K. (2016) "The effect of monovalent cations on the collective dynamics of water and on a model protein", *Journal of Molecular Liquids* 215, 197-203.

8. I have also contributed to the following publications:

1. Samanta, N., Das Mahanta, D., Patra, A., and Mitra, R. K., (2018) "Soft Interaction and excluded volume effect compete as polyethylene glycols modulate enzyme activity", *International Journal of Biological Macromolecules*, 118, 209-215.
2. Pal, S., Samanta, N., Das Mahanta, D., Mitra, R. K., and Chattopadhyay A. (2018) "Effect of phospholipid headgroup charge on the structure and dynamics of water at the membrane interface: A Terahertz spectroscopic study", *Journal of Physical Chemistry B*, 122, 19, 5066-5074.
3. Samanta, N., Das Mahanta, D., Choudhury, S., Barman, A., and Mitra, R. K. (2017) "Collective Hydration dynamics in some amino acid solutions: A combined GHz-THz Spectroscopy study", *Journal of Chemical Physics* 146 (12), 125101-125108.

4. Samanta, N., Luong, T. Q., Das Mahanta, D., Mitra, R. K., and Havenith, M. (2016) "Effect of Short Chain Polyethyleneglycols on the Hydration Structure and Dynamics around Human Serum Albumin", *Langmuir*.32(3), 831-837.
5. Samanta, N., Das Mahanta, D., and Mitra, R. K. (2015) "Urea and guanidinium chloride act as 'water structure breakers': The debate revisited by dielectric relaxation study in THz range", *Infrared, Millimeter, and Terahertz waves (IRMMW-THz), 2015 40th International Conference*, IEEE.
6. Samanta, N., Das Mahanta, D., and Mitra, R. K. (2014) "Does Urea Alter the Collective Hydrogen Bond Dynamics in Water: A Dielectric Relaxation Study in the THz Frequency Region", *Chemistry - An Asian Journal* 9, 3457-346.
7. Samanta, N., Das Mahanta, D., Hazra, S., Kumar, G. S., and Mitra, R. K. (2014) "Short Chain Polyethylene Glycols Unusually Assist Thermal Unfolding of Human Serum Albumin", *Biochimie* 104, 81-89.
8. Samanta, N., Das Mahanta, D., and Mitra, R. K. (2014) "Collective Hydration Dynamics of Guanidinium Chloride Solutions and its Possible Role in Protein Denaturation: A Terahertz Spectroscopic Study", *Physical Chemistry Chemical Physics* 16, 23308-23315.
9. Samanta, N., Das Mahanta, D., and Mitra, R. K., "THz spectroscopic study unravels why chloride salt of guanidinium is a protein denaturing agent while sulphate salt is not" (*Manuscript to be submitted*).
10. Das, D., Das Mahanta, D., and Mitra, R. K., "Modulation of Coherent Oscillation in Micro-heterogeneous Environment: Effect of Solvent Isotopes" (*Manuscript to be submitted*).

Cover Art:

	
<p>Back Cover: Nonmonotonic Hydration Behaviour of Bovine Serum Albumin in Alcohol/Water Binary Mixtures: A Terahertz Spectroscopic Investigation.</p>	<p>Cover Art: Effect of Phospholipid Headgroup Charge on the Structure and Dynamics of Water at the Membrane Interface: A Terahertz Spectroscopic Study.</p>

Acknowledgements

It has been an incredible journey so far. I start from a small village Kandara, district Burdwan, state West Bengal, India. I would graciously take this pleasant opportunity to acknowledge some nice persons who helped and encouraged me directly or indirectly during my PhD. My journey towards PhD would have been impossible without their help. I am so greatly indebted to all of them.

First of all, I express my deepest love and respect for the very first teacher in my life, my parents. It is due to their unconditional love, affection, support, ideology and guidance that I am here today. They always encouraged me to be a perfect man with full of humanities and love. They plant the seeds of morality in my mind from my early childhood. I would like to express my love to my grandfather, grandmother and to my elder sister (Kakuli) for being the perfect sibling. They are the biggest inspiration of my life.

It's my pleasure to express my heartiest thanks and sincere gratitude to my PhD advisor Dr. Rajib Kumar Mitra for his valuable guidance, contagious encouragement, illuminating discussions and insightful comments. His constant motivation, assistance and support help me to grow as a researcher. He trained me about the research topics, the instrumentations and about how to present or write the findings in a proper scientific way. Besides a patient guide and a good teacher, he is a very good human being and process a beautiful sense of humour. "*Brahmastra*", the most powerful weapon he gave to me, is the motivation and inspiration to do any kind of work. It is always satisfying to talk with him and listen to his views in different aspects of science as well as in life. I am lucky enough to work with such a man with goodness, calmness and welcoming behaviour. I have been fortunate to have him as my supervisor.

I would like to thank my past and present lab mates from "*THz Spectroscopy Lab*" (Dr. Dipak Kumar Das, Dr. Animesh Patra, Dr. Nirnay Samanta, Dr. Arindam Das, Dr. Debanjan Polley, Dr. Chaitrali Sengupta, Debkumar Rana, Kumar Neeraj, Amit Barh, Sk Imadul Islam, Partha Pyne, Saikat Pal, Didhiti Bhattacharya, Anulekha De, Sayantan Adak and Sudip Majumder) for cheerful discussions and for the healthy and friendly atmosphere in the lab. I am very much thankful to them for all the fun that we have during the last five years. They are a great bunch of guys and I am really happy to share the lab with them. A special thanks to Nirnay da. I learnt almost each and every step about working in lab, handling chemistry samples, processing and explaining the data. It has been a real pleasure to

work with him. I thank Dipak da for giving fruitful ideas, helpful discussions to understand the instrumentations and also the topics. He used to aware me about the literature, the work doing by the other researchers in the world in my research field. In research where one doesn't know what will be the exact answer, basic ideas become very much helpful. In this regard, I would like to thank Animesh da for long discussions and debate that helped me to design my experimental projects or to explain the data. The discussions with Dipak da, Animesh da, and Nirnay da help me to understand the THz Spectroscopy, Pump-probe Spectroscopy, and Fluorescence Spectroscopy as a chemist's point of view. I learnt a lot of things about the THz spectroscopy from Debanjan da. I have also learnt many technical things (using lab software and some useful tips in using other software such as "Endnote", "MS Word", "MS PowerPoint", "Igor", "Origin", "SigmaPlot" and many more) from my seniors. The juniors Didhiti, Partha, Saikat and Imadul always insist me to participate in their discussions. They used to ask a lot of questions. Their queries contend me to know the subject deeply with clear descriptions. I thank Partha for the final proof corrections of my thesis.

We enjoy some delightful dinner party in various restaurants as well as in sir's home. Thanks to sir and madam (Dr. Sukanya Chakrabarty) for those special dinners, delicious dishes an cheerful moments. I also like to thank Animesh da and Sonali di for those dinner parties in their room. I always love to taste those mouth-watering divine foods prepare by Nirnay da, Dipak da, Animesh da, Imadul and Didhiti.

I heartily acknowledge my collaborators. A special thanks to Prof. Anjan Barman and Samiran who permit me to access their lab at SNBNCBS, and perform experiments with the VNA instrument in the GHz frequency region. I convey my sincere thanks to Dr. Biswaroop Mukherjee (recently shifted to University of Sheffield, UK). It's being a very nice experience to work with him. I learnt some very basic and important steps of MD simulation techniques. I also like to acknowledge my other collaborators Prof. Amitabha Chattopadhyay (CCMB, Hyderabad), Sreetama pal, Prof. G. Suresh Kumar (IICB, Kolkata), Dr. Soumitra Banerjee, Dr. Trung Quan Luong (Germany), Prof. Martina Havenith (Rurh University, Germany), Dr. Sayan Bagchi (NCL Pune).

My "Pranam" to my respected teachers from my early childhood (Prabir sir, Dipali mam), from Ramakrishna mission, Kandara (Amal sir, Tushar sir, Ranjit sir, Kesan sir, Sujan sir), from school time (Bhinod sir, Kesan sir, Maya didimoni, Sawilaswar sir, Uday babu), from high school time (Asish babu, Goutam babu, Buro da, Monohar da, Partha babu), from graduate time (Kali babu, Arun da, Sutanu babu, Dayamoy babu, Joytipratim (JRC) sir,

Bharat babu). I owe my success to them. I also cannot forget the moments spent with my friends, we share our foods, we argue, we quarrel, we play together. It is my privilege to extend a vote of thanks to my childhood friends Debabrata, Ankhi, Lipika, Ankita, Tanusree, Paltu, Kanchan, Sujit, Azahar, Sukanta, Thirtha. A special thanks to Sushobhan, Debu and Nitish. They stay with me in each and every step of my life. I thank my graduation batch mates (Anowar, Arghya, Subir, Janardan, Tanmoy, Anamika, Saheli, Sanjana, Kousik), and some other college days friends (Sanjay da, Madhab, Subhankar da, Sandip da, Balaram da, Arjun da, Rahul da, Tuhin da). Thanks for being with me. Their support was my biggest strength during that difficult time. I appreciate the positive influence you had on my life in that certain period of time.

I am grateful to all the faculty members, research scholars, academic and non-academic staffs at SNBNCBS for their help and cooperation. I wish to thank my integrated PhD batch mates (Souvik, Sumanta, Dilip, Somnath, Saheli, Deblina, Chandryee, Anita, Shauri). I am incredibly fortunate to have such nice batch mates. I would like to convey my gratitude to those faculty members who had taken our IPhD classes (Prof. J. K. Bhattacharjee, Prof. S. S. Manna, Prof. M. Mathur, Prof. Biswajit Chakraborty, Prof. T. Saha-Dasgupta, Prof. Kalyan Mondal, Prof. A. Lahiri, Prof. S. K. Pal, Prof. P. K. Mukhopadhyay, Prof. Jaydeb Chakrabarti, Dr. R. K. Mitra, Dr. P. Pradhan, Dr. M. Kumar, Prof. M. S. Kumar, Dr. S. Barman). Sincere thanks to my master project supervisors Prof. A. Lahiri & Dr. R. K. Mitra. I learnt a lot from those teachers. I also want to thank to the administrative staffs of SNBNCBS. Words cannot express how grateful I am for their support. I want to thank SNBNCBS centre for providing me experimental, computational and other facilities. I thankfully acknowledge my centre SNBNCBS and Inspire, Department of Science & Technology (DST, India) for financial assistance.

My dear friends, colleagues and beloved seniors at SNBNCBS have been an integral part of this journey. They are my family. We used to cherish the occasional get-togethers, gossips, playing cards & monopoly game, enjoy food and drinks in my hostel room that made this place a home away from home. Though it's very hard to list all of them, yet some close and dear "*Gobesok Bandhugans*" are Subrata da (*nayak*), Sarower da (*goba*), Vinood, Subhadip (*lalu*), Ananda (*bachha*), Souvanik (*sova*), Arindam da (*dadda*) Kartik da, Dhimadri (*khata*), Sudipta (*poty*), Abhishek da, Arunava, Dipak da, Subhasish da etc. I thank them for such homely environment. We used to play various games like badminton, football and cricket at SNBNCBS. These games are my daily refreshments. I learn the power of unity and enjoy the spirit of the games. There are many unforgettable moments with my co-players

that certainly increase the bonding among us. It's my pleasure to acknowledge those co-players of badminton (vinood, samiran, shaili, lalu, nayak, chaoba di, sreeraj da, kallol da, aslam da, kartik, ejaj, amit, sourav, goba, mehabub, semanti di, neeraj), football (ransell, nayak, dipanjan, neeraj, mahebab, smrat, khata, dhiraj, edwine, prantik), cricket (rakesh, sumanta, sova, shankar, imadul, panda, supriyo da, abhishek, vinood, samiran, dipanjan, subrata, kallol da, ejaj, amit, sourav, goba, mehabub). I was the coordinator (2013-17) of the sports activity group of Mukatangan (a Bose Centre Recreation club). We often organised tournaments among ourselves and also among other institutes. In the year of 2014, 2016 and 2017 we organised the inter-institute badminton tournament. It was a great experience to work with the working committee of Mukatangan. I am also closely attached to some musical groups "*SNB Khaja Band*" (international musical band) and "*Music group SNB*" that entertain & energize me. It's been very pleasant to play *Tabla* and *Cajon* with those singers and other instrument players (goba, nayak, lalu, chaitrali di, ransell, bachha, shaili, jayita, anwasha, soumi di, subhasish da). I also acknowledge Horen da and Dulal da for their tea shop. Almost every day, I enjoy the tea and evening snacks from their tea-shop.

Last but not the least it is my world, my would be wife, Anamika who is beyond acknowledgement. I would like to add a special note of thanks to her for immense support and encouragement, for always being there with me through ups and downs of my life, for all those wonderful fights we had and for accepting me with all my madness.

Finally I acknowledge the whole team of a TV serial "*Star Plus Mahabharat*" and some daily checked websites like Youtube, Hotstar, Google, Researchgate, Google scholar, Sci-finder and the social networking sites; WhatsApp, Facebook etc. The characters of "*Star Plus*" *Mahabharat* strongly influenced my mind and heart. The songs by "*Wind of Change*" and "*Coke Studio*" are mind-blowing, I love the musical teams. Many thanks to the teams, they used to change my mood in my tuff times.

This page is kept blank intentionally.

Acronyms

BSA	Bovine serum albumin
CD	Circular dichroism
DLS	Dynamic light scattering
DME	1,2-Dimethoxy ethane
DMSO	Dimethyl sulfoxide
DRS	Dielectrics relaxation spectroscopy
FIR	Far infrared
FTIR	Fourier transform infrared spectroscopy
GdmCl	Guanidinium chloride
GHz	Gigahertz (10^9 Hz)
H-bond	Hydrogen bond
MD	Molecular dynamics
MIR	Mid infrared
PEG	Poly(ethylene) glycol
SASA	Solvent accessible surface area
TCSPC	Time correlated single photon counting
TEAC	Tetra ethyl ammonium chloride
THz	Terahertz (10^{12} Hz)
TMAC	Tetra methyl ammonium chloride
TMGdm	Tetra methyl guanidinium
TPAC	Tetra propyl ammonium chloride
TRFS	Time-resolved fluorescence spectroscopy
Tri EAC	Tri ethyl ammonium chloride
TTDS	Terahertz time domain spectroscopy
UV	Ultra violet
VNA	Vector network analyser

Table of Contents

Abstract	I
List of Publications	II
Acknowledgements	IV
Acronyms	IX
1. Introduction	1
1.1. References	9
2. Instrumentation and the Underline Basic Theories	14
2.I. Experimental Techniques	14
2.I.1. Ultra Violet-Visible Spectroscopy (UV-Vis)	14
2.I.2. Circular Dichroism (CD) Spectroscopy	15
2.I.3. Steady State Fluorescence Spectroscopy	15
2.I.4. Time-Resolved Fluorescence Spectroscopy (TRFS)	16
2.I.5. Dynamic Light Scattering (DLS)	17
2.I.6. Fourier Transform Infrared (FTIR) Spectroscopy	18
2.I.7. Terahertz (THz) Spectroscopy	18
2.I.8. Terahertz Time Domain Spectroscopy (TTDS)	19
2.I.9. Vector Network Analyser (GHz Frequency Region)	21
2.I.10. Pump Probe Spectroscopy	22
2.II. Methods and Underline Basic Theories	23
2.II.1. Theory of Dielectric Polarization.....	23
2.II.2. Dielectric Relaxation (DR) “Debye Model”	27
2.II.3. Generation and Detection of THz Radiation.....	28
2.II.4. THz Measurement.....	29
2.II.5. Dielectric Relaxation Fitting (GHz-THz Regime).....	30
2.II.6. Tetrahedral Hydrogen Bond Networks	32
2.II.7. Cooperative Hydrogen Bond Network	32
2.II.8. Depolarization.....	33
2.II.9. Investigation of the Secondary and Tertiary Structure of Protein by CD Spectroscopy.....	34
2.II.10. Thermal Stability of Protein.....	35
2.II.11. OD Stretching mode	36
2.III. References	36

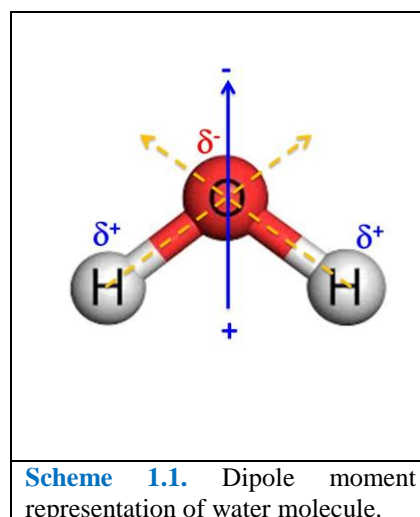
3. Molecular Dynamics Simulation Analysis Protocol.....	39
3.I. Simulation Details	39
3.II. Analysis Protocol	40
3.II.1. Hydrogen Bonding.....	40
3.II.2. Reorientation of water via Jump Mechanism	42
3.II.3. Waiting Periods.....	44
3.II.4. Tetrahedral Order Parameter.....	45
3.III. References.....	46
4. Effect of Monovalent Electrolytes on Water Structure and Dynamics of Water and on a Globular Protein	47
4.1. Introduction.....	47
4.2. Materials and Methods.....	49
4.3. Results and Discussion	50
4.4. Summary	60
4.5. References.....	62
5. Investigation of the Heterogeneous Hydration and Solvation Dynamics of Binary Mixtures of Water and a Small Hydrophobic Molecule 1,2-Dimethoxy Ethane	65
5.1 Introduction.....	65
5.2 Materials and Methods.....	68
5.3. Results and Discussions	68
5.3.I. Experimental Findings	68
5.3.II. MD simulation study	80
5.4. Summary	92
5.5. References.....	94
6. Non-monotonous Hydration Behaviour of Bovine Serum Albumin in Alcohol-Water Binary Mixtures: A THz Spectroscopic Investigation.....	98
6.1. Introduction.....	98
6.2. Materials and Methods.....	100
6.3. Results and Discussions.....	101

6.4. Summary	109
6.5. References	110
7. Contrasting Hydration Behaviour of DME and DMSO	113
7.1. Introduction.....	113
7.2. Materials and Methods.....	116
7.3. Results and Discussions	117
7.4. Summary	129
7.5. References	134
8. Decisive Role of Hydrophobicity over Electrolytes on Protein Stability	137
8.1. Introduction.....	137
8.2. Materials and Methods.....	141
8.3. Results and Discussions	142
8.4. Summary	153
8.5. References	155
9. Reorientational Relaxation via Large Amplitude Angular Jumps and Its Connections to the Dynamic Heterogeneity.....	159
9.1. Introduction.....	159
9.2. Results and Discussions	161
9.3. Summary	172
9.4. References	173
10. Summary and Future Perspective	174
10.1. Summary	174
10.2. Future Perspective.....	177

1. Introduction

Liquid water at ambient condition is a disordered ensemble of highly polar molecules which possesses several fascinating anomalous and complex properties.¹ Some of these are: (a) an abnormally large dielectric constant ($\epsilon_s \sim 80$), (b) high melting point (273 K), (c) high boiling point (~ 373 K),² (d) high surface tension, (e) high heat capacity, (f) high solubilisation capability and (g) a solid phase that is less dense than its liquid phase. Such unusual properties of this small, otherwise innocent molecule, are linked with its unique ability to form an intricate, robust and dynamic three dimensional tetrahedral hydrogen bond (H-bond) network.^{3,4} Water molecule, one of the most abundant molecules in biophysical

systems, consists of two hydrogen atoms and an oxygen atom attached through two covalent OH bonds. Being a high electronegative candidate compared to the hydrogen atoms, the oxygen atom pulls the electron density away from the two hydrogen atoms. As a result, the oxygen atom enjoys a partial negative charge whereas the hydrogen atoms have partial positive charge that gives rise to two electric dipole moments; both of them are directed towards the oxygen atom (see scheme 1.1). These opposite partial charges on oxygen and hydrogen atoms can also originate



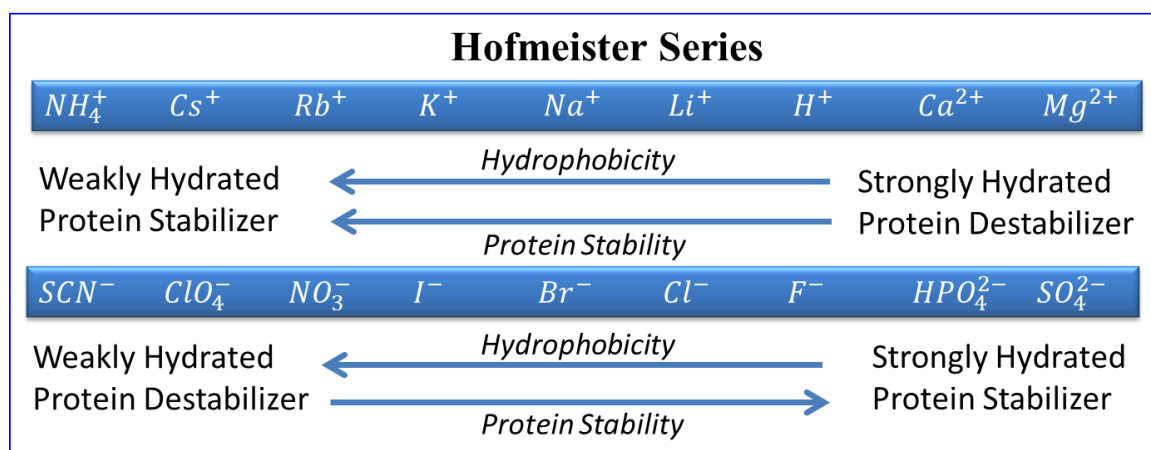
an attractive force between nearby water molecules, known as H-bond. The unusually high dielectric constant of water may be explained as being due to a large liquid phase dipole moment (~ 2.95 D),^{5,6} as well as a high degree of correlation between neighbouring dipoles which is maintained by their transient H-bond networks.⁷ It is due to the local H-bond interactions that make liquid water to possess large dipole moment than its gas phase ($\mu_{\text{gas}} \sim 1.85$ D). In real systems, water is not found in its pure bulk form, rather found being in a micro-heterogeneous confined environment. Water in restricted environment such as aqueous ionic solution,⁸⁻¹⁵ reverse micellar systems,^{16,17} ionic liquids,^{18,19} inside carbon nanotubes and nanodroplets,²⁰⁻²⁴ in contact with organic molecules²⁵⁻³⁰ and in most general biological and chemical possesses³¹ show distinct properties compared to pure water.^{4,32-35} Perturbation of

the H-bonded network results in temporal fluctuations which are the origin of their orientation relaxations (translations coupled with rotations) and are governed by the breaking and making of H-bonds with random waiting periods. Hynes et al.³⁶⁻³⁸ first pictorially demonstrated this restructuring with wait and switch model known as “H-bond jump mechanism”.^{24,36} According to this model a rotating water molecule breaks a H-bond with an over-coordinated first shell neighbour to form H-bond with the under-coordinated second shell neighbour and this process involves a large-amplitude angular jump. Such processes are quite different from the conventional Debye small step diffusion processes. Hence it is of utmost importance to investigate the H-bonded network structure of water and understand their various inter and intra molecular interaction modes in such altered and confined environments as compare to that of pure bulk water.

Hydrogen bonds are particular types of dipole-dipole interactions where a hydrogen atom is sandwiched between two electro negative atoms and is covalently bound to one of them. It had earlier been an issue of debate about the number of H-bonds formed by a single water molecule. It has now been well established that each water molecules can form four H-bonds (average coordination number ~ 3.5 in bulk water) with four other water molecules; two as H-bond donor and two as H-bond acceptor.^{1,39} A small number of water molecules could also remain single or isolated from others (zero H-bond). This fully connected extended water network of pure water is dynamic in nature. In liquid water the molecules are too restless to align in just the right way with four other water molecules which results in the jiggling motions of water. The H-bonds are continuously breaking and forming where they last only for a few hundreds of femtoseconds (fs). Generally in micro-heterogeneous and/or in confined environments the motions of the water network gets sluggish with an increase in the H-bond lifetime. Water molecules residing at interfaces are often termed as hydration water and they possess significantly altered properties due to specific interactions with the solutes surfaces. These water molecules in the hydration layers around biomolecules also control their structure and activity.⁴⁰

The way of interactions of water with hydrophobic and hydrophilic molecules are different and undoubtedly the most critical and important phenomenon that governs most of the biological processes such as protein folding-unfolding, membrane formation etc. There are three major types of non-covalent interactions: electrostatics, hydrophobic and hydrophilic (which includes dipolar, H-bonding, van der Waals interactions etc.) interactions that govern all possible mechanisms in bio-physical systems.^{41,42} Non-covalent interactions (energy lesser than 30 kJ/mol) are basically weak interactions as compared to the covalent

interactions (200-800 kJ/mol). The main aim of this research thesis is to systematically investigate these interactions individually first to have a detail understanding about the situations when more than one interactions are acting simultaneously as is mostly evidenced in real biophysical systems. It also emphasises on the detail studies about the various aspects of solute-solute, solute-solvent and solvent-solvent interaction patterns. In the following section we have discussed the nature of those interactions in detail.



Scheme 1.2. The hydration and protein destabilization capability of the cations and the anions (The Hofmeister series).

Long-range electrostatic interactions are based on the attractions of opposite charges and a repulsion of like charges. In dielectric medium it somehow gets weaker due to screening of the ions by the medium depending upon the dielectric constant of that particular medium. Due to their polar nature, water molecules are excellent solvent candidate of the ions. Ion-water interaction plays important role in biology e.g. in signal transduction and controlling the cell volume.⁴³ Human cells contain negative potassium ions inside the cell and positive sodium ions outside; several biomolecules such as protein, DNA also contain charges. These ion-water interaction pattern can also changes the stability and solubility of proteins in the solution. The phenomena in which the solubility of any molecules in water decreased when electrolytes samples are added in the solution, is known as “*Salting-out*”. A century ago the great scientist “Hofmeister”⁴⁴ arranged the ions based on their hydrophobic effect and the ability to salt-out protein molecules (scheme 1.2).⁴⁵⁻⁴⁷ Thus it is very important to study aqueous electrolyte solutions that can be modelled to understand the electrostatic interactions in real biological systems.⁴⁶⁻⁴⁹ Ions that dissolve in water can strengthen the water network (called as kosmotropes) as well as can rapture the network structure of water (chaotropes) owing to their specific nature of influence on the water-water network.⁵⁰⁻⁵⁴ Introduction of charged ions forces the water molecules to fix themselves around that ions

with electrostatic interactions by pointing one of its OH bonds toward an anion while its dipole points away from a cation.^{15,53,55} Ions pull the water molecules and holds it electrostatically; as a result it breaks the water network structure, forming a semi-rigid hydration shell. As the salt concentration is increased, higher numbers of water molecules start interacting with the ions. For smaller size ions; Li⁺ (the smallest radius among the alkali metal cations), the effective charge density is very high; thus the largest effect is expected to be observed in Li⁺. However, it stands also to consider the dipole-dipole interaction among the water molecules associated with the ion which limits the hydration shell thickness⁵⁴ and eventually minimize the effect. While many of the previous studies indicate that the effect of ions is negligible beyond the first hydration shell, there are certain reports which indicate the effect to be extended to the second and third hydration layers.^{9,56,57} It is important to systematically understand size and/or charge density dependent water-water, ion-water and ion-ion interactions. The main question to address here is how the ions perturb the structure as well as the dynamics of water. It is still a matter of debate that what factors determine the structure maker and breaker properties, and how far the perturbations extend.⁵⁸ In *chapter 4*, we take the opportunity to investigate the collective H-bond network and also the cooperative hydration dynamics of water in presence of some monovalent salts.^{12-14,53,59-62}

Nonpolar molecules also known as hydrophobic molecules do not prefer to stay in pure water. This phenomenon is called “*hydrophobic effect*”.^{41,42,63-66} The associated free energy of the system increases when hydrophobic molecules (called as hydrophobes) are added in liquid water. Hydration of such hydrophobic molecules is associated with entropy loss and heat capacity gets anomalously high. This makes hydration of hydrophobic molecule thermodynamically unfavourable, famously coined as “*hydrophobic hydration*”. Hydrophobic interactions⁶⁷⁻⁷² do not involve bond formations and crucially they are not based on the attractive forces between molecules. Rather hydrophobic molecules have only a few or no polar bonds and thus cannot engage in H-bonds with polar water molecules. True hydrophobic molecules are purely non polar and do not solubilize in water. So in present day research, amphiphilic molecules that contain both hydrophobic and hydrophilic moieties are taken as model systems to understand the hydrophobic effects in aqueous environments. The H-bonding ability of water is a major concern in the role of hydrophobic phenomenon. There are two types of hydrophobic effects; i) *preferential hydrophobic interaction* and ii) *hydrophobic hydration*. Amphiphilic molecules generally consist of some polar groups (e.g. oxygen atom, C=O bond, S=O bond, O-H bond) along with some hydrophobic groups (mostly CH_n group). Some of the amphiphilic molecules such as 1,2-dimethoxy ethane

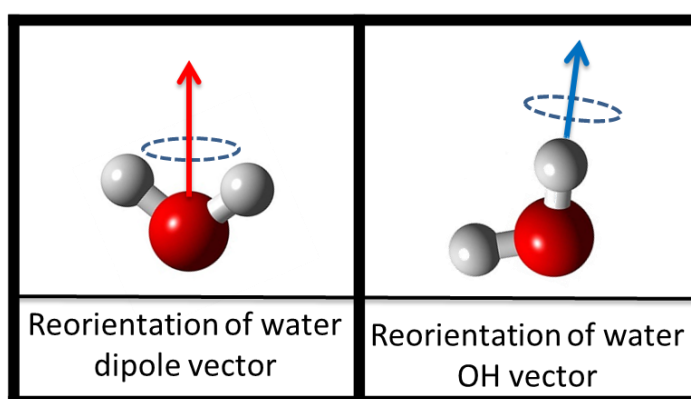
(DME), dimethyl sulfoxide (DMSO), ethanol (EtOH), propanol (PrOH), tertiary butyl alcohol (TBA) in aqueous solutions are been exploited in this particular thesis. In amphiphilic molecules the polar moieties can form H-bonds with solvents like water; whereas the hydrophobic groups assist the cooperative accumulation through hydrophobic hydration. This phenomenon is often termed as “hydrotaxis”, where the preferential movement of certain hydrophobic part of a molecule can sense the presence of other hydrophobic moieties. Amphiphilic molecules dissolved in water force the water molecules to reorient in a specific arrangement around them compared to bulk water where they are free to rotate and form H-bonds in all directions. To minimize the surface contact, these systems are forced to form cluster or aggregation of hydrophobic molecules in a more ordered arrangement. This enhances water-water tetrahedral ordering and association of hydrophobic molecules in aqueous solutions which eventually gives rise to the well-known “*Ice-berg model*”⁷³ and/or “*hydrophobic hydration model*”, where hydrophobic groups aggregates to hide from water and the water molecules surrounding the hydrophobic moieties create an ice-like clathrate structure.^{28,64,67,74,75} Preferential hydrophobic interactions, in which the hydrophobic molecules preferentially attack and bind to the hydrophobic part of another large molecule, are one of the major driving forces for protein folding/unfolding, membrane formations, molecular assembly recognition.^{41,42,65,67,76-79} Such interactions are efficiently replicated in binary aqueous mixtures as the physical properties of the system could easily be tuned by varying the non-aqueous solvent and their compositions.²⁸ There has been a plethora of effort put forward by researchers that has characterized various binary solvents.^{15,80,81} It has grossly been concluded that these interactions are non-specific in nature and depend on the solute type and dimension.^{82,83} Small amphiphilic solutes can fit themselves in a slightly deformed cage of water whereas in large solutes water molecules fail to uphold its H-bonding network that results in a defect in the network. In *chapter 5 & 7* we have investigated the perturbation produced by the amphiphilic molecule; DME on water structure and dynamics. We also compare the findings with another amphiphilic molecule DMSO. In *chapter 6*, we take the opportunity to study the effect of amphiphilic molecules (we have taken three alcohol molecules with varying hydrophobicity) on the structure and hydration of the BSA protein.

In most of the biological systems the situations are somehow complicated. Instead of individual hydrophobic or hydrophilic or electrostatic interactions, there exists a subtle interplay between all these interactions. As for example, there exist several organic and inorganic compounds including macromolecules like sugar, lipids, nucleic acids, proteins, osmolytes in the intra and extra cellular environments. These interactions can be replicated in

complex molecules which contain both electric charge as well as water repelling hydrophobic moieties; some complexes are ionic liquids⁸⁴⁻⁸⁶ and tetra-n-alkylammonium ions ($N(C_nH_{2n+1})_4^+$, TAA).^{11,67,83,87,88} Owing to their unique hydration behaviour, the molecules have attracted the attention of researchers to investigate their effect on the structure, dynamics and activity of water and on biomolecules. The main motivation of these studies involves to model systems which experience combinations of hydrophilic, hydrophobic and electrostatic interactions to gain enough information about the processes involved in real systems (see *chapter 8*). The investigation of the interactions of these molecules with water helps to understand the effect of those molecules on proteins in aqueous environments. Interactions of these molecules with proteins include direct interactions where hydrophobic molecules preferentially bind to the hydrophobic core of the proteins, and also the indirect effect in which they perturb the water network structure around proteins.^{89,90}

Various experimental techniques have been employed through ages to examine the structure and dynamics of bulk and confined water in heterogeneous environments; starting from some very basic such as NMR relaxation,⁹¹ Fourier transform infrared (FTIR),⁹² Raman spectroscopy,^{24,93-95} X-ray diffraction,²² X-ray absorption spectroscopy,²³ volumetric thermodynamic measurements⁹⁶ and steady state fluorescence to state-of-the-art ultrafast techniques like fs IR pump-probe spectroscopy,^{18, 25} optical pump-probe,⁹⁷⁻⁹⁹ THz spectroscopy,¹⁰⁰⁻¹⁰⁷ broadband dielectric spectroscopy,²⁶⁻²⁷ 2D-IR vibrational echo experiments,^{28-29,108} optical Kerr rotation spectroscopy,³⁰ vibrational sum frequency generation spectroscopy³¹⁻³² various non-linear spectroscopy techniques etc. Several theoretical and simulation procedures¹⁰⁹⁻¹¹⁴ are also utilized with those experimental techniques. To understand the H-bond dynamics in water, it is essential to design experiments which can provide information in a wide range (from tens of fs to a few ns) of timescale. It often also becomes necessary to employ more than one technique to probe the whole time span. Ultrafast inferred investigation of stretching vibrational modes can infer accurately about the structural aspect of the water H-bonding connectivity. We have explicitly employed FTIR and DRS techniques in this thesis to understand H-bond structure and dynamics of water in presence of various co-solutes and solvents. To have a time averaged understanding about solvent-solvent and solute-solvent intra and intermolecular interactions FTIR spectroscopy is a very useful technique. Frequency dependent OH stretching mode can directly correlate to the local inter molecular H-bond network. In this thesis, the H-bonded configuration in various aqueous solution has been obtained using FTIR investigation by measuring the O-H stretching ($3000-3800\text{ cm}^{-1}$), O-D stretching ($2200-2800\text{ cm}^{-1}$) and CN

stretching ($2200\text{--}2250\text{ cm}^{-1}$) modes in different physical systems. Dielectric relaxation spectroscopic (DRS) studies probe the correlation of microscopic polarization of samples and could reveal better understanding of hydrogen bonding and intermolecular interactions. This makes DRS a useful technique to monitor cooperative processes. Such studies can also provide with information about the collective response of polarization relaxation of dipolar solvents in terms of the complex permittivity $\tilde{\epsilon}(\nu) = \epsilon_{real}(\nu) - i\epsilon_{img}(\nu)$ of the solutions, where $\epsilon_{real}(\nu)$ is the real part of the dielectric function which is proportional to the energy stored reversibly in the system per period, $\epsilon_{img}(\nu)$ is the imaginary part of the complex permittivity which is proportional to the energy dissipated per period. The dependency on the angular frequency (ω) of that complex dielectric function originates from different processes such as (i) microscopic fluctuations of permanent molecular dipoles (rotational diffusion), (ii) propagation of mobile charge carriers (translational diffusion of electrons, holes or ions) and (iii) separation of charges at interfaces which gives rise to an additional induced polarization. All of these specific processes have their individual contributions towards the frequency dependent real and imaginary part of the complex dielectric functions. While both of these techniques can explore the H-bonding status inside the solutions, the basic difference between them is that the stretching mode of OH bond depends on the local H-bonding whereas DRS study is global in nature. Regarding to their sensitivity DRS is sensitive to the reorientation of the dipole vector of the water molecules around the solute whereas it is the OH vector in case of MIR studies (scheme 1.3).



Scheme 1.3. DRS probes the reorientation of the permanent water dipole vector whereas MIR study probes the rotation of the water OH hand.

Hydration dynamics around electrolytes, biologically important cosolvents and proteins has been measured by two complementary techniques: *THz time domain spectroscopy* (TTDS) and *time-resolved fluorescence spectroscopy* (TRFS). TRFS was measured using ps-resolved *time-correlated single photon counting* (TCSPC) technique,¹¹⁵⁻¹¹⁷

which manifests the stabilization or relaxation of an instantaneously created dipole by the reorientation of the surrounding polar dipoles (water). The structural stability and the hydrodynamic diameter of proteins in aqueous medium and in presence of co-solutes have been investigated with *circular dichroism* (CD) spectroscopy and *dynamic light scattering* (DLS) study. The principle objective of this thesis is to understand the nature of the extended three dimensional H-bonded networks of water in altered environments. Besides experimental investigations this thesis used all-atom classical *molecular dynamics* (MD) simulation technique to obtain microscopic view about various H-bonded configurations, cluster formation in presence of hydrophobic solute particles, the tetrahedral structural order parameter and the H-bond breaking and making dynamical mechanisms of water molecules in presence of amphiphilic solutes molecules. Another aspect of this present thesis is also to discuss about how the perturbations of the hydration water by the co-solutes and co-solvents perturb the stability of a model protein *bovine serum albumin* (BSA).

The motivation and interest of this thesis is to model different interactions and understand them in detail that present in various physical chemistry and biological systems. The curiosity is on the effect of water structure and dynamics in presence of some guest molecules as they found in real systems or maybe they can mimic the real biophysical processes. To gain a broad understanding of the real interactions one has to first understand the electrostatics, hydrophilic and hydrophobic interactions individually. With this brief introduction, the theses describe the findings and try to explain the individual interactions in *chapter 4, 5, 6 & 7* in detail. And finally in *chapter 8* it discusses such cases where all these interactions are present simultaneously and also compare such scenario with the individual one. This thesis consists of the following ten chapters as described in brief.

Chapter 1 discusses a very general introduction and motivation behind this thesis work. The discussions about previous findings by other researchers are also described briefly in the introduction section of each chapter.

Chapter 2 is based on some relevant basic theories; working principles and information about all the instruments that have been used in this thesis.

Chapter 3 provides a complete description of the all-atom molecular dynamics (MD) simulation methods and analysis protocols.

Chapter 4 describes the effect of monovalent salt on the structure and dynamics of water. It also discusses about the perturbation produced by those ions on the physical properties of BSA protein. We investigated the secondary structure of the protein by CD spectroscopy and

its hydration by the state of the art THz TDS. We found that the relaxation time constants of water dipoles in presence of salts as obtained from the fitting of real and imaginary parts of permittivity (ϵ) show an accelerated reorientation dynamics, which is an indirect support of the structure breaking ability of the ions. We also found that the salts have negligible effect on the structure of BSA, the salt hydration and protein hydration act independently.

Chapter 5 argues on the nature of hydration of a biologically important amphiphilic molecule DME to understand the phenomena of “hydrophobic hydration”. A combination of experimental and simulation techniques are implemented to understand the heterogeneous structure and dynamics of water-DME binary mixtures in the whole concentration region. We try to correlate the experimental findings with that of simulation results.

Chapter 6 reveals the study of the preferential hydrophobic interactions, where being a hydrophobic candidate the alcohol molecules prefer to interact with the hydrophobic core of the BSA protein molecules that ensure its rapture of the secondary structure and also its hydration.

Chapter 7 compares about microscopic features of the contrasting hydration behaviours of two amphiphilic molecules DME and DMSO. Being a more polar candidate compare to DME molecules, DMSO shows a more H-bonding affinity towards water molecules.

Chapter 8 reveals the study of the effect of cations that contain some hydrophobic moieties along with a monovalent electrostatic charge. It also compares the results that are found in *chapter 4* due to the presence of electrostatic charge only (monovalent cations). This chapter combines the findings of *chapter 4,5 & 7*.

Chapter 9 gives a very brief overview of how one can investigate the microscopic features of translational and rotational dynamics of liquid water with the “*wait and jump model*”. This chapter describe the parameters of the “*wait and jump model*” during the transition states (H-bond partner exchange events). It also consists of some results that can probe the dynamic heterogeneity of the aqueous solutions of hydrophobic molecules.

Chapter 10 provides the summary of the present thesis and discussed about the current findings. It also briefly discuss about some future plans that one can perform in future.

1.1. References

- (1) Chaplin, M. [Internet URL] <http://www1.lsbu.ac.uk/water/anmlies.html>. April, 2010.
- (2) Yuan, R.; Yan, C.; Tamimi, A.; Fayer, M. D. *The Journal of Physical Chemistry B* **2015**, *119*, 13407-13415.
- (3) Nandi, N.; Bhattacharyya, K.; Bagchi, B. *Chem. Rev.* **2000**, *100*, 2013-2045.

- (4) Levinger, N. E. *Science* **2002**, 298, 1722-1723.
- (5) Badyal, Y. S.; Saboungi, M.-L.; Price, D. L.; Shastri, S. D.; Haeffner, D. R.; Soper, A. K. *The Journal of Chemical Physics* **2000**, 112, 9206-9208.
- (6) Gubskaya, A. V.; Kusalik, P. G. *The Journal of Chemical Physics* **2002**, 117, 5290-5302.
- (7) Kirkwood, J. G. *The Journal of Chemical Physics* **1939**, 7, 911-919.
- (8) Chen, T.; Hefter, G.; Buchner, R. *J. Phys. Chem. A* **2003**, 107, 4025-4031.
- (9) Wachter, W.; Fernandez, S.; Buchner, R.; Hefter, G. *J. Phys. Chem. B* **2007**, 111, 9010-9017.
- (10) Turton, D. A.; Hunger, J.; Hefter, G.; Buchner, R.; Wynne, K. *J. Chem. Phys.* **2008**, 128, 161102.
- (11) van der Post, S. T.; Scheidelaar, S.; Bakker, H. J. *The Journal of Physical Chemistry B* **2013**, 117, 15101-15110.
- (12) Samanta, N.; Das Mahanta, D.; Mitra, R. K. *Physical Chemistry Chemical Physics* **2014**, 16, 23308-23315.
- (13) Das Mahanta, D.; Samanta, N.; Mitra, R. K. *Journal of Molecular Liquids* **2016**, 215, 197-203.
- (14) Schmidt, D. A.; Birer, Ö.; Funkner, S.; Born, B.; Gnanasekaran, R.; Schwaab, G.; Leitner, D. M.; Havenith, M. *J. Am. Chem. Soc.* **2009**, 131, 18512-18517.
- (15) Tielrooij, K. J.; van der Post, S. T.; Hunger, J.; Bonn, M.; Bakker, H. J. *J. Phys. Chem. B* **2011**, 115, 12638-12647.
- (16) Das, A.; Patra, A.; Mitra, R. K. *The Journal of Physical Chemistry B* **2013**, 117, 3593-3602.
- (17) Hou, M. J.; Shah, D. O. *Langmuir* **1987**, 3, 1086-1096.
- (18) Wong, D. B.; Giammanco, C. H.; Fenn, E. E.; Fayer, M. D. *The Journal of Physical Chemistry B* **2013**, 117, 623-635.
- (19) Shin, J. Y.; Yamada, S. A.; Fayer, M. D. *The Journal of Physical Chemistry B* **2018**, 122, 2389-2395.
- (20) Mukherjee, B.; Maiti, P. K.; Dasgupta, C.; Sood, A. K. *ACS Nano* **2010**, 4, 985-991.
- (21) Mukherjee, B.; Maiti, P. K.; Dasgupta, C.; Sood, A. K. *The Journal of Chemical Physics* **2007**, 126, 124704.
- (22) Dokter, A. M.; Woutersen, S.; Bakker, H. J. *Proceedings of the National Academy of Sciences USA* **2006**, 103, 15355-15358.
- (23) Kumar, H.; Mukherjee, B.; Lin, S.-T.; Dasgupta, C.; Sood, A. K.; Maiti, P. K. *The Journal of Chemical Physics* **2011**, 134, 124105.
- (24) Mukherjee, B.; Maiti, P. K.; Dasgupta, C.; Sood, A. K. *The Journal of Physical Chemistry B* **2009**, 113, 10322-10330.
- (25) Yoshio Miyazaki, H. M. *Bulletin of the Chemical Society of Japan* **1991**, 64, 288-290.
- (26) Takamuku, T.; Yamaguchi, A.; Tabata, M.; Nishi, N.; Yoshida, K.; Wakita, H.; Yamaguchi, T. *J. Mol. Liq.* **1999**, 83, 163-177.
- (27) Kustov, A. V.; Antonova, O. A.; Korolev, V. P. *Journal of Solution Chemistry* **2002**, 31, 671-680.
- (28) Fenn, E. E.; Moilanen, D. E.; Levinger, N. E.; Fayer, M. D. *J. Am. Chem. Soc.* **2009**, 131, 5530-5539.
- (29) Wong, D. B.; Sokolowsky, K. P.; El-Barghouthi, M. I.; Fenn, E. E.; Giammanco, C. H.; Sturlaugson, A. L.; Fayer, M. D. *The Journal of Physical Chemistry B* **2012**, 116, 5479-5490.

- (30) Das Mahanta, D.; Patra, A.; Samanta, N.; Luong, T. Q.; Mukherjee, B.; Mitra, R. K. *The Journal of Chemical Physics* **2016**, *145*, 164501.
- (31) Ebbinghaus, S.; Kim, S. J.; Heyden, M.; Yu, X.; Heugen, U.; Gruebele, M.; Leitner, D. M.; Havenith, M. *Proc. Natl. Acad. Sci. USA* **2007**, *104*, 20749-20752.
- (32) Levinger, N. E.; Swafford, L. A. *Annual Review of Physical Chemistry* **2009**, *60*, 385-406.
- (33) Fayer, M. D. *Physiology* **2011**, *26*, 381-392.
- (34) Fayer, M. D.; Levinger, N. E. *Annual Review of Analytical Chemistry* **2010**, *3*, 89-107.
- (35) Moilanen, D. E.; Levinger, N. E.; Spry, D. B.; Fayer, M. D. *J. Am. Chem. Soc.* **2007**, *129*, 14311-14318.
- (36) Laage, D.; Hynes, J. T. *Science* **2006**, *311*, 832-835.
- (37) Laage, D.; Hynes, J. T. *J. Phys. Chem. B* **2008**, *112*, 14230-14242.
- (38) Laage, D. L.; Hynes, J. T. *Proc. Natl. Acad. Sci. U.S.A.* **2007**, *104*, 11167-11172.
- (39) Sharp, K. A.; Vanderkooi, J. M. *Accounts of Chemical Research* **2010**, *43*, 231-239.
- (40) Kropman, M. F.; Bakker, H. J. *Science* **2001**, *291*, 2118-2120.
- (41) Tanford, C. *The Hydrophobic effect: formation of micellar and biological membranes*; 2nd ed.; Wiley Interscience: New York, **1980**.
- (42) Blokzijl, W.; Engberts, J. B. F. N. *Angewandte Chemie International Edition in English* **1993**, *32*, 1545-1579.
- (43) Ward, J. M.; Pei, Z. M.; Schroeder, J. I. *The Plant Cell* **1995**, *7*, 833-844.
- (44) F., H. *Arch. Exp. Pathol. Pharmacol.* **1888**, *24*, 247-260.
- (45) Baldwin, R. L. *Biophys. J.* **1996**, *71*, 2056-2063.
- (46) Cacace, M. G.; Landau, E. M.; Ramsden, J. J. *Q. Rev. Biophys.* **1997**, *30*, 241-277.
- (47) Lo Nostro, P.; Ninham, B. W. *Chem. Rev.* **2012**, *112*, 2286-2322.
- (48) Dill, K. A. *Biochemistry* **1990**, *29*, 7133-7155.
- (49) Rupley, J. A.; Careri, G. *Adv. Prot. Chem.* **1991**, *41*, 37-172.
- (50) Marcus, Y. *Ion solvation*; Wiley-Interscience: New York, **1985**.
- (51) Kunz, W. N. B.; Henle, J.; Ninham, B. W. *Curr. Opin. Colloid Interface Sci.* **2004**, *9*, 19-37.
- (52) Tobias, D. J.; Hemminger, J. C. *Science* **2008**, *319*, 1197-1198.
- (53) Tielrooij, K. J.; Garcia-Araez, N.; Bonn, M.; Bakker, H. J. *Science* **2010**, *328*, 1006-1009.
- (54) Hribar, B.; Southall, N. T.; Vlachy, V.; Dill, K. A. *J. Am. Chem. Soc.* **2002**, *124*, 12302-12311.
- (55) Omta, A. W.; Kropman, M. F.; Woutersen, S.; Bakker, H. J. *Science* **2003**, *301*, 347-349.
- (56) Mancinelli, R.; Botti, A.; Bruni, F.; Ricci, M. A.; Soper, A. K. *Phys. Chem. Chem. Phys.* **2007**, *9*, 2959-2967.
- (57) Buchner, R.; Chen, T.; Hefter, G. *J. Phys. Chem. B* **2004** *108*, 2365-2375.
- (58) Marcus, Y. *Chem. Rev.* **2009**, *109*, 1346-1370.
- (59) Tielrooij, K. J.; Timmer, R. L. A.; Bakker, H. J.; Bonn, M. *Phys. Rev. Lett.* **2009**, *102*, 198303.
- (60) Ottosson, N.; Hunger, J.; Bakker, H. J. *J. Am. Chem. Soc.* **2014**, *136*, 12808-12811.
- (61) Funkner, S.; Niehues, G.; Schmidt, D. A.; Heyden, M.; Schwaab, G.; Callahan, K. M.; Tobias, D. J.; Havenith, M. *J. Am. Chem. Soc.* **2012**, *134*, 1030-1035.

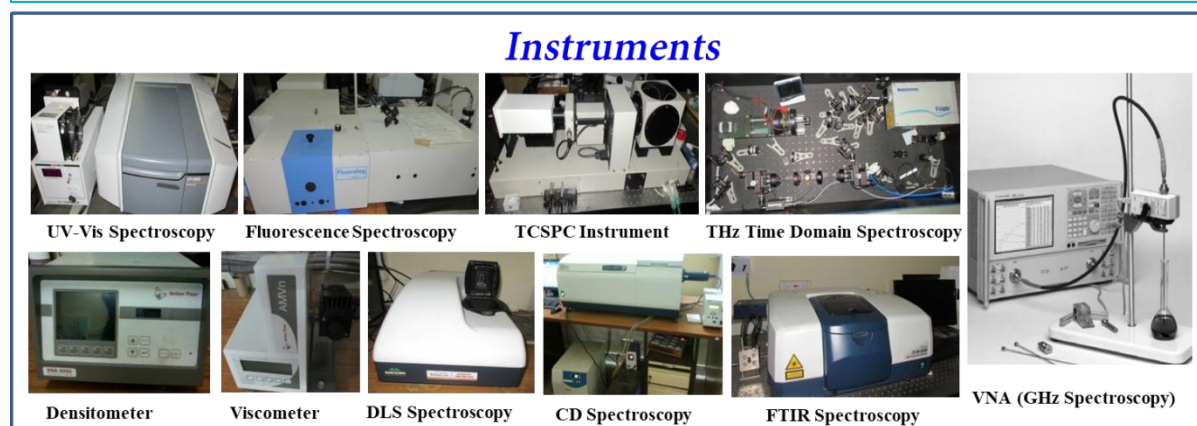
- (62) Buchner, R. *Pure Appl. Chem.* **2008**, *80*, 1239-1252.
- (63) Strazdaite, S.; Versluis, J.; Bakker, H. J. *The Journal of Chemical Physics* **2015**, *143*, 084708.
- (64) Bakker, H. J. *Nature* **2012**, *491*, 533-535.
- (65) Southall, N. T.; Dill, K. A.; Haymet, A. D. J. *The Journal of Physical Chemistry B* **2002**, *106*, 521-533.
- (66) Widom, B.; Bhimalapuram, P.; Koga, K. *Physical Chemistry Chemical Physics* **2003**, *5*, 3085-3093.
- (67) Das Mahanta, D.; Samanta, N.; Mitra, R. K. *The Journal of Physical Chemistry B* **2017**, *121*, 7777-7785.
- (68) Rakshit, S.; Saha, R.; Chakraborty, A.; Pal, S. K. *Langmuir* **2013**, *29*, 1808-1817.
- (69) Pascal, T. A.; Goddard, W. A. *The Journal of Physical Chemistry B* **2012**, *116*, 13905-13912.
- (70) Huang, N.; Schlesinger, D.; Nordlund, D.; Huang, C.; Tylliszczak, T.; Weiss, T. M.; Acremann, Y.; Pettersson, L. G. M.; Nilsson, A. *J. Chem. Phys.* **2012**, *136*, 074507.
- (71) Davis, J. G.; Gierszal, K. P.; Wang, P.; Ben-Amotz, D. *Nature* **2012**, *491*, 582-585.
- (72) Tomlinson-Phillips, J.; Davis, J. G.; Ben-Amotz, D.; Spångberg, D.; Pejov, L.; Hermansson, K. *J. Phys. Chem. A* **2011**, *115*, 6177-6183.
- (73) Frank, H. S.; Evans, M. W. *The Journal of Chemical Physics* **1945**, *13*, 507-532.
- (74) Li, I. T. S.; Walker, G. C. *Proceedings of the National Academy of Sciences* **2011**, *108*, 16527-16532.
- (75) Grdadolnik, J.; Merzel, F.; Avbelj, F. *Proceedings of the National Academy of Sciences* **2017**, *114*, 322-327.
- (76) Das, D. K.; Das Mahanta, D.; Mitra, R. K. *ChemPhysChem* **2017**, *18*, 749-754.
- (77) Ide, M.; Maeda, Y.; Kitano, H. *The Journal of Physical Chemistry B* **1997**, *101*, 7022-7026.
- (78) Wiggins, P. M. *Physica A: Statistical Mechanics and its Applications* **1997**, *238*, 113-128.
- (79) O'Brien, E. P.; Dima, R. I.; Brooks, B.; Thirumalai, D. *J. Am. Chem. Soc.* **2007**, *129*, 7346-7353.
- (80) Chandler, D. *Nature* **2002**, *417*, 491-491.
- (81) Zangi, R.; Zhou, R.; Berne, B. J. *J. Am. Chem. Soc.* **2009**, *131*, 1535-1541.
- (82) Chandler, D. *Nature* **2005**, *437*, 640-647.
- (83) Buchner, R.; Holzl, C.; Stauber, J.; Barthel, J. *Physical Chemistry Chemical Physics* **2002**, *4*, 2169-2179.
- (84) Mann, J. P.; McCluskey, A.; Atkin, R. *Green Chem.* **2009**, *11*, 785-792.
- (85) Araque, J. C.; Daly, R. P.; Margulis, C. J. *The Journal of Chemical Physics* **2016**, *144*, 204504.
- (86) Wijaya, E. C.; Separovic, F.; Drummond, C. J.; Greaves, T. L. *Physical Chemistry Chemical Physics* **2016**, *18*, 25926-25936.
- (87) Strazdaite, S.; Versluis, J.; Bakker, H. J. *The Journal of Physical Chemistry C* **2016**.
- (88) Shimizu, A.; Taniguchi, Y. *Bull. Chem. Soc. Jpn.* **1990**, *63*, 3255- 3259.
- (89) Rossky, P. J. *Proc. Nat. Acad. Sci.* **2008** *105*, 16825-16826.
- (90) Schellman, J. A. *Biophys. Chem.* **2002**, *96*, 91-101.
- (91) Kříž, J.; Dybal, J. *Chem. Phys.* **2011**, *382*, 104-112.

- (92) Matsuura, H.; Sagawa, T. *J. Mol. Liq.* **1995**, 65-66, 313-316.
- (93) Goutev, N.; Nickolov, Z. S.; Matsuura, H. *J. Mol. Liq.* **1998**, 76, 117-126.
- (94) Nickolov, Z. S.; Goutev, N.; Matsuura, H. *J. Phys. Chem. A* **2001**, 105, 10884 - 10889.
- (95) Goutev, N.; Ohno, K.; Matsuura, H. *J. Phys. Chem. A* **2000**, 104, 9226-9232.
- (96) Douheret, G.; Reis, J. C. R.; Davis, M. I.; Fjellanger, I. J.; Høiland, H. *Phys. Chem. Chem. Phys.* **2004**, 6, 784-792.
- (97) Berera, R.; van Grondelle, R.; Kennis, J. T. M. *Photosynth. Res.* **2009**, 101, 105-118.
- (98) Rosspeintner, A.; Lang, B.; Vauthey, E. *Annual Review of Physical Chemistry* **2013**, 64, 247-271.
- (99) Kumpulainen, T.; Lang, B.; Rosspeintner, A.; Vauthey, E. *Chemical Reviews* **2017**, 117, 10826-10939.
- (100) Beard, M. C.; Turner, G. M.; Schmittenmaer, C. A. *J. Phys. Chem. B* **2002**, 106, 7146-7159.
- (101) Heyden, M.; Ebbinghaus, S.; Havenith, M. In *Encyclopedia of Analytical Chemistry*; John Wiley & Sons, Ltd: **2006**.
- (102) Tonouchi, M. *Nat Photon* **2007**, 1, 97-105.
- (103) Lee, Y. S. *Principles of Terahertz Science and Technology*; Springer US, **2009**.
- (104) Baxter, J. B.; Guglietta, G. W. *Anal. Chem.* **2011**, 83, 4342-4368.
- (105) Kindt, J. T.; Schmittenmaer, C. A. *J. Phys. Chem.* **1996**, 100, 10373-10379.
- (106) Venables, D. S.; Schmittenmaer, C. A. *J. Chem. Phys.* **1998**, 108, 4935-4943.
- (107) Schmittenmaer, C. A. *Chem. Rev.* **2004**, 104, 1759-1780.
- (108) Hamm, P.; Zanni, M. *Concepts and Methods of 2D Infrared Spectroscopy*; Cambridge University Press, **2011**.
- (109) Bedrov, D.; Borodin, O.; Smith, G. D. *J. Phys. Chem. B* **1998**, 102, 5683-5690.
- (110) Bedrov, D.; Smith, G. D. *J. Phys. Chem. B* **1999**, 103, 3791-3796.
- (111) Bedrov, D.; Pekny, M.; Smith, G. D. *J. Phys. Chem. B* **1998**, 102, 996 - 1001.
- (112) Smith, G. D.; Bedrov, D.; Borodin, O. *Phys. Rev. Lett.* **2000**, 85, 5583.
- (113) Hezaveh, S.; Samanta, S.; Milano, G.; Roccatano, D. *J. Chem. Phys.* **2011**, 135, 164501.
- (114) Bedrov, D.; Borodin, O.; Smith, G. D. *J. Phys. Chem. B* **1998**, 102, 9565-9570.
- (115) Lakowicz, J. R. *Principles of Fluorescence Spectroscopy*; 2nd ed.; Kluwer Academic/Plenum: New York, **2006**.
- (116) O'Connor, D. *Time-correlated single photon counting*; Academic Press, **2012**.
- (117) Amiri, M.; Jankeje, K.; Albani, J. R. *JFlu* **2010**, 20, 651-656.

2. Instrumentation and the Underline Basic Theories

This chapter discuss some experimental techniques & methods, that are applied in chapters 4, 5 & 6. It will briefly describe basic theories and information behind those techniques. To explain the findings one should have clear concepts about the instrumentations and the underline physical processes involved.

Instruments



2.I. Experimental Techniques

2.I.1. Ultra Violet-Visible Spectroscopy (UV-Vis)

Here in this thesis the UV-Vis absorption spectra are measured with Shimadzu UV-2600 spectrophotometer where a tungsten lamp (W_1) is used as visible light source and a deuterium lamp (D_2) is used as an ultraviolet light source with a lamp interchange wavelength of 282-293 nm. The monochromator consists of high performance blazed holographic grating that can divide the beam of light into its component wavelengths. It is a typical double beam instrument; the light emanating from source is split into two beams. One of them is used as reference beam and the other is the sample beam. A photomultiplier tube (PMT) is used as a detector.

When continuous radiation passes through a material, a portion of the radiation may be absorbed. If that occurs, the residual radiation, when it is passed through a prism, yields a spectrum with gaps in it, called an absorption spectrum. By absorbing the electromagnetic radiation, the molecules excite from lower energy electronic state (S_0) to higher energy state

(S₁). Such electronic transition of any molecule is always associated with both vibrational and rotational transitions. But the electronic energy states consist of a vast number of closely spaced rotational and vibrational levels that not every spectrophotometer can resolve. Rather, the instrument traces an envelope. That's why the UV absorption spectrum of a molecule usually provides a broad distribution band with a central peak wavelength where the major transition happens. Regarding the extent of absorption of a molecule there is an empirical equation known as Beer-Lambert law as given below,

$$A = \log(I_0/I) = \epsilon cl \quad (\text{for a given wavelength}) \quad (2.1)$$

where A is the absorption, I_0 is the intensity of light incident upon sample cell, I is the intensity of light leaving sample cell, ϵ is molar absorptivity, c is the molar concentration of solute and l is the length of sample cell. This absorption is linearly proportional to the concentration of the molecules (c) and the path length (l) of the absorbing medium.

2.1.2. Circular Dichroism (CD) Spectroscopy

CD data, provided in the following chapters, are measured with JASCO J-815. Spectropolarimeter with a Peltier temperature controller attached with that. A Xe-lamp is used as a source of light. N₂ is purged to remove O₃ gas from the chamber. CD is defined as the difference in absorbance of left-handed (L) and right-handed (R) circularly polarized light and have a non-zero value when a molecule contains one or more chiral chromophores (light absorbing groups) in it.

$$CD = A_L(\lambda) - A_R(\lambda) \quad (2.2)$$

Molar ellipticity $[\theta]$ is defined as,

$$[\theta] = \frac{\theta \text{ (mdeg)}}{C_M \times l \times 10} \text{ (deg cm}^2 \text{ decmol}^{-1}) \quad (2.3)$$

where θ (mdeg) is the CD in mdeg unit, C_M is the molar concentration of the sample, l is the path length of the cell in cm unit.

2.1.3. Steady State Fluorescence Spectroscopy

Steady-state emission spectra are measured with Fluorolog, Horiba-Jobin Yvon, Edison, NJ (Model LFI-3751). Ozone free Xe-Arc lamp has been used as a source of continuous wave light. There are two monochromators¹ which are excitation and emission monochromator. The reflection gratings of the monochromator contain 1200 grooves/mm and are blazed at

330 nm (excitation) and 500 nm (emission). These gratings can give excitation wavelength coverage from 220-600 nm and emission wavelength coverage 290-850 nm.

2.1.4. Time-Resolved Fluorescence Spectroscopy (TRFS)

Picosecond-resolved fluorescence² transients are recorded using time correlated single photon counting (TCSPC) technique.¹ The fluorescence decays were recorded with the TCSPC setup (Edinburgh instruments, U.K.). The instrument response functions (IRFs) of the laser sources at different excitation wavelengths varied from 60 ps to 400 ps (~70 ps for the laser of excitation wavelength 309 nm). Fluorescence signal from the samples was detected by a photomultiplier after dispersion through a grating monochromator. For all the transient decays, the polarizer in the emission side was adjusted to be at magic angle (54.7°) with respect to the polarization axis of the excitation pulse.

Solvation Dynamics: Generally the fluorescent probes are non-polar in its ground state, but possesses a large dipole moment in the excited state. At t=0, when the fluorophore is excited by the ultrafast (ps or fs duration) laser pulse, a dipole moment is created instantaneously in its excited state. Since the electronic excitation is much faster than the nuclear motion of atoms in molecules (according to Frank-Condon principle), the instantaneously excited probe in the vicinity of the solvent molecules find themselves in a relatively high energy configuration. As time passes, the solvent molecules begin to diffuse via rotation and translation to get a new equilibrium position. Thus the fluorescent maxima gradually shift to lower energy (longer wavelength) which results a time dependent fluorescence Stokes shift (TDFSS). This wavelength dependency of the fluorescence decays manifests the solvation dynamics. Time-resolved fluorescence solvation dynamics manifests the stabilization of the instantaneously created solute dipoles (fluorophore) by the reorientation of the solvent dipoles. We measure the wavelength dependent emission transients of the fluorophore in solution. Then we fit those emission transient decays with exponential decay functions using an iterative re-convolution least-square algorithm. Using the transient fitting parameters and the steady state emission spectra, we construct the corresponding time-resolved emission spectra (TRES) using equation 2.4, as given by,

$$I(\nu, t) = I_{SS}(\nu) \frac{\sum_{i=1}^N \alpha_i(\nu) e^{-t/\tau_i(\nu)}}{\sum_{i=1}^N \alpha_i(\nu) \tau_i(\nu)} \quad (2.4)$$

where $I_{ss}(\nu)$ is the steady state fluorescence intensity. The TRES were used to construct the normalised spectral shift correlation function defined as,

$$C(t) = \frac{\tilde{\nu}(t) - \tilde{\nu}(\infty)}{\tilde{\nu}(0) - \tilde{\nu}(\infty)} \quad (2.5)$$

where $\tilde{\nu}(0)$, $\tilde{\nu}(t)$ and $\tilde{\nu}(\infty)$ are the emission maxima at time *zero*, time *t*, and at *infinity* respectively. The time dependent solvation correlation functions $C(t)$ are fitted using a bi-exponential decay function. The average solvation time is calculated as $\langle \tau_s \rangle = \sum a_i \tau_i$. Further details of the solvation dynamics and the data analysis procedure can be found elsewhere.³⁻⁶

2.1.5. Dynamic Light Scattering (DLS)

DLS, also known as photon correlation spectroscopy (PSC) or quasi elastic light scattering (QELS) is one of the reliable technique to determine the hydrodynamic diameter of the particle. DLS measurements were carried out with *Nano S Malvern* instrument employing a 4mW He-Ne LASER ($\lambda = 632.8$ nm) equipped with a thermostated sample chamber. When light hits small particles compared to the wavelength, the light scatters in all directions (Rayleigh scattering). For the monochromatic and coherent light, the scattering intensity fluctuates over time due to small molecules in solutions undergoing *Brownian motion*. Hence the distance between the scatterers in the solution is constantly changing with time. This scattered light then undergoes either constructive or destructive interference by the surrounding particles, and within this intensity fluctuation, information is contained about the time scale of movement of the scatterers. All the scattered photons are collected at 173° scattering angle.⁷⁻⁹ The measured data in DLS experiment is the correlation curve. The correlation curves contain all of the information regarding the diffusion of particles within the samples. By fitting the correlation curve to an exponential function, the diffusion coefficient (D) can be calculated (D is proportional to the lifetime of the exponential decay). Hydrodynamic diameter (d_H) of the particle is estimated from the intensity autocorrelation function of the time-dependent fluctuation in intensity. According to Stokes-Einstein (SE) model, the d_H is related to the viscosity and the diffusion coefficient of the solution as given below,

$$d_H = \frac{K_B T}{3\pi\eta D} \quad (2.6)$$

where K_B is the Boltzmann constant, T is the temperature, η is the viscosity, and D is the translational diffusion coefficient. The viscosities of the solutions are taken from the literature.¹⁰

2.1.6. Fourier Transform Infrared (FTIR) Spectroscopy

Mid Infrared (MIR) Study: FTIR measurements are performed on a JASCO FTIR-6300 spectrometer (transmission mode). Michelson interferometer is the heart of FTIR spectrometer.¹¹ It consists of a fixed mirror, a moving mirror and a beam-splitter (BS). The collimated IR beam from the source is partially transmitted to the moving mirror and partially reflected to the fixed mirror by the beam-splitter. The two IR beams are then reflected back to the beam-splitter by the mirrors. The detector then senses the transmitted beam from the fixed mirror and reflected beam from the moving mirror, simultaneously. The two combined beams interfere constructively or destructively depending on the wavelength of the light (or frequency) and the optical path difference introduced by the moving mirror. The resulting signal is called an interferogram which has the unique property that every data point (a function of the moving mirror position) have information about every infrared frequency which comes from the source. The measured interferogram signal is then Fourier transformed to obtain the final spectrum. Each spectrum consists of 120 scans and the spectral range can be varied from 1500 to 4000 cm^{-1} (MIR region) acquired at 0.5 cm^{-1} resolution.

Far Infrared (FIR) Study: FTIR spectra in far infrared region were recorded using a VERTEX 80v FTIR Spectrometer (Bruker Optics) under nitrogen gas flow in the sample compartment. The data were collected and processed using OPUS software. For spectra acquisition in the FIR region (30-450 cm^{-1}), a mercury-lamp served as an FIR source, a liquid-helium-cooled silicon bolometer was used as a detector. All the measurements were performed using a liquid cell (model A145, Bruker Optics, diamond windows) with a thickness of $28.5 \pm 0.3 \mu\text{m}$.

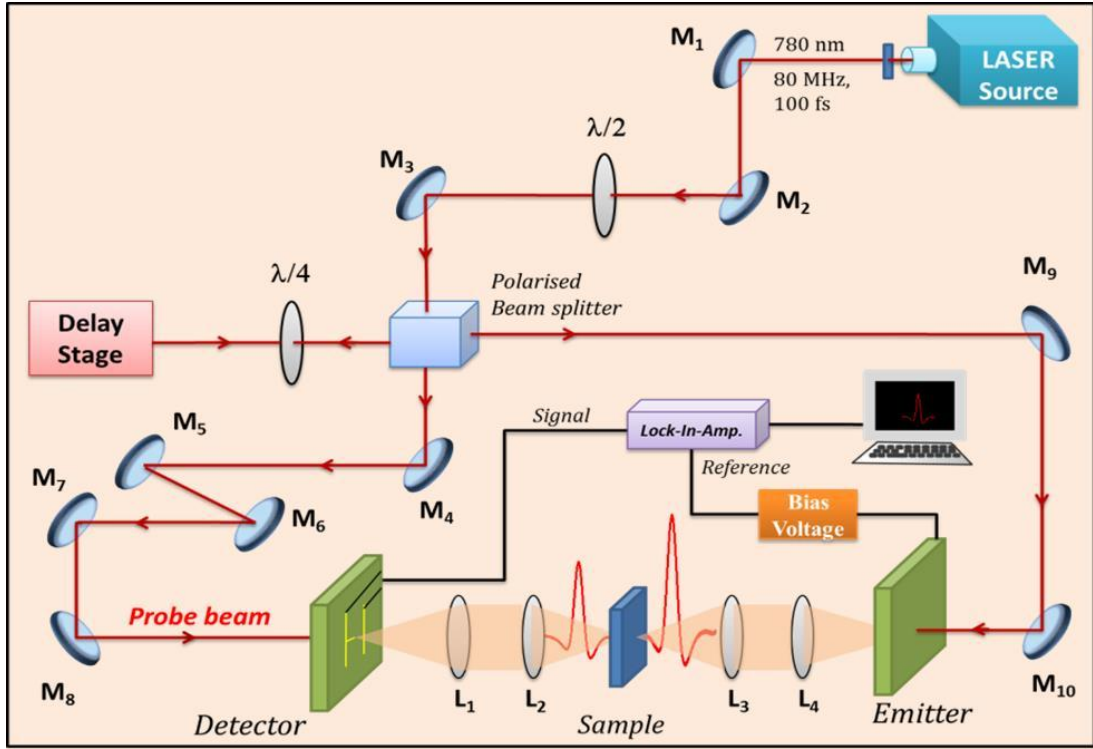
2.1.7. Terahertz (THz) Spectroscopy

Electromagnetic radiation has an electric (\vec{E}) and magnetic field (\vec{B}) that oscillates at mutually perpendicular to its propagation (\vec{k}) vector ($\vec{E} \perp \vec{B} \perp \vec{k}$). In the electromagnetic spectrum, the gap in between microwaves and infrared region, the combination of electronics and optics open up a new “Tera-Era”^{12,13} that spans from 300 GHz to 10 THz. 1 THz corresponds to a timescale of $\sim 1 \text{ ps}^{-1}$, a wavelength of 300 μm , a wave number of 33.3 cm^{-1} . Such energy is not enough for electronic transition. THz is in between the microwave, which probes the rotational motions of the molecules and the IR, which is sensitive to the vibrational motions. Such spectroscopic tool is useful in radio astronomy and bio-chemistry research. THz spectroscopy provides information on the collective H-bond dynamics.

Rotational frequencies of light molecules and vibrational frequencies of large molecules with many functional groups including some biological molecules have broad resonance in this region. This so-called “THz gap” arises due to lack of inexpensive and convenient commercial spectrometers operating in this elusive spectral region. Due to the unavailability of the efficient detectors the THz/microwave radiation coming from universe, different galaxies and stars, also emitted from living objects are remain undetected. The main disadvantage with the electronic is that one cannot go beyond 0.3 THz due to the inherent restriction of the fast electron oscillation time, and with the semiconductors materials one cannot go below 10 THz. The conventional band gaps of the semiconductors are of the order of few electron-volts (eV), an order of magnitude higher than the THz energy.¹⁴ This THz radiation cannot be produced or detected by lasers or commercial photo diodes. The energy of 1 THz (10^{12} Hz) photon is about 4.1 meV much smaller than the quantized thermal unit of $k_B T$ ($1 k_B T \sim 25$ meV at room temperature, $T = 300$ K). So the quantized nature of the radiation can be neglected. Rather it can be think that THz regime is a natural bridge between the classical and quantum description of the EM waves and their interaction with matter. In the last 20-30 years of extensive research people have almost filled the Tera gap. There are three different types of spectroscopic measurement techniques are available now-a-days, namely i) THz time domain spectroscopy (THz-TDS), in which ground state properties of the sampled are measured in a non-invasive way ii) THz time-resolved spectroscopy (TRTS) and iii) THz emission spectroscopy (TES). In this thesis we are only interested on the THz-TDS technique.

2.I.8. Terahertz Time Domain Spectroscopy (TTDS)

TTDS measurements are carried out in a commercial THz spectrophotometer (*TERA K8, Menlo System*).^{15,16} A 780 nm Er doped fiber laser having pulse width of <100 fs and a repetition rate of 100 MHz excites a THz emitter antenna that produce a THz radiation having a bandwidth up to 3.0 THz (> 60 dB). This THz radiation is then focused on sample and the transmitted THz radiation is further focused on a THz detector antenna which is gated by the probe laser beam (scheme 2.I.1). Both the THz antennas are gold dipoles with a dipole gap of $5\mu\text{m}$ deposited on LT (low temperature grown) GaAs substrate (mobility $\mu \sim 400$ cm/s, carrier lifetime $\tau \sim 1$ ps) (scheme 2.I.2).



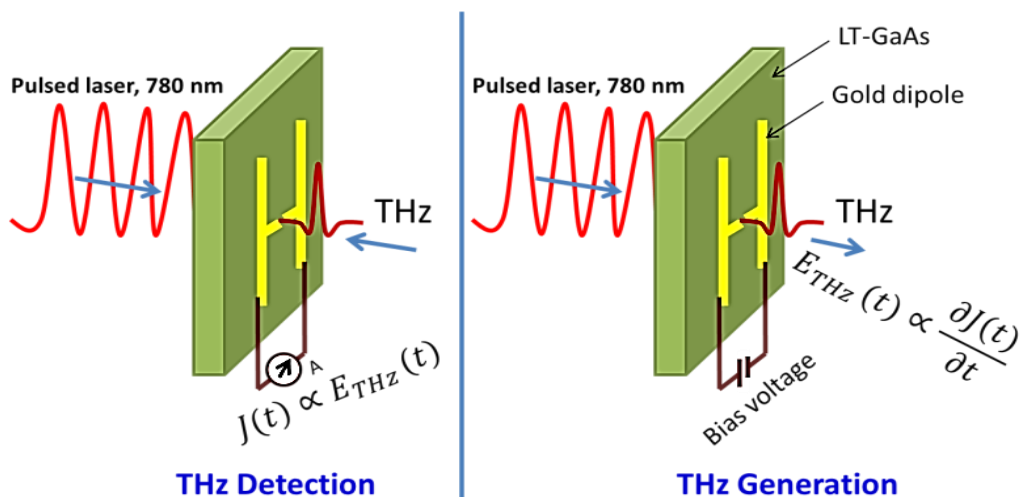
Scheme 2.I.1. Schematic diagram of Terahertz time domain spectroscopy. M, L, $\lambda/2$ and $\lambda/4$ representing mirror, TPX polymer convex lens, half wave plate and quarter wave plate respectively. Both the detector and emitter are photo conductive antennas made of gold dipole deposited on GaAs semiconductor (low temperature grown).

When laser light focuses on the gap, electron hole pairs are created. These charge carriers are accelerated by a bias voltage (~ 20 V, 10 kHz) which is attached to the detector antenna. In this case, the fs laser pulses act transient switches to open the stored electric energy and releases it in the form of the emission of a time dependent THz field $E_{THz}(t)$ which is proportional to the derivation of the current density $J(t)$.

$$E_{THz}(t) = \frac{1}{4\pi\epsilon_0} \frac{A}{zc^2} \frac{\partial J(t)}{\partial t} \quad (2.7)$$

$$J(t) = N(t)e\mu E_b \quad (2.8)$$

By varying the time delay between the pump and the probe beams the amplitude and phase of the THz electric field are measured as a function of time. Frequency dependent power and phase of the transmitted pulse are then obtained using Fourier transform of the measured electric field amplitude $E_{THz}(t)$ (figure 2.I.1).



Scheme 2.I.2. THz generation and detection by using photo conducting antenna.

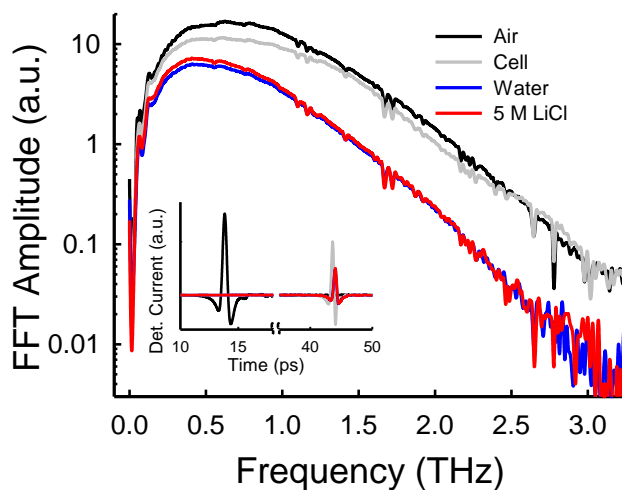


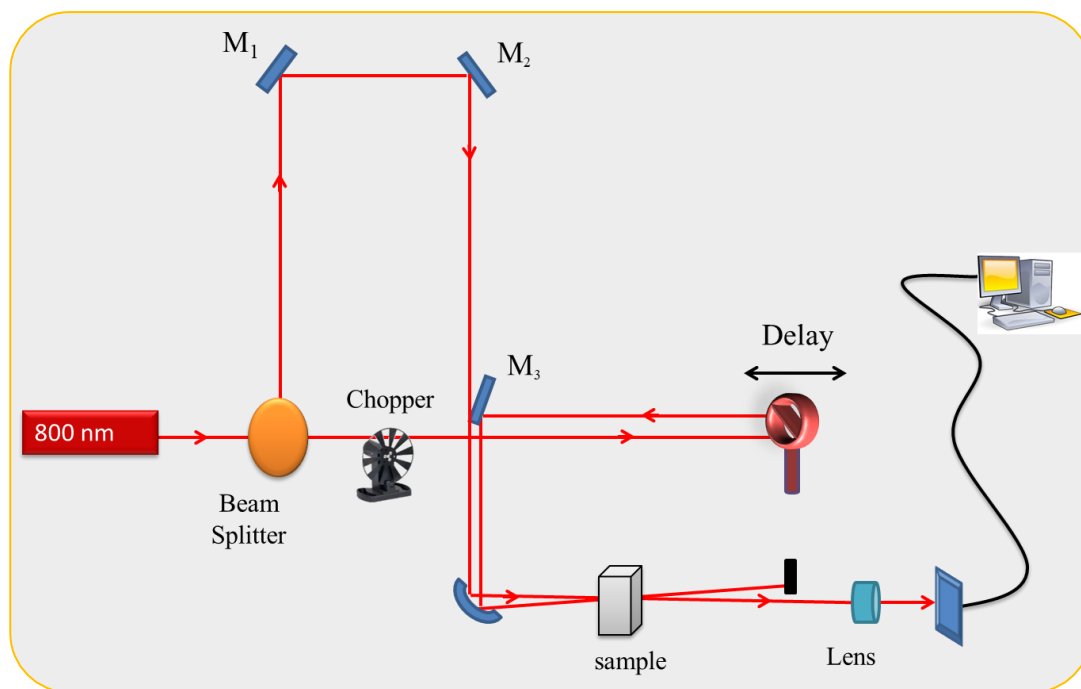
Figure 2.I.1. Fourier transformed spectra of the transmitted THz signals through air, empty cell, water and 5M LiCl aqueous solution.

2.I.9. Vector Network Analyser (GHz Frequency Region)

Dielectric relaxation (DR) in GHz frequency regime is measured with PNA-L network analyser with an open ended coaxial probe which is in direct contact with the solutions. Both the magnitude and phase of the reflected power are measured by the network analyser to acquire information of real and imaginary permittivity at each frequency sweep. DR study probes the dipolar reorientation of all polar species in a particular frequency range in terms of the complex dielectric constants given as $\tilde{\epsilon} = \epsilon'(v) - i\epsilon''(v)$. Here v is the field frequency, $\epsilon'(v)$ is the real (in-phase part) and $\epsilon''(v)$ is the imaginary (out of phase or dissipative part) part of the total complex dielectric constant. A phase stable coaxial cable is connected at the measurement port of the vector network analyser (VNA). Before each experiment it is calibrated with open air, short standards and water samples at 20⁰C.

2.I.10. Pump Probe Spectroscopy

To gain enough information about the non-equilibrium excited state dynamics, the transient measurements become popular in recent photo-physical and photochemical research. Femtosecond transient absorption technique is a sensitive and powerful technique to study the ground and excited dynamics in aqueous medium. We build the transient absorption “*optical pump optical probe*” setup in our lab. We use an excitation pulse to pump the dye molecule from equilibrium ground state to the higher electronic excited states (S_n ; $n \geq 1$). We have used a regeneratively amplified Ti:sapphire near infrared (NIR) laser system (Libra HE, Newport, USA, Inc.) with a central wavelength of 800 nm ultrashort pulses (4.2 mJ/pulse), operating at 1 kHz repetition rate with 40 fs pulse durations. The amplified laser beam has divided into two beams by using an ultrafast thin beam splitter (scheme 2.I.3). The transmitted pump beam has then guided to the sample through a retro reflector optical delay stage (Newport, Model: M-IMS600CC) with resolution of 6.67 fs to generate variable time delay between the pump and the probe beam. The probe beam is guided to the sample directly just after the pump beam. We determine the zero delay by putting a BBO (β -BaB₂O₄) type-I crystal in the focal point of the two beams. The pump and the probe beams are focused on a 1 mm thin quartz sample cell containing the dye solution by using a 10 cm focal length off-axis parabolic mirror. The intensity of the probe beam is modulated by a variable neutral density filter (NDL-25C-2, Thor Labs, USA, Inc.). We keep the pump power ~100 times higher compared to the probe power at the sample. The transmitted probe beam is detected by using a silicon photodiode (DET10A, Thor Labs, USA). The output of the photodiode is connected with a lock-in amplifier (SR-830, Stanford research system, USA). To modulate the pump pulse we use an optical chopper (MC2000, Thor Labs, USA) in the pump arm. The chopper is kept at frequency 200 Hz to chop the pump beam and was used as a reference in lock-in amplifier. The data acquisition is performed as a function of delay with a LabVIEW program. The time-resolved traces are fitted in IGOR software program. DET210A photo diode is used as the detector to detect the probe pulse amplitude (Thor Lab). The spectral response of this photo diode falls in the range of 200 nm – 1100 nm, with a peak wavelength ~780 nm.



Scheme 2.I.3. Ray diagram of the single colour pump probe setup. M represents the mirrors.

2.II. Methods and Underline Basic Theories

2.II.1. Theory of Dielectric Polarization

Dielectric relaxation measurement is a robust and versatile technique that measures the correlation among the dipoles present in the system, and can give information about the intermolecular interactions, the structure and dynamics of complex systems and the cooperative processes at the molecular level.¹⁷⁻²⁰ Here the time or frequency dependent response of the samples with the varying electric field is measured in terms of polarization that is related to the orientation of the free charges and the dipoles in the system, that finally gives rise to a dimensionless quantity, the complex dielectric constant. Basic principles and the underline theories about dielectric polarization are discussed in the following section.

Linear Dielectric Polarization in Static Electric Field

On the basis of electrical conductivity all the objects are classified into three classes: *conductors* (substances that contain infinite supply of free charge carriers), *insulators* (substances that do not contain any mobile charges), and *dielectric* (materials contain permanent or induced dipole moment). Now the question here to ask is what happens to a piece of dielectric material when it is placed in an external electric field. If the substance contains neutral atoms or nonpolar molecules there occurs a charge displacement inside dielectric materials that creates a *macroscopic dipole moment* (\vec{M}). The field will induce tiny

dipole moments pointing in the direction of the field. If the material is made up with polar molecules each permanent dipoles are forced to orient in the direction of the field. This process is known as polarization (\vec{P}). Polarization is defined as the dipole moment $\langle \vec{M} \rangle$ per unit volume of the sample.

$$\vec{P} = \frac{\langle \vec{M} \rangle}{V} \quad (2.9)$$

In presence of static electric field of strength \vec{E} the macroscopic polarization of linear uniform dielectrics are proportional to the field (provided \vec{E} is not too strong).

$$\vec{P} = \epsilon_0 \chi \vec{E} \quad (2.10)$$

where χ is the dielectric susceptibility of the isotropic and uniform dielectric material, ϵ_0 is the permittivity in free space ($8.854 \times 10^{-12} \text{ C}^2/\text{N.m}^2$). The electric displacement (electric induction) vector, \vec{D} can be written as,

$$\vec{D} = \epsilon_0 \vec{E} + \vec{P} = \epsilon_0(1 + \chi)\vec{E} = \epsilon \vec{E} \quad (2.11)$$

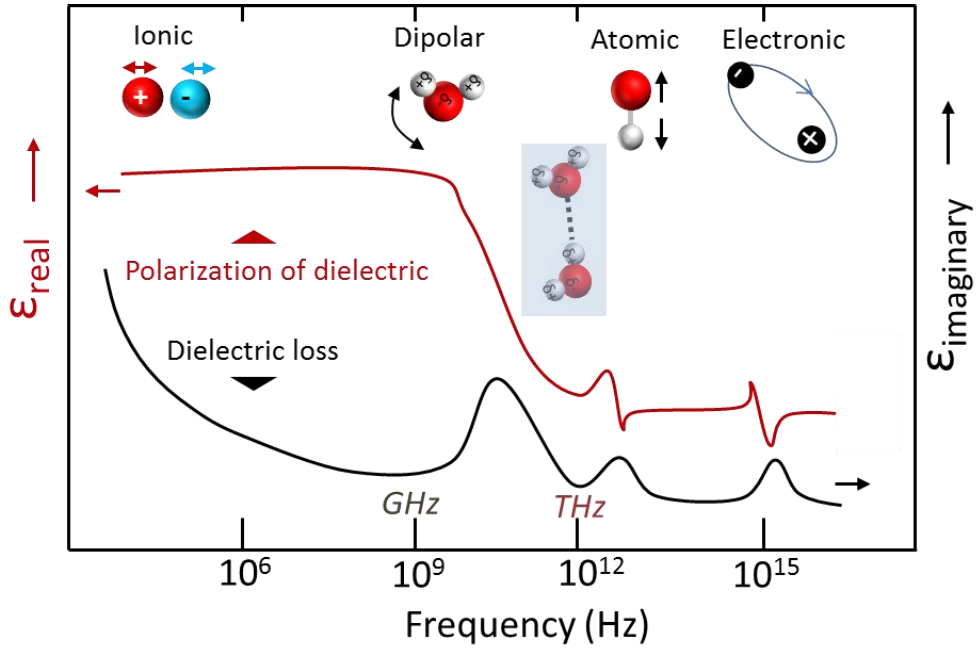
D is also proportional to \vec{E} . The new constant ϵ is the permittivity of the material. Hence the relative dielectric permittivity or *dielectric constant* (a dimensionless quantity) is given by $\epsilon_r = \frac{\epsilon}{\epsilon_0} = k = 1 + \chi$. It is also known as *static dielectric permittivity* or *low-frequency permittivity*. In other way dielectric constant may be define as the factor by which the force between two point charges decreases in the material relative to vacuum. From Columb's law, the force between two point charges in air and inside material is,

$$F_{vacuum} = \frac{1}{4\pi\epsilon_0} \frac{q_1 q_2}{r^2} \quad (2.12)$$

$$F_{material} = \frac{1}{4\pi\epsilon} \frac{q_1 q_2}{r^2} \quad (2.13)$$

$$Dielectric\ constant = k = \frac{F_{air}}{F_{material}} = \frac{\epsilon}{\epsilon_0} = \epsilon_r \quad (2.14)$$

In general it is a complex quantity. Dielectric polarization function depends on the frequency of the applied electric field. The total polarization appears due to the various polarization mechanisms in different frequency regions. They are (scheme 2.II.1): i) *Orientation or dipolar rotation polarization*, ii) *Distortion (Atomic and Electronic) polarization* and iii) *Ionic polarization*.



Scheme 2.II.1: Frequency dependent real and imaginary permittivity and corresponding processes: ionic, dipolar relaxations and atomic, electronic resonances. [Reference: Wikipedia]

Orientation Polarization (P_o): The dielectric material may contains permanent dipole moments, which is mainly due to the unbalanced sharing of the electrons by atoms of the molecule. In room temperature the dipoles are randomly oriented. So there is no net dipole moment. In presence of external applied electric field the dipoles are forced to orient along the field direction gives rise to a net dipole moment. That is known as orientational polarization. The orientation of the dipoles can follow the periodic change of \vec{E} if the frequency is lower than 10^{11} Hz. Usually any molecule takes of the order of 1 ps time to rotate within any fluid. So if the external electric fields switch over in frequency larger than 10^{11} Hz then the orientational polarization ceased to contribute. Orientation polarization is given by the volume density of the permanent dipoles $\vec{\mu}_d$. Let us consider a sphere with volume V comprised of dipoles, then the *orientation polarization* (P_o) can be written as,

$$\vec{P}_\mu = \frac{\langle \vec{M}_d \rangle}{V} = \frac{\sum_i (\vec{\mu}_d)_i}{V} \quad (2.15)$$

Distortion Polarization: The *atomic* (\vec{P}_α) and *electronic polarization* (\vec{P}_e) (*distortion polarization*) are independent of dipole orientation. Suppose a molecule contains positive and negative atoms. Due to the external field these positive and negative atoms or atom groups displaced from each other resulting a net dipole moment. This is known as *atomic polarization* (\vec{P}_α). Its frequency falls in the infrared region (10^{11} - 10^{14} Hz). When a neutral

atom is placed in an external field the centre of the negative electron cloud displaced from the positive nucleus. As a result a dipole is induced. This is known as electronic polarization. It can follow the frequency in the visible and UV region (10^{15} - 10^{17} Hz).

Ionic Polarization (\vec{P}_i): In any ionic crystal (such as NaCl) positive and negative ions are displaced in the direction and opposite to the direction of the external electric field respectively. That induces a macroscopic polarization, known as ionic polarization. *Distortion and ionic polarization* are sometimes called as *induced polarization*.

Therefore the total polarization (\vec{P}) is the sum of orientation polarization and *induced polarization*.

$$\vec{P} = \vec{P}_o + \vec{P}_\alpha + \vec{P}_e + \vec{P}_i \quad (2.16)$$

Linear Dielectric Polarization in Time Dependent Electric Field:

The electric polarization induced by a static electric field is always in equilibrium with the applied external electric field. But in dynamic case when a time dependent electric field is switched on, the molecules take some times to achieve a certain value of polarization. The time dependent displacement vector is proportional to the time dependent applied electric field is given by,

$$\vec{E}^*(t) = E_0 e^{i\omega t} \quad (2.17)$$

$$\vec{D}^*(t) = D_0 e^{i(\omega t - \delta(\omega))} \quad (2.18)$$

where $\delta(\omega)$ is the phase difference between the \vec{D} and \vec{E} field. In line with the relationship $\vec{D} = \epsilon \vec{E}$ in static case here also it can be written by introducing a complex frequency dependent dielectric permittivity

$$\epsilon^*(\omega) = \frac{D_0}{E_0} e^{-i\delta(\omega)} \quad (2.19)$$

By using Euler's relations ($\exp(i\theta) = \cos \theta + i \sin \theta$) the complex dielectric constant can be written as,

$$\epsilon^*(\omega) = \epsilon'(\omega) - i\epsilon''(\omega) \quad (2.20)$$

where $\epsilon'(\omega) = \frac{D_0(\omega)}{E_0(\omega)} \cos[\delta(\omega)]$, $\epsilon''(\omega) = \frac{D_0(\omega)}{E_0(\omega)} \sin[\delta(\omega)]$,

$D_0(\omega) = E_0(\omega) \sqrt{\epsilon'(\omega)^2 + \epsilon''(\omega)^2}$ and $\tan[\delta(\omega)] = \frac{\epsilon''(\omega)}{\epsilon'(\omega)}$.

2.II.2. Dielectric Relaxation (DR) “Debye Model”

When the field is suddenly removed the relaxation function or decay function or correlation function of the dielectric polarization is given by,

$$\phi(t) = \frac{\vec{P}(t)}{\vec{P}(0)} \quad (2.21)$$

where $\vec{P}(t)$ is the time dependent polarization decay vector. For time dependent electric field the time dependent displacement vector may be written as, $\vec{D}(t) = \epsilon_0 \vec{E}(t) + \vec{P}(t)$. Any material cannot be polarized instantaneously in response to the external electric field. It depends on the response of the material to the external field. A more general formulation of $\vec{P}(t)$ is given by,

$$\begin{aligned} \vec{P}(t) &= \epsilon_0 \int_{-\infty}^t \Phi(t') \vec{E}(t-t') dt' \\ \vec{D}(t) &= \epsilon_0 \left[\epsilon_\infty \vec{E}(t) + \int_{-\infty}^t \Phi(t') \vec{E}(t-t') dt' \right] \end{aligned} \quad (2.22)$$

where $\Phi(t)$ is the dielectric response function of the material, $\Phi(t) = (\epsilon_s - \epsilon_\infty)/[1 - \varphi(t)]$. ϵ_s and ϵ_∞ are the dielectric permittivity at very low and high frequency, respectively. The frequency dependent complex permittivity $\epsilon^*(\omega)$ is related to the time derivative of the relaxation function through Laplace transformation,²¹⁻²³

$$\frac{\epsilon^*(\omega) - \epsilon_\infty}{\epsilon_s - \epsilon_\infty} = \hat{L} \left[-\frac{d}{dt} \varphi(t) \right] \quad (2.23)$$

where \hat{L} is the well-known Laplace transformation operator is given by,

$$\hat{L}[f(t)] \equiv F(\omega) = \int_0^\infty e^{-pt} f(t) dt \quad (2.24)$$

where $f(t)$ is any arbitrary time dependent function, $p = x + i\omega$ and $x \rightarrow 0$.

Equation 2.22 gives equivalent information on dielectric relaxation properties of the sample both in frequency domain and time domain measurements. Hence experimentally one can measure the dielectric response in either time or frequency domain. For instance, neglecting inertia effects let us assume that the change of the polarization is directly proportional to its actual value (only in first order)²⁴

$$\frac{d\vec{P}(t)}{dt} = -\frac{1}{\tau_D} \vec{P}(t) \quad (2.25)$$

where τ_D is the characteristics relaxation time. Such dependency leads to exponential decay of the macroscopic relaxation function or correlation function.

$$\varphi(t) = \exp\left(-\frac{t}{\tau_D}\right) \quad (2.26)$$

Using equation 2.21 we can write the following relations,

$$\frac{\varepsilon^*(\omega) - \varepsilon_\infty}{\varepsilon_s - \varepsilon_\infty} = \frac{1}{1 + i\omega\tau_D} \quad (2.27)$$

$$\varepsilon^*(\omega) = \varepsilon_\infty + \frac{\varepsilon_s - \varepsilon_\infty}{1 + i\omega\tau_D} \quad (2.28)$$

This is known as the *Debye relaxation model* for frequency dependent dielectric permittivity. However only in rear cases such relaxation behaviour matches with experimentally measured dielectric data. The Debye conjecture is simple and elegant. Hence in many cases one has to use a superposition of multi Debye functions with different relaxation times. The dispersion (real part) and the loss factors (imaginary contribution) are

$$\varepsilon'(\omega) = \varepsilon_\infty + \frac{\varepsilon - \varepsilon_\infty}{1 + \omega^2\tau_D^2}$$

$$\varepsilon''(\omega) = \omega\tau \frac{\varepsilon - \varepsilon_\infty}{1 + \omega^2\tau_D^2}$$

The real part is a monotonically decreasing function whereas the imaginary part has a maximum at $\omega = 1/\tau_D$.

2.II.3. Generation and Detection of THz Radiation

Let's begin with the well-known Maxwell equations of electromagnetic (EM) field in free space

- 1) $\vec{\nabla} \cdot \vec{E} = \frac{\rho}{\varepsilon_0}$ Gauss's Law
- 2) $\vec{\nabla} \cdot \vec{B} = 0$ Magnetic monopole doesn't exist
- 3) $\vec{\nabla} \times \vec{E} = -\frac{\partial \vec{B}}{\partial t}$ Faraday's Law
- 4) $\vec{\nabla} \times \vec{B} = \mu_0 \vec{J} + \mu_0 \varepsilon_0 \frac{\partial \vec{E}}{\partial t}$ Ampere's Law with the Maxwell correction term

Inside matter the charge density (ρ) of the medium may be expressed as a combination of the charge density for the free electrons (ρ_f) and due to the bound polarization charges ($\rho_{bound} = -\vec{\nabla} \cdot \vec{P}$), \vec{P} is the polarization density. The total charge density can also be expressed as a combination of the conduction current density due to free electrons (\vec{J}_f), the magnetization or bound current density ($\vec{J}_{bound} = \vec{\nabla} \times \vec{M}$), and the displacement or

polarization current density ($\vec{J}_{polarization} = \frac{\partial \vec{P}}{\partial t}$). So the Maxwell's equation inside matter can be written as,

$$\begin{aligned} 1) \quad \vec{\nabla} \cdot \vec{D} &= \rho_f \\ 2) \quad \vec{\nabla} \cdot \vec{B} &= 0 \\ 3) \quad \vec{\nabla} \times \vec{E} &= -\frac{\partial \vec{B}}{\partial t} \\ 4) \quad \vec{\nabla} \times \vec{H} &= \vec{J}_f + \frac{\partial \vec{D}}{\partial t} \end{aligned}$$

where, \vec{D} is the electric displacement current ($\vec{D} = \epsilon_0 \vec{E} + \vec{P}$), and \vec{H} is the magnetic field strength ($\vec{H} = \vec{B}/\mu_0 - \vec{M}$). Taking curl of the third equation and combining the other equations into the general wave equation as given below,

$$\nabla^2 \vec{E} - \frac{1}{c^2} \frac{\partial^2 \vec{E}}{\partial t^2} = \mu \left(\frac{\partial \vec{J}}{\partial t} + \frac{\partial^2 \vec{P}}{\partial t^2} \right) \quad (2.29)$$

where, $c = \frac{1}{\sqrt{\mu_0 \epsilon_0}}$. The wave equation indicates that there are two time varying source term for any electric field. One can change the current density or the polarization with time to generate any field. There are various techniques available for generation and detection of pulsed as well as continuous wave (CW) THz radiation based on photoconductive antenna switch, nonlinear crystal, and air plasma. This thesis is only concerned about the generation and detection of pulsed THz with photoconductive antenna switch where time dependent current density is the source of THz radiation and with non-linear crystal by electro-optic effect where a time dependent change of polarization is used as the source of THz pulse.

2.II.4. THz Measurement

THz (1 THz = 10^{12} Hz = 1 ps^{-1}) spectroscopy has recently been evolved as a potential and sensitive tool to label free probe the sub-ps intermolecular collective dynamics of water network which is otherwise wiped off in conventional spectroscopic techniques.^{16,25,26} The GHz as well as MIR frequency range are limited to the intra-molecular stretching band of various molecules and does not protrude into the global collective motion. It also can give information about the hydrated water that extends to more than one or two hydration layer around molecules.²⁵ Such global collective information can only be realized by this THz spectrometer that works in the THz frequency domain.²⁷

Data analysis: By varying the time delay between the probe and the pump beam (*section 2.I.8*) the amplitude and phase of the THz electric field are measured as a function of time. Frequency dependent power and phase of the transmitted pulse are obtained using Fourier analysis of the measured electric field amplitude $E_{THz}(t)$. This thesis used ‘Tera K8, Menlo Systems’ THz TDS where the extracted frequency domain THz spectra in air is fairly smooth with a high signal to noise ratio and minimal water absorption lines up to ~2.5 THz which enables us to extract the optical parameters with high precision up to ~2 THz (Figure 2.I.1). Different optical parameters are extracted from this frequency domain data such as absorption coefficient is given by,

$$\alpha(\nu) = \frac{\ln I_0(\nu) - \ln I_s(\nu)}{d} \quad (2.30)$$

where $I_0(\nu)$ and $I_s(\nu)$ represent the intensities in air (reference) and in presence of sample, d indicates the sample thickness. This α_{THz} is a direct manifestation of the cooperative dynamics of water.^{4, 20, 55-56} The refractive index can be calculated by measuring the phase in air and in sample,

$$n(\nu) = \frac{\phi_s(\nu) - \phi_0(\nu)}{2\pi\nu d} \quad (2.31)$$

The imaginary refractive index,

$$k(\nu) = \frac{c\alpha(\nu)}{4\pi\nu} \quad (2.32)$$

The frequency dependent real (ϵ') and imaginary (ϵ'') dielectric constants of the samples are extracted as, $\epsilon'(\nu) = n^2(\nu) - k^2(\nu)$ and $\epsilon''(\nu) = 2n(\nu)k(\nu)$, where the complex refractive index is given as, $\tilde{n}(\nu) = n(\nu) - ik(\nu)$. We have extracted all the parameters by commercially available TeraLyzer software

(<http://www.menlosystems.com/products/thz-time-domain-solutions/teralyzer-single/>).

2.II.5. Dielectric Relaxation Fitting (GHz-THz Regime)

In *section 2.II.2*, this thesis already described about one of the dielectric relaxation models, “*Debye Model*”. To analyse multi component complex dipolar liquids one has to include several dispersion steps related to different relaxation processes. This thesis mainly employed a multiple mode *Debye model*^{16,28,29} to describe the frequency dependent relaxation dynamics of the dipoles present in the systems. According to the Debye model, the complex frequency dependent dielectric response [$\tilde{\epsilon}(\nu) = \epsilon_{real}(\nu) - i\epsilon_{imaginary}(\nu)$] can be described as:

$$\tilde{\epsilon}(\nu) = \epsilon_{\infty} + \sum_{j=1}^m \frac{\epsilon_j - \epsilon_{j+1}}{1 + i2\pi\nu\tau_j} + \frac{\sigma}{i2\pi\nu\epsilon_0} \quad (2.33)$$

where, ϵ_0 is the permittivity in free space ($=8.854 \times 10^{-12}$ F/m), $\omega = 2\pi\nu$ is the angular frequency, τ_j is the relaxation time for the j -th relaxation mode, ϵ_1 is the static dielectric constant, ϵ_j are the dielectric constants for different relaxation processes, ϵ_∞ is the extrapolated dielectric constant at a very high frequency and m describes the number of relaxation modes. For charged species the d.c. conductivity σ creates an additional Ohmic loss to the total polarization.³⁰ The magnitude of induced polarization of each type of dipoles is given by the dispersion amplitude, $S_j = \epsilon_j - \epsilon_{j+1}$. The *Debye model* with $m=1$ is the simplest case associated with a single relaxation mode that describes the total motion. We fit the relaxation data of water and other aqueous solutions in the THz frequency range with triple *Debye relaxation model* is given by,

$$\tilde{\epsilon}(\omega) = \epsilon_\infty + \sum_{j=1}^3 \frac{S_j}{1+i\omega\tau_j} + \frac{\sigma}{i\omega\epsilon_0} \quad (2.34)$$

The first mode describes the co-operative rearrangement of the bulk-like water with strength $S_1 = S_{\text{bulk}}$, and $\tau_1 = \tau_{\text{bulk}}$ (~ 9 ps).^{14,31-34} The second and the third terms correlate the large angular rotations of water molecules (~ 200 fs) and the H-bond bending mode (~ 80 fs).^{14, 55}

In the GHz frequency region (0.2 – 50 GHz) we employ double *Debye relaxation model*. One (~ 8 ps) mode corresponds to the cooperative relaxation of water whereas the other relaxation mode is for the solute rotational mode.

$$\tilde{\epsilon}(\omega) = \epsilon_\infty + \frac{S_{\text{water}}}{1+i\omega\tau_{\text{water}}} + \frac{S_{\text{solute}}}{1+i\omega\tau_{\text{solute}}} \quad (2.35)$$

However, the most of the experimental data are better describe by non-exponential relaxation laws (non-Debye behaviour). Besides *Debye model*, there are some other model exist in the literature that also can describe the frequency dependent relaxation pattern of the complex dielectric function of liquids. Some of them are, *Cole-Cole model*,^{35,36}

$$\tilde{\epsilon}(\nu) = \epsilon_\infty + \sum_{j=1}^m \frac{\epsilon_j - \epsilon_{j+1}}{1+(i\omega\tau_j)^{(1-\alpha)}} \quad (2.36)$$

Cole-Davidson model,³⁷

$$\tilde{\epsilon}(\nu) = \epsilon_\infty + \frac{\epsilon_S - \epsilon_\infty}{(1+i\omega\tau_j)^\beta} \quad (2.37)$$

Havriliak-Negami (NH) model,³⁸

$$\tilde{\epsilon}(\nu) = \epsilon_\infty + \frac{\epsilon - \epsilon_\infty}{[1+(i\omega\tau_j)^\alpha]^\beta} \quad \alpha \geq 0, \beta \leq 1 \quad (2.38)$$

and the *Damped Harmonic Oscillator model*,

$$\tilde{\epsilon}(\nu) = \epsilon_\infty + \frac{(\epsilon - \epsilon_\infty)\omega_0^2}{(\omega_0^2 - \omega^2) + i(\omega/\tau_D)} \quad (2.39)$$

The symbols have their usual meanings.

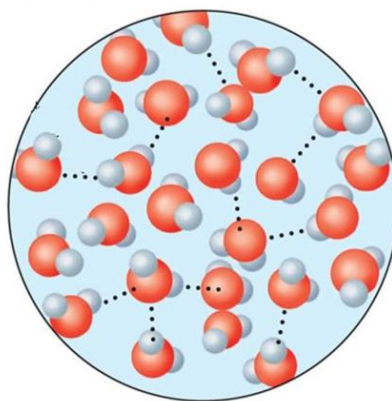
2.II.6. Tetrahedral Hydrogen Bond Networks

H-bond is a weak electrostatic attraction of the hydrogen atom towards the oxygen atom of a neighbouring water molecule. These are stronger than van der Waals or dipole-dipole interaction and weaker than covalent or ionic bonds. It is generally a proton shared by two lone electron pairs. H-bond may be defined in many different ways depending on their geometrical criteria, energy consideration and also with orbital occupancy criteria.^{39,40} According to the geometrical criteria based on the distance and angle is, “a H-bond donor (D) and an acceptor (A) are considered to be H-bonded if and only if (i) the distance between them (R_{DA}) is less than a cut off (R_{cut}) and (ii) the angle (for water-water H-bond) between the OH vector of water and the vector joining the two oxygen atom (θ_{OOH}) is less than a cut-off (θ_{cut})”. These cut off distances are evaluated from the radial distribution functions of the D and A atoms. In energetic definition that used the same distance condition but instead of angle criteria there is an energy criterion that their interaction energy must be less than threshold energy (E_{th}). One water molecule can produce two H-bonds through their H-atoms (H-bond donor) plus two further H-bonds through their oxygen atom utilizing the H-atoms of their neighbouring water molecules. That creates the average structure of water network (mesh) similar to a tetrahedral arrangement.^{41,42} Such local structuring of liquid water can be defined in terms of “*tetrahedral order parameter*” (see section 3.II.3 for further details).

2.II.7. Cooperative Hydrogen Bond Network

The non-additive nature of H-bonds is often termed as cooperativity. Two hydrogen bonds may strengthen (cooperative) or weaken (non-cooperative) each other depending on their orientation structures. Each H-bond can assist its neighbouring H-bond to get stronger.⁴³ Each H-bond is affected due to the presence of other: if one is removed the entire network could get weaker; add one and the whole system could get stronger. Cooperativity in any interaction means the interaction (such as binding) with one site on a macromolecule, influence the interaction on another site of the same macromolecule. The H-bond in water is cooperative in nature where formation of one bond can assist the formation of several other bonds and when one bond breaks typically the whole clusters dissolved.⁴⁴ A long time back Frank and Wen,⁴⁵ confirm that H-bonding in any particular site of a molecule or ion fade the strength of the neighbouring site of the same nature. There are various types of contributions to this cooperative force. One of them is the long range electrostatic attraction or repulsion between like and unlike charge distributions. The intermolecular forces between a pair of

charges or dipoles may modify due to presence of other species into the system. The complexity arises due to the secondary interactions when H-bond donors with positive charge clouds and acceptor present in the same molecule. Repulsion between the donors/acceptors can destabilize the H-bond strength between donor-acceptor, which also depends on the specific position and orientation of the donor/acceptor. The cooperativity of H-bonding also induces by the binding in the active site and the conformational change of biological samples.



Scheme 2.II.2. Hydrogen bonding in water

2.II.8. Depolarization

Depolarization as measured by the change in the dielectric relaxation strength (ΔS) signifies the alteration in the cooperative H-bond structure of polar solvents. Typically dielectric response strength ($S = \epsilon_s - \epsilon_\infty$) decreases as compare to the bulk strength when one increase the concentration of the solute particles in the aqueous solution. The failure of the water dipoles to follow and reorient themselves with an applied oscillating electric field generates depolarization. It has grossly been believed that there exist three reasons behind such depolarization.⁴⁶ (a) *Dilution effect*: as one dissolve solute molecules in the solution the effective concentration of water decreases than bulk water, (b) *Kinetic depolarization*: if the solute particles contain charge, they move towards the external electric field and hence the water molecules are forced to reorient via another local electric field in the opposite direction to the external field, and (c) *Static depolarization*: if the water dipoles are H-bonded to the solute particles, they are forced to orient and/or attached to the solute molecules. Such frozen water molecules fail to follow the external field and cannot participate in the DR processes. This thesis tries to describe another possibility of depolarization in *chapter 7* with specific explanations.

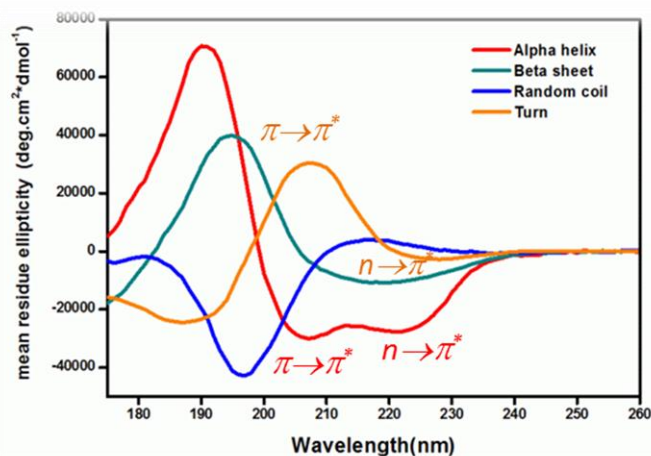
2.II.9. Investigation of the Secondary and Tertiary Structure of Protein by CD Spectroscopy

CD spectroscopy is a useful and reliable tool to probe secondary and tertiary structures of proteins. It can provide information about the possible conformational changes in protein molecules due to the presence of macromolecular crowding or cosolvents. ‘Dichroism’ is used to denote directional dependent light absorption. For linearly or plane polarized light, the electric field of the photons oscillate in a plane, whereas for circularly polarized light the electric field vector traces out a helix about the propagation direction with constant magnitude in time. The combination of two circular polarised lights of equal magnitude with 90° phase difference (one that rotates in counter clockwise direction; the left handed polarized and the other rotating in clockwise direction; the right handed polarised light) can produces a plane polarised light. The interaction between a chiral molecule and left and right handed polarised waves are different. CD refers to the absorption difference of these two components.

$$CD = \Delta A = A_L - A_R = \Delta \epsilon cl \quad (2.40)$$

where $\Delta \epsilon = \epsilon_{lcp} - \epsilon_{rcp}$, from the Beer-Lambert law absorption (see equation 2.1). That will happen only for chiral (optically active) chromophores. Chirality means the molecule that cannot be superimposed on its mirror image. It appears due to its intrinsic structure, for example a carbon atom with four different substitutes, or may be the dihedral bonds are chiral due to the dihedral angles of the (C-S-S-C) chain. It may be covalently linked to any chiral centre in the molecule, or it is placed in an asymmetric environment. Far-UV region (190-260 nm) and near-UV region (250-310 nm) are sensitive to the secondary and tertiary structures, respectively. α -helix, β -sheet, and a random coil have amide bonds in different orientations at different distances and thus give CD signals with different amplitudes of different signs as a function of wavelength. For each pure secondary conformation the distinctive CD spectrums are shown in scheme 2.II.3. The CD spectra of α -helices contain a negative peak with two separate maxima at 208 nm and 222 nm with comparable magnitude. The negative 222 nm band arises due to the peptide $n \rightarrow \pi^*$ transition, while the 208 nm band results from the exciton splitting of the lowest peptide $\pi \rightarrow \pi^*$ transition.^{47,48} The far-UV spectrum of protein molecules is sensitive to their secondary structure that contains various pattern such as α -helix, β -sheet, random coil etc. The secondary structural analysis is done by deconvoluting the CD spectra using CDNN software (<http://bioinformatik.biochemtech.uni-halle.de/cdnn>).

The near UV spectrum is due to the absorption of the aromatic residues (phenylalanine, tyrosine, and tryptophan) and di sulphide bonds.



Scheme 2.II.3. Typical CD spectra for each secondary structure content.⁴⁹

2.II.10. Thermal Stability of Protein

With the CD spectroscopy, one can also investigate the temperature induce changes in the folding and unfolding populations of a protein molecule. According to two-state model of thermal denaturation process ($N(\text{native}) \rightleftharpoons D(\text{denatured})$) of a protein folded native form of protein is directly converted into denatured or unfolded states,^{50,51} The corresponding equilibrium constant for the unfolding process (K_u) can analytically be expressed as,

$$K_u = \frac{\text{Fraction of the denatured protein } (f_D)}{\text{Fraction of the native protein } (f_N)} \quad (2.41)$$

The native fraction (f_N) of any protein can be calculated by the temperature dependent spectroscopic study e.g., CD, fluorescence or UV. The native fraction is defined as,

$$f_N = \frac{\theta_T - \theta_D}{\theta_N - \theta_D} \quad (2.42)$$

where θ_T , θ_N and θ_D represent the optical property at a particular wavelength at any temperature T, completely in its native state (N) and in the complete denatured state (D), respectively. The change in Gibbs free energy in this unfolding process is given by,

$$\Delta G_u = -RT \ln K_u = -RT \ln \left(\frac{1-f_N}{f_N} \right) \quad (2.43)$$

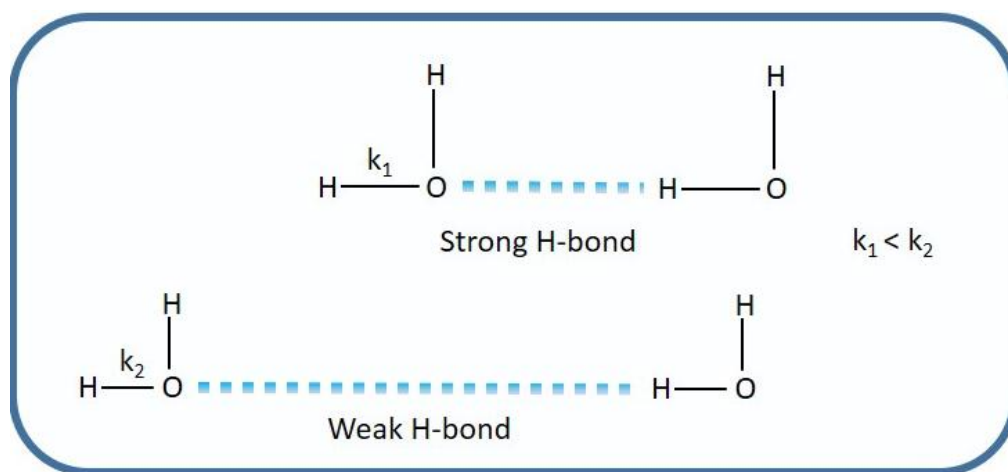
where R is the gas constant.

2.II.11. OD Stretching mode

The hydroxyl OD stretch is extremely sensitive to local H-bond environments. This OD stretching band is wide ($\sim 170 \text{ cm}^{-1}$ full width at half maxima, FWHM) centred at $\sim 2505 \text{ cm}^{-1}$. The reason behind this is, there exists a large distribution in the lengths and the strength of the H-bonds in aqueous solution. The OD covalent bond can be thought of as a linear harmonic oscillator, and the spring constant (k) is given by

$$\nu = \frac{1}{2\pi} \sqrt{\frac{k}{\mu}} \quad (2.44)$$

where μ is the effective mass of oxygen (O) and deuterium (D) atoms, and ν is the stretching frequency of the OD oscillator.



Scheme 2.II.4. Representation of the OD covalent bonds with the H-bonds.

In presence of any solute molecules, if the H-bonds of any water or solute molecules with the HOD molecule become stronger then the OD covalent bonds become weaker (scheme 2.II.4). Hence ν_{max} shifted to lower frequency region (red side). Whereas if the H-bond becomes weaker, OD covalent bond becomes stronger, ν_{max} goes to some higher value (blue shift). Now if the peak frequency (ν_{max}) remains same but the width of the distribution (FWHM) decreases, it indicates that the hydrogen bonding status become more homogenous.

2.III. References

- (1) Lakowicz, J. R. *Principles of fluorescence spectroscopy*; Springer Science & Business Media, 2013.

- (2) O'Conner, D. V.; Philips, D. *Time correlated single photon counting*; Academic Press: London, **1984**.
- (3) Periasamy, N.; Koti, A. S. R. *Proc. Indian Natn. Sci. Acad.* **2003**, 69A, 41-48.
- (4) Maroncelli, M.; Fleming, G. R. *J. Chem. Phys.* **1987**, 86, 6221-6238.
- (5) Horng, M. L.; Gardecki, J. A.; Papazyan, A.; Maroncelli, M. *J. Phys. Chem.* **1995**, 99, 17311-17337.
- (6) Lakowicz, J. R. *Principles of fluorescence spectroscopy*; Kluwer Academic/Plenum: New York, **1999**.
- (7) Mitra, R. K.; Sinha, S. S.; Pal, S. K. *Langmuir* **2007**, 23, 10224-10229.
- (8) Samanta, N.; Mahanta, D. D.; Hazra, S.; Kumar, G. S.; Mitra, R. K. *Biochimie* **2014**, 104, 81-89.
- (9) Mitra, R. K.; Sinha, S. S.; Pal, S. K. *Langmuir* **2007**, 23, 10224-10229.
- (10) Buchner, R.; Holzl, C.; Stauber, J.; Barthel, J. *Physical Chemistry Chemical Physics* **2002**, 4, 2169-2179.
- (11) Saptari, V. *Fourier transform spectroscopy instrumentation engineering*; SPIE Optical Engineering Press, **2004**.
- (12) Lee, Y. S. *Principles of Terahertz Science and Technology*; Springer US, **2009**.
- (13) Dexheimer, S. L. *Terahertz Spectroscopy: Principles and Applications*; CRC Press, **2007**.
- (14) Baxter, J. B.; Guglietta, G. W. *Anal. Chem.* **2011**, 83, 4342-4368.
- (15) Polley, D.; Ganguly, A.; Barman, A.; Mitra, R. K. *Opt. Lett.* **2013**, 38, 2754-2756.
- (16) Polley, D.; Patra, A.; Mitra, R. K. *Chem. Phys. Lett.* **2013** 586, 143-147.
- (17) Nee, T. W.; Zwanzig, R. *The Journal of Chemical Physics* **1970**, 52, 6353-6363.
- (18) Nandi, N.; Bhattacharyya, K.; Bagchi, B. *Chemical Reviews* **2000**, 100, 2013-2046.
- (19) Agieienko, V.; Horinek, D.; Buchner, R. *Physical Chemistry Chemical Physics* **2017**, 19, 219-230.
- (20) Yuri Feldman, P. B. I., Alexander Puzenko, Valerică Raicu; Oxford University Press: Oxford, **2015**.
- (21) Fröhlich, H. *Theory of dielectrics: dielectric constant and dielectric loss*; Clarendon Press, **1958**.
- (22) Bötcher, C.; Bordewijk, P.; Elsevier Science: **1978**.
- (23) Feldman, Y.; Puzenko, A.; Ryabov, Y. *Adv. Chem. Phys.* **2006**, 133, 1.
- (24) Debye, P. J. W. *Polar molecules*; Chemical Catalog Company, Incorporated, **1929**.
- (25) Heyden, M.; Sun, J.; Funkner, S.; Mathias, G.; Forbert, H.; Havenith, M.; Marx, D. *Proc. Natl. Acad. Sci. USA* **2010**, 107, 12068-12073.
- (26) Heugen, U.; Schwaab, G.; Bründermann, E.; Heyden, M.; Yu, X.; Leitner, D. M.; Havenith, M. *Proc. Natl. Acad. Sci. USA* **2006**, 103, 12301-12306.
- (27) Ebbinghaus, S.; Kim, S. J.; Heyden, M.; Yu, X.; Heugen, U.; Gruebele, M.; Leitner, D. M.; Havenith, M. *Proc. Natl. Acad. Sci. USA* **2007**, 104, 20749-20752.
- (28) Kindt, J. T.; Schmuttenmaer, C. A. *J. Phys. Chem.* **1996**, 100, 10373-10379.
- (29) Rønne, C.; Åstrand, P. O.; Keiding, S. R. *Phys. Rev. Lett.* **1999**, 82, 2888-2891
- (30) van der Post, S. T.; Tielrooij, K.-J.; Hunger, J.; Backus, E. H. G.; Bakker, H. J. *Faraday Discuss.* **2013**, 160, 171-189.
- (31) Samanta, N.; Das Mahanta, D.; Mitra, R. K. *Chem. Asian J.* **2014**, 9, 3457-3463.

- (32) Samanta, N.; Das Mahanta, D.; Mitra, R. K. *Physical Chemistry Chemical Physics* **2014**, *16*, 23308-23315.
- (33) Das Mahanta, D.; Patra, A.; Samanta, N.; Luong, T. Q.; Mukherjee, B.; Mitra, R. K. *The Journal of Chemical Physics* **2016**, *145*, 164501.
- (34) Das Mahanta, D.; Samanta, N.; Mitra, R. K. *Journal of Molecular Liquids* **2016**, *215*, 197-203.
- (35) Cole, K. S.; Cole, R. H. *The Journal of Chemical Physics* **1941**, *9*, 341-351.
- (36) Cole, K. S.; Cole, R. H. *The Journal of Chemical Physics* **1942**, *10*, 98-105.
- (37) Davidson, D. W.; Cole, R. H. *The Journal of Chemical Physics* **1951**, *19*, 1484-1490.
- (38) S. Havriliak, S. N. *Journal of Polymer Science Part C: Polymer Symposia* **1966**, *14*, 99-117.
- (39) Starr, F. W.; Nielsen, J. K.; Stanley, H. E. *Physical Review Letters* **1999**, *82*, 2294-2297.
- (40) Luzar, A.; Chandler, D. *Physical Review Letters* **1996**, *76*, 928-931.
- (41) Head-Gordon, T.; Johnson, M. E. *Proceedings of the National Academy of Sciences* **2006**, *103*, 7973-7977.
- (42) Chaplin, M. [Internet URL] <http://www1.lsbu.ac.uk/water/anmlies.html>.
April, 2010.
- (43) Williamson, M. *How Proteins Work*; Garland Science, Taylor & Francis Group, LLC: USA, **2012**.
- (44) Ohno, K.; Okimura, M.; Akai, N.; Katsumoto, Y. *Physical Chemistry Chemical Physics* **2005**, *7*, 3005-3014.
- (45) Frank, H. S.; Wen, W.-Y. *Discuss. Faraday Soc.* **1957**, *24*, 133-140.
- (46) Tielrooij, K. J.; van der Post, S. T.; Hunger, J.; Bonn, M.; Bakker, H. J. *The Journal of Physical Chemistry B* **2011**, *115*, 12638-12647.
- (47) Woody, R. W.; Tinoco Jr., I. *J. Chem. Phys.* **1967**, *46*, 4927-4945.
- (48) Nordén, B. *Circular dichroism and linear dichroism*; Oxford University Press, **1997**; Vol. 1.
- (49) Rodger, A.; Ismail, M. A. In *Spectrophotometry and Spectrofluorimetry A Practical Approach*; Gore, M. G., Ed.; Oxford University Press: Oxford, New York, **2000**, p 99-139.
- (50) A A Saboury, A. A. M.-M. *BIOCHEMICAL EDUCATION* **1994**, *22*, 210-211.
- (51) Tamura, Y.; Gekko, K. *Biochemistry* **1995** *34*, 1878-1884.

3. Molecular Dynamics Simulation Analysis Protocol

This chapter describes about the molecular dynamics simulation techniques & methods that are applied for the chapters 5 and 9. It will briefly describe basic principles and the analysis protocols.

3.I. Simulation Details

All atom classical molecular dynamics (MD) simulations of DME and SPC/E water^{1,2} binary mixtures was performed in canonical ensemble (constant N, V, T).³ A detailed description of the force field parameters can be found in these references.³⁻⁶ The initial configurations were built using Packmol³ and equilibrated in the NPT ensemble at 1 atm pressure for 500 ps. Nose-Hoover thermostat⁴ and barostat⁷ were used to control the temperature and pressure with time constants of 0.5 and 1.0 ps, respectively. Subsequently, further equilibration of 1 ns followed by a production run of 5 ns was carried out in NVT ensemble. MD simulations were performed using GROMACS (version 4.6.5) software package⁵ using the constant temperature and pressure methods. All bonds were constrained using the LINCS algorithm.⁸ Periodic boundary conditions were employed in all three directions and the equations of motions were integrated using a time step of 1 fs employing the velocity Verlet algorithm.⁹ The long ranged electrostatic interactions were calculated using the particle-mesh Ewald method with a real space cut-off of 0.9 nm, a Fourier mesh spacing of 0.12 nm, and a fourth-order interpolation. Here the unified atom models for DME molecules were used. The DME and water molecules interacted via a potential function that consists of two types of interactions, bonded and non-bonded interactions.

$$\begin{aligned}
 V(r_1, r_2, r_3, \dots, r_n) = & \\
 & \sum_{bond} \frac{1}{2} K_r (r - r_{eq})^2 + \sum_{angles} \frac{1}{2} K_\theta (\theta - \theta_0)^2 + \sum_{proper\ dihedral} \sum_{i=0}^4 C_i [\cos(\theta)]^i + \\
 & \sum_{improper\ dihedral} \frac{1}{2} K_\xi (\xi - \xi_0)^2 + \sum_i \sum_{j>i} \left(\frac{C_{ij}^{12}}{r_{ij}^{12}} - \frac{C_{ij}^6}{r_{ij}^6} \right) + \sum_i \sum_{j>i} \left(\frac{q_i q_j}{4\pi\epsilon_0 r_{ij}} \right)
 \end{aligned} \tag{3.1}$$

where, K_r is the bond constant with r_{eq} is the equilibrium bond distance, K_θ is the angle constant with the equilibrium angle θ_{eq} , C_i is the dihedral constant r_{ij} is distance between i-th and j-th atoms with partial charges q_i and q_j , respectively. The first four term of equation 3.1 represents the bonded interactions and the last two terms represents the non-bonded interactions. The short range van der Waals interactions are represented by the Lennard-Jones (LJ) potential. The details of the force parameterization are given in the table 3.I.1. Every simulated system consists of approximately 1000 molecules with different ratios of water and DME molecule in a 4 nm cubical box. The Lennard-Jones (LJ) interactions were computed using a cut-off of 1.4 nm. Snapshots were saved in every 5 fs for further data analyses. It is to note that the simulations were carried out at a fixed temperature 293 K in order to avoid complexity which may arises due to temperature change. We have computed six different water/DME binary mixture systems at various water mole fractions (X_w) correspondingly ($X_w \sim 0.06, 0.25, 0.45, 0.70, 0.85$ and 0.90).

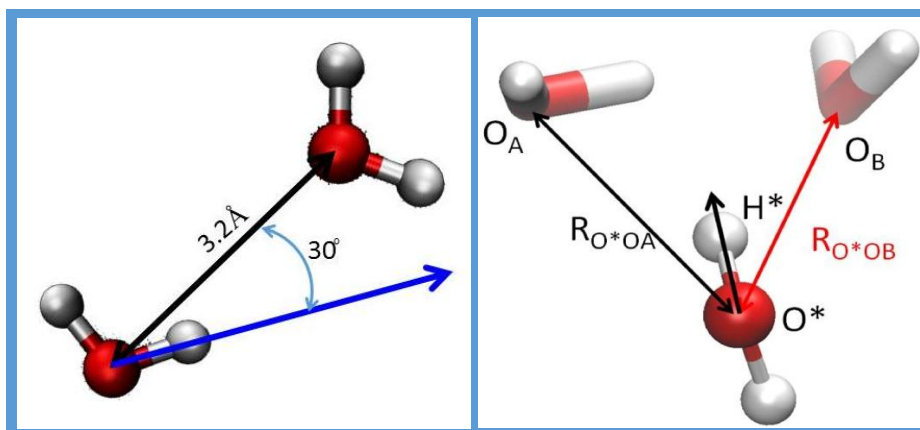
3.II. Analysis Protocol

3.II.1. Hydrogen Bonding

H-bonds can be defined in a number of ways based on geometric criteria, energy consideration as well as orbital occupancy.¹⁰ In order to identify the hydrogen bonded clusters one first needs to decide a suitable criteria whether a given pair of water molecules are hydrogen bonded or not. Here we have chosen the widely accepted geometric definition (see scheme 3.II.1 for details) based on a distance (R) and an angle (θ) criteria. According to this definition, a H-bond donor (D) and an acceptor (A) molecules are considered to be H-bonded iff (i) the distance between D and A atoms (R_{DA}), is less than a cut off distance, R_{cutoff} ($\sim 3.2 \text{ \AA}$ for water-water H-bond) at that certain time and (ii) the angle between the OH vector of water and the vector joining the two oxygen atoms of water-water or water-DME molecules (θ_{O-O-H}) is less than θ_{cutoff} ($\approx 30^\circ$). We have taken care of all the possible H-bonds (water-water and also water DME). The cut off distances were fixed from the radial distribution functions (RDF). From the first minima of the radial distribution function of donor and acceptor atom one can fix the R_{cutoff} . To compute the spatial distribution of the atoms of the molecules in all those binary mixtures we compute the radial distribution functions (RDF) of various possible pairs of oxygen following the equation as given below,

$$RDF_{ij}(r) = \langle \sum_{ij} \delta(r - r_{ij}) \rangle \quad (3.2)$$

where r_{ij} is the distance between any i-th and j-th oxygen atoms.



Scheme 3.II.1. Geometric criteria (both the distance and the angle criteria) of the definition of H-bond between two neighbouring water molecules (left panel). The distances between the oxygen atom O^* of the rotating water molecule and the oxygen atom of initial O_A ($R_{O^*O_A}$) and final O_B ($R_{O^*O_B}$) H-bond partners. The transition angle is define as the angle between the projection of the O^*H^* vector on the $O_AO^*O_B$ plane and the angle bisector of plane $O_AO^*O_B$ (right panel).

We compute water-water, water-DME and DME-DME RDFs from the MD trajectories of all the atoms of all the mixtures. Conventionally R_{cutoff} has been considered as the distance at which the first minimum of the simulated radial distribution function ($g(r)$) (see figure 3.II.1) for each DME-water mixture system appears. We have taken the value of $R_{\text{cutoff}} \sim 3.2 \text{ \AA}$ that certainly covers the first hydration shell of DME for the whole concentration range. An oxygen atom could belong either to a DME or to a water molecule. The first peaks for the water-water and water-DME RDF's arise at distances of 2.78 \AA and 3.12 \AA respectively. In the mixture the position of the water-DME peak remains almost unaltered indicating that hydration of DME molecules could be achieved without significant perturbation of H-bond network of water molecules. The first peak of DME-DME RDF occurs at 2.9 \AA (figure 3.II.1), which is higher than that in water-water but smaller than that in water-DME signifying hydrophobically induced aggregation of DME molecules.

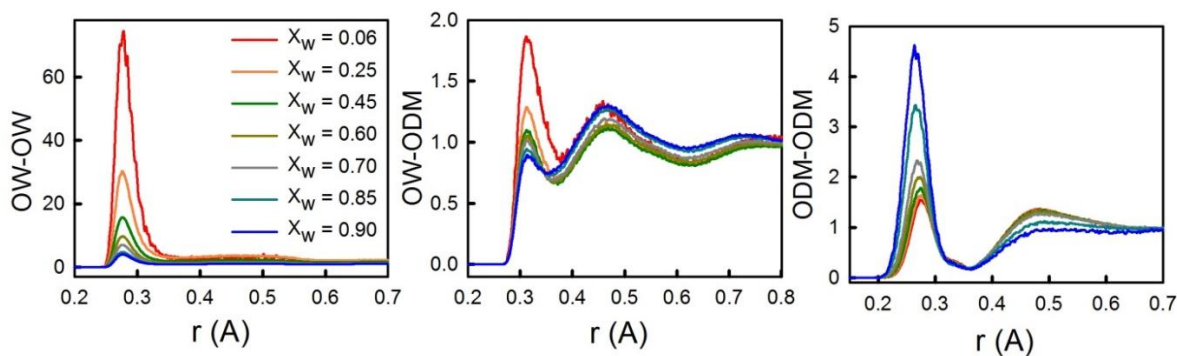


Figure 3.II.1. Radial distribution functions of (a) water oxygen-oxygen, (b) water oxygen-DME oxygen, (c) DME oxygen-oxygen.

3.II.2. Reorientation of water via Jump Mechanism

We compute the time evolution of the cosine of the angle made by of the backbone of any one of the OH vector of water molecules with the z-axis of the simulation box (figure 3.II.2). Figure 3.II.2 clearly indicates that the water molecules executes diffusive reorientation along with large amplitude angular jumps; sometimes as large as 90° . Such combine features of large amplitude angular jumps sandwich with diffusive reorientations are quite different from the traditional *Debye* picture of orientation in liquid water that led to the reinterpretation of several previous findings (both experiment and simulation results).

The angular feature is a direct and clear proof of the large angular jump motions of water orientation. However we made an elaborate attempt to have microscopic picture of the jump orientations of water. It has been recently shown that both aqueous¹¹ and non-aqueous¹² H-bonded fluids exhibit orientational jump reorientations. During these jumps the translational degrees of freedom of the rotating molecule and its initial and final H-bond partners are strongly coupled to their rotational degrees of freedom. During the orientational jump the initial H-bond acceptor recedes from the first hydration shell of the rotating molecule to the second shell and the final H-bond acceptor moves towards the first shell in from the second shell.

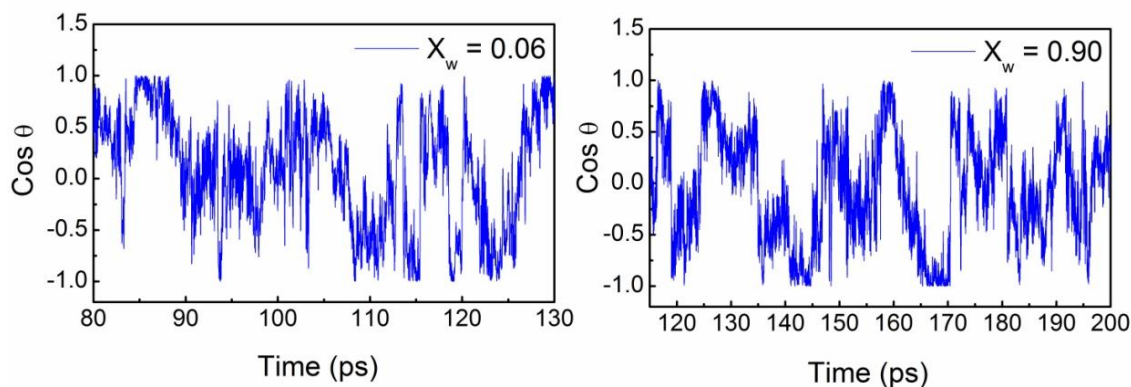
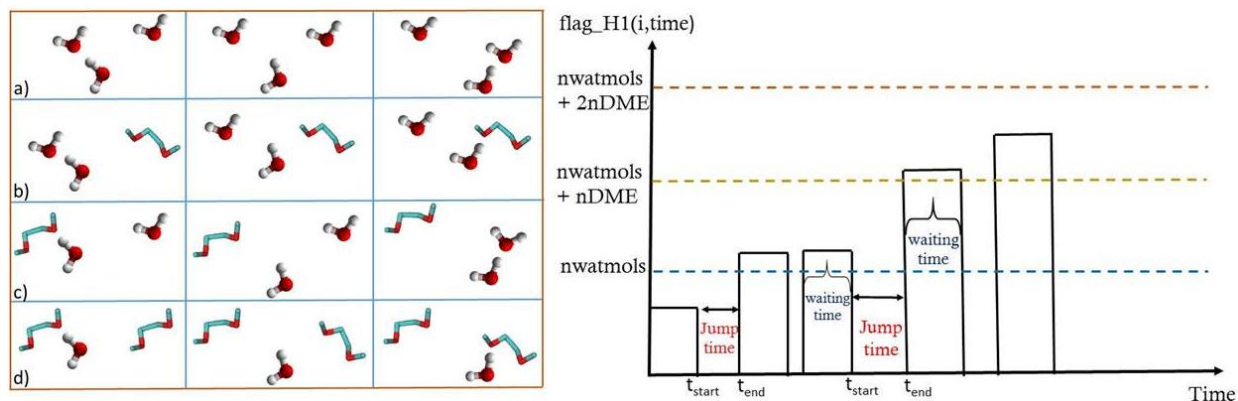


Figure 3.II.2. The time evolution of the cosine of the angle of the OH vector makes with the Z-axis of the simulation box of any randomly chosen water molecule.

Our primary focus is to identify the large amplitude angular jumps and characterized the H-bond breaking and forming events. To have the detail information about the H-bond partner exchange events we first tag each water molecule at each time step and identify its H-bond partner. There are several definition of H-bonds based on geometric criteria, energy consideration as well as orbital occupancy. Here we choose a widely accepted geometric definition based on both distance between donor and acceptor ($R_{\text{cutoff}} \sim 3.0 \text{ \AA}$) along with angle between the vector joining water-water or water-DME molecule ($\theta_{\text{cutoff}} \approx 30^\circ$) cut off

condition (scheme 3.II.1). We develop in-house code to label the H-bond exchange events, the initial and final H-bond partners, the starting and ending times of the H-bond switching events. We assign two flag variables $\text{flag}^{\text{H1}}(i,\text{time})$ and $\text{flag}^{\text{H2}}(i,\text{time})$ for each i -th water molecule at each simulation time step (scheme 3.II.2). At any time t , if the i -th water molecule donates H-bond to the oxygen atom of the j -th water molecule via its one of the H atom (say H_1) then we assign the value of $\text{flag}^{\text{H1}}(i,\text{time})$ is equal to j . If it donates H-bond to the 1st oxygen atom or 2nd oxygen atom of the j th DME molecule then $\text{flag}^{\text{H1}}(i,\text{time})$ became $(n_{\text{watmols}} + j)$ or $(n_{\text{watmols}} + n_{\text{DME}} + j)$. If the central water molecule does not connected to any water or DME molecule then the flag value remains zero. It is to note here the reason behind the H-bond exchange is the thermal and density fluctuations; after breaking the H-bond if the central molecule again reconnects with the same molecule via H-bond (librational motion), we have not considered this as a successful H-bond exchange event. These are not a H-bond partner exchange event, so it is not connected with large amplitude jumps. We also tag each time of the H-bond breaking as well as making. The same algorithm is followed for H_2 atom of each water molecule. Thus in each step the flag variables signifies the H-bonding state of the two H-atom of any water molecule. From the dynamics of this flag variables one can easily compute further detail of the large amplitude angular jumps. Any H-atom of i -th water molecule can undergo a jump from initial partner water or DME to final partner water or DME. These jumps are labelled as homo-molecular events (water to water (ww), DME to DME (dd)) and hetero-molecular jumps (water to DME (wd), and DME to water (dw)) jump. In scheme 3.II.2 we try to provide pictorial representation of these different types of H-bond exchange events where the rotating water molecule undergoes water-water (panel a), water-DME (panel b), DME-water (panel c) and DME-DME (panel d) large amplitude angular jump. The microscopic jump time (τ_{jump}) is defined as the difference between ending and starting times of a reorientational jump ($\tau_{\text{jump}} = t_{\text{end}} - t_{\text{start}}$), similarly the waiting time (τ_{wait}) is the time duration of the end time of the i -th jump and the starting time of the $(i+1)$ -th jump (scheme 3.II.2), where t_{start} is the last instant when the water molecule was H-bonded with its initial partner, and the end time (t_{end}) is the first instant when that is H-bonded to its final partner. Similarly waiting time corresponding to any one of the OH vector of any water is the time period on which that OH vector is connected to any water or DME molecule. Eventually the molecules are not in rest at waiting periods since the librational or frame vibration is present at that time. In waiting periods the water molecule may H-bonded or wait with any water molecule or any DME molecule. We already reported the waiting time distributions

and the waiting times calculated by fitting the long-time tail of the waiting time distributions with exponentially decay function.



Scheme 3.II.2. The left panel describes all the four possible reorientational jumps (hydrogen bond exchange) of any water molecule, (a) water to water (*ww*), (b) water to DME (*wd*), (c) DME to water (*dw*) and (d) DME to DME (*dd*), jumps. The flag variable of any OH vector of any water molecule, and the jump and waiting times are described in the right panel.

3.II.3. Waiting Periods

Waiting time corresponding to any one of the OH vector of any water is the time period on which that OH vector is connected to any water or DME molecule. Truly speaking the molecules are not in rest at waiting periods since the H-bond vibrations are present at that time instant also. There are two options available: (i) waiting periods when the water molecule is H-bonded to any water, and (ii) when it is connected to any DME molecule. We have analysed the waiting time distributions and the waiting times are calculated by fitting those long-time tails of the waiting time distributions. The computed waiting time distributions, $y(t)$ have been fitted to exponential time dependence of the form,

$$y(t) = y_0 + Ae^{-t/\tau} \quad (3.3)$$

where y_0 is a constant value, A is the amplitude of the exponential term and τ is the characteristic timescale. The long-time portion of the waiting time distributions were fitted to the above form and from the fitted parameters one can estimate the waiting periods of water in that frame. The waiting time distributions have been computed for the time intervals during which a tagged water molecule is H-bonded to another water and during those periods when it is H-bonded to a DME. In figure 3.II.3 we provide a representative waiting time distributions computed for the mixture for which the mole fraction of water $X_w = 0.85$.

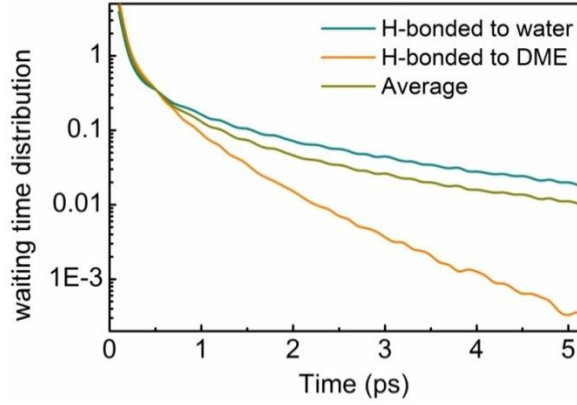


Figure 3.II.3. The waiting time distributions at $X_w = 0.85$ of the rotating water molecule for the durations during which the H-bond partner is a water molecule (blue line) and a DME molecule (orange line). The waiting time distribution considering all waiting times is the average distribution, denoted by the yellow line.

3.II.4. Tetrahedral Order Parameter

H-bond interactions ensure that locally there is a tetrahedral arrangement of with the water molecules surrounding the target molecule. To probe the local tetrahedral water network of the H-bonded water clusters, we compute *tetrahedral order parameter*(q),^{13,14} is defined as,

$$q_i = \frac{9}{8N(N+1)} \sum_{j=1}^{(N-1)} \sum_{k=(j+1)}^N (\cos\varphi_{ijk} + 1/3)^2 \quad (3.4)$$

where N ($2 \leq N \leq 4$) denotes the number of nearest neighbours of the i -th water molecule, φ_{ijk} is the angle formed by the bond vectors connecting the oxygen atoms of molecules i and j (r_{ij}) and molecules i and k (r_{ik}). A perfect tetrahedral arrangement corresponds to $q = 0$, whereas, an extreme non-tetrahedral arrangement (random alignment of bonds) corresponds to $q = 1$. For bulk water ($X_w = 1$), $p(q)$ is bimodal in nature. As X_w is decreased, the population of $p(q)$ systematically shifts from the location of the peak ($q \sim 0.09$) for pure water to lower and higher values of q . This signifies a disruption of bulk water like environments and a simultaneous appearance of more ordered “ice-like” ($q = 0$) as well as disordered ($q = 1$) local environments. After normalising the distribution of the order parameter ($\int_0^1 p(q) dq = 1$), we calculate the relative fraction of the population of three regions of q (see *chapter 5* for the results). We define,

$$\begin{aligned} n_a &= \int_0^{0.03} p(q) dq \\ n_b &= \int_{0.03}^{0.25} p(q) dq \\ n_c &= \int_{0.25}^1 p(q) dq \end{aligned} \quad (3.5)$$

where n_a and n_b are the population of the ice-like (high tetrahedral order) and “bulk-like” environment and n_c is for the tetrahedral disordered environment.

Table 3.I.1. DME force field parameters:

LJ parameters					
Atom types	C_6 (KJ.mol ⁻¹)	C_{12} (KJ.mol ⁻¹ nm ¹²)	Charge (e)	Mass (amu.)	
C(H ₃)	9.3547×10^{-3}	3.6075×10^{-3}	0.225	15.035	
C(H ₂)	5.9491×10^{-3}	1.7912×10^{-3}	0.225	14.027	
O	2.0751×10^{-6}	1.5127×10^{-3}	-0.450	15.999	
Modified atom pairs					
Atom pair type	C_6 (KJ.mol ⁻¹)	C_{12} (KJ.mol ⁻¹ nm ¹²)			
O _{DME} -O _W	0.6082×10^{-2}	0.5475×10^{-5}			
Bonds Distance (in nm)					
C-C			C-O		
0.153			0.141		
Bond angles					
Angles	Φ (deg)		K_Φ (KJ.mol ⁻¹ rad ⁻²)		
C-C-O	109.5		418.68		
C-O-C	109.5		501.22		
Proper dihedrals					
Dihedrals	C_0 (KJ.mol ⁻¹)	C_1 (KJ.mol ⁻¹)	C_2 (KJ.mol ⁻¹)	C_3 (KJ.mol ⁻¹)	C_4 (KJ.mol ⁻¹)
O-C-C-O	-3.10	-0.74	-4.69	-6.87	15.4
C-O-C-C	1.12	-3.51	-2.54	0.03	4.90

3.III. References

- (1) Berendsen, H. J. C.; Grigera, J. R.; Straatsma, T. P. *The Journal of Physical Chemistry* **1987**, *91*, 6269-6271.
- (2) Mukherjee, B. *The Journal of Chemical Physics* **2015**, *143*, 054503.
- (3) Nosé, S. *J. Chem. Phys.* **1984**, *81*, 511.
- (4) Smith, G. D.; Jaffe, R. L.; Yoon, D. Y. *Macromolecules* **1993**, *26*, 298-304.
- (5) Hess, B.; Kutzner, C.; van der Spoel, D.; Lindahl, E. *J. Chem. Theory Comput.* **2008**, *4*, 435-447.
- (6) Hezaveh, S.; Samanta, S.; Milano, G.; Roccatano, D. *The Journal of Chemical Physics* **2011**, *135*, 164501.
- (7) Hoover, W. G. *Phys. Rev. A* **1985**, *31*, 1695-1697.
- (8) Hess, B.; Bekker, H.; Berendsen, H. J. C.; Fraaije, J. G. E. M. *J. Comput. Chem.* **1997**, *18*, 1463-1472.
- (9) Allen, M. P.; Tildesley, D. J. *Computer Simulation of Liquids*; Oxford University Press: New York, **1989**.
- (10) Starr, F. W.; Nielsen, J. K.; Stanley, H. E. *Physical Review Letters* **1999**, *82*, 2294-2297.
- (11) Laage, D.; Hynes, J. T. *J. Phys. Chem. B* **2008**, *112*, 14230-14242.
- (12) Das, S.; Biswas, R.; Mukherjee, B. *J. Phys. Chem. B* **2015**, *119*, 274-283.
- (13) Chau, P. L.; Hardwick, A. J. *Mol. Phys.* **1998**, *93*, 511-518.
- (14) Errington, J. R.; Debenedetti, P. G. *Nature* **2001**, *409*, 318-321.

4. Effect of Monovalent Electrolytes on Water Structure and Dynamics of Water and on a Globular Protein

Experimental evidences of the ultrafast (sub-ps to ps) collective hydrogen bond dynamics of water in the extended hydration layers of alkali metal chlorides are provided using THz TTDS and FTIR spectroscopic techniques. We detect the cooperative hydrogen bond restructuring dynamics of water that occurs in ps to sub-ps time with the TTDS technique in the terahertz frequency region (0.3-2.1 THz; 10-70 cm^{-1}). The frequency dependent absorption coefficient (α), refractive index (n) and the dielectric relaxation response time (τ) obtained by fitting both real and imaginary part of the dielectric constant (ϵ) using a triple Debye relaxation model. The relaxation time constant of the water dipoles in presence of the salt shows an accelerated reorientation dynamics, which, in turn, renders an indirect support for the 'water structure breaking' ability of those monovalent cations. The effect is observed to be highly ion specific, depends on the cations radius and charge densities. Further we have studied the effect of these electrolytes on the structure and hydration dynamics of a model protein BSA and found that the structure and hydration of the protein suffer negligible perturbation in presence of the alkali metal chlorides. We also conclude that the hydration of the metal ions and the globular protein acts independently of each other.

4.1. Introduction

Hydration of ions is a broad topic in physical chemistry and biology. Ions dissolved in water produce a significant amount of perturbation of the hydrogen-bonded structure. However the extent of the perturbation is highly ion specific¹⁻³ in nature. Some of the ions tend to strengthen the water structure whereas there are some ions which induce its rupture also.⁴ It is the utmost important to understand these ion-water interactions in biology and chemistry, since several biophysical and biochemical processes are determined by these interactions.⁵⁻⁸ There have been extensive studies that highlight the hydration of salts; however, the challenge is to sketch a molecular picture to understand how these electrolytes perturb the structure and dynamics of its surrounding H-bonded water network. Structural information of ion hydration has so far been examined by several research groups by neutron and X-ray diffraction,⁹ X-ray absorption spectroscopy,¹⁰ IR and Raman spectroscopy¹¹ while the corresponding dynamics has been revealed using various techniques like fs IR pump-probe spectroscopy,¹²⁻¹⁴ broadband dielectric spectroscopy,^{15,16} two dimensional (2D) IR vibrational echo experiment,^{17,18} optical Kerr rotation spectroscopy¹⁹ as well as various

methods of computer simulation studies.²⁰⁻²² Many of these studies point out that the effect of ions is negligible beyond their first hydration shell. However there are effects that can extend up to second and third hydration layers.²³⁻²⁵ The structure-making (kosmotrope) and structure-breaking (chaotrope) influence of ions on water has been manifested as a delicate balance between the water–water and ion–water interactions, that may vary considerably with the size and charge density on the solute surface properties.

The network structures of the water are mainly governed by the continuous restructuring of its H-bonds. It is therefore important to realize the effect of ions on the H-bond breaking and making dynamics in water molecules within the H-bonded network which occurs in ps to sub-ps timescale and leave their traces in the elusive THz ($=10^{12}$ Hz) frequency range.^{26,27} A few experimental surveys exist in this frequency window to elucidate the collective H-bond dynamics in presence of electrolytes by the research groups of Bakker et al.^{14,28-30} and Havenith et al.^{31,32} and Buchner et al.^{24,25,33} The solvation dynamics in presence of ions is cooperative in nature that depends strongly upon the hydration of the counter ions also.¹⁴ A measurement of the absorption coefficient in the frequency of ~ 2.5 THz coupled with MD simulation study by Havenith et al.^{31,32} has established a strong correlation between the observed solvation dynamics with the ‘rattling motion’ of the metal ions, which in turn is also ion specificity. A recent study by Kondoh et al.³⁴ concluded the structure breaking ability of monovalent metal ions. Recently ab-initio MD simulation study by Marx et al.³⁵ probed the spectral responses of the solvation shell around ions in the infrared and THz frequency region. They found that the dipolar couplings between the solute and the solvent molecules and the dipole-dipole correlations are the most important factors in these frequency regions. Our group has initiated a systematic study to understand the collective dynamics of water around some biologically important solutes like urea,³⁶ guanidinium hydrochloride (GdmCl)³⁷ and alcohols³⁸ using dielectric relaxation (DR) study³⁹⁻⁴¹ in the THz frequency range. We concluded that the water structure breaking ability of the solutes might influences the much debated denaturation mechanism of proteins. DR studies of water can probe various dynamical modes associated with time scales extending from tens of fs to several ns.⁴² DR measures the frequency dependent behaviour of various optical parameters (viz. refractive index and absorption coefficient) owing to the failure of water dipoles to reorient themselves in accordance with the applied oscillating electrical field leading to depolarization. Due to the technical difficulties most of the earlier DR studies have essentially been restricted to frequencies in the GHz range. Introduction of table top THz

sources makes it possible to access the collective network dynamics of water in recent past.^{41,43}

We measure the THz response (0.3-2.1 THz) of aqueous solutions of alkali metal chlorides MCl (where M = Li, Na, K and Cs) to understand the systematic effect of changing the ionic radius and consequently the charge density of the cations on the collective solvation dynamics of water. We carefully choose Cl⁻ as a common anion, since its size falls in the middle in the monovalent anions. This allows us to investigate the effect predominantly by the systematic variation of the charge density of the metal cations. The hydration nature of the cations and the anions are structurally very much different. The cationic hydration shells are semi-rigid in nature where the rotation of the water molecules does not lead to the reorientation of the water dipole vectors making the OH transition dipoles random. Whereas in anionic hydration shell, the OH transition dipoles are fixed results with a randomization of the water dipole moment.¹⁴ That makes the DR study mostly effective to underline the hydration around the positively charged ions making the contribution of the anions less specific.¹² We extend our study to investigate the effect of these metal cations on a model transport protein BSA. The effect of ions on proteins has traditionally been explained on the basis of specific (Hofmeister) or non-specific (Coulombic) effects.⁴⁴⁻⁴⁶ Hofmeister ions could either behave as “chaotropes” or “kosmotropes” and earlier studies have mostly been concentrated on the competition between the salt ions and water for interactions with the protein surfaces. It has been concluded that monovalent cations having radius smaller than 1.06 Å are repelled by hydrophobic surface while larger monovalent cations stick to the surface.⁴⁷ Such conclusion has strongly been challenged on account of the unusual hydrophobicity exhibited by some of these ions.^{48,49} Our aim is to explore whether the perturbation of the collective water dynamics by metal ions leaves any imprint on the structure and/or hydration of protein.

4.2. Materials and Methods

The monovalent salts (LiCl, NaCl, KCl, CsCl) and the BSA protein were purchased from Sigma Aldrich with highest available purity and were used without further purification. The aqueous solutions of the monovalent salts were prepared using deionized Milli-Q water. To fix the pH of the solutions at 7.0, the protein aqueous solutions were prepared in sodium phosphate buffer (10 mM). *FTIR spectroscopy* measurements in the MIR region (2200–2800 cm⁻¹) were carried out in a JASCO FTIR-6300 spectrometer using circular CaF₂ windows with a spacer thickness of 25 μm. HOD samples were prepared by vigorous mixing of 4%

D₂O in pure water. All the data represented here are difference absorbance spectrums with pure water/salt aqueous solutions are used as reference. Protein secondary structure was measured by the *CD spectroscopy*. *TTDS* measurements of the salt solutions were carried out in a commercial THz spectrophotometer (TERA K8, Menlo System).^{37,50} To investigate the dielectric relaxation response we employ the extensively used *Debye model*^{39,41,51,52} that describe the dynamics of water molecules in various salt solutions. We have used the literature values of some parameters in GHz range of the salts in aqueous solutions^{16,24,53-57} to fit our data in triple *Debye model*. Further details about the instruments and the methodology can be found in *chapter 2*.

4.3. Results and Discussion

MIR Study: To understand of the water structure around metal ions, we study the MIR spectra (2400-2700 cm⁻¹) of the OD oscillators in aqueous salt solutions. The O-D vibrational stretch of HOD molecules (figure 4.1 and 4.2) is an ideal tool to study solute hydration.⁵⁸ These absorbance data explicitly involve the signature of water and the composition dependent MIR features correspond to the changes in the structure of water. The difference normalised absorption spectra of the aqueous salt solutions at different concentrations are shown in figure 4.1. For all the monovalent salt solutions the peak frequency gets slightly blue shifted compared to that of pure water (~2509 cm⁻¹). The OD stretching spectra in pure water are Gaussian in nature with the full width half maxima (FWHM) is ~170 cm⁻¹. We plot the frequency corresponding to the absorption maximum (ν_{peak}) and the FWHM of the MIR spectrums with the concentration of the salts in figure 4.2a and b respectively. It is evident that ν_{peak} suffers progressive blue shift with a nearly linear dependency on the salt concentration. This is due to the asymmetric redistribution of the H-bond strengths in presence of the salts.⁵⁹⁻⁶² The blue shifted narrower spectra indicate weakening of the water-water tetrahedral bulk like coordination in presence of those salts.

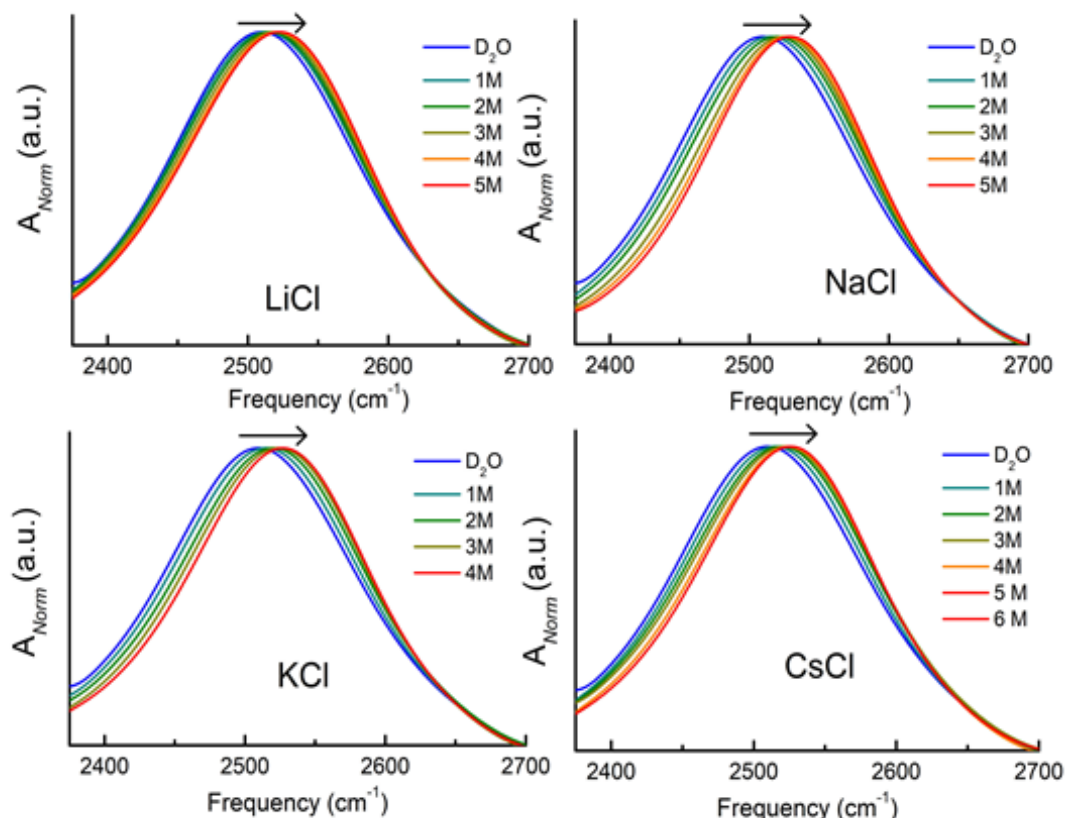


Figure 4.1. The FTIR absorption spectra of the OD stretch of HOD molecules in water and for various salt solutions. The arrows represent increasing salt concentrations.

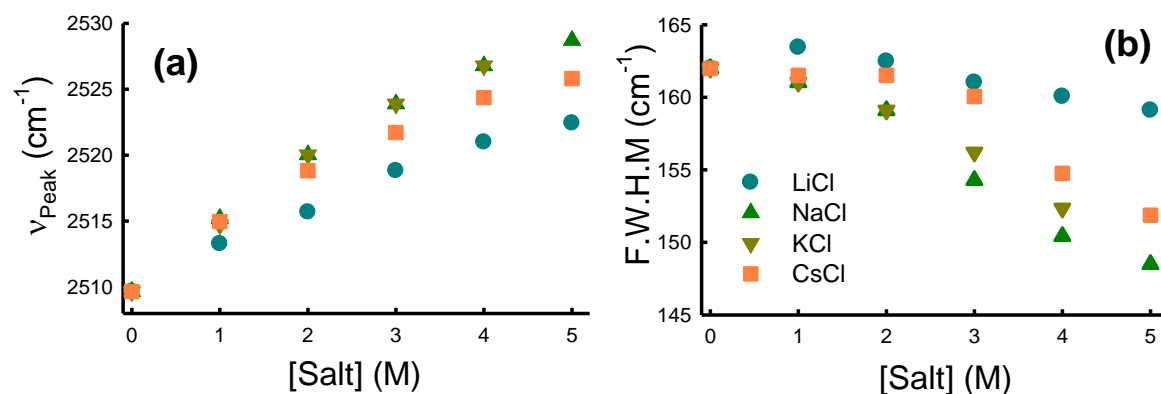


Figure 4.2. (a) Shift of the maximum absorption Frequency and (b) full width & half maxima of the absorption spectra of the OD stretch of HOD molecules in different salts solutions.

THz TDS Study

A representative transmitted THz pulse (in inset) and the corresponding FFT signals through air, empty cell, water and 5 M LiCl are depicted in figure 4.3. The THz spectra in the frequency domain in air is found to be fairly smooth with a high signal to noise ratio and nominal water absorption lines up to ~ 2.5 THz which enables us to extract the optical parameters with high precision up to ~ 2 THz.

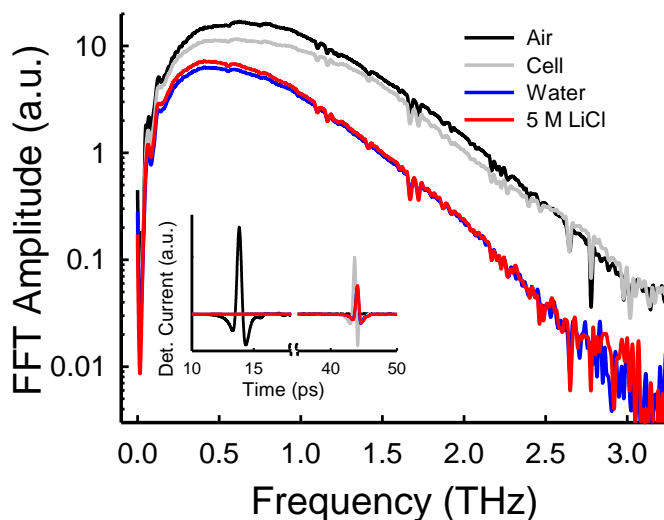


Figure 4.3. The inset shows representative THz signals in air, in presence of cell, water and 8M LiCl. The corresponding FFT diagrams are shown in the main figure.

The extracted frequency dependent optical parameters, viz. refractive index, $n(\nu)$ and absorption coefficient, $\alpha(\nu)$ for various salt solution in the THz frequency region are shown in figure 4.4a-d. A ‘THz excess’⁶³ has been observed in which $\alpha_{\text{salt solution}}(\nu)$ shows a higher value than $\alpha_{\text{water}}(\nu)$, the effect being more prominent for larger cations.

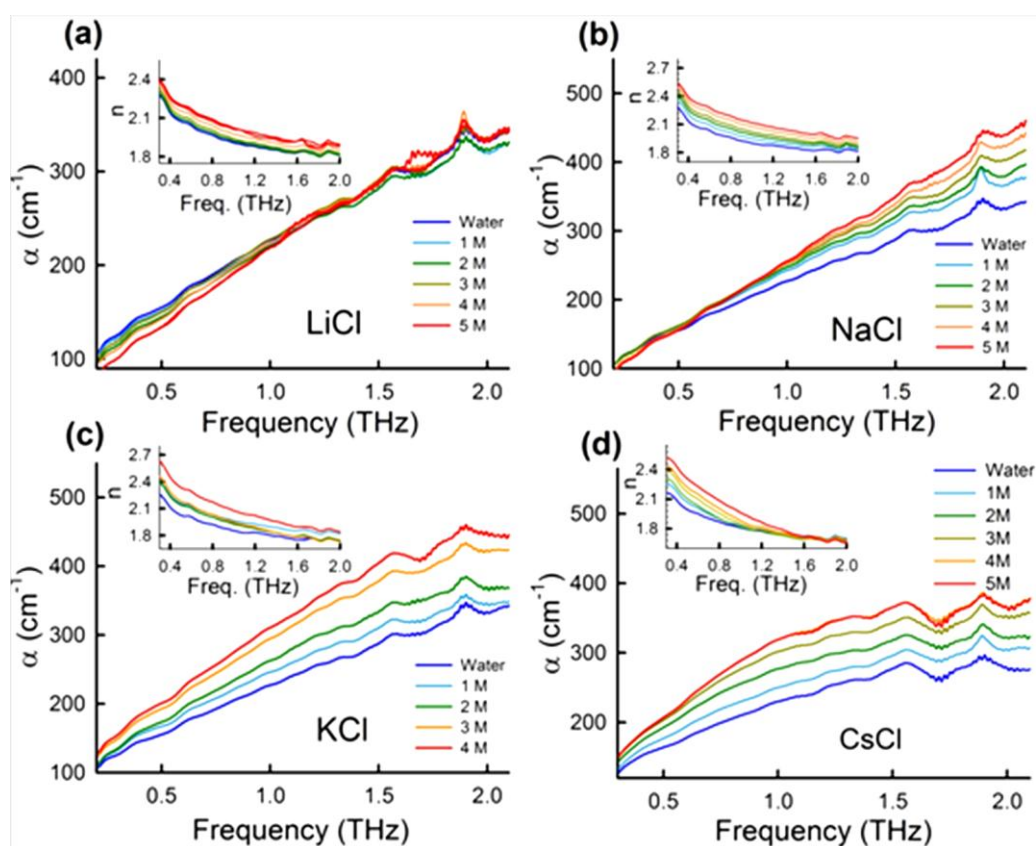


Figure 4.4. Frequency dependent absorption coefficient, $\alpha(\nu)$ and refractive index, $n(\nu)$ (in the insets) of aqueous solution of different salts (a) LiCl, (b) NaCl, (c) KCl, and (d) CsCl at different concentrations.

To obtain a more quantitative understanding, we plot the change in absorption coefficient ($\Delta\alpha = \alpha_{\text{solution}} - \alpha_{\text{water}}$) measured at 1 THz (see figure 4.5). $\Delta\alpha$ does not effectively change for the smallest cation Li^+ , however, for the rest of the ions it increases almost linearly with salt concentration. Such linearity in $\Delta\alpha$ profile has previously been reported by Havenith et. al. around 2.4 THz using the same group of ions.³¹ The slope of the curves increases with the ionic radius of the cations. We assume that the measured α_{solution} has cumulative contribution from pure water, cation, anion, and their respective hydration shells. Thus, a simple three component model can be formulated as,

$$\Delta\alpha = \alpha_{\text{solution}} - \alpha_{\text{water}} = (\phi_c\alpha_c + \phi_{ch}\alpha_{ch} + \phi_a\alpha_a + \phi_{ah}\alpha_{ah} + \phi_{\text{water}}\alpha_{\text{water}}) - \alpha_{\text{water}} \quad (4.1)$$

where, ϕ stands for mole fraction, 'c' and 'a' stand for cation and anion while 'ch' and 'ah' stand for the corresponding hydration terms, respectively. Neglecting the contribution of the volume fraction of the cations and anions towards the total volume (V_t), equation 4.1 simplifies to,

$$\Delta\alpha = \frac{V_{ch}}{V_t}(\alpha_{ch} - \alpha_{\text{water}}) + \frac{V_{ah}}{V_t}(\alpha_{ah} - \alpha_{\text{water}}) \quad (4.2)$$

Since the anion is fixed the second term in equation 4.2 contributes the same share for each salt. Thus $\Delta\alpha$ is expected to vary linearly with the salt concentration, the magnitude of the slope being dependent on the terms V_{ch} and α_{ch} . The observed linear increase of $\Delta\alpha$ clearly identifies the increase in the number of ion associated hydrated water molecules and that the hydration layers of individual ions do not overlap within the studied concentration range. The ionic radii increases in the order Na^+ (0.095 nm) < K^+ (0.133 nm) < Cs^+ (0.169 nm)¹ and their hydration number also follows that similar sequence.⁶⁴ Assuming that the ions hydrate individually, the observed difference in the slope for Na^+ and K^+ (or Cs^+) can be due either to the increase in V_{ch} or α_{ch} . However, the similarity in the slopes of Cs^+ and K^+ in spite of their varied hydration number signifies a trade-off between these two factors. It is also worth mentioning here that the collective dynamics of water as probed in the THz frequency domain extends several layers beyond the first solvation shell and a mere consideration of the first solvation shell hydration while formulating equations 4.1-4.2 is insufficient to account for the observed changes in the THz domain.

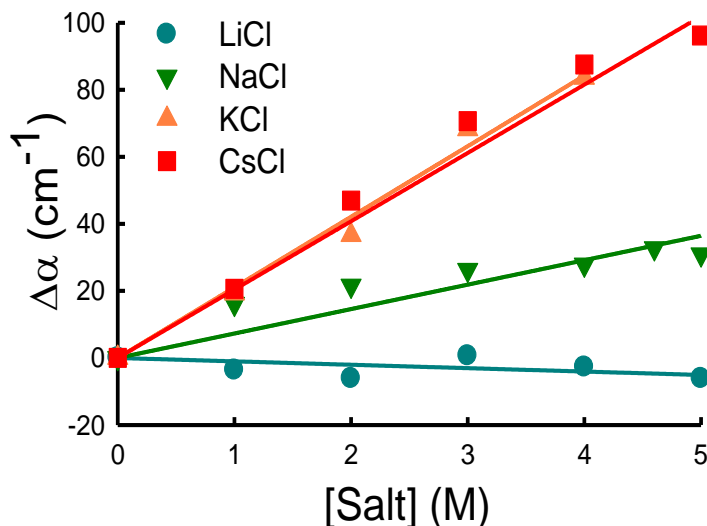


Figure 4.5. The change in the absorption coefficient, $\Delta\alpha$ measured at 1 THz as function of salt concentration.

It is important to note that the dynamic hydration shell around ions which involves rearrangement in the associated H-bonded network offers an absorption coefficient different from that of pure water.⁶⁵ As the salt concentration is increased larger numbers of water molecules start interacting with the ions eventually increasing $\alpha(\nu)$. Li^+ has the smallest radius among the alkali metals and hence the effective charge density is also the highest, therefore the largest effect is expected to be observed in Li^+ . However, the dipole-dipole interaction among the water molecules associated with the ions limits the hydration shell thickness⁶⁶ eventually producing a moderate effect only.

We found that both real and imaginary part of the permittivity increases with increasing salt concentration. We fit both the real and the imaginary dielectric constant with a triple *Debye model*. Some representative fitted curves are shown in figure 4.6a-d and the fitting parameters are presented in table 4.I-4.IV. It is important to remember here that there might remain an appreciable fraction of water molecules in the first solvation layer that strongly bind to the ions which rotates rather slowly (in the timescale of tens to hundreds of ps).¹⁶ But the dynamics of those first hydration shell water molecules are not detectable in THz domain. For pure water, we obtain the relaxation timescales of 8.9 ps (τ_1), 207 fs (τ_2), and 71 fs (τ_3).^{36,37} The ~9 ps and ~200 fs timescales are associated to the well-known cooperative rearrangement of the H-bonded network and the small angular rotational modes of individual polar water molecules, respectively.^{41,43} We also found another timescale ~70 fs, has its origin rooted to the 60 cm^{-1} (1.8 THz) vibrational band owing to the H-bond

bending and the related transverse acoustic phonons, which propagate in a direction normal to the hydrogen bonds between two neighbouring water molecules.^{67,68} We observe that, τ_1 gradually decreases with salt concentration (figure 4.7a) that indicates an accelerated dynamics of the cooperative H-bond rearrangement in presence of the ions and consequently invokes the notion of “structure breaking” ability of these ions corroborating the FTIR results. It is interesting to note that at a fixed concentration the maximum acceleration in τ_1 occurs in Na^+ and K^+ , which also supports the FTIR data. For Li^+ and Cs^+ the changes are relatively smaller and comparable. The time scale τ_2 suffers only negligible change with salt concentration (figure 4.8) which indicates a marginal change in the rotational modes of individual water dipoles within the water network corroborating earlier reports involving IR pump-probe studies.^{30,69}

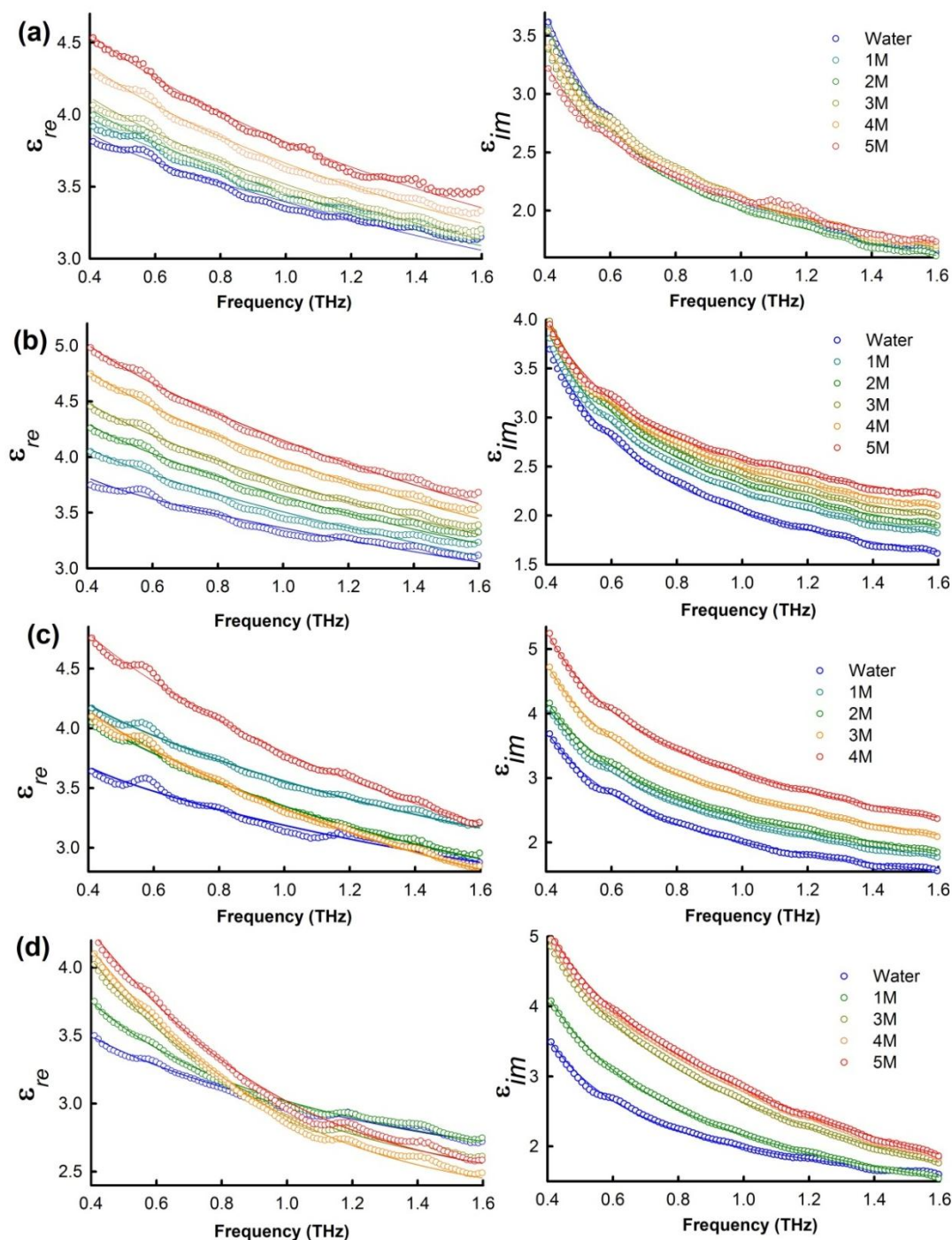


Figure 4.6. The real (ϵ') and imaginary (ϵ'') dielectric constants of various concentration of different salts (a) LiCl, (b) NaCl, (c) KCl, (d) CsCl as a function of frequency. The dotted curves are for experimental and the solid curve represents the fitted data.

We plot the first relaxation strength ($S_1 = \epsilon_S - \epsilon_1$) with salt concentration in figure 4.7b. The salt solutions produce smaller S_1 values compared to that of pure water, implying a ‘depolarization’ phenomenon.⁷⁰ The observed depolarization is partly kinetic in nature, in which the water molecules are forced to reorient in the local electric field direction caused by the movement and charge of the ions,^{71,72} while on the other hand the local electric field of

the ions binds water molecules resulting in a static depolarization.⁷³ The relative contribution of these two terms towards the total depolarization is debatable and the dynamical contribution has been considered to be significantly smaller compared to that of the static term.⁵⁷ The depolarization strength is found to follow the order: $\text{Li}^+ \sim \text{Cs}^+ < \text{Na}^+ < \text{K}^+$ which in turn reciprocates the acceleration in τ_1 values (figure 4.7a). It is interesting to note that Li^+ and Cs^+ produce comparable S_1 but distinct $\alpha(v)$ profiles. Depolarization is essentially an optimization of two opposing effects: formation of ion bound water and rupture of the network water structure. The high charge density of Li^+ makes the first solvation shell water molecules highly oriented, however, does not protrude into the subsequent layers of hydration. The optimization is found to be the most efficient in the middle of the alkali metal group (K^+) producing the most prominent rupture in the extended network dynamics.

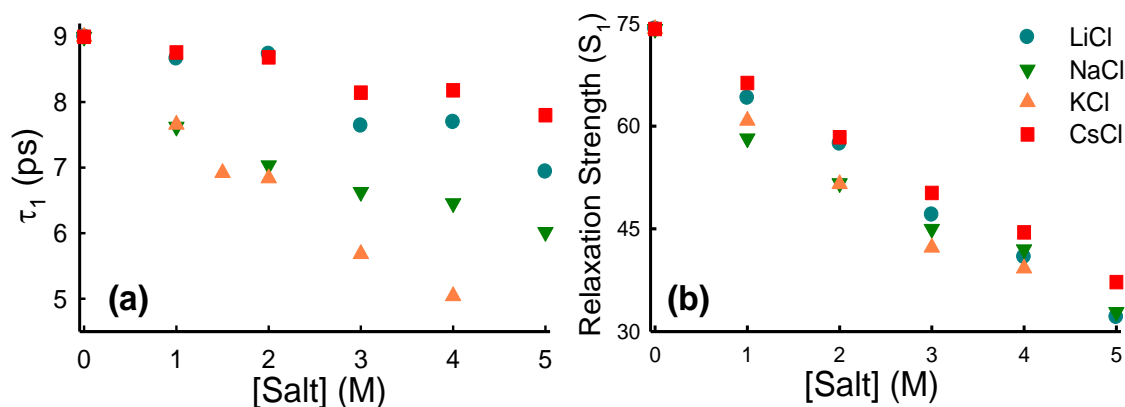


Figure 4.7. (a) Time constant (τ_1) as function of salts concentration. (b) Relaxation strength (S_1) as a function of salt concentration

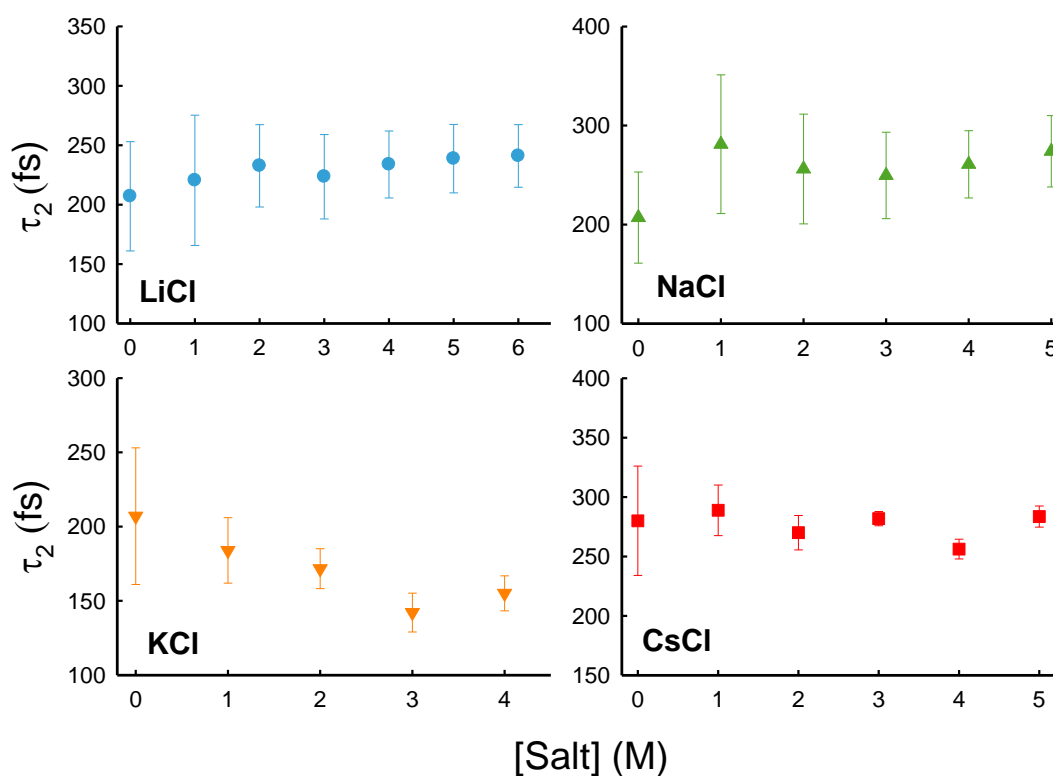


Figure 4.8. The Debye timescale τ_2 for various concentrations of LiCl, NaCl, KCl, and CsCl.

We now investigate the effect of these salts on the secondary structure of a model protein, BSA using CD spectroscopy (figure 4.9a). To get a comparative view we include HCl as it is a well-known denaturant agent to BSA.^{74,75} Two representative CD spectra of BSA in presence of 1M LiCl and HCl are depicted in figure 4.9a (insets). The secondary structure of the protein does not suffer noticeable perturbation in the presence of LiCl, similar results are also observed in the other metal cations. However, in case of HCl a noticeable decrease in the CD signal is observed indicating a significant rupture of the secondary structure of the protein. For a more quantitative insight we plot the relative abundance of the α -helix structure in the protein as a function of salt concentration (figure 4.9a). The relative abundance α -helical structure in BSA is relatively high (~70%) and does not change appreciably in presence of the metal cations. However, it decreases drastically with a concomitant increase in the random coil structure in presence of H^+ which signifies the unfolding of the protein.

To determine the changes in the hydration structure of both the protein and the cations, we measure the THz response of BSA in presence of these salts. The $\alpha(v)$ profile of the protein solution lies lower than that of bulk water (figure 4.9b, inset), which is intuitive

considering the replacement of highly THz absorbing water molecules with the relatively low THz absorbing protein molecules. However, the extent of the observed decrease in the $\alpha(\nu)$ profile can only be explained by taking into consideration the solvation sheath associated with the protein surface (similar to that for the salts in equation 4.2) with the added complexity that the volume of the protein is no longer negligible compared to the total volume V_t . We plot the change in protein hydration ($\Delta\alpha_{ph} = \alpha_p - \alpha_h$ where α_p is the absorption coefficient of the protein while α_h is that of the salt solution only) measured at 1 THz at a fixed cation concentration of 1 M (circles, figure 4.9b). All the $\Delta\alpha_{ph}$ values are found to be negative and do not suffer noticeable change in presence of the metal cations. The observed cation independency of $\Delta\alpha_{ph}$ values strongly correlate the unaltered CD spectra (figure 4.9a), the cations thus not only remain indifferent to the protein structure they also do not perturb the hydration structure of BSA. For H^+ , however, $\Delta\alpha_{ph}$ is noticeably smaller than that of pure water. The observed change in $\Delta\alpha_{ph}$ can be explained on the basis of the proton induced rupture of the protein structure (figure 4.9a, inset). Unfolding of the protein's secondary structure from α -helix to random coil expose the buried hydrophobic moiety of the protein into bulk water which in turn considerably modifies the long range collective hydration dynamics as the mode of interaction of the exposed hydrophobic amino acids are different from the hydrophilic amino acids present at the folded protein surface.

We also consider the changes in the salt hydration $\Delta\alpha_{sh} = \alpha_s - \alpha_h$ where α_s and α_h are the absorption coefficients in presence and in absence of 1 M salt measured at 1 THz. We plot $\Delta\alpha_{sh}$ both in absence (open triangles) and in presence (filled triangles) of 0.8 mM BSA (figure 4.9b). As evidenced from the figure all the $\Delta\alpha_{sh}$ values are positive correlating the 'THz excess' of these salt solutions (see figure 4.4). $\Delta\alpha_{sh}$ does not change appreciably in presence of the protein corroborating the fact that ion and protein hydration stay independent of one another. The small decrease observed in the $\Delta\alpha_{sh}$ in presence of the protein could be accounted for considering the volume changes associated with the protein itself. It is, however, intriguing that an identical and negligible change is also observed in H^+ , which signifies that although H^+ induces a considerable rupture of the protein hydration, whereas the associated ion hydration remains nearly unaffected. This apparent ambiguity can be understood in the light of protein denaturation mechanism by the solutes, which ironically is still a much debated issue.⁷⁶ The most extensively used protein denaturants like guanidinium chloride and urea are classically explained to denature proteins either by directly binding to the proteins or by modifying the properties of aqueous solutions. We have recently shown

that GdmCl does alter the collective water dynamics around protein surface that plays pivotal role in the protein denaturation.³⁷ The key mechanism of proton mediated protein unfolding initiates with the ionization of the surface exposed amino acid residues of proteins which in turn induces electrostatic interactions resulting in the unfolding of the protein. Our results unambiguously reveal that similar to the monovalent metal cations, the collective hydration dynamics of proton does not change much upon protein denaturation. The findings of the present study could likely lead to a new avenue towards understanding the molecular mechanism of the process involved. A detailed and systemic investigation in this topic is of certain demand.

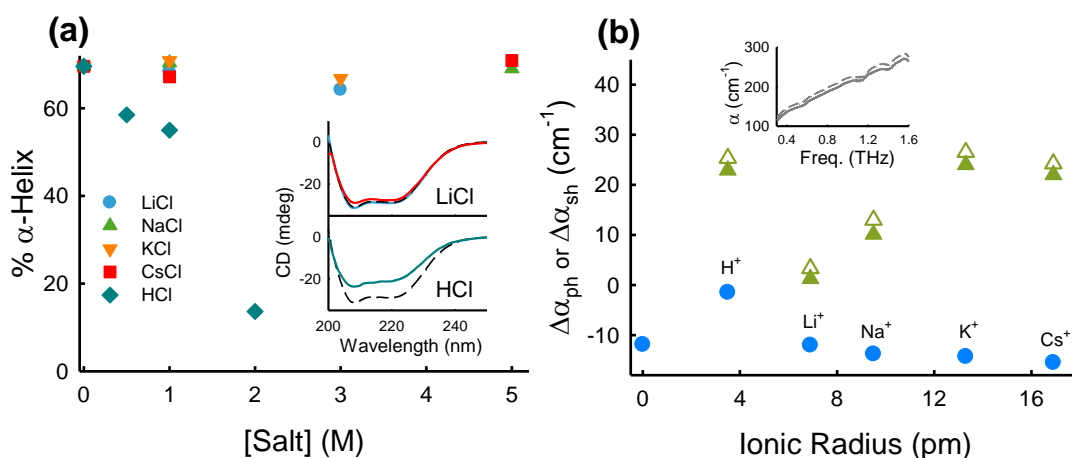


Figure 4.9. (a) Content of α -Helix of BSA in presence of ions of different concentrations. Representative CD signals of BSA in water (broken lines) and presence of 1M LiCl and HCl (solid lines) are shown in the insets. (b) The inset shows $\alpha(v)$ profile of water (broken line) and 0.8 mM BSA solution (solid line). The main figure depicts the changes in protein hydration (circles) and ion hydration in absence (open triangle) and in presence (solid triangle) of protein.

4.4. Summary

We have studied the effect of monovalent cations on the collective hydration dynamics of the water dipoles and found that these ions unambiguously accelerate the cooperative hydrogen bond dynamics. It affirms a positive support towards the most debated notion of these ions to act as water structure breakers. The extent of this effect has been found to be mostly ion specific, K^+ being the most effective ion and a simple consideration of ionic charge density is insufficient to account for the observed changes. It has also been concluded that the hydration structure of the metal cations and the globular protein BSA act independent of each other. In case of proton, however, the protein hydration gets significantly perturbed owing to its unfolding, surprisingly keeping the proton hydration unaltered. This observation is intriguing in order to establish the molecular mechanism of proton induced denaturation of proteins.

Table 4.I. Debye relaxation fitting parameters of aqueous solutions of LiCl at different concentrations

[LiCl] (M)	ϵ_{∞}	S_1	S_2	S_3	τ_1 (ps)	τ_2 (fs)	τ_3 (fs)	σ (S m ⁻¹)
0	1.99	75.27	0.475±0.03	1.41±0.1	8.89±0.10	207±46	70.8	0.00
1	2.21	64.10	0.435±0.06	1.35±0.07	8.66±0.11	220±54	70.8	6.03
2	2.16	53.51	0.65±0.03	1.34±0.08	8.73±0.13	233±34	70.8	10.87
3	2.18	47.03	0.67±0.03	1.36±0.08	7.64±0.11	223±35	70.8	14.12
4	2.24	40.87	0.846±0.05	1.40±0.09	7.69±0.12	234±28	70.8	16.11
5	2.26	32.09	0.979±0.03	1.53±0.06	6.94±0.16	239±28	70.8	16.00

Table 4.II. Debye relaxation fitting parameters of aqueous solutions of NaCl at different concentrations

[NaCl] (M)	ϵ_{∞}	S_1	S_2	S_3	τ_1 (ps)	τ_2 (fs)	τ_3 (fs)	σ (S m ⁻¹)
0	1.99	75.27	0.475±0.03	1.41±0.10	8.89±0.10	207±46	70.8	0.00
1	1.99	58.20	0.394±0.06	1.74±0.07	7.62±0.14	281±90	70.8	8.26
2	2.07	51.66	0.556±0.03	1.74±0.08	7.04±0.11	256±55	70.8	11.96
3	2.05	44.97	0.671±0.03	1.86±0.08	6.63±0.10	249±43	70.8	16.02
4	2.07	36.58	0.857±0.03	2.05 ±0.06	6.46±0.12	261±33	70.8	21.60
5	2.05	32.83	0.891±0.03	2.30±0.06	6.01±0.04	274±35	70.8	22.29

Table 4.III. Debye relaxation fitting parameters of aqueous solutions of KCl at different concentrations

[KCl] (M)	ϵ_{∞}	S_1	S_2	S_3	τ_1 (ps)	τ_2 (fs)	τ_3 (fs)	σ (S m ⁻¹)
0	1.99	75.27	0.475±0.03	1.41±0.09	8.89±0.10	207±46	70.8	0.00
1	1.95	63.11	0.627±0.06	1.54±0.07	7.66±0.11	225±39	70.8	9.13
1.5	2.03	56.09	0.762±0.03	1.44±0.08	6.92±0.07	201±27	70.8	12.70
2	1.95	52.62	0.960±0.03	1.46±0.08	6.84±0.07	201±21	70.8	18.98
3	1.91	44.74	1.220±0.03	1.48±0.06	5.68±0.04	181±15	70.8	22.05
4	1.80	38.70	1.470±0.03	1.60±0.06	5.003±0.04	181±14	70.8	29.87

Table 4.IV. Debye relaxation fitting parameters of aqueous solutions of CsCl at different concentrations

[CsCl] (M)	ϵ_{∞}	S_1	S_2	S_3	τ_1 (ps)	τ_2 (fs)	τ_3 (fs)	σ (S m ⁻¹)
0	1.99	75.27	0.475±0.03	1.41±0.10	8.89±0.10	207±46	70.8	0.00
1	2.21	66.29	1.163±0.06	0.66±0.07	8.76±0.08	288±21	70.8	10.36
2	2.23	58.38	1.864±0.03	0.21±0.08	8.68±0.08	270±14	70.8	22.36
3	2.19	50.24	2.364±0.05	0.21±0.08	8.14±0.08	281±06	70.8	30.00
4	2.02	44.49	2.726±0.07	0.12±0.06	8.18±0.07	256±08	70.8	35.60
5	2.03	37.20	2.745±0.02	0.39±0.10	7.80±0.09	283±07	70.8	40.50

4.5. References

- (1) Marcus, Y. *Ion solvation*; Wiley-Interscience: New York, **1985**.
- (2) Kunz, W. N. B.; Henle, J.; Ninham, B. W. *Curr. Opin. Colloid Interface Sci.* **2004**, *9*, 19-37.
- (3) Tobias, D. J.; Hemminger, J. C. *Science* **2008**, *319*, 1197-1198.
- (4) Marcus, Y. *Chem. Rev.* **2009**, *109*, 1346-1370.
- (5) Dill, K. A. *Biochemistry* **1990**, *29*, 7133-7155.
- (6) Rupley, J. A.; Careri, G. *Adv. Prot. Chem.* **1991**, *41*, 37-172.
- (7) Cacace, M. G.; Landau, E. M.; Ramsden, J. J. *Q. Rev. Biophys.* **1997**, *30*, 241-277.
- (8) Lo Nostro, P.; Ninham, B. W. *Chem. Rev.* **2012**, *112*, 2286-2322.
- (9) Mancinelli, R.; Botti, A.; Bruni, F.; Ricci, M. A.; Soper, A. K. *J. Phys. Chem. B* **2007**, *111*, 13570-13577.
- (10) Cappa, C. D.; Smith, J. D.; Messer, B. M.; Cohen, R. C.; Saykally, R. J. *J. Phys. Chem. B* **2006**, *110*, 5301-5309.
- (11) Smith, J. D.; Saykally, R. J.; Geissler, P. L. *J. Am. Chem. Soc.* **2007**, *129*, 13847-13856.
- (12) Tielrooij, K. J.; van der Post, S. T.; Hunger, J.; Bonn, M.; Bakker, H. J. *J. Phys. Chem. B* **2011**, *115*, 12638-12647.
- (13) Onfelt, B.; Lincoln, P.; Norden, B.; Baskin, J. S.; Zewail, A. H. *Proc. Natl. Acad. Sci. USA* **2000**, *97*, 5708-5713.
- (14) Tielrooij, K. J.; Garcia-Araez, N.; Bonn, M.; Bakker, H. J. *Science* **2010**, *328*, 1006-1009.
- (15) Buchner, R.; Hefter, G. *Phys. Chem. Chem. Phys.* **2009**, *11*, 8984-8999.
- (16) Chen, T.; Hefter, G.; Buchner, R. *J. Phys. Chem. A* **2003**, *107*, 4025-4031.
- (17) Moilanen, D. E.; Wong, D.; Rosenfeld, D. E.; Fenn, E. E.; Fayer, M. D. *Proc. Natl. Acad. Sci. U.S.A.* **2009**, *106*, 375-380.
- (18) Fayer, M. D. *Acc. Chem. Res.* **2012**, *45*, 3-14.
- (19) Turton, D. A.; Hunger, J.; Hefter, G.; Buchner, R.; Wynne, K. *J. Chem. Phys.* **2008**, *128*, 161102.
- (20) Laage, D. L.; Hynes, J. T. *Proc. Natl. Acad. Sci. U.S.A.* **2007**, *104*, 11167-11172.

- (21) Gallo, P.; Corradini, D.; Rovere, M. *Phys. Chem. Chem. Phys.* **2011**, *13*, 19814-19822.
- (22) Stirnemann, G.; Wernersson, E.; Jungwirth, P.; Laage, D. *J. Am. Chem. Soc.* **2013**, *135*, 11824-11831.
- (23) Mancinelli, R.; Botti, A.; Bruni, F.; Ricci, M. A.; Soper, A. K. *Phys. Chem. Chem. Phys.* **2007**, *9*, 2959-2967.
- (24) Wachter, W.; Fernandez, S.; Buchner, R.; Hefter, G. *J. Phys. Chem. B* **2007**, *111*, 9010-9017.
- (25) Buchner, R.; Chen, T.; Hefter, G. *J. Phys. Chem. B* **2004** *108*, 2365-2375.
- (26) Heyden, M.; Sun, J.; Funkner, S.; Mathias, G.; Forbert, H.; Havenith, M.; Marx, D. *Proc. Natl. Acad. Sci. USA* **2010**, *107*, 12068-12073.
- (27) Penkov, N.; Shvirst, N.; Yashin, V. A.; Fesenko, E. E.; Fesenko, E. E. *The Journal of Physical Chemistry B* **2015**.
- (28) Tielrooij, K. J.; Timmer, R. L. A.; Bakker, H. J.; Bonn, M. *Phys. Rev. Lett.* **2009**, *102*, 198303.
- (29) Ottosson, N.; Hunger, J.; Bakker, H. J. *J. Am. Chem. Soc.* **2014**, *136*, 12808-12811.
- (30) van der Post, S. T.; Tielrooij, K.-J.; Hunger, J.; Backus, E. H. G.; Bakker, H. J. *Faraday Discussions* **2013**, *160*, 171-189.
- (31) Schmidt, D. A.; Birer, Ö.; Funkner, S.; Born, B.; Gnanasekaran, R.; Schwaab, G.; Leitner, D. M.; Havenith, M. *J. Am. Chem. Soc.* **2009**, *131*, 18512-18517.
- (32) Funkner, S.; Niehues, G.; Schmidt, D. A.; Heyden, M.; Schwaab, G.; Callahan, K. M.; Tobias, D. J.; Havenith, M. *J. Am. Chem. Soc.* **2012**, *134*, 1030-1035.
- (33) Brandes, E.; Stage, C.; Motschmann, H.; Rieder, J.; Buchner, R. *The Journal of Chemical Physics* **2014**, *141*, 18C509.
- (34) Kondoh, M.; Ohshima, Y.; Tsubouchi, M. *Chem. Phys. Lett.* **2014**, *591*, 317-322.
- (35) Smiechowski, M.; Sun, J.; Forbert, H.; Marx, D. *Physical Chemistry Chemical Physics* **2015**, *17*, 8323-8329.
- (36) Samanta, N.; Das Mahanta, D.; Mitra, R. K. *Chem. Asian J.* **2014**, *9*, 3457-3463.
- (37) Samanta, N.; Das Mahanta, D.; Mitra, R. K. *Phys. Chem. Chem. Phys.* **2014**, *16*, 23308--23315.
- (38) Das, D. K.; Das Mahanta, D.; Mitra, R. K. *ChemPhysChem* **2017**, *18*, 749-754.
- (39) Polley, D.; Patra, A.; Mitra, R. K. *Chem. Phys. Lett.* **2013** *586*, 143-147.
- (40) Ro/nne, C.; Thrane, L.; Åstrand, P.-O.; Wallqvist, A.; Mikkelsen, K. V.; Keiding, S. r. R. *The Journal of Chemical Physics* **1997**, *107*, 5319-5331.
- (41) Kindt, J. T.; Schmuttenmaer, C. A. *J. Phys. Chem.* **1996**, *100*, 10373-10379.
- (42) Buchner, R. *Pure Appl. Chem.* **2008**, *80*, 1239-1252.
- (43) Rønne, C.; Åstrand, P. O.; Keiding, S. R. *Phys. Rev. Lett.* **1999**, *82*, 2888-2891
- (44) von Hippel, P. H.; Schleich, T. *Acc. Chem. Res.* **1969**, *2*, 257-265.
- (45) Baldwin, R. L. *Biophys. J.* **1996**, *71*, 2056-2063.
- (46) Zhou, H.-X. *Proteins* **2005**, *61*, 69-78.
- (47) Collins, K. D. *Proc. Nat. Acad. Sci.* **1995**, *92*, 5553-5557.
- (48) Borén, K.; Grankvist, H.; Hammarström, P.; Carlsson, U. *FEBS Lett.* **2004**, *566*, 95-99.
- (49) Ebel, C.; Faou, P.; Kernel, B.; Zaccai, G. *Biochemistry* **1999**, *38*, 9039-9047.
- (50) Polley, D.; Ganguly, A.; Barman, A.; Mitra, R. K. *Opt. Lett.* **2013**, *38*, 2754-2756.

- (51) Nandi, N.; Bagchi, B. *J. Phys. Chem. B* **1997**, *101*, 10954-10961.
- (52) Rønne, C.; Lars Thrane, L.; Åstrand, P.-O.; Wallqvist, A.; Mikkelsen, K. V.; Keiding, S. R. *J. Chem. Phys.* **1997**, *107*, 5319-5331.
- (53) Hasted, J. B.; Ritson, D. M.; Collie, C. H. *J. Chem. Phys.* **1948**, *16*, 1-21.
- (54) Nörtemann, K.; Hilland, J.; Kaatze, U. *J. Phys. Chem. A* **1997**, *101*, 6864-6869.
- (55) Lileev, A.; Lyashchenko, A. *J. Mol. Liq.* **2009**, *150*, 4-8.
- (56) Wang, P.; Anderko, A. *Fluid Phase Equilib.* **2001**, *186*, 103-122.
- (57) Chandra, A. *J. Chem. Phys.* **2000**, *113*, 903-905.
- (58) Śmiechowski, M.; Stangret, J. *Pure Appl. Chem.* **2010**, *82*, 1869-1887.
- (59) Verma, P. K.; Lee, H.; Park, J.-Y.; Lim, J.-H.; Maj, M.; Choi, J.-H.; Kwak, K.-W.; Cho, M. *The Journal of Physical Chemistry Letters* **2015**, *6*, 2773-2779.
- (60) Nickolov, Z. S.; Miller, J. D. *J. Colloid Interface Sci.* **2005**, *287*, 572-580.
- (61) Li, R.; Jiang, Z.; Chen, F.; Yang, H.; Guan, Y. *J. Mol. Struct.* **2004**, *707*, 83-88.
- (62) Mähler, J.; Persson, I. *Inorg. Chem.* **2012**, *51*, 425-438.
- (63) Heyden, M.; Havenith, M. *Methods* **2010**, *52*, 74-83.
- (64) Lee, S. H.; Rasaiah, J. C. *J. Phys. Chem.* **1996**, *100*, 1420-1425.
- (65) Heyden, M.; Bründermann, E.; Heugen, U.; Niehues, G.; Leitner, D. M.; Havenith, M. *J. Am. Chem. Soc.* **2008**, *130*, 5773-5779.
- (66) Hribar, B.; Southall, N. T.; Vlachy, V.; Dill, K. A. *J. Am. Chem. Soc.* **2002**, *124*, 12302-12311.
- (67) Vij, J. K.; Simpson, D. R. J.; Panarina, O. E. *J. Mol. Liq.* **2004**, *112*, 125-135.
- (68) Walrafen, G. E. *J. Phys. Chem.* **1990**, *94*, 2237-2239.
- (69) Omta, A. W.; Kropman, M.; Woutersen, S.; Bakker, H. J. *Science* **2003**, *301*, 347-349.
- (70) Kaatze, U. *Z. Phys. Chem.* **1983**, *135*, 51-75.
- (71) Hubbard, J.; Onsager, L. *J. Chem. Phys.* **1977**, *67*, 4850.
- (72) Hubbard, J. B.; Onsager, L.; van Beek, W. M.; Mandel, M. *Proc. Nat. Acad. Sci.* **1977**, *74*, 401-404.
- (73) Barthel, J.; Buchner, R.; Bachhuber, K.; Hetzenauer, H.; Kleebauer, M.; Ortmaier, H. *Pure Appl. Chem.* **1990**, *62*, 2287-2296.
- (74) Goto, Y.; Calciano, L. J.; Fink, A. L. *Proceedings of the National Academy of Sciences* **1990**, *87*, 573-577.
- (75) Fink, A. L.; Calciano, L. J.; Goto, Y.; Kurotsu, T.; Palleros, D. R. *Biochemistry* **1994**, *33*, 12504-12511.
- (76) England, J. L.; Haran, G. *Ann. Rev. Phys. Chem.* **2011**, *62*, 257-277.

5. Investigation of the Heterogeneous Hydration and Solvation Dynamics of Binary Mixtures of Water and a Small Hydrophobic Molecule 1,2-Dimethoxy Ethane

We explore properties of water (both structure and dynamics) in its binary mixtures with a small hydrophobic molecule 1,2-dimethoxy ethane with a combined experimental (THz TDS (0.3-1.6 THz), TCSPC and mid- and far-infrared FTIR spectroscopy) and classical MD simulation study. Our aim is to understand the evolution of the structure and dynamics of water over the entire concentration region. We found a non-monotonic nature in the cooperative hydrogen bond dynamics as well as in solvation dynamics of water as obtained from Debye relaxation of TTDS data and TCSPC measurements respectively. The concentration dependence of the reorientation times of water, calculated from the MD simulations also captures such non-monotonous character. The MD simulation trajectories reveal presence of large amplitude angular jumps, which dominate the orientational relaxation. We rationalize the non-monotonous concentration dependent orientational dynamics by identifying two different physical mechanisms which operate at high and low water concentration regions.

5.1 Introduction

Water molecules, in most practical circumstances are found in micro-heterogeneous environments rather than in its pure bulk form. Liquid water is a disordered ensemble of highly polar molecules. It possesses several charming complex properties owing to its three dimensional intermolecular H-bonded networks¹⁻³ which makes water to play ‘the key’ role in many biophysical as well as chemical processes.^{2,3} Perturbation of such H-bond network results in temporal fluctuations, which is the origin of their orientational relaxations⁴ that is governed by the making and breaking of H-bonds.⁵⁻⁸ While the various dynamical modes of pure bulk water has been well understood,⁹ its behaviour in the vicinity of an amphiphilic (i.e. partly hydrophilic and partly hydrophobic) molecule or macromolecular fragment has still been a popular subject in scientific community.¹⁰ A proper apprehension of ‘hydrophobic hydration’¹¹ model is of prime importance in order to understand its behaviour in the real biological milieu. In this regard polymer–water binary mixtures are of potential interest since they could often mimic biological environments¹².

The polymer poly (oxyethylene) (POE) is a perfect candidate to model such systems owing to its varied conformational properties,¹³ amphiphilic character and high solubility in

water.¹⁴ The interaction pattern of water with POE changes with the composition of the mixture,¹⁵ and this phenomenon provides with a unique opportunity to study water dynamics in varied hydrophobic environments without essentially altering the chemical nature of the system. DME is the shortest ether molecule and the building blocks of the POE family.¹⁶ The choice of this solvent is justified from its unlimited solubility and stress free hydration in water which allows probing the entire concentration range in which water evolves from being a solute to a solvent. Oligomers of DME, namely PEO (or PEG), has tremendous technological importance with wide spread applications¹⁷⁻¹⁹ mostly due to their water solubility, flexible structure, non-reactivity and low toxicity. It has been shown that the H-bond distribution in water-PEO and water-DME mixtures are comparable, and therefore, studies on water-DME binary mixture could provide meaningful insights into the otherwise complex water-polymer interactions.²⁰ Such small amphiphilic polymer units in aqueous environments provides with a model platform for studying the highly debated phenomenon of “hydrophobic hydration”.^{15,21-23} Moreover, DME ($\text{CH}_3\text{-O-CH}_2\text{-CH}_2\text{-O-CH}_3$) is structurally related to two water insoluble hydrophobic polymers: poly-(oxymethylene), with one $-\text{CH}_2$ group less in the monomer unit, and poly-(oxytrimethylene), with one $-\text{CH}_2$ group more.²⁴ DME-water mixture has been a subject of various experimental investigations including NMR relaxation,²⁵ FTIR,²⁶ Raman spectroscopy,²⁷⁻²⁹ volumetric and thermodynamic measurements³⁰ as well as several simulation studies.³¹⁻³⁶ Previous studies have revealed that many macroscopic thermodynamic parameters of this binary mixture, e.g., viscosity,³⁷ partial molar volume³⁰ including some microscopic parameters like diffusion coefficient³⁶ pass through an inflation point in the composition profile, which clearly identifies the micro-heterogeneous environment of the mixtures. While most of these aforementioned studies have been carried out addressing the conformational changes of DME, the associated changes in structure and dynamics have received comparatively lesser attention.

We explore the OD stretching mode of water to investigate the structure of water in its mixture with DME at varied compositions using FTIR spectroscopy in the mid-IR region. We have also studied the collective vibrational modes of water which essentially leaves their imprint in the far-infrared (FIR) frequency region using FTIR measurements. The evolution of the cooperative dynamics of water in the mixture is explored using TTDS technique in the frequency window of 0.3-1.6 THz ($1 \text{ THz} \approx 33.3 \text{ cm}^{-1}$). TTDS is a label free tool that can probes the collective hydration dynamics of water which extends beyond the first few hydration layers and essentially leaves its imprint in this elusive THz frequency region.^{38,39} This technique thus offers a unique advantage to examine the fate of the H-bonded network

dynamics of water in otherwise less polar environments including biological interfaces.⁴⁰⁻⁴³ Various frequency-dependent optical parameters of the solution such as absorption coefficient, $\alpha(\nu)$, complex refractive index, $\tilde{n}(\nu)$, complex dielectric constants, $\tilde{\epsilon}(\nu)$ etc. can be extracted from a single measurement⁴⁴ and the dynamics of water can be obtained following a *Debye relaxation model*.⁴⁵ The composition of the mixture is varied carefully and since one of our major emphases is on the low water content region where water is expected to be present mostly in its isolated form; such an environment experimentally reproduces the notion of ‘*hydrophobic hydration*’. It has been observed that the collective dynamics of water shows a non-monotonous behaviour as a function of the mixture composition.

DR study provides information about the collective response of polarization relaxation of dipolar solvents, is often complemented by time-resolved fluorescence (TRF) measurements which is more sites specific in nature and could often found to be of better relevance for specific processes. Time-resolved fluorescence spectroscopy (TRFS) manifests the stabilization of instantaneously created solute dipoles (fluorophore) by the reorientation of solvent dipoles. We study ps-resolved solvation dynamics of DME/water binary mixtures using coumarin 500 (C500)⁴⁶ as the fluorophore. While TRFS has extensively been employed to understand unusual hydration in many binary mixtures⁴⁷⁻⁵⁰ no such study is reported for the DME-water mixtures. Since water can form H-bond to both neighbouring water as well as DME, one could apprehend microscopic heterogeneity in the mixture, which in turn is expected to provide its imprint in the TRFS measurements.

In order to acquire a further molecular level apprehension of micro-heterogeneity in the H-bonded structure we perform all-atom classical MD simulation of water-DME mixed systems. MD simulation is an incisive tool to study these binary mixtures as it provides a complete molecular picture of microscopic mechanisms involved, at the same time it is also possible to calculate quantities that can be directly compared with experimental measurements.^{51,52} There exist complementary theoretical⁵³ and MD simulations^{54,55} studies that looks at the properties and H-bond connectivity of the solute (not water) molecules and relate that to the static and dynamic anomalies and non-idealities of the mixtures. The MD simulation results show that the structure of water evolves from linear H-bonded chains at low water concentrations to a bulk tetrahedral like network structure at higher simulated concentrations. Investigation of the concentration dependence of the time-scales associated with the re-orientational and translational motion calculated from MD trajectories reveals a non-monotonic dependence on water concentration. We present an explanation of this

observed non-monotonicity by identifying two different physical mechanisms which manifest at low and high water concentrations.

5.2 Materials and Methods

DME, D₂O and benzonitrile (PhCN) were purchased from Sigma Aldrich (stated purity 98%). Binary solutions were prepared using deionize Milli-Q water. All the experiments were done in room temperature. MIR-FTIR spectroscopy measurements were recorded in a JASCO FTIR-6300 spectrometer using two CaF₂ windows (3 mm thickness) with the spacer thickness of 25 μm, in the frequency region of 2200–2250 cm⁻¹ (CN stretching mode) and 2250-2700 cm⁻¹ (OD stretching mode). Samples were prepared by vigorous mixing of 2% PhCN and 4% D₂O with the binary mixtures. All the data represented here are difference absorbance spectra where the absorption spectrums of the corresponding DME/water binary mixtures were used as the references. FTIR spectra in the FIR region (50-350 cm⁻¹) were recorded using VERTEX 80v under constant nitrogen gas flow. The samples were measured with a liquid cell (model A145, Bruker Optics) with diamond windows, a cell path length of 28.5 ± 0.2 μm, as defined by a Teflon spacer placed between two parallel windows. The FIR spectra also correspond to the difference absorbance between the measured absorbance of the samples and the measured absorbance of pure DME. Steady-state emission spectra were measured with a Jobin Yvon Fluorolog fluorimeter (Fluoromax-3). We used a non-covalent fluorescent solvation probe C500 at very low concentration (~4 μM). Time-resolved emission measurements were performed using a previously described⁵⁶ commercially available TCSPC instrument with an overall instrument response function (IRF) ~ 80 ps. We perform all-atom classical MD simulations of DME and SPC/E water binary mixtures using force-field as described elsewhere.^{5,33,35} Further details about the instrumental as well as simulation methods are available in *chapter 2 and chapter 3*.

5.3. Results and Discussions

5.3.I. Experimental Findings:

MIR (OD stretching) study: OD vibrational stretch in MIR region (2400–2700 cm⁻¹) of HOD oscillators is highly sensitive to the strength of the local intra and inter-molecular H-bond,^{57,58} is an ideal tool to study solute hydration. It is to remember that the difference absorbance spectra reported here (figure 5.3.I.1) involve explicitly the signature of water molecules only. Figure 5.3.I.1a represents the O-D stretching of HOD in pure water and in water-DME mixtures at different mole fraction of water (X_w). Pure water yields an broad (~170 cm⁻¹

FWHM) absorption band with peak value at 2505 cm^{-1} (designated as ν_w).⁵⁹ This peak suffers a progressive blue shift with an associated asymmetric deformation of the absorption profile as we increase DME content. These are especially prominent in the low water content region.^{15,28,41,60} The observed blue shift can be explained in terms of the reduction of the electric field along the OD stretch⁶¹ as well as weakening of the H-bond strength,^{15,25} the effect being more prominent in the low water content region where enhanced DME-water H-bond formation prevails.

In order to obtain a quantitative insight about the H-bonding states we deconvolute the absorption spectra of DME-water mixtures into three Gaussian sub-bands. For a comparative understanding we keep one peak fixed at 2505 cm^{-1} corresponding to bulk water.^{28,41} Two such representative spectra for $X_w = 0.03$ and 0.6 are presented in figure 5.3.I.1b. For the systems with $X_w \geq 0.8$, the spectra can be fitted with two such Gaussian sub-bands; apart from the bulk water (2505 cm^{-1}) band, a new blue shifted band appears (designated as ν_2) furnishing the evidence of water-DME H-bond formation which in turn weakens the water-water H-bonds. The frequency ν_2 gradually increases with decreasing X_w (figure 5.3.I.1c) which signifies an increase in the number of DME-water H-bonds formation with increasing DME content. In low water content region ($X_w \leq 0.6$), the total spectra could only be fitted considering a new band (designated as ν_1) appearing around $\sim 2610\text{ cm}^{-1}$ region. This band is associated with the vibrational stretch of isolated or uncoordinated water molecules that share H-bonding with DME oxygen atoms only or water molecules that do not share any H-bond with any neighbouring molecule.^{62,63} The water/DME binary mixtures thus correspond to three types of water molecules associated with three different Gaussian peaks, ν_w , ν_2 and ν_1 . The relative abundance of these three types of water could approximately be estimated by calculating the relative area under each Gaussian band that contributes to the observed spectra. The relative population profile is provided in figure 5.3.I.1d. We found that at high water content the population is effectively governed by the bulk like water (ν_w) with a steady growth of the ν_2 population. Whereas, in low water content region water molecules contribute primarily to the frequencies around ν_1 and ν_2 and as a result the contribution around ν_w is decreases for these water concentrations.

At low DME concentrations, ($0.8 \leq X_w \leq 1$) DME molecules fit themselves into a slightly distorted network structure of liquid water. The average maximum hydration number per ether oxygen of DME is ~ 1.8 ,⁶⁴ as revealed previously by Brillouin light scattering and sound velocity measurements, which corresponds to $X_w \sim 0.8$. It can be concluded that in this

region all the DME molecules are fully hydrated and can fit themselves in a slightly deformed H-bonded water cage. On further increase in the DME content the bulk water contribution decreases considerably only to be compensated with a concomitant increase in the ν_1 water content and where the ν_2 population is modestly increased. It could be noted that with increasing DME concentration the number of water molecules available to hydrate DME molecules decreases. As a result the fully H-bonded water network structure melts down to form ν_2 and ν_1 water molecules.²⁵ At $X_w < 0.1$ the ν_1 water contributes significantly with negligible abundance of bulk water. However, a notable abundance of ν_2 type of water even in this small water content indicates the presence of discrete water clusters^{15,28} which also gets support from the MD simulation results (see later).

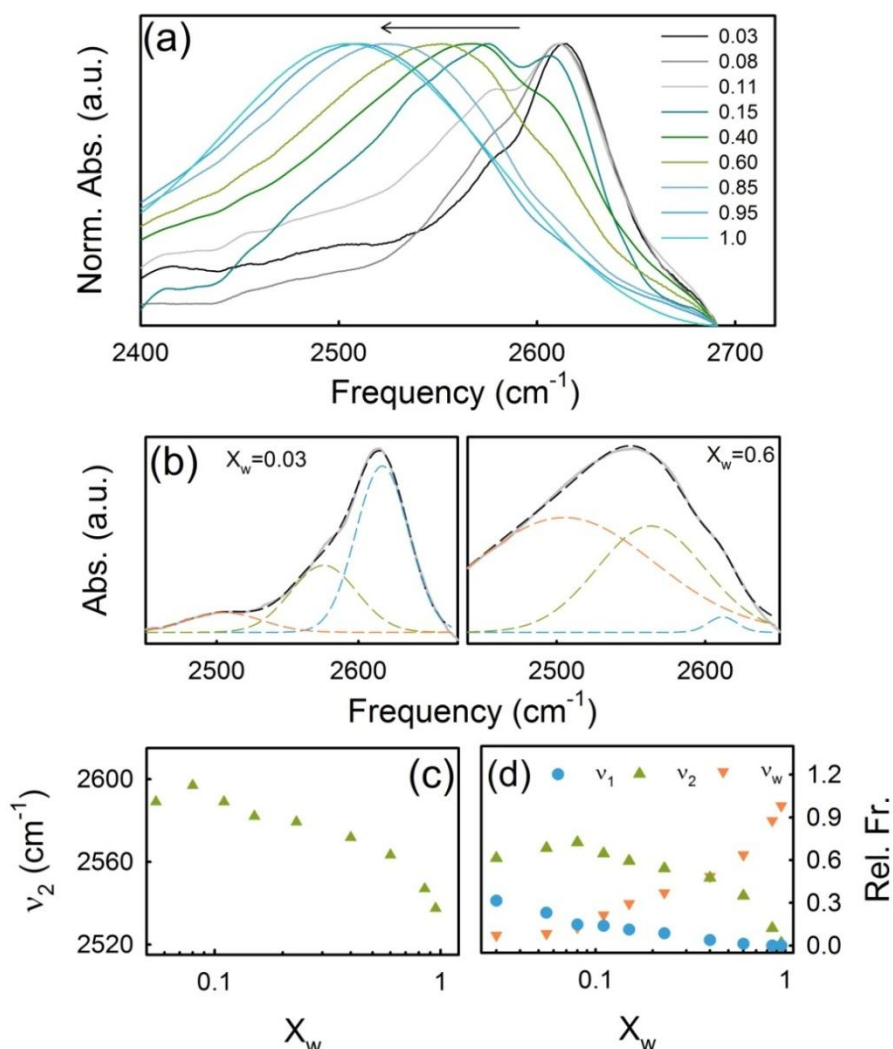


Figure 5.3.I.1 (a) FTIR absorption spectra of the OD stretch of HOD in water for water/DME mixtures at different mole fractions of water (X_w) ranging from 0.03 to 1.0. The arrow indicates increasing water content. (b) Deconvoluted O-D stretching spectrum of HOD in water-DME mixture at $X_w = 0.03$ and 0.6. The orange broken line is centred at 2505 cm^{-1} and corresponds to bulk water. The black broken line represents the overall fitting. (c) Peak frequency ν_2 as a function of X_w . (d) Relative population of different types of water present at different water/DME mixing ratios.

MIR (CN stretching) study: As discussed previously FTIR experiments in the mid IR region provide meaningful information about the H-bonding status and can sense the polarity of the environment.⁶⁵⁻⁶⁷ Nitrile ($C\equiv N$) is an efficient IR spectroscopic probe to investigate the intermolecular interactions, solvent polarity, and formation of non-covalent H-bonding in liquids⁶⁵. Figure 5.3.I.2a shows the MIR absorption spectra of PhCN in water/DME binary mixtures at various X_w . DME being a relatively less polar molecule ($\epsilon_s \sim 7$) can hardly form H-bond with its neighbouring PhCN molecules and the IR peak frequency (ν_{NHB}) for the unbound CN molecules in DME continuum is observed at $\sim 2229 \text{ cm}^{-1}$. On the other hand, the protic solvent water generously forms H-bond with CN and the IR peak suffers noticeable blue shift to appear at $\nu_{HB} = 2235 \text{ cm}^{-1}$. The IR peak (ν_{peak}) profile exhibits a non-monotonic nature in the binary mixtures (figure 5.3.I.2b). We observe that in low X_w region (from pure DME to $X_w \sim 0.6$) ν_{peak} suffers nominal red shift while on further addition of water, at $X_w > 0.6$ ν_{peak} increases sharply (figure 5.3.I.2b). The mixed system thus offers significant deviation from the otherwise expected ideal linear mixing behaviour^{5,68}. IR characteristic of nitriles is driven mostly by solvent induced changes in the local electric field of the environment.^{65,69}

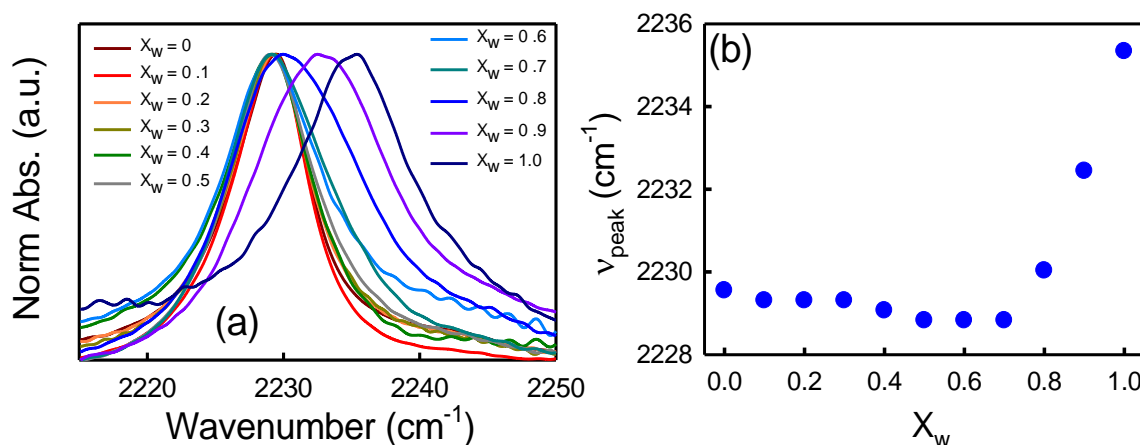


Figure 5.3.I.2. (a) FTIR absorption spectra of CN stretch frequency of PhCN in DME-water solutions at different mole fraction of water. (b) The absorption maxima are plotted as function of the mole fraction of water.

In conventional IR probes (e.g. OD or CO), as one increases water content, the probe bond length increases due to the extensive H-bonding and eventually the IR peak frequency suffers red shift.^{5,68} However, the length of the strong triple covalent CN bond could hardly be perturbed by relatively weak non-covalent H-bonding. As water molecules form H-bonds with the N terminal (H-bond acceptor) of PhCN, the partial charge difference between C and N decreases. Hence the effective dipole moment of CN decreases increasing the corresponding potential energy which eventually leads to a blue shift of the IR peak

frequency.⁶⁵ This rationale corroborates with the sharp increase in IR peak frequency in the high X_w region. Whereas, at low X_w region, due to the confinement of water clusters in the vicinity of DME clusters,⁵ free water is less available to form H-bonds with PhCN. A modest red shift is observed in this region due to the increase in the polarity of the medium.

Steady state fluorescence study: Steady state absorption spectra of C500 in the water-DME binary mixtures are shown in figure 5.3.I.3. We found a progressive red shift of the absorption peak with increasing water content.

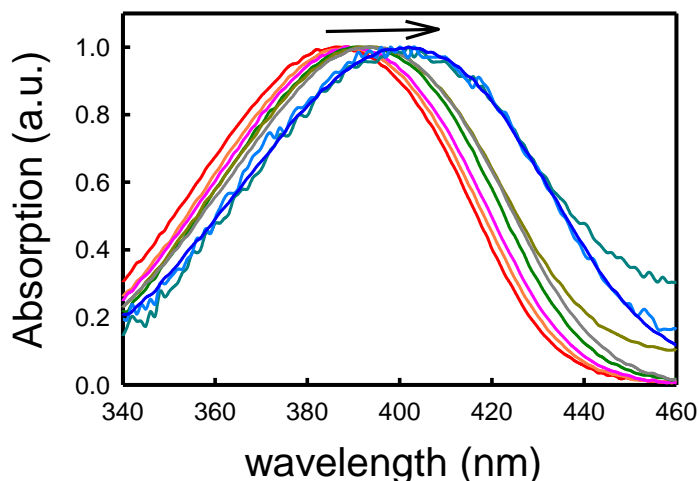


Figure 5.3.I.3. Steady state absorption spectra of cumarin 500 fluorophore in DME-water binary mixtures.

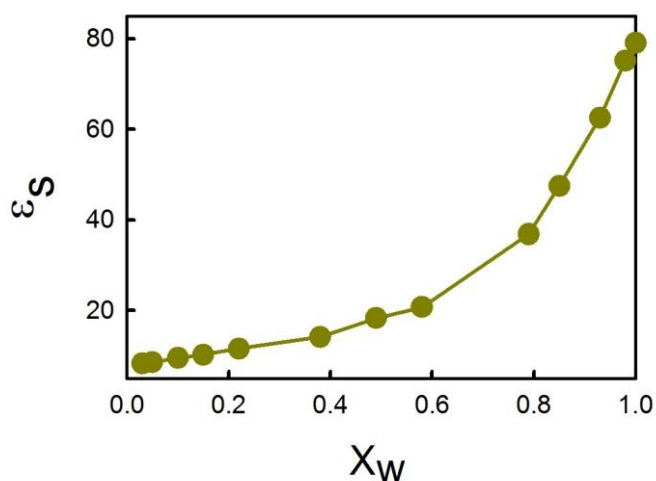


Figure 5.3.I.4. The static dielectric constant of water/DME binary mixtures with different water concentration.

We also observe a progressive red shift of the emission peak with increasing X_w (figure 5.3.I.5). The emission maximum at 459 nm in pure DME appears at 499 nm at $X_w = 0.9$, which in turn is blue shifted compared to the 508 nm peak observed in pure water.⁵⁰ We plot the peak maxima with X_w , and found that the red shift is progressive but not linear. A

distinct change in the slope is observed at $X_w \sim 0.2$. Such red shift has classically been explained as the manifestation of increasing polarity of the mixture.

To rationalized the polarity of the samples we plot the static dielectric constant (ϵ_s) of each mixtures as a function of X_w (figure 5.3.I.4) and observe a non-linear change at $X_w \sim 0.6$. The non-monotonous red shift of the emission peak thus cannot be explained solely on the basis of the change in the dielectric constant in such H-bonded system, rather one also needs to consider that DME has a capability to form extensive H-bonding with the neighbouring water molecules through its two oxygen atoms, which can cause the probe to be distributed in different heterogeneous locations in the mixture and can influence the fluorescence characteristics accordingly. We try to deconvolute the emission profile of C500 in the mixtures with two Gaussian envelopes keeping the centre frequencies fixed at 459 nm (C500 in pure DME) and at 508 nm (C500 in pure water). The spectra could not be deconvoluted into these sub-bands with reasonable accuracy which unambiguously concludes that the probe might also reside at the interfaces of DME and water.

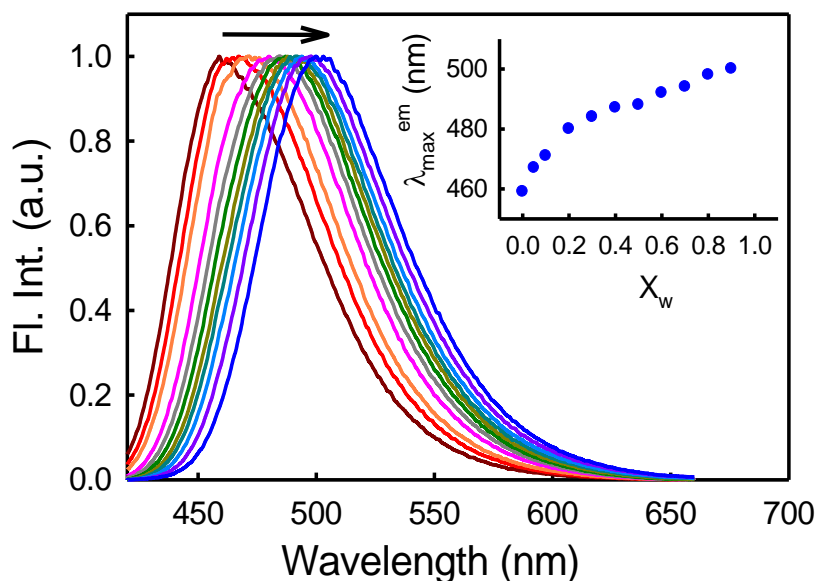


Figure 5.3.I.5. Steady state emission spectra of cumarin 500 fluorophore in DME-water binary mixtures. Emission peak frequencies are plotted in inset as function of mole fraction of water.

TRFS measurements: We measure the wavelength dependent emission transients of C500 in different DME-water mixtures; the tri-exponential fits of these transients reveal that the decay parameters in the blue end differ significantly than those in the red end (figure 5.3.I.6a), which strongly indicates solvation of the probe.⁷⁰ Using the transient fitting parameters and the steady state emission spectra we construct the corresponding time-resolved emission

spectra (TRES) (figure 5.3.I.6b). We, however, could not find noticeable differences in the time-resolved spectra of C500 in the neat liquids (DME and water).

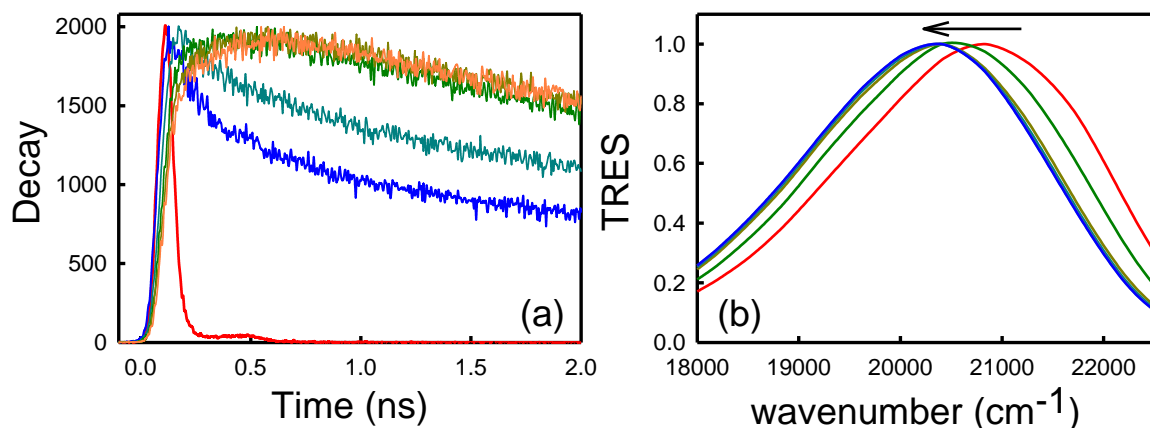


Figure 5.3.I.6. A representative decay and time-resolved emission spectra (TRES) of the DME/water mixture at X_w 0.6.

Solvation of fluoroprobes in neat polar solvents generally occurs in ps to sub-ps timescales^{50,71} which is undetectable in the TCSPC measurements. However, the molecular heterogeneity in the mixed systems hinders the reorientation and/or translational diffusion of the solvents which eventually retards the solvation process to produce considerable dynamical Stokes shift be detected in TCSPC measurements.⁵⁰ All the $C(t)$ curves (as described in chapter 2) are fitted bi-exponentially with time constants of sub hundred and a few hundreds of ps (table 5.3.I.1). It is to be noted that we miss a significant fraction of the ultrafast fluorescence signal due to the limited resolution of the TCSPC setup. We estimate the extent of the loss (instrumental resolution) of our setup using a methodology developed by Fee and Maroncelli,⁷²

$$\tilde{\nu}_{emi}^p(0) = \tilde{\nu}_{abs}^p - (\tilde{\nu}_{abs}^{np} - \tilde{\nu}_{emi}^{np}) \quad (5.1)$$

where $\tilde{\nu}_{abs}^p$, $\tilde{\nu}_{abs}^{np}$ and $\tilde{\nu}_{emi}^{np}$ are the peak absorption frequency of polar and nonpolar solvent and the emissive peak frequency of nonpolar solvent, respectively. We found ~70% of the ultrafast signal, which arises from the bulk water, goes undetected (table 5.3.I.1).

We calculate the average solvation time $\langle\tau\rangle$ and plot it against X_w in figure 5.3.I.7b. $\langle\tau\rangle$ decreases first modestly (up to $X_w=0.6$) and then sharply. The solvation profile can well be rationalized in the light of MIR measurements. In low X_w region, water molecules are rather confined and/or strongly H-bonded in the DME continuum, as inferred from the MIR measurements, which inhibits them to reorient and/or translate in response to the instantaneously created C500 dipole resulting in slow solvation. In the high X_w region (>0.6) the mixture contains DME-free water molecules as indicated by their ability to form

extensive H-bond with the PhCN molecules (figure 5.3.I.2a). Gradual increase in X_w starts forming water molecules which are not H-bonded to more than one DME molecule (see MD simulation results) and can form large clusters with flexible structures around DME molecules. Such water network acts in comparable manner to that of bulk water and are available for the solvation of the excited C500 dipoles, which eventually accelerates the solvation process (figure 5.3.I.7b). The increased missing fraction of the Stokes shift (table 5.3.I.1) is also a manifestation of the fact.

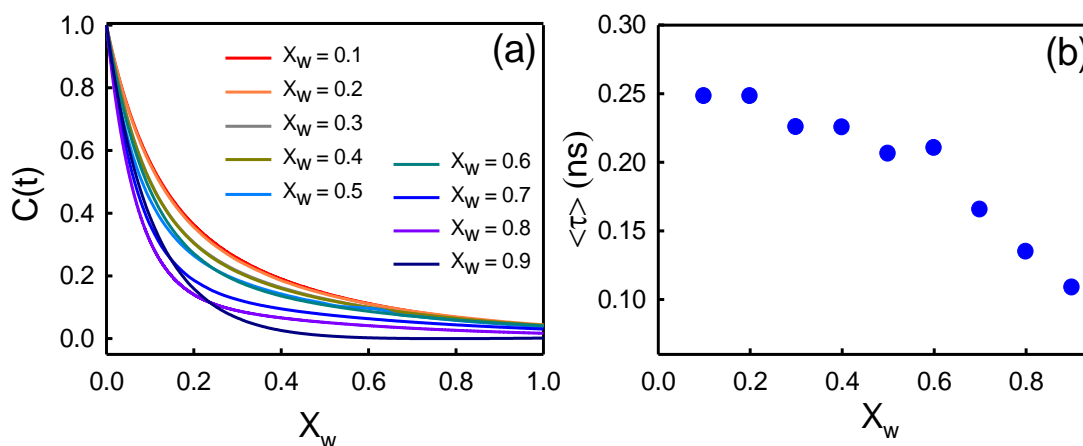


Figure 5.3.I.7. Average solvation timescales as function of mole fraction of water.

FIR study: The energies corresponding to the intermolecular motions that arise due to the fluctuations in the H-bond network are lower than those of intra-molecular covalent bonds. Their spectral signatures range correspondingly shifts to lower wavenumber region. The FIR (50-350 cm^{-1}) spectra (occasionally referred to as the connectivity band⁷³) of water in DME-water binary mixture at different compositions are shown in figure 5.3.I.8a. Water, in the FIR frequency range produces two characteristic peaks, one at $\sim 200 \text{ cm}^{-1}$ which is distinctly collective in nature. It corresponds to the hindered longitudinal motion of water molecules along hydrogen bonds and the other peak occurs at comparatively higher frequency $\sim 650 \text{ cm}^{-1}$. The former peak arises due to acoustic branch (due to the hydrogen bond vibration) while the latter mode one is in the optical band (due to librational motion of water). It is evident from the figure 5.3.I.8a that with increasing water concentration the absorbance increases which corroborates our findings of increasing size of the water clusters. For a more comprehensive understanding of the evolution of the network structure of water, we deconvolute the FIR spectra of different solutions and plot the peak frequency and the full width at half maximum (FWHM) (see figure 5.3.I.8b) of the hydrogen bond stretching vibration band (\sim at 200 cm^{-1}), which is predominantly collective in nature.^{42,74} At low water

concentrations, the band is noticeably red shifted indicating an abundance hetero-molecular hydrogen bond formation.^{60,75} As the concentration of water increases this band gets blue shifted, first sharply and then modestly, along with an increase in the FWHM. The initial sharp blue shift indicates the progressive formation of homo-molecular hydrogen bonds between water molecules (formation of water clusters) which then spread to form an overall tetrahedral network. This evolution of the collective nature of hydrogen bond formation in water is supported from the MD simulation studies also.

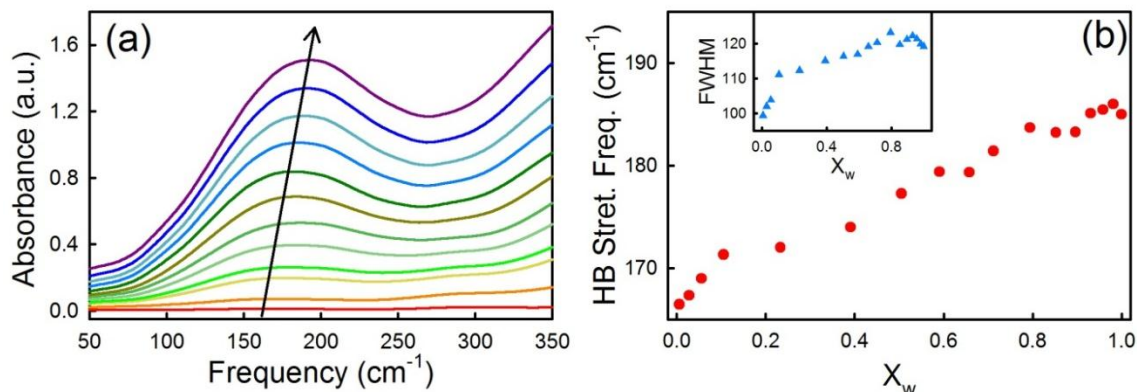


Figure 5.3.I.8. (a) FIR Absorption spectrum of DME aqueous solutions at different mole fraction of water (X_w), the arrow indicates an increasing of water content. (b) The peak frequency of the hydrogen bond stretching mode ($\sim 200 \text{ cm}^{-1}$) in the mixed binary solvent as a function of water concentration. The corresponding change in the FWHM is shown in the inset.

THz TDS study: The optical parameters of water-DME mixtures obtained from TTDS measurements (0.3-1.6 THz) are summarized in figure 5.3.I.9. The frequency dependent absorption coefficient, $\alpha(\nu)$, of water and DME-water mixtures are presented in figure 5.3.I.9a. $\alpha(\nu)$ increases gradually with increasing X_w , the observed increase can be understood considering the replacement of low absorbing DME molecules with high THz absorbing water.⁷⁶ In figure 5.3.I.9b, we plot the absorption coefficient measured at 1 THz, as a function of mole fraction of water X_w for the mixtures. One can estimate the absorption coefficient (α_{ideal}) for an ideal mixture from the following relation,^{41,52}

$$\alpha_{ideal} = \frac{\rho_{real}}{\rho_{ideal}} \sum_i \phi_i \alpha_i(\nu) \quad (5.2)$$

where ϕ_i is the volume fraction of the i -th species, ρ_{real} is the measured density of the mixture and $\rho_{ideal} = \sum_i X_i \rho_i$.

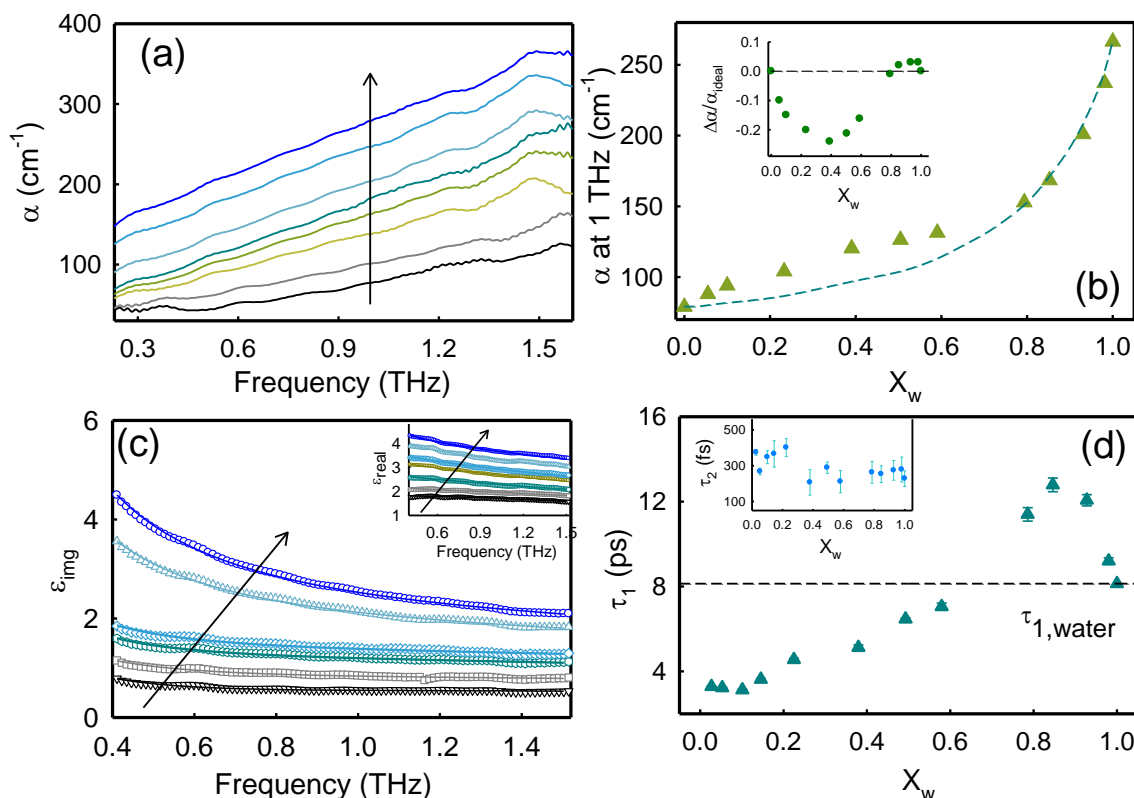


Figure 5.3.I.9. (a) Frequency dependent absorption coefficient (α) of water-DME mixtures. (b) α value measured at 1 THz as a function of X_w . The broken line represents calculated α_{ideal} of the mixture assuming an ideal mixing. The inset shows the extent of deviation from the calculated values. (c) Real (ϵ_{real}) and imaginary (ϵ_{img}) dielectric constant of water-DME mixtures at different mole fractions of water in the THz region. The solid lines represent the triple Debye relaxation fittings. (d) Debye relaxation time scales (τ_1 and τ_2) as a function of X_w . The broken line is a measure of cooperative hydrogen bond relaxation time of pure water. All the arrows indicate increasing water mole fraction in the mixtures.

We include the value of α_{ideal} values in the same plot. It is evident that the measured values deviate significantly from the calculated ones, especially in the low water content region. The inset of figure 5.3.I.9b shows the relative deviation of α ($\Delta\alpha = \alpha_{ideal} - \alpha_{real}$) with X_w , and the non-ideal behaviour of the mixture seems evident from it. Such non-idealities in the low water concentration region has previously been observed for water-dioxane⁴¹ and water-acetonitrile⁵² mixtures. The deviation of this ideal behaviour at low X_w also reciprocates the MIR results which show clear evidence of the existence of isolated or uncoordinated water. For high X_w mixtures, the deviation of α from ideality is marginal (figure 5.3.I.9b, inset). It is now interesting to investigate whether the observed non-ideal to near-ideal transition would also be reflected in the corresponding hydration dynamics.

The frequency dependent real and imaginary permittivity profiles of water-DME mixtures at different compositions are presented in figure 5.3.I.9c. Both ϵ_{real} and ϵ_{img} show

gradual increase with increasing X_w (in the direction of the arrow in figure 5.3.I.9c). The complex dielectric profiles have been fitted using the triple *Debye relaxation model*.^{45,77,78} We fixed the static dielectric constant (ϵ_s) value from the literature.⁷⁹ The fitted parameters are presented in table 5.3.I.2. Dielectric spectra of pure water in THz region reveals three relaxation time scales of ~ 8 ps (τ_1), ~ 200 fs (τ_2) and ~ 90 fs (τ_3). The ~ 8 ps timescale associated with the spontaneous restructuring of the H-bond network,^{80,81} whereas the ~ 200 fs timescale is due to either quick jumps of under-coordinated water or a small angular rotation preceding a large angle jump.^{7,82} The ~ 80 fs timescale is related to the 60 cm^{-1} vibrational band responsible for the H-bond bending and the transverse acoustic phonons which propagate in a direction normal to the H-bonds from one water molecule to other.^{83,84} We plot τ_1 and τ_2 as a function of X_w in figure 5.3.I.9d. The τ_1 profile has two distinct features. For $X_w \leq 0.6$, the τ_1 values lie well below $\tau_{1,\text{water}}$ and increases linearly with increasing X_w . As discussed earlier this mode is assigned to the cooperative relaxation of H-bond network and at these concentrations the associated timescale is much smaller than that of pure water. This occurs due to the rupture of the tetrahedral H-bonding network and is also observed for reverse micellar waterpool.⁸⁵ At such low water content the dynamics is found to be 3-4 times faster than the bulk water. This indicates the lack of any cooperative H-bonded network and supports the notion of the formation of under-coordinated water or the formation of some dangling OH. These thoughts also are in agreement with the FTIR measurements and simulation results. With increase in X_w , more water molecules participate in the H-bond network which eventually forms larger water clusters and increases τ_1 .⁴¹ In the region $X_w > 0.6$, an intriguing retardation of the dynamics compared to bulk water, and at $X_w = 0.85$, this slowest timescale becomes as large as ~ 12 ps. The retardation in τ_1 is correlated with DME hydration by solvent water molecules wherein DME-water interaction slows down the cooperative rearrangement of water network and similar effect has previously been observed for sucrose hydration.⁷⁷

In the moderate to high water concentration region ($X_w \geq 0.3$) the obtained τ_2 values are more or less comparable to bulk water timescale and the changes are within the error bar associated with the experimental measurements and the fitting programme. In the low X_w region the observed values of τ_2 are somewhat slower than that of $\tau_{2,\text{water}}$, a behaviour contrary to what has been observed for τ_1 . This apparent dissimilarity can be rationalized from the different origins of these two timescales. As mentioned earlier, while a cooperative rearrangement is responsible for the timescale τ_1 , τ_2 essentially originate from a small angular

rotation of water molecules followed by a jump. At low X_w , the water molecules are primarily bonded to one or more DME molecules, which perhaps hinder the small rotation and jump dynamics and thus slowdown τ_2 . At a higher X_w , when the formation of water cluster predominates, the jump motion gradually gets eased and τ_2 approaches $\tau_{2,\text{water}}$. TTDS studies thus establish the evolution of collective hydration dynamics as water switches from being solute to a solvent in the mixture. Such transition can be explained by apprehending a structural transition from small water clusters to a fully grown H-bonded structure.

Table 5.3.I.1. Solvation relaxation parameters of C500 in DME-water binary mixtures at different mole fraction of water

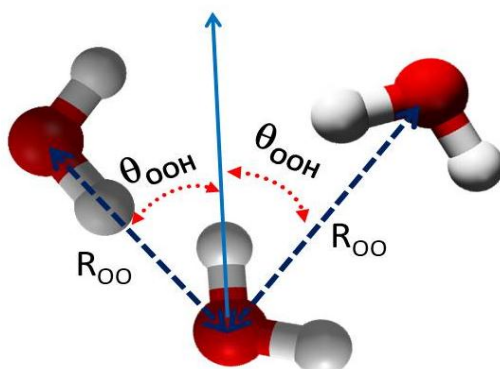
X_w	a_1	τ_1 (ns)	a_2	τ_2 (ns)	$\langle\tau\rangle$ (ns)	Loss (%)
0.1	0.51	0.097	0.49	0.403	0.248	79
0.2	0.56	0.099	0.44	0.433	0.248	72
0.3	0.63	0.089	0.37	0.457	0.225	59
0.4	0.64	0.089	0.36	0.465	0.225	67
0.5	0.65	0.075	0.35	0.448	0.205	65
0.6	0.73	0.093	0.27	0.524	0.210	70
0.7	0.80	0.075	0.20	0.529	0.162	62.
0.8	0.87	0.075	0.13	0.528	0.126	72
0.9	0.42	0.080	0.59	0.128	0.108	90

Table 5.3.I.2. Triple Debye relaxation fitting parameters with error bars for water-DME mixtures at different compositions. We have fixed the value of ϵ_s from literature.

X_w	ϵ_s	τ_1 (in ps)	τ_2 (in fs)	τ_3 (in fs)
0.03	8.29	3.28±0.02	374.5±15.7	88.00
0.05	8.55	3.22±0.02	267.7±18.6	81.00
0.10	9.40	3.12±0.02	347.8±36.5	74.00
0.15	10.19	3.62±0.04	365.7±73.7	94.36
0.22	11.58	4.55±0.06	402.7±62.5	96.45
0.38	14.14	5.12±0.13	206.8±71.0	71.00
0.49	18.22	6.46±0.05	289.0±31.8	78.84
0.58	20.72	7.05±0.17	210.7±61.9	76.32
0.79	36.80	11.40±0.32	262.4±60.6	84.00
0.85	47.46	12.78±0.32	252.9±46.8	78.07
0.93	62.55	12.06±0.27	273.7±54.9	77.30
0.98	75.09	9.20±0.15	278.3±70.0	78.40
1.00	79.05	8.10±0.10	227.6±43.6	71.89

5.3.II. MD simulation study:

In order to obtain some microscopic insight into the concentration dependences, we have performed all-atom classical MD simulation study on the water-DME mixtures at several concentrations. For further details about the analysis methods please see *chapter 3*.



Scheme 5.3.II.1. Geometrical criteria of hydrogen bonding among water molecules.

Hydration structure: To obtain a microscopic realization of the observed structural and dynamical features, classical MD simulation of the DME/water binary mixtures is performed. From the MD trajectories we compute the radial distribution functions (RDF) for various possible pairs of oxygen atoms. The results are shown in figure 5.3.II.1. An oxygen atom could belong either to a DME or to a water molecule. The first peaks for the water-water and water-DME RDF's arise at distances of 2.78 and 3.12 Å respectively. In the mixture the position of the water-DME peak remains almost unaltered indicating that hydration of DME molecules could be achieved without significant perturbation of H-bond network of water molecules. The first peak of DME-DME RDF occurs at 2.9 Å (figure 5.3.II.1), which is higher than that in water-water but smaller than that in water-DME signifying hydrophobically induced aggregation of DME molecules.

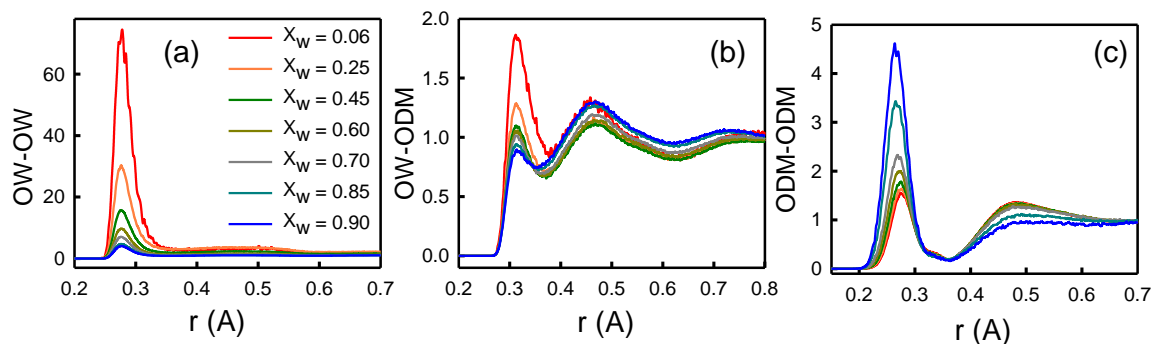


Figure 5.3.II.1. Radial distribution function of (a) water oxygen-oxygen, (b) water oxygen-DME oxygen, (c) DME oxygen-oxygen.

We define “*coordination number*” or “*hydration number*” as the number of neighbours (water molecules) in the hydration shell of DME that are connected to the DME molecules through H-bonds. In figure 5.3.II.2a we display the hydration number of DME molecules as a function of X_w . We have used the geometrical criteria (scheme 5.3.II.1) for deciding whether a pair of molecules is H-bonded or not. Details of the H-bond criteria are provided in *chapter 3*. The hydration number profile shows a nonlinear dependence on X_w (figure 5.3.II.2a). In the low X_w region (<0.6), it increases slowly indicating towards a non-classical hydrophobic hydration of DME.²² On the other hand, beyond $X_w=0.6$ it increases sharply as DME molecules starts forming extensive H-bonds with water and consequently high content ($\sim 80\%$) of open H-bonded structures (see later) are produced. We also calculate the relative abundance of the non H-bonded dangling OH bonds at different water concentrations (figure 5.3.II.2b). Dangling water molecules are identified as those which are H-bonded through one of its OH-hand while the other O-H hand does not participate in any H-bond formation.^{6,86,87} We found that the abundance of dangling bonds is presumably high with more than 20% of water molecules to remain in the dangling state in the low to moderate X_w region. With increasing X_w the relative population of the dangling water molecules decreases gradually.

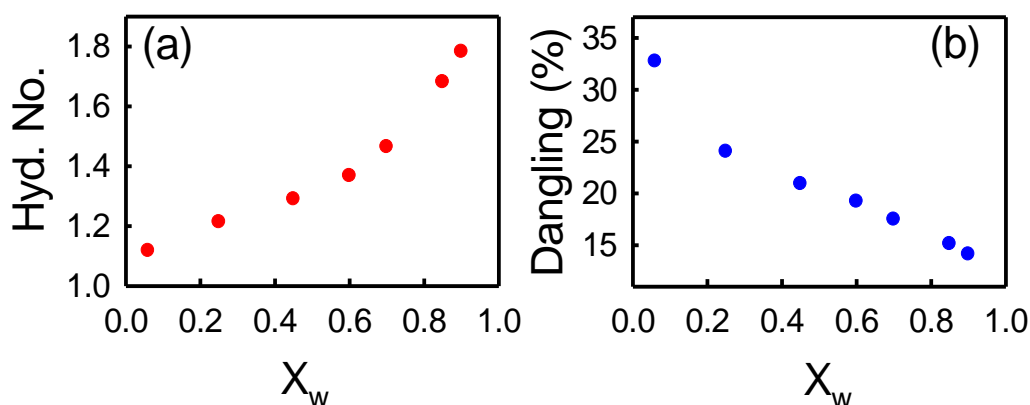


Figure 5.3.II.2. (a) Water concentration dependent average hydration number of DME molecules. (b) The abundance of the dangling H-bond.

Water can donate as well as can accept H-bonds with any other water and/or DME molecule, whereas DME molecules always act as H-bond acceptors. Aggregation of DME molecules can create void spaces that could induce defects in H-bonding network. So it is of utmost importance to examine the relative percentage of H-bond weights. We tag each H-bond formed by any water molecule in the mixture and group them in three possible categories: bonded to water, bonded to DME and non H-bonded or single (figure 5.3.II.3). Water prefers to bind with neighbouring water molecules forming water clusters, however,

water molecules in the vicinity of DME molecules could hardly connect to their polar partners and thus prefer to remain single rather than connected to other DME molecules. This eventually results in a considerable abundance of single and DME-connected water molecules at low X_w (figure 5.3.II.3). With increase in X_w the relative population of these water molecules decreases with a concomitant increase in the H-bonded water abundance.

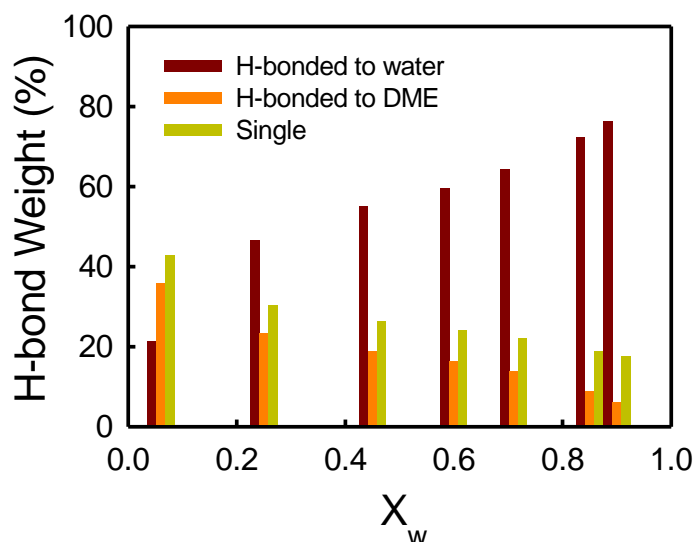
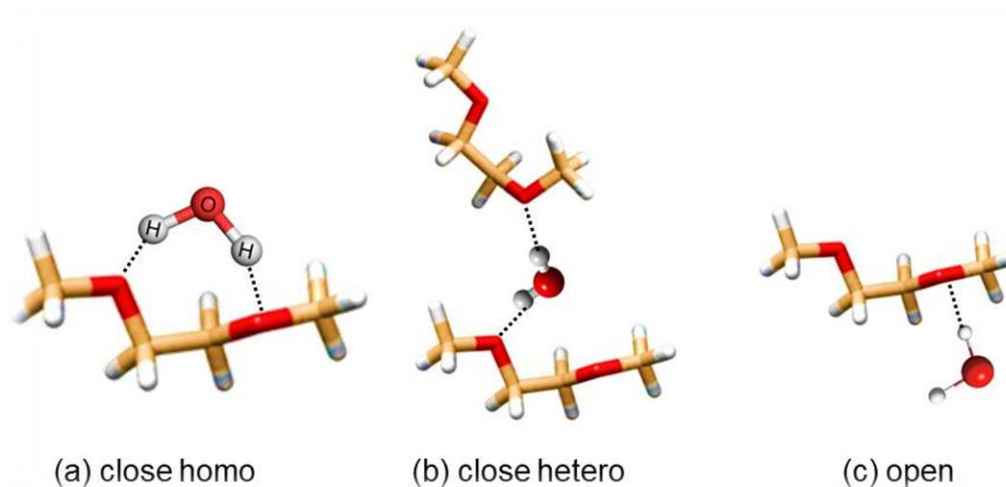


Figure 5.3.II.3. The relative percentage weight of H-bond of water as function of the mole fraction of water (X_w).



Scheme 5.3.II.2. Various degrees of configuration of water molecules in the vicinity of DME molecules, (a) close homo structure, (b) close hetero structure and (c) open structure.

As observed in figure 5.3.II.2, at low X_w there exist under coordinated water molecules in DME continuum with dangling OH bonds. These dangling water molecules are connected to an oxygen atom of neighbouring DME via H-bonding, and correspondingly unable to participate in bulk like H-bond network that results a sluggish solvation of C500 molecules (figure 5.3.I.7). For a detailed microscopic view we divide the hydration status into

three different plausible configuration and identified the relative abundance of those local H-bonded configurations (scheme 5.3.II.2): (a) “*close-homo structure*”, in which a single water molecule is connected to two oxygen atoms of the same DME molecule, (b) “*close-hetero structure*”, where a single water molecule binds to two oxygen atoms of two different DME molecules, and (c) “*open structure*”, in which one of the O-H hands of a single water molecule is connected to a DME oxygen atom, the other O-H hand does necessarily not bind to DME, however, can bind to any neighbouring water molecule or could remain dangling as well. We compute the relative population of all these configurations and the results are represented in figure 5.3.II.4. We found that the population of the *close-homo* structure is rather low (<2 %) in the mixtures even in the very low water concentration regions. Perhaps the oxygen-oxygen distance in DME molecule is not optimally fit for a single water molecule to bridge them. The low abundance of such conformation also corroborates an earlier report which concludes 3-7 water molecules to form chain like structures to bridge the two oxygen atoms of a single DME molecule.²⁵

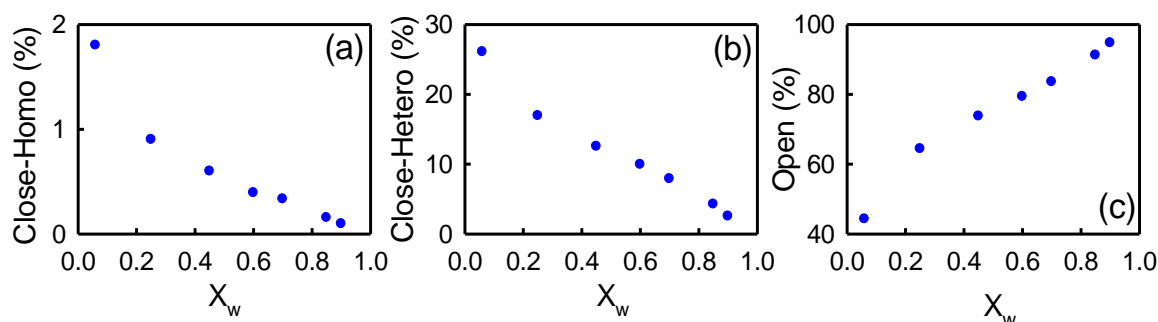


Figure 5.3.II.4. Relative abundance of different structure of water molecules in the close approximate of DME molecules.

It is also noted that the population of *close-homo* structures diminishes with increasing X_w , which is anticipated with the increasing abundance of water into the mixture. At low X_w , the relative populations of *close-hetero* is ~25% and that of the open structure is ~45%, however, with increasing X_w , the former decreases at the expense of the increase in the population of the *open* structures. Relatively high *hetero* structure abundance at low X_w region suggests the encapsulation of water molecules within DME clusters. With increasing X_w such clusters dissolve and DME gets essentially solvated by water molecules. At high X_w , no water molecule is H-bonded to more than one DME molecule (high abundance of *open* structure).

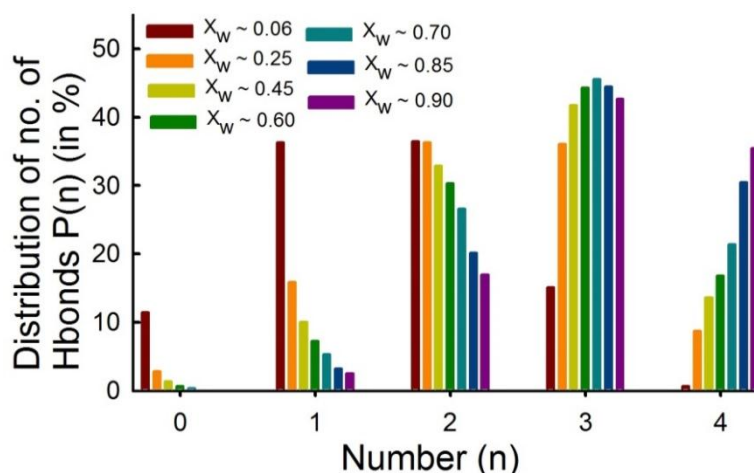


Figure 5.3.II.5. The probability distributions of the number of H-bonds formed by any water molecule in the whole concentration range.

Water molecule can donate two H-bonds through its H-atoms and/or can also accept two H-bonds through the O-atom. Hence it can have a maximum coordination number of four with an approximately tetrahedral arrangement.^{10,88} The possibility of the formation of otherwise stable five member bifurcated H-bond structure is rather low in presence of hydrophobic polymers due to the defect and the fluctuation of H-bond network.⁸⁹ The probability distribution of the number of H-bonds made by individual water molecules can provide with a better understanding of the hydration in presence of hydrophobic solutes. We compute the probability distribution of the number of H-bonds per water molecules in all the mixtures (figure 5.3.II.5). These H-bonds are formed with neighbouring water and/or DME molecules present in the mixture. At low water concentration ($X_w \sim 0.06$) at least 10% of the total water population form no H-bond (remain as single, see figure 5.3.II.3); perhaps these water molecules get arrested in the hydrophobic framework of DME molecular clusters. At low X_w water molecules preferentially stay either in dangling form or in two H-bonded structures. The negligible abundance of three or four H-bonded structure unambiguously confirms the lack of tetrahedral connectivity and abundance of linear water clusters at these concentrations. At moderate to high X_w the water molecules start connecting with each other and form percolating water clusters around DME molecules. The relative growth of the three and four member water signifies the completion of the bulk-like tetrahedrality of the water network.

In order to visualize how the local environment around water molecules changes with X_w we study the properties of clusters of the water molecules at various simulated concentrations. We have used a modified version of the algorithm by Stoddard et al.⁹⁰

(applying the angle cut-off condition along with distance cut-off) to identify the largest H-bonded clusters appearing at each simulated concentration. At very low water concentration ($X_w \sim 0.06$) we find linear water clusters which contain up to six water molecules forming H-bonded chains. Snapshots of the largest water cluster for each simulated concentration are shown in figure 5.3.II.6. The H-bonding structure of these linear clusters supports the inference drawn from the FTIR and TTDS experiments which concluded the existence of water clusters having dangling OH bonds (figure 5.3.II.2b). As X_w increases larger sized water clusters appear with increasing tetrahedral coordination among neighbouring water molecules resulting in non-linear structures. At $X_w=0.25$ we observe water clusters with more complex topologies, where cyclic pentamers of water are a part of the cluster. Eventually one observes bulk like tetrahedrally correlated water clusters upon increase in X_w .

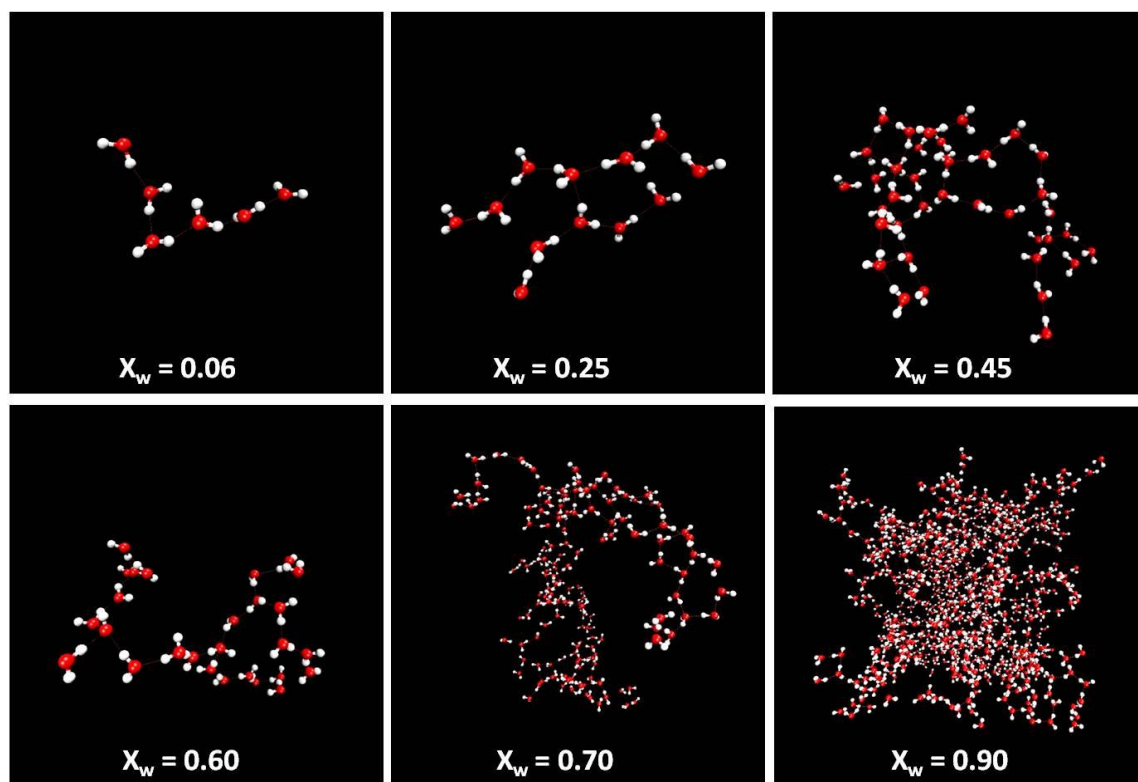


Figure 5.3.II.6. The largest water clusters observed at each simulated concentration. The concentrations of water are mentioned in the respective panels.

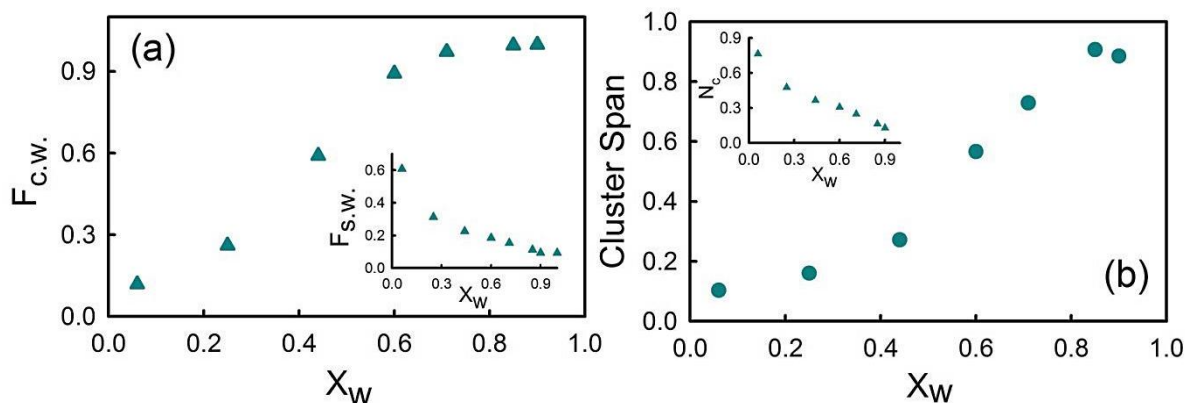


Figure 5.3.II.7. (a) The variation of the fraction of coordinated water ($F_{C.W.}$) and the fraction of single water ($F_{S.W.}$) (in inset), (b) the span of the largest water cluster and the number of clusters in the system (in inset) as a function of the mole fraction of water, X_w .

In order to acquire the microscopic parameters which characterize these water clusters we have calculated, “*fraction of coordinated water ($F_{C.W.}$)*” (figure 5.3.II.7a) which is defined as the ratio of the number of water molecules in the largest cluster to the total number of water molecules. We have also calculated “*fraction of single water ($F_{S.W.}$)*” (figure 5.3.II.7a, in inset) that is the ratio of the number of water molecules that are not H-bonded to any other water molecule to the total number of water molecules. To estimate the spatial extent of these water clusters, we computed the, “*cluster span*” which is the ratio of the longest possible linear dimension of the largest cluster and the diagonal length of the simulation box. The calculated values of these parameters are shown in figures 5.3.II.7a and b as function of X_w . In figure 5.3.II.7b (inset) we have also shown “*fraction of cluster number (N_c)*” that is the ratio of the total number of water clusters in the system to the number of water molecules. At low X_w region, the fraction of un-coordinated water molecule is high enough and that corroborates the MIR OD stretching results (figure 5.3.I.1d). The appearance of different vibrational bands of water in the FIR spectrum (figure 5.3.I.8) can be rationalized by the observation of the small chain like water clusters. These clusters eventually grow with increasing water concentration. It is evident that between $X_w = 0.6$ to 0.8 almost 94% of the total water molecules become the member of the largest water cluster family that nearly spans the whole simulations box. By visually inspecting the dynamics of these clusters we observed that they remain H-bonded upto ~ 5 to 10 ps. The snapshots of the water clusters at various water concentrations indicate that a percolation like transition takes place at $X_w \sim 0.7$ to 0.8 , where the largest water cluster spans the whole simulation box. Percolating water clusters are known to have important consequences on the functioning of biological molecules.⁹¹⁻⁹³

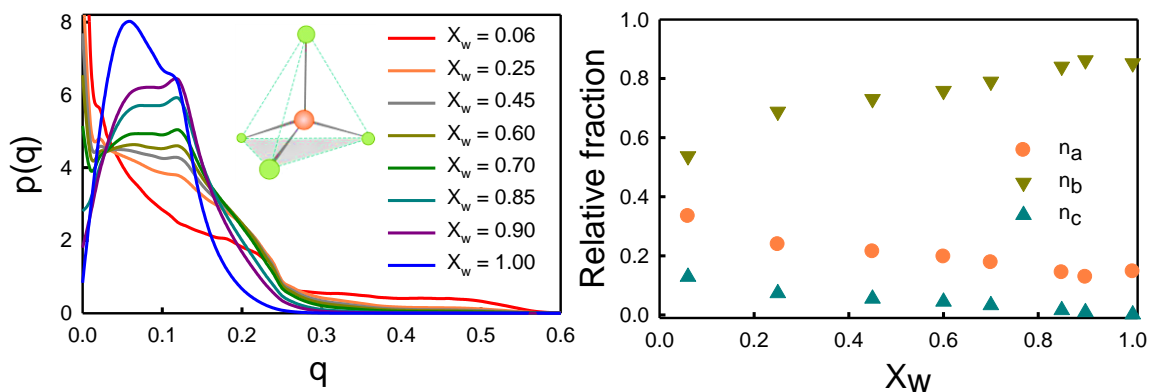


Figure 5.3.II.8. The distribution of the tetrahedral order parameter, $p(q)$ (left panel) and the population of various types of water (right panel) at all simulated water concentrations.

In figure 5.3.II.8 (left panel) we calculate the tetrahedral order parameter which shows that as we decrease X_w , the population of the “bulk-like” water decreases, which migrates towards the “ice-like” (more ordered) as well as to the disordered regions. The distribution of q , $p(q)$, is qualitatively different for water concentration at $X_w = 0.06$ and $X_w = 1$, which indicates a complete disruption of the “bulk-like” tetrahedrality at low water concentrations which corroborates our FIR results. In right panel of the figure 5.3.II.8 shows the evolution of the relative populations n_a , n_b and n_c as a function of the water concentration X_w (for definition of n_a , n_b and n_c see *chapter 3*). With increasing DME content bulk like tetrahedrality transform to both the “ice-like” and “non-tetrahedral” arrangements.⁹⁴ To understand the primary experimental observation, as obtained from TTDS measurements, which shows a non-monotonic dependence of the collective reorientational timescales on water concentration (X_w). We also calculate the single particle reorientational time-scales from simulated *orientational correlation functions (OCF)*. Strictly speaking these single particle reorientation timescales⁹⁵ and the timescales extracted from TTDS measurements are different in their origin. The TTDS experiments probe the rate of change of the collective dipole moment auto-correlation function in response to an externally applied time-dependent electric field, which is related to the relaxation time of the collective dipole moment. The single molecule reorientational times, estimated from MD simulations, also contain multi-body effects as they are calculated in “exact” way from the dynamics of the tagged molecule in presence of other molecules in the system. Several conceptual difficulties arise when one tries to correlate the single molecule reorientation relaxation time (a microscopic time-scale) and the collective relaxation time (a macroscopic time-scale).⁹⁶⁻⁹⁸ However, given the fact that effects of single molecule reorientation times obtained from MD simulations already contains significant

multi-body correlations, we expect that the concentration timescales will also exhibit the non-monotonicity dependency with water concentration. The orientational time correlation function (tcf) are computed by using the following expression^{67, 68}

$$C_n(t) = \langle P_n[u_{OH}(0) \cdot u_{OH}(t)] \rangle \quad (5.3)$$

where P_n is the n^{th} -rank Legendre polynomial and u_{OH} is an unit vector along the OH-bond direction vector. The relaxation dynamics of these OH vectors is bi-exponential in nature with two distinct time scales, one shorter (faster timescale ~ 0.1 -1 ps) and another larger timescale in the range of (4-8 ps).

The computed orientational correlation functions provide very important guideline for interpreting the timescales obtain from experiments. The anisotropy decay measured from pump-probe IR spectroscopy^{9,99} approximately correlate with the time dependence of $C_2(t)$ and the corresponding timescales agree well with the experimental results.^{7,95} We have calculated the first and the second rank orientational time correlation functions $C_1(t)$ and $C_2(t)$ and the results are shown in figure 5.3.II.9a and c and the corresponding bi-exponential fitting parameters are presented in tables 5.3.II.1 and 5.3.II.2 respectively. The concentration dependent time scales extracted from bi-exponential fits of these OCF are presented in figures 5.3.II.9b and d. The two time-scales associated with the orientational correlation functions (reorientation relaxation) show non-monotonic dependence with X_w . This behaviour qualitatively mimics the experimental scenario. We try to figure out microscopic reasons for this observed non-monotonic behaviour.

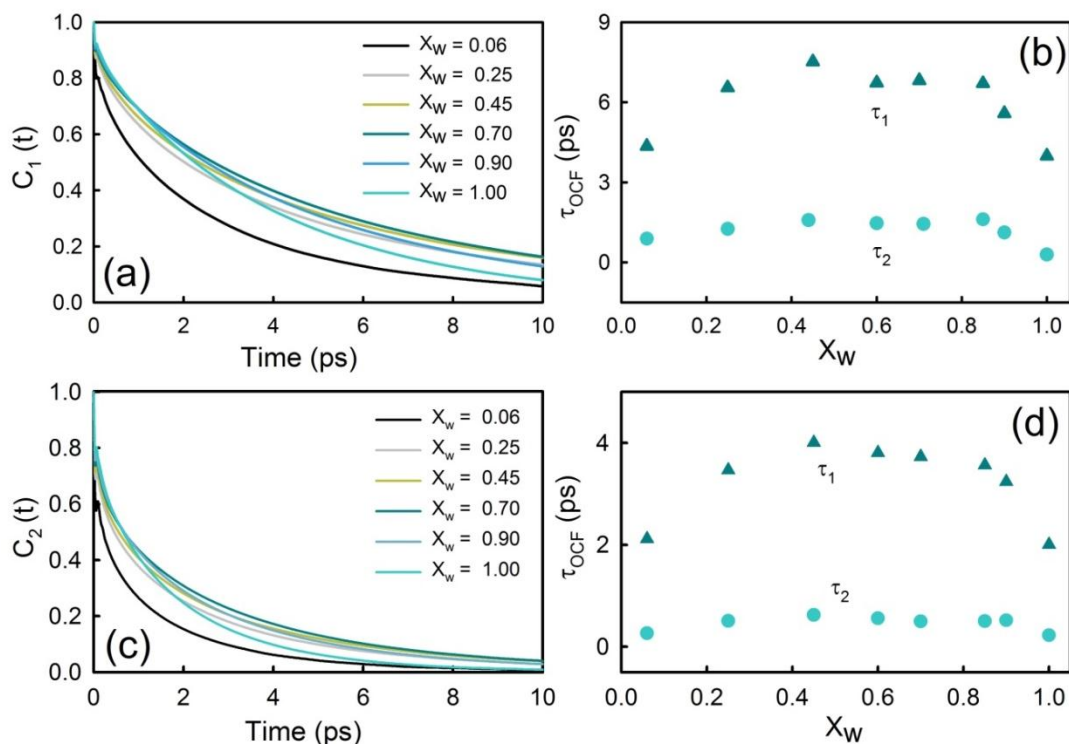


Figure 5.3.II.9. (a) the 1st order and (c) the 2nd order orientational time correlation function $C_n(t) = \langle P_n[\mathbf{u}_{OH}(0) \cdot \mathbf{u}_{OH}(t)] \rangle$, where P_n is the n -th order Legendre polynomial and \mathbf{u}_{OH} the rotating OH bond direction, are calculated with the ensemble of all OH bonds from MD simulation. The bi-exponentially fitted timescale of the 1st (b) and 2nd (d) τ_{OCF}

The single molecule reorientation behaviour of molecules in liquid water has its own peculiar features, owing to the extensive hydrogen bonding in water. It has been shown in a set of very important publications^{7,95,100} that driven by the fluctuations in the hydrogen bond coordination, water molecules reorient via a combination of orientational diffusion and large amplitude angular jumps. This picture of molecular reorientation is quite different from the traditional Debye picture of orientation and has led to the reinterpretation of several experimental data, particularly the understanding of the quasi-elastic neutron scattering (QENS) spectra of liquid water.¹⁰¹ It has been recently shown that both aqueous⁹⁵ and non-aqueous¹⁰² H-bonded fluids exhibit orientational jumps and during these jumps the translational degrees of freedom of the rotating molecule and its initial and final H-bond acceptor are strongly coupled to the rotational degrees of freedom of the orienting molecule and one cannot occur without influencing the other one. During the orientational jump the initial H-bond acceptor recedes from the first hydration shell of the rotating molecule to the second and the final H-bond acceptor moves in from the second to the first shell.

The ratios of the timescales associated with the decay of the orientational correlation functions provide an important insight into the detailed nature of the orientational dynamics.

For purely diffusive reorientational motion the time-scale associated with the n -th order orientational correlation function is related to the rotational diffusional constant (D) by the following relation,^{95,102}

$$\tau_n = \frac{1}{n(n+1)D} \quad (5.4)$$

This implies that for purely diffusive (Debye like) reorientational process the ratio of the characteristic timescales of decay of the first and second order reorientational correlation functions is 3.^{95,102} In the present system the ratio of the longer timescales associated with $C_1(t)$ and $C_2(t)$ is found to be ~ 2 for all the simulated concentrations (see table 5.3.II.3), a value which indicates a marked deviation from the Debye diffusion model and indicates the presence of large amplitude angular jumps. This points to a break-down of the picture of continuous hydrodynamic reorientation at short timescales and these orientational jumps are observed in aqueous (bulk water, confined water¹⁰³, ionic solutions¹⁰⁴ etc.) and non-aqueous (deep-eutectic mixtures^{105,106}, ionic liquids¹⁰⁷ etc.) liquids.^{7,95} Although the deviation of the ratio of the longer timescales from three is a rough pointer towards the presence of orientational jumps, a conclusive proof of the existence of the jump reorientations is presented in figure 5.3.II.10. Panel (a) depicts the time-evolution of the distances between the oxygen atom of the rotating water molecule and the oxygen atom of its initial (shown in black line) and final (red line) H-bond partners. Panel (a), inset, depicts the time-evolution of the projection of the O^*H^* vector on the $O_AO^*O_B$ plane (see *chapter 3* for definition of this angle) and clearly shows that the O^*H^* vector suddenly rotates via an angle of almost 80 degrees during a time of about a few hundreds of fs. This clearly shows that the orientational dynamics proceeds by the jump reorientations. These average trajectories indicate that the initial H-bond accepting water molecule recedes from the first hydration shell to the second, simultaneously the final H-bond acceptor water molecule moves in from the second hydration shell to the first. The angular reorientation of the O^*H^* vector occurs in phase with the hydration layer exchange translations, thus exhibiting the extent of rotation-translation coupling in these systems.¹⁰⁸

The time-scale associated with the orientational dynamics is provided by a combination of two timescales, one is the waiting time between orientational jumps (exchange of H-bond acceptors) and another, of relatively lesser importance, the timescale associated with reorientations during periods when the hydrogen bond connectivity is intact.^{95,101} By following the OH bonds of each individual water molecule in time, we have identified the periods of orientational jumps (during which a rapid exchange of H-bond

acceptors occur ~ 100 fs) and the much longer periods (\sim several ps) of waiting between two consecutive orientational jump events. The most important quantity is the waiting time distributions that a molecule waits for time t_w between successive jumps. In other way we may think that every jump is followed by a wait.¹⁰⁹ During the waiting times the local connectivity of the tagged water molecule remains intact. Since the present system is a binary mixture, the tagged water molecule can be H-bonded to another water and/or a DME molecule during the periods of waiting. Thus the waiting times of the OH bonds of the tagged water molecules can be grouped into two different categories, (a) when the tagged water molecule is H-bonded to another water and (b) when the tagged water molecule is H-bonded to a DME molecule. The waiting time distributions of the OH bonds of water are shown in *chapter 9*.

The waiting time distribution is an exponential one that also indicates that the jump originates from a Poissonian process. By fitting the long-time tails of these waiting time distributions to an exponential function of time, we obtain the corresponding “mean waiting times” at each simulated concentrations. Figure 5.3.II.10b shows the concentration dependence of the mean waiting time. The average waiting time distribution and the corresponding mean average waiting times have been calculated at each concentration by not differentiating between the two types of waiting time intervals. All waiting time intervals have been included in these calculations. The detailed procedure used for the computation of the waiting time is provided in *chapter 3*.¹⁰⁸

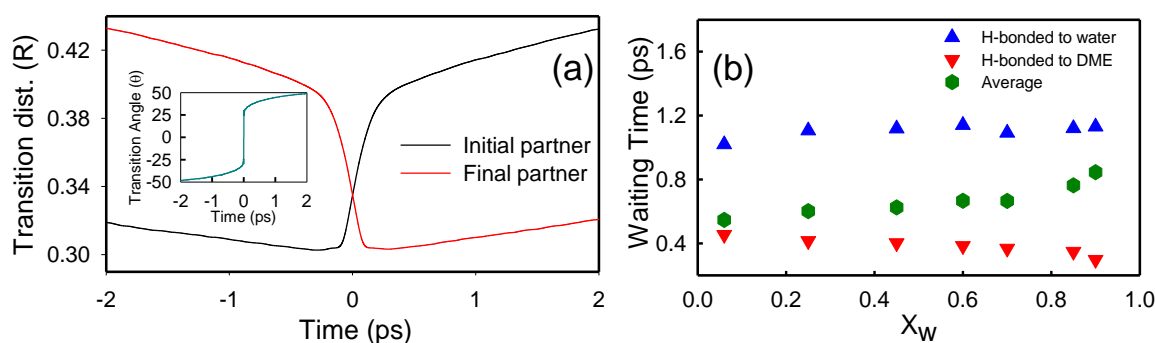


Figure 5.3.II.10. Water molecules performing large amplitude angular jump orientation. (a) The left panel shows the distance from the centre water molecule to the initial H-bond partner (black line), and the final H-bond partner (red line). The time evolution of the transition angle is shown in inset. (a representative fig for X_w 0.85) (b) The average waiting time (green symbol) and the waiting time of the rotating water molecule when it is H-bonded to water (blue symbol) and DME (red symbol) for various water concentrations.

To understand the non-monotonic dependence of the reorientation times on the concentration of water one has to appreciate that two competing mechanisms are at work. When one starts from high water concentrations, $X_w \sim 1$, the reorientational dynamics is

dominated by the water-water waiting times due to the presence of more water-water H-bonds than water-DME H-bonds. The water-water waiting time is longer than the water-DME waiting times at all simulated concentrations (figure 5.3.II.10b). Incidentally, this underlines the hydrophobic nature of DME molecules as a given water molecule prefers to stay H-bonded with another water molecule rather than a DME molecule. At these concentrations, the water dynamics slows down in the vicinity of the DME molecules due to the fact that these molecules fail to find other suitable water molecules with which it can form H-bonds leading to longer waiting times. It has been shown in reference¹¹⁰ that a transition state excluded volume theory leads to a quantitative understanding of the rotational slowdown of water in the vicinity of hydrophobic solutes.

At moderate to low water concentrations, the dynamics of water molecules accelerate. The acceleration of the water dynamics can be understood by the behaviour of the average waiting time shown in figure 5.3.II.10. The average waiting time smoothly interpolates from the blue dots (water-water waiting time) to the red (water-DME waiting time) upon decreasing X_w . At low X_w , there are many more water-DME H-bonds and thus the average waiting time is essentially governed by the water-DME waiting time. These effects thus lead to the acceleration of water orientational dynamics in the moderate to low water concentrations, in line with what has been observed in the TTDS experiment.

5.4. Summary

The structure and dynamics of water in its binary mixture with a less polar liquid DME are investigated by both experimental as well as computer simulation study. MIR FTIR measurements reveal the existence of under-coordinated water molecules in DME continuum with dangling O-H bonds at low water concentrations. With increasing X_w bulk like water evolves with the establishment of H-bonded network. FIR FTIR measurements identify the different vibrational bands of water in the low X_w region; at higher water concentration these bands merge to form the well-known collective band at $\sim 200 \text{ cm}^{-1}$. This band exhibits a considerable red shift in DME continuum and then is progressively blue shifted with increasing water concentration. The collective H-bond relaxation dynamics, as determined from *Debye relaxation* in THz region, is found to be accelerated in the low X_w region while at $X_w \sim 0.8$ region it is intriguingly slower than that of pure water. We have identified the local structure of water clusters that appear in various concentration regimes via MD simulations. We found that these H-bonded water clusters are quite stable and exist at all simulated concentrations. We also observe similar non-monotonic dependence in the water

reorientation times, calculated from the MD simulations. Water reorientations are found to occur via a combination of large amplitude angular jumps and diffusive reorientations. We observe a non-monotonic concentration dependence of the simulated reorientation timescales. The slowing down of the orientations at high water concentrations is due to slower H-bond exchanges in the vicinity of the DME molecules. At lower water concentrations, there is a complete breakdown of the tetrahedral H-bond structure in water and the timescale associated with the orientational dynamics is dominated by water-DME waiting times, which is much less than the water-water waiting time. This abundance of water-DME H-bond, lead to an acceleration of the rotational dynamics at these concentrations. We think that such interplay of two different physical mechanisms to understand the concentration dependence of reorientation times should be a universal feature of any aqueous binary mixture.

Table 5.3.II.1. Bi-exponential fitting parameters of the 1st order time correlation function $C_1(t)$ of OH vector for water-DME mixtures at different compositions.

X_w	A_1	τ_1 (ps)	A_2	τ_2 (ps)
0.06	0.51	4.35±0.00849	0.32	0.88±0.00528
0.25	0.59	6.54±0.00818	0.28	1.24±0.00566
0.45	0.57	7.52±0.01263	0.30	1.58±0.00769
0.60	0.63	6.72±0.00924	0.24	1.46±0.00835
0.70	0.67	6.81±0.00841	0.22	1.44±0.00878
0.85	0.67	6.70±0.00932	0.22	1.61±0.01012
0.90	0.74	5.58±0.00375	0.16	1.11±0.00615
1.00	0.86	3.99±0.00201	0.08	0.29±0.00191

Table 5.3.II.2. Bi-exponential fitting parameters of the 2nd order time correlation function $C_2(t)$ of OH vector for water-DME mixtures at different compositions.

X_w	A_1	τ_1 (ps)	A_2	τ_2 (ps)
0.06	0.40	2.11±0.00534	0.31	0.26±0.00233
0.25	0.43	3.46±0.00649	0.31	0.50±0.00314
0.45	0.43	4.00±0.00771	0.32	0.62±0.00365
0.60	0.47	3.81±0.00583	0.29	0.55±0.00322
0.70	0.51	3.73±0.0045	0.27	0.49±0.00283
0.85	0.52	3.56±0.00421	0.27	0.50±0.00283
0.90	0.52	3.24±0.00416	0.27	0.51±0.00291
1.00	0.66	2.01±0.00224	0.21	0.22±0.00157

Table 5.3.II.3. Ratio of the fitted time scales of 1st and 2nd order tcf.

X _w	0.06	0.25	0.45	0.60	0.70	0.85	0.90	1.00
Ratio of the longer time scales	2.06	1.89	1.88	1.77	1.83	1.88	1.72	1.99
Ratio of the shorter time scales	3.38	2.45	2.55	2.63	2.91	3.22	2.15	1.32

5.5. References

- (1) Roberts, S. T.; Ramasesha, K.; Tokmakoff, A. *Acc. Chem. Res.* **2009**, *42*, 1239-1249.
- (2) Ball, P. *Chem. Rev.* **2008**, *108*, 74-108.
- (3) Halle, B. *Philos. Trans. R. soc. London B* **2004**, *359*, 1207-1224.
- (4) Mukherjee, B. *J. Chem. Phys.* **2015**, *143*, 054503.
- (5) Das Mahanta, D.; Patra, A.; Samanta, N.; Luong, T. Q.; Mukherjee, B.; Mitra, R. K. *J. Chem. Phys.* **2016**, *145*, 164501.
- (6) Eaves, J. D.; Loparo, J. J.; Fecko, C. J.; Roberts, S. T.; Tokmakoff, A.; Geissler, P. L. *Proc. Natl. Acad. Sci. U. S. A.* **2005**, *102*, 13019-13022.
- (7) Laage, D.; Hynes, J. T. *Science* **2006**, *311*, 832-835.
- (8) Loparo, J. J.; Roberts, S. T.; Tokmakoff, A. *J. Chem. Phys.* **2006**, *125*, 194522 (194521-194512).
- (9) Bakker, H. J.; Skinner, J. L. *Chem. Rev.* **2010**, *110*, 1498-1517.
- (10) Fayer, M. D. *Physiology* **2011**, *26*, 381-392.
- (11) Yaminsky, V. V.; Voglerb, E. A. *Curr. Op. Colloid Interface Sci.* **2001**, *6*, 342-349.
- (12) Smith, G. D.; Bedrov, D.; Borodin, O. *Phys. Rev. Lett.* **2000**, *85*, 5583-5586.
- (13) Begum, R.; Matsuura, H. *J. Chem. Soc., Faraday Trans.* **1997**, *93*, 3839-3848.
- (14) Molyneux, P. *Water-Soluble Synthetic Polymers Properties and Behavior*; CRC Press: Boca Raton, FL, **1983**; Vol. 1.
- (15) Fenn, E. E.; Moilanen, D. E.; Levinger, N. E.; Fayer, M. D. *J. Am. Chem. Soc.* **2009**, *131*, 5530-5539.
- (16) Smith, G. D.; Bedrov, D. *Macromolecules* **2002**, *35*, 5712-5719.
- (17) Bailey, F. E. J.; Koleske, J. V. In *Poly (Ethylene Oxide)*; Elsevier: **1976**, p 163-169.
- (18) Martin, L. M.; Rajabi-Siahboomi, A. R. In *Hydrophilic Matrix Tablets for Oral Controlled Release*; Timmins, P., Pygall, S. R., Melia, C. D., Eds.; Springer: New York, **2014**, p 123-141.
- (19) Dhawan, S.; Dhawan, K.; Varma, M.; Sinha, V. R. *Pharm. Technol.* **2005**, *29*, 82-96.
- (20) Smith, G. D.; Bedrov, D. *Macromolecules* **2002**, *35*, 5712-5719.
- (21) Li, I. T. S.; Walker, G. C. *Proc. Natl. Acad. Sci. U. S. A.* **2011**, *108*, 16527-16532.
- (22) Grdadolnik, J.; Merzel, F.; Avbelj, F. *Proc. Natl. Acad. Sci. U. S. A.* **2017**, *114*, 322-327.
- (23) Das Mahanta, D.; Samanta, N.; Mitra, R. K. *J. Phys Chem. B* **2017**, *121*, 7777-7785.
- (24) Wada, R.; Fujimoto, K.; Kato, M. *J. Phys. Chem. B* **2014**, *118*, 12223-12231.

- (25) Kříž, J.; Dybal, J. *Chem. Phys.* **2011**, 382, 104-112.
- (26) Matsuura, H.; Sagawa, T. *J. Mol. Liq.* **1995**, 65-66, 313-316.
- (27) Goutev, N.; Nickolov, Z. S.; Matsuura, H. *J. Mol. Liq.* **1998**, 76, 117-126.
- (28) Nickolov, Z. S.; Goutev, N.; Matsuura, H. *J. Phys. Chem. A* **2001**, 105, 10884-10889.
- (29) Goutev, N.; Ohno, K.; Matsuura, H. *J. Phys. Chem. A* **2000**, 104, 9226-9232.
- (30) Douheret, G.; Reis, J. C. R.; Davis, M. I.; Fjellanger, I. J.; Høiland, H. *Phys. Chem. Chem. Phys.* **2004**, 6, 784-792.
- (31) Bedrov, D.; Borodin, O.; Smith, G. D. *J. Phys. Chem. B* **1998**, 102, 5683-5690.
- (32) Bedrov, D.; Smith, G. D. *J. Phys. Chem. B* **1999**, 103, 3791-3796.
- (33) Bedrov, D.; Pekny, M.; Smith, G. D. *J. Phys. Chem. B* **1998**, 102, 996 - 1001.
- (34) Smith, G. D.; Bedrov, D.; Borodin, O. *Phys. Rev. Lett.* **2000**, 85, 5583.
- (35) Hezaveh, S.; Samanta, S.; Milano, G.; Roccatano, D. *J. Chem. Phys.* **2011**, 135, 164501.
- (36) Bedrov, D.; Borodin, O.; Smith, G. D. *J. Phys. Chem. B* **1998**, 102, 9565-9570.
- (37) Saleh, M. A.; Akhtar, S.; Ahmed, M. S. *Phys. Chem. Liq.* **2008**, 46, 140-153.
- (38) Schmuttenmaer, C. A. *Chem. Rev.* **2004**, 104, 1759-1780.
- (39) Heyden, M.; Sun, J.; Funkner, S.; Mathias, G.; Forbert, H.; Havenith, M.; Marx, D. *Proc. Natl. Acad. Sci. USA* **2010**, 107, 12068-12073.
- (40) Tielrooij, K. J.; Paparo, D.; Piatkowski, L.; Bakker, H. J.; Bonn, M. *Biophys. J.* **2009**, 97, 2484-2492.
- (41) Luong, T. Q.; Verma, P. K.; Mitra, R. K.; Havenith, M. *J. Phys. Chem. A* **2011**, 115, 14462-14469.
- (42) Heyden, M.; Havenith, M. *Methods* **2010**, 52, 74-83.
- (43) He, Y.; Ku, P. I.; Knab, J. R.; Chen, J. Y.; Markelz, A. G. *Phys. Rev. Lett.* **2008**, 101, 178103.
- (44) Beard, M. C.; Turner, G. M.; Schmuttenmaer, C. A. *J. Phys. Chem. B* **2002**, 106, 7146-7159.
- (45) Polley, D.; Patra, A.; Mitra, R. K. *Chem. Phys. Lett.* **2013** 586, 143-147.
- (46) Patra, A.; Luong, T. Q.; Mitra, R. K.; Havenith, M. *Phys. Chem. Chem. Phys.* **2013**, 15, 930-939.
- (47) Sarangi, M. K.; Mitra, A. K.; Sengupta, C.; Ghosh, S.; Chakraborty, S.; Saha, C.; Basu, S. *J. Phys. Chem. C* **2013**, 117, 2166-2174.
- (48) Banik, D.; Kundu, N.; Kuchlyan, J.; Roy, A.; Banerjee, C.; Ghosh, S.; Sarkar, N. *J. Chem. Phys.* **2015**, 142 054505.
- (49) Pradhan, T.; Ghoshal, P.; Biswas, R. *J. Chem. Sci.* **2008**, 120, 275-287.
- (50) Sinha, S. S.; Mitra, R. K.; Verma, P. K.; Pal, S. K. *J. Phys. Chem. B* **2009**, 113, 4744-4750.
- (51) Wensink, E. J. W.; Hoffmann, A. C.; van Maaren, P. J.; van der Spoel, D. *J. Chem. Phys.* **2003**, 119, 7308-7317.
- (52) Venables, D. S.; Schmuttenmaer, C. A. *J. Chem. Phys.* **2000**, 113, 11222-11236.
- (53) Kashyap, H. K.; Biswas, R. *J. Chem. Phys.* **2007**, 127, 184502.
- (54) Roy, S.; Banerjee, S.; Biyani, N.; Jana, B.; Bagchi, B. *J. Phys. Chem. B* **2011** 115 685-692.
- (55) Roy, S.; Bagchi, B. *J. Chem. Phys.* **2013**, 139, 034308.
- (56) Patra, A.; Verma, P. K.; Mitra, R. K. *J. Phys. Chem. B* **2012**, 116, 1508-1516.
- (57) Śmiechowski, M.; Stangret, J. *Pure Appl. Chem.* **2010**, 82, 1869-1887.

- (58) Das Mahanta, D.; Samanta, N.; Mitra, R. K. *Journal of Molecular Liquids* **2016**, *215*, 197-203.
- (59) Stangret, J.; Gampe, T. *J. Phys. Chem. B* **1999**, *103*, 3778-3783.
- (60) Cringus, D.; Yeremenko, S.; Pshenichnikov, M. S.; Wiersma, D. A. *J. Phys. Chem. B* **2004**, *108*, 10376-10387.
- (61) Smith, J. D.; Saykally, R. J.; Geissler, P. L. *J. Am. Chem. Soc.* **2007**, *129*, 13847-13856.
- (62) Graener, H.; Seifert, G. *J. Chem. Phys.* **1993**, *98*, 36-45.
- (63) Scatena, L. F.; Brown, M. G.; Richmond, G. L. *Science* **2001**, *292*, 908-912.
- (64) Matsuura, H.; Fukuhara, K. *Biull. Chem. Soc. Jpn.* **1986**, *59*, 763-768.
- (65) Deb, P.; Haldar, T.; Kashid, S. M.; Banerjee, S.; Chakrabarty, S.; Bagchi, S. *J. Phys. Chem. B* **2016**, *120*, 4034-4046.
- (66) Brubach, J.-B.; Mermet, A.; Filabozzi, A.; Gerschel, A.; Roy, P. *J. Chem. Phys.* **2005**, *122*, 184509.
- (67) Haldar, T.; Bagchi, S. *J. Phys. Chem. Lett.* **2016**, *7*, 2270-2275.
- (68) Luong, T. Q.; Verma, P. K.; Mitra, R. K.; Havenith, M. *J. Phys. Chem. A* **2011**, *115*, 14462-14469.
- (69) Choi, J.-H.; Oh, K.-I.; Lee, H.; Lee, C.; Cho, M. *J. Chem. Phys.* **2008**, *128*, 134506.
- (70) Maroncelli, M.; Fleming, G. R. *J. Chem. Phys.* **1987**, *86*, 6221-6238.
- (71) Jimenez, R.; Fleming, G. R.; Kumar, P. V.; Maroncelli, M. *Nature* **1994**, *369*, 471-473.
- (72) Fee, R. S.; Maroncelli, M. *Chemical Physics* **1994**, *183*, 235-247.
- (73) Brubach, J.-B.; Mermet, A.; Filabozzi, A.; Gerschel, A.; Roy, P. *The Journal of Chemical Physics* **2005**, *122*, 184509.
- (74) Zelsmann, H. R. *Journal of Molecular Structure* **1995**, *350*, 95-114.
- (75) Mitra, R. K.; Verma, P. K.; Pal, S. K. *The Journal of Physical Chemistry B* **2009**, *113*, 4744-4750.
- (76) Heugen, U.; Schwaab, G.; Bründermann, E.; Heyden, M.; Yu, X.; Leitner, D. M.; Havenith, M. *Proc. Natl. Acad. Sci. USA* **2006**, *103*, 12301-12306.
- (77) Samanta, N.; Das Mahanta, D.; Mitra, R. K. *Chem. Asian J.* **2014**, *9*, 3457-3463.
- (78) Samanta, N.; Das Mahanta, D.; Mitra, R. K. *Phys. Chem. Chem. Phys.* **2014**, *16*, 23308--23315.
- (79) Marcheselli, L.; Marchetti, A.; Tagliazucchi, M.; Tassi, L.; Tosi, G. *Aust. J. Chem.* **1993**, *46*, 633-639.
- (80) van der Post, S. T.; Tielrooij, K.-J.; Hunger, J.; Backus, E. H. G.; Bakker, H. J. *Faraday Discuss.* **2013**, *160*, 171-189.
- (81) Fukasawa, T.; Sato, T.; Watanabe, J.; Hama, Y.; Kunz, W.; Buchner, R. *Phys. Rev. Lett.* **2005**, *95*, 197802.
- (82) Fecko, C. J.; Eaves, J. D.; Tokmakoff, A. *J. Chem. Phys.* **2002**, *117*, 1139-1154.
- (83) Walrafen, G. E.; Chu, Y. C.; Piermarini, G. J. *J. Phys. Chem.* **1996**, *100*, 10363-10372.
- (84) Vij, J. K.; Simpson, D. R. J.; Panarina, O. E. *J. Mol. Liq.* **2004**, *112*, 125-135.
- (85) Patra, A.; Luong, T. Q.; Mitra, R. K.; Havenith, M. *Phys. Chem. Chem. Phys.* **2014**, *16*, 12875-12883.
- (86) Tomlinson-Phillips, J.; Davis, J. G.; Ben-Amotz, D.; Spångberg, D.; Pejov, L.; Hermansson, K. *J. Phys. Chem. A* **2011**, *115*, 6177-6183.

- (87) Davis, J. G.; Rankin, B. M.; Gierszal, K. P.; Ben-Amotz, D. *Nat. Chem.* **2013**, *5*, 796-802.
- (88) Sharp, K. A.; Vanderkooi, J. M. *Acc. Chem. Res.* **2010**, *43*, 231-239.
- (89) Mancera, R. L. *J. Chem. Soc., Faraday Trans.* **1996**, *92*, 2547-2554.
- (90) Stoddard, S. D. *J. Comput. Phys.* **1978**, *27*, 291-293.
- (91) Rupley, J. A.; Careri, G. *Adv. Prot. Chem.* **1991**, *41*, 37-172.
- (92) Oleinikova, A.; Brovchenko, I. *J. Phys. Chem. Lett.* **2011**, *2*, 765-769.
- (93) Brovchenko, I.; Krukau, A.; Oleinikova, A.; Mazur, A. K. *Phys. Rev. Lett.* **2006**, *97*, 137801.
- (94) Godec, A.; Smith, J. C.; Merzel, F. *Physical Review Letters* **2011**, *107*, 267801.
- (95) Laage, D.; Hynes, J. T. *J. Phys. Chem. B* **2008**, *112*, 14230-14242.
- (96) Powles, J. G. *The Journal of Chemical Physics* **1953**, *21*, 633-637.
- (97) Madden, P.; Kivelson, D. In *Adv. Chem. Phys.*; John Wiley & Sons, Inc.: **2007**, p 467-566.
- (98) Chandra, A.; Bagchi, B. *J. Phys. Chem.* **1990**, *94*, 1874-1876.
- (99) Woutersen, S.; Bakker, H. J. *Nature* **1999**, *402*, 507-509.
- (100) Laage, D. L.; Hynes, J. T. *Proc. Natl. Acad. Sci. U.S.A.* **2007**, *104*, 11167-11172.
- (101) Laage, D. *J. Phys. Chem. B* **2009**, *113*, 2684-2687.
- (102) Das, S.; Biswas, R.; Mukherjee, B. *J. Phys. Chem. B* **2015**, *119*, 274-283.
- (103) Duboué-Dijon, E.; Fogarty, A. C.; Hynes, J. T.; Laage, D. *Journal of the American Chemical Society* **2016**, *138*, 7610-7620.
- (104) Laage, D.; Hynes, J. T. *Proceedings of the National Academy of Sciences* **2007**, *104*, 11167-11172.
- (105) Das, S.; Biswas, R.; Mukherjee, B. *The Journal of Chemical Physics* **2016**, *145*, 084504.
- (106) Das, S.; Biswas, R.; Mukherjee, B. *The Journal of Physical Chemistry B* **2015**, *119*, 11157-11168.
- (107) Araque, J. C.; Daly, R. P.; Margulis, C. J. *The Journal of Chemical Physics* **2016**, *144*, 204504.
- (108) Mukherjee, B. *The Journal of Chemical Physics* **2015**, *143*, 054503.
- (109) Pastore, R.; Coniglio, A.; Candia, A. d.; Fierro, A.; Ciamarra, M. P. *Journal of Statistical Mechanics: Theory and Experiment* **2016**, *2016*, 054050.
- (110) Laage, D.; Stirnemann, G.; Hynes, J. T. *J. Phys. Chem. B* **2009**, *113*, 2428-2435.

6. Non-monotonous Hydration Behaviour of Bovine Serum Albumin in Alcohol-Water Binary Mixtures: A THz Spectroscopic Investigation

We report the experimental observation on non-monotonous change in the collective hydration of BSA in presence of alcohols of varying carbon chain lengths: ethanol, 2-propanol and t-butanol (TBA) using THz TDS technique. We measure the THz absorption coefficient (α) of the protein solutions and find that α fluctuates periodically with alcohol concentration at a fixed protein concentration. For a fixed alcohol concentration, increase in protein concentration shows a non-monotonous change in α , it first decreases rapidly, and then increases followed by a shallow decrease. An alcohol induced α -helix to random coil transition of the protein secondary structure is revealed from CD spectroscopic measurement, the effect being more prominent in TBA. The anomalous change in the hydration is a delicate balance between the various interactions present in the three component system.

6.1. Introduction

Addition of small guest molecules often brings about noticeable changes in the structure and functionality of proteins.^{1,2,3} These co-solvents can preferentially solvate certain segments of proteins, thereby perturbing the hydration network at the protein surface.⁴ The preferential hydration of protein in presence of co-solvents may be regarded as a result of the delicate balance of three different contributions: a repulsion and an attraction between protein and cosolvent, and the steric exclusion of the co-solvents acting as classical ‘crowders’. In this regard water-alcohol binary mixtures have evoked a considerable attention in recent past owing to their various anomalous behaviours which is found to be dependent on the chain length and the hydrophobicity of the alcohols.⁵⁻⁸ Anomalous hydration behaviour of alcohols has extensively been studied using various experimental and simulation techniques.⁸⁻¹⁷ It has been concluded that the conventional “iceberg” model is not appropriate to explain the experimental results. Presence of hydrophobic moieties of alcohol are found to be responsible for the unusual rotational mobility of water.¹⁸

Alcohol-water mixtures are not homogeneous throughout the entire concentration range,¹⁹ the heterogeneity arises due to incomplete mixing as a result of cluster formation as well as self-aggregation of the alcohols.¹⁶ Being amphiphilic in nature, alcohol molecules can

induce opposite effects in water, while the hydrophilic part can form favourable H-bonds with water, the hydrophobic part tend to self-aggregate and disrupt the water structure by hydrophobic hydration.¹⁷ These two opposing effects combine together to modify the extensive H-bond network of water depending upon the composition of the binary mixtures.²⁰ The extent of heterogeneity is found to be dependent on the hydrophobic nature of the alcohol; e.g. it is observed that water-t-butyl alcohol (TBA) shows strong cluster formation at a relatively low alcohol concentration compared to that in water-ethanol (EtOH) and water-methanol (MeOH) mixtures.¹⁷ The effect of such inhomogeneous mixing is expected to affect the long-range collective H-bond dynamics of water which leaves its imprint in the elusive THz frequency regime.²¹ Some recent reports on the aqueous solutions of a series of alcohols have indeed identified long range structural heterogeneity in the mixtures.^{20,22} A combined THz spectroscopic and MD simulation study from our group has also established a non-monotonous dynamics of water-dimethoxy ethane (DME) mixture.²³

The inherent heterogeneity of water-alcohol mixture makes the study of biomolecular hydration in such binary solvents even more complex. There have been a few experimental and simulation reports investigating the effect of different alcohols on protein structural perturbation.^{24,25} It was known for long that at low concentrations alcohols stabilize proteins as a result of preferential solvation of alcohols at protein surface²⁶, addition of alcohol induces propensity of α -helical formation in certain class of proteins^{27,28,29} the effect being dependent on the carbon chain length of alcohols. The carbon chain promotes the transition according to their size, the hydroxyl group suppresses that. At high alcohol concentration, proteins get destabilized and could even get precipitated due to alcohol binding to the active sites of proteins; also the self-aggregation of alcohols might incorporate protein molecules.^{30,31,32} Recent fluorescence correlation spectroscopy (FCS) measurements on a model protein lysozyme by the group of Bhattacharyya et al.²⁴ and MD simulation studies on chicken villin headpiece (HP-36) by the group of Bagchi et al.²⁵ have unambiguously established strong modulation of the protein hydrodynamic radius as a function of ethanol concentration due to the interaction and preferential binding of the alcohol to the active sites of the proteins. The protein structure exhibits a unique oscillating fluctuation due to the different concentration dependent binding modes of alcohols with the protein.²⁴ Most of these earlier studies were concerned to the changes of the protein structure while the associated hydration remained mostly unaddressed. It therefore stands interesting to investigate whether the aforementioned changes in the protein conformational behaviour also get manifested in

the hydration behaviour of the proteins. In this present study, we have investigated the effect of three different alcohols: ethanol (EtOH), 2-propanol (2-PrOH) and tert-butanol (TBA) on a model protein BSA. The choice of the alcohols lies on their unlimited water solubility irrespective of the progressively increased carbon chain length. The protein BSA is responsible for the transport of various nutrients in animals, and is structurally analogous to the human serum albumin (HSA). The crystal structure of this protein is well established.³³ It also has been studied extensively as a model protein for protein stability, folding, and denaturation,^{34,35} and is found to be responsive of the addition of various co-solutes in its aqueous solution.³⁶⁻³⁸ In a recent study³⁶ the effect of ethanol on BSA has been found to be bimodal; the abundance of secondary structural content has been found to be dependent on ethanol concentration, which in turn is contrary to other proteins like lysozyme³² or melittin²⁸. This makes a systematic study on the effect of alcohols on BSA interesting. We obtain structural information of BSA in presence of the alcohols using CD spectroscopy. The hydration dynamics is obtained using THz TDS technique that is able to probe the rotational and vibrational dynamics of molecules in the frequency range of 0.1-4 THz. It covers part of the far-infrared region of the electromagnetic spectrum and probes molecular motions arising from inter-molecular interactions, in particular hydrogen bonds.^{39,40,41} THz spectroscopy measurements of aqueous systems provide with pivotal information on the various collective vibrational modes of water which occur in hundreds of fs to tens of ps timescale. This technique has successfully been employed to extract hydration dynamics in both binary mixtures^{20,23,42} as well as in biomolecules.^{43,44,45,46} In this present contribution, we aim to address the issue that how the addition of alcohols modulate the structure as well as the hydration associated with a model protein. The results could be found helpful in pharmaceutical applications as alcohols are used as the solvent of various drugs and understanding how biomolecules interact with alcohols serves as a prerequisite for that.

6.2. Materials and Methods

BSA (lyophilized powder, > 98% Purity), HPLC grade alcohols, namely, ethanol (EtOH), 2-propanol (2-PrOH) and tertiary butanol (TBA) are procured from Sigma-Aldrich and are used as received. Deionize Milli-Q water is used for preparation of the aqueous solutions. Aqueous BSA solutions are prepared in Milli-Q water also. We kept BSA concentration as 1 mg ml⁻¹ for alcohol concentration dependent study. For the protein concentration dependent study we fixed the alcohol concentration (alcohol 5% mole), prepared 30 mg ml⁻¹ stock solution of the protein and the desired concentrations were achieved through dilution. All the measurements

are carried out at room temperature ($\sim 293\text{K}$). CD measurements in the far-UV (200-250 nm) and near-UV (250-350 nm) region were recorded in a JASCO J-815 spectropolarimeter using quartz cuvettes of 1 mm and 10 mm path length, respectively. The sample scan speed was kept at 50 nm min^{-1} with response time of 2 sec. Three CD spectra were recorded in continuous mode and averaged for each CD experiment. THz TDS measurements were carried out in a commercial THz spectrophotometer (TERA K8, Menlo Systems).^{46, 47} Further details about the instruments and the underline methods can be found in *chapter 2*.

6.3. Results and Discussions

CD measurements: The secondary structure of BSA in presence of alcohols is investigated by CD spectroscopy in the far UV region (200-250 nm) (figure 6.1a-c). Two negative bands appearing in the far-UV region (at 208 and 222 nm) typify the predominant secondary ($\sim 60\%$) α -helical structure of BSA.⁴⁸ The intensity of CD signal is found to decrease with increasing alcohol concentration. At higher alcohol concentration the shape of the CD profile gets significantly perturbed compared to that in the native state. To investigate the tertiary structure of the protein we measure the CD profiles in the near-UV region (250-350 nm) (figure 6.1d-f). We notice two minima at 261 and 268 nm along with a shoulder at 287 nm. These peaks correspond to the transitions of the tryptophan residues of the protein and thus provide information on the tertiary structure of the protein. We notice that with increasing alcohol concentration the intensity of the two minima decreases and at $X_{\text{alcohol}} > 0.1$ these two peaks disappear. This indicates a considerable perturbation of the protein tertiary structure as a result of its binding with the alcohols. The intensity of these two minima also varies with the variation of the hydrophobicity of the alcohols.

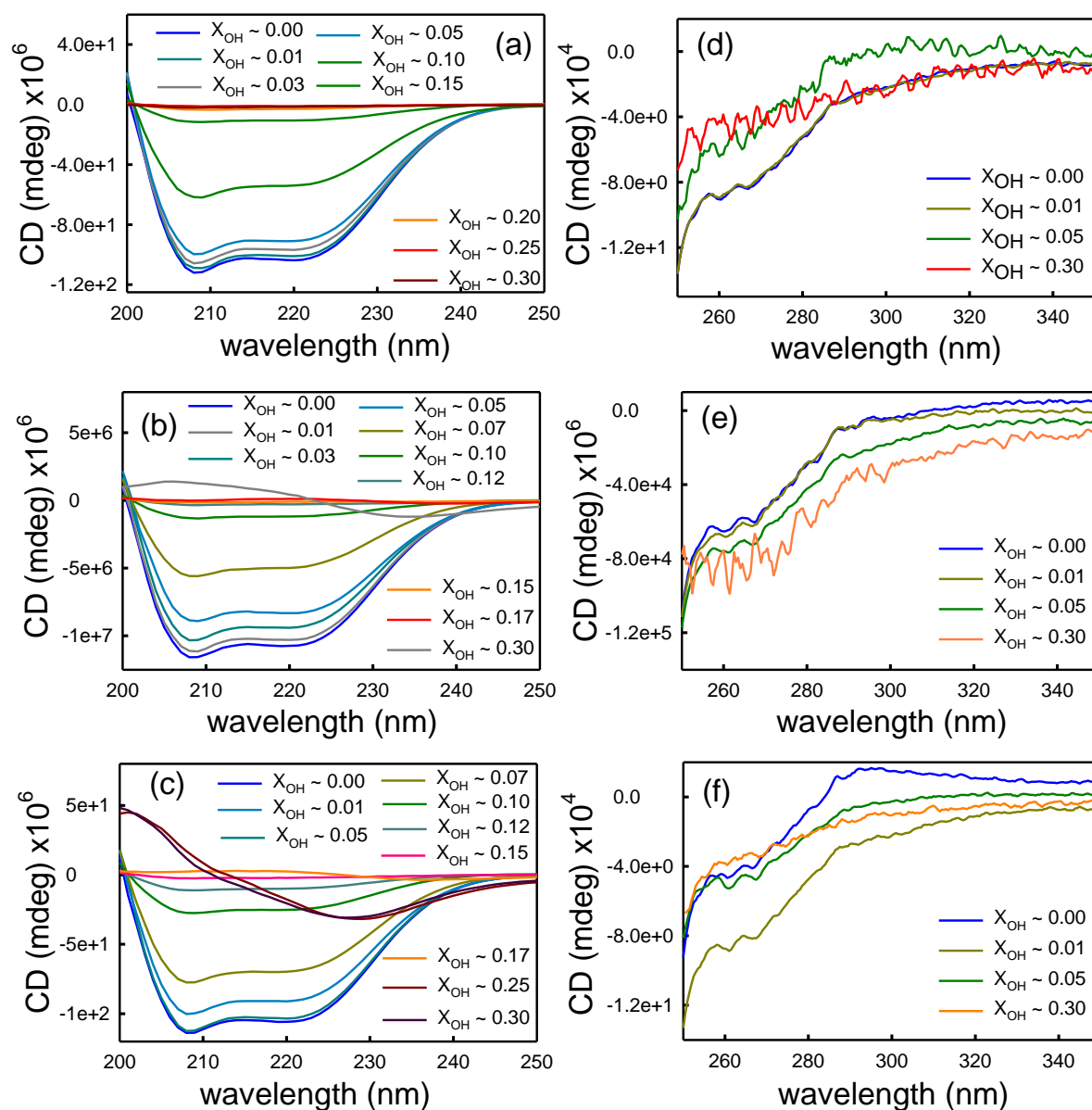


Figure 6.1: CD spectra of BSA in three different alcohols, namely, EtOH, 2-PrOH, TBA. The changes of secondary structure of BSA in different alcohol are shown in figure 1, (a) EtOH (b) 2-PrOH and (c) TBA respectively. The changes of the tertiary structure of BSA in presence of alcohol for three different alcohol are shown in figure (d) EtOH, (e) 2-PrOH and (f) TBA respectively.

For a better comprehension of the effect of alcohols on BSA we plot the CD signal at 208 and 222 nm as a function of alcohol concentration (figure 6.2a-b). It is evident that in both the cases the CD signal decreases rapidly with alcohol concentration; at any fixed alcohol concentration the changes are found to be alcohol specific following the sequence TBA>2-PrOH>EtOH, which exactly also corroborates the extent of hydrophobic content of the alcohols. We calculate the relative content of the secondary structures as a function of alcohol concentration (figures 6.2c-e).

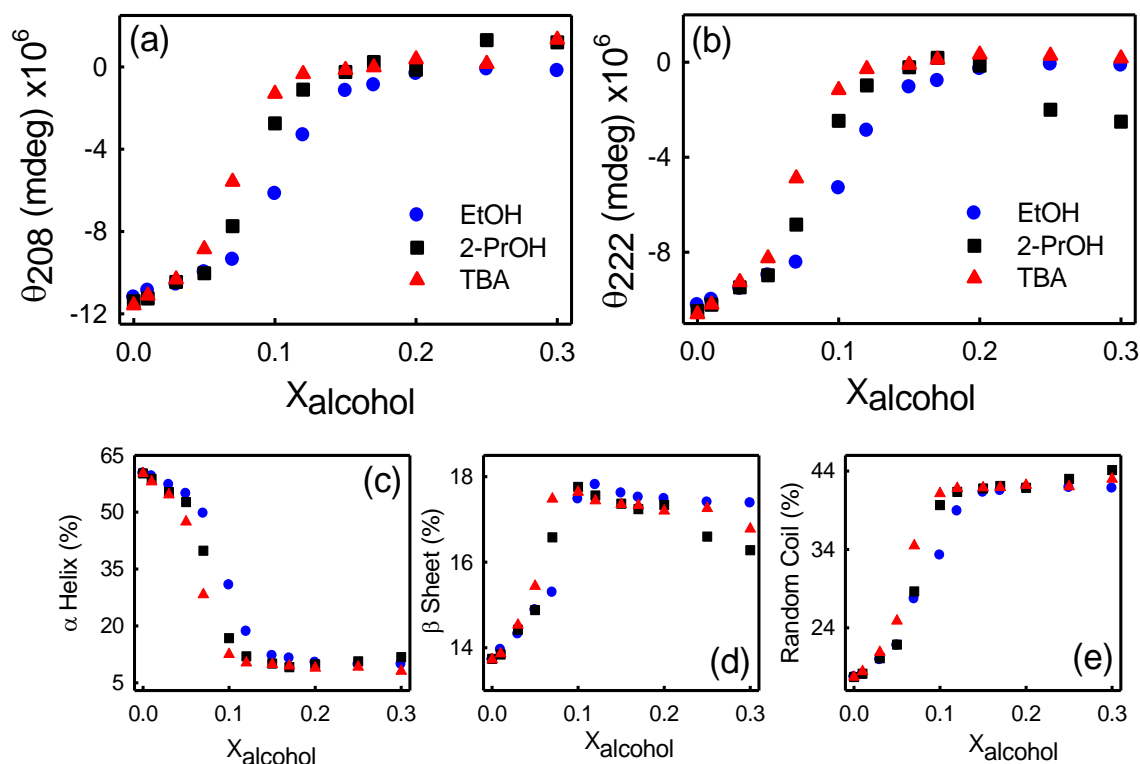


Figure 6.2. The changes of CD signal at (a) 208 nm and (b) 222 nm as a function of alcohol concentration for EtOH, 2-PrOH and TBA. The relative changes in the α -helix (c), β -sheet (d) and random coil (e) content are also shown.

We find that the abundance of α -helix decreases mostly at the expense of relatively non-structured random coils. This suggests an exposure of the hydrophobic moieties of the protein towards the solvent. Such a decrease in the α -helical content is in contrast with other proteins like lysozyme³², β -lactoglobulin²⁷ or melittin.²⁸ The results are indicative of the specific nature of the protein-alcohol interaction; while in some cases alcohol induces volume exclusion to stabilize the helical content, it may also solvate the hydrophobic side chains and destabilize the helical content. As alcohol molecules are introduced into aqueous BSA solution they serve as a good solvent for the protein's hydrophobic milieu.³⁶ With increasing concentration, alcohol molecules actively bind to the protein surface replacing hydrated water and subsequently produce strong perturbation in the protein structure as it exposes its hydrophobic residues towards the alcohols. During this process the more structured helical structures convert into random coils, the effect being more intense for more hydrophobic alcohols.

TTDS measurements: We study the hydration dynamics of alcohol-water binary mixtures (figure 6.3). The frequency dependent absorption coefficient ($\alpha(\nu)$) in the THz region

correlates the cooperative hydrogen bond dynamics of water as it manifests the density of states of molecules undergoing such motions.⁴⁹

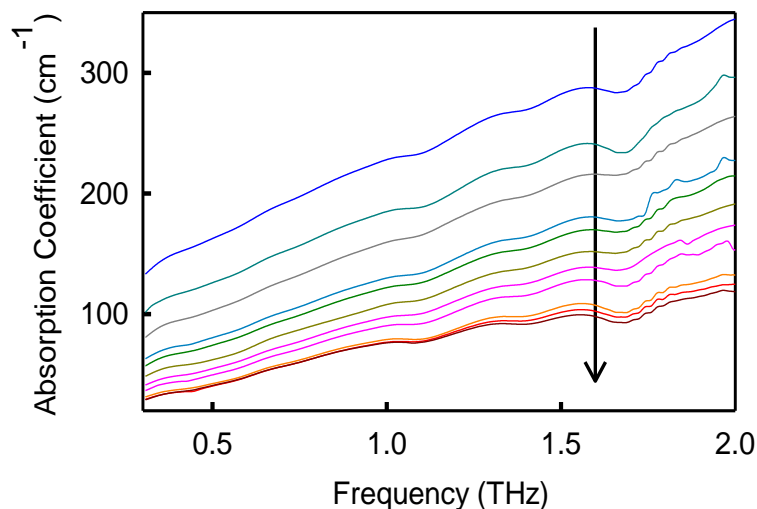


Figure 6.3: The THz absorption coefficient, $\alpha(\nu)$ of EtOH-water binary mixtures as a function of EtOH concentration (arrow indicates decreasing of water content).

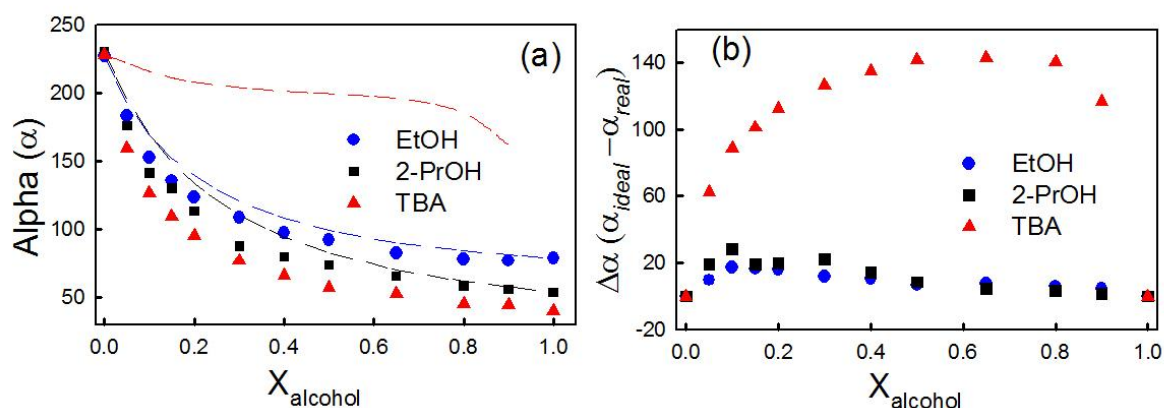


Figure 6.4. (a) Represented α measured (symbol) at 1 THz for alcohol-water binary mixture as a function of alcohol mole fraction. The dotted lines indicate the corresponding α_{ideal} . The changes in $\Delta\alpha(\alpha_{ideal} - \alpha_{real})$ are shown in (b).

Water has very high absorbance in this frequency region compared to other molecules^{20,50, 51} which provides a unique advantage to identify the changes in these parameter and extract information on the alteration in hydration dynamics. Our previous studies concluded that monovalent salts⁵² act as water structure breakers whereas a structure making trend is more evident in otherwise naive or protein stabilizing polymers.⁵³ We measure the THz frequency dependent parameters of different alcohol-water mixtures (figure 6.3). Figure 6.4a depicts the absorption coefficient measured at 1 THz for all the three binary mixtures. With increasing alcohol concentration α expectedly decreases, the extent of decrease follows the order $\alpha_{EtOH} > \alpha_{2-PrOH} > \alpha_{TBA}$, higher the carbon chain length, lower is

the absorption coefficient. The order is anticipated from the increasing size as well as the increasing hydrophobicity of the molecule. We calculate α_{ideal} assuming an ideal mixing of the components: $\alpha_{ideal} = \frac{\rho_{real}}{\rho_{ideal}} \sum_i \phi_i \alpha_i(\nu)$ where ϕ_i is the volume fraction of the i -th species, ρ_{real} is the measured density of the mixture and $\rho_{ideal} = \sum_i X_i \rho_i$, we found that the measured values of α deviate strongly from the calculated ones (broken lines in figure 6.4a), specially for TBA. A similar non-ideal mixing behaviour has also been observed in water-DME,²³ water-dioxane⁴² binary mixtures. For a better apprehension we plot the relative change in α ($\Delta\alpha = \alpha_{ideal} - \alpha_{real}$) as a function of alcohol concentration (figure 6.4b). We observe decent changes in $\Delta\alpha$ for EtOH and PrOH, the change is found to be drastic in TBA-water mixture. In a recent THz study Li et al²⁰ reported a bell-shaped α profile in alcohol-water binary mixtures using MeOH, EtOH and PrOH. The observed non-ideality emanates either from the formation of defects in the hydrogen bonding network of water or alcohol-alcohol aggregation and formation of clathrate-like structure or more likely due to a delicate interplay between all these factors. It has been reported that the entropy of the alcohol-water mixture increases far less than that expected for an ideal solution of randomly mixed molecules⁵⁴, which supports their strong mutual interaction as has also been reciprocated in the unusual changes in volume and density.^{55,56,57} The marked deviation in TBA is perhaps rooted in its large size and the presence of hydrophobic butyl groups which sets in the inter-molecular aggregations (even at 5% TBA concentration) thereby inducing incomplete mixing with water.⁵⁸

We measure the frequency dependent α of aqueous BSA solutions [at a fixed protein concentration of 1 mg ml⁻¹] in presence of alcohols (some representative profiles are shown in figure 6.5). The protein concentration is low enough to avoid self-aggregation. It is observed that protein solutions have lower $\alpha(\nu)$ than that of pure water as intuited from the fact of replacing high absorbing water molecules with proteins.⁵⁹

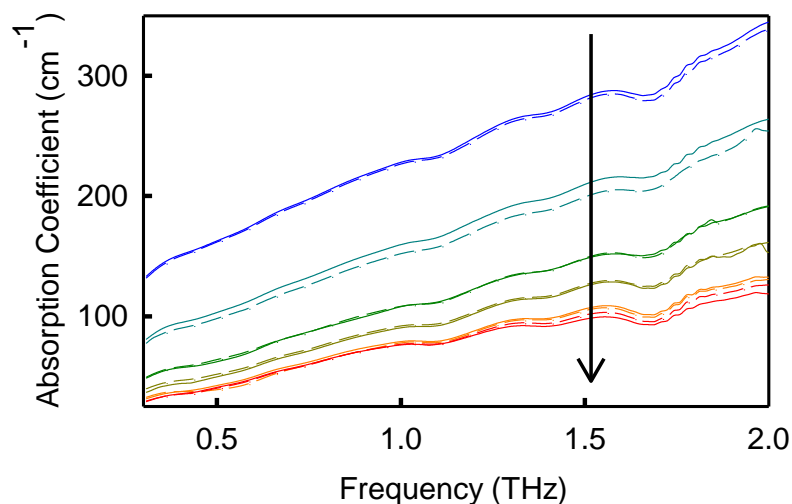


Figure 6.5: The THz absorption coefficient, $\alpha(\nu)$ of BSA in presence (dotted line) and absence (solid line) of EtOH as a function of EtOH concentration (arrow indicates decreasing of water content).

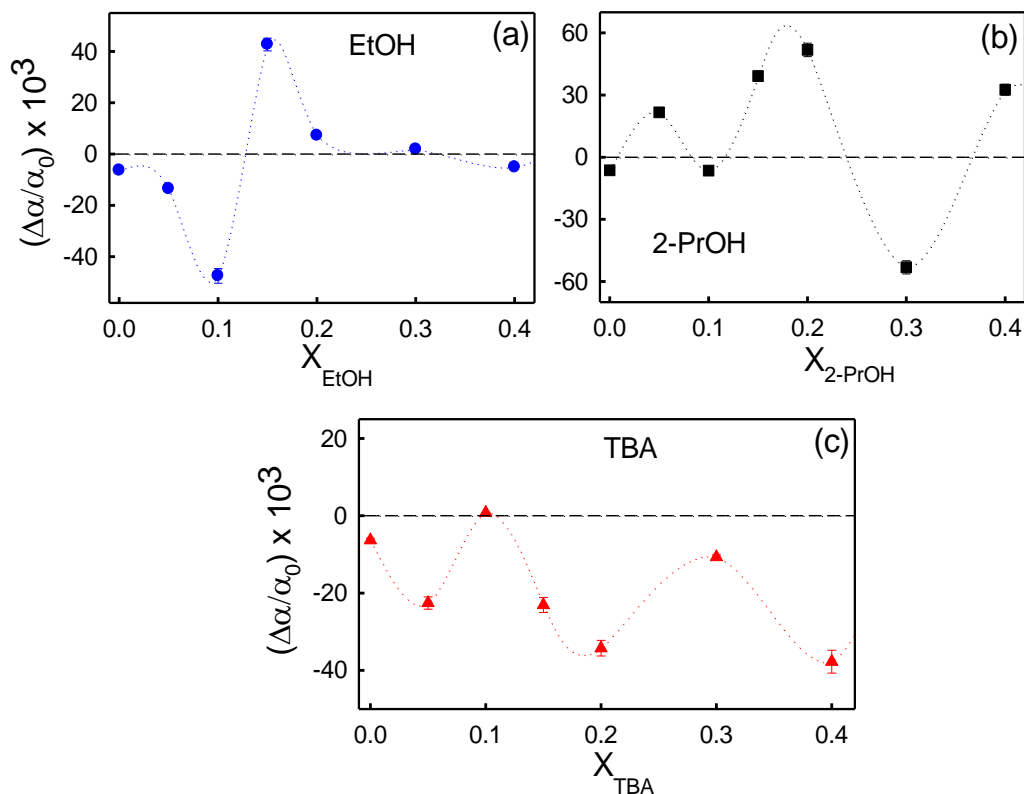


Figure 6.6. The relative terahertz absorption coefficient (at 1 THz), $(\Delta\alpha/\alpha_0)$ in presence of BSA as a function of alcohol concentration for (a) EtOH (b) 2-PrOH and (c) TBA. The dotted lines are guide to the eyes.

We observe that the THz absorption of protein-water-alcohol mixtures do not change linearly and to obtain a better apprehension we plot the relative change in absorption (defined

as, $\frac{\Delta\alpha}{\alpha_0} = \frac{\alpha_{\text{protein+alcohol+water}} - \alpha_{\text{alcohol+water}}}{\alpha_{\text{alcohol+water}}}$) as a function of alcohol concentration (figure

6.6). The parameter $\Delta\alpha/\alpha_0$ bears the signature of protein hydration explicitly.⁴⁶ The nature of all the curves deviate strongly from linearity and show an unusual oscillating trend. A simple three-component model (water-alcohol-protein) does not suffice to explain the observed trend as has also been observed in DMSO-water-lysozyme mixtures.⁴⁶ It is also worth noting that the oscillating feature is distinct for different alcohols; for EtOH and PrOH the parameter oscillates between positive and negative values of $\Delta\alpha$, whereas, for TBA, it is always negative. To understand the fluctuations it is important to consider that the overall hydration dynamics is a delicate balance between competing interactions: alcohols preferentially solvate the protein surface and deplete the hydration layer, this in turn increases the abundance of bulk water. Considering that the absorbance of hydrated and bulk water is different^{46,49} this factor leads to a change in $\Delta\alpha$. Moreover with progressive addition of alcohol the protein's buried part get exposed (as evidenced from the CD results wherein we observe an increase in the random coil content at the expense of more structured α -helical content) increasing the non-polar solvent accessible surface area (SASA). This facilitates alcohol binding at the protein surface. This process is opposed by a possible alcohol-alcohol self-aggregation which certainly modifies the hydration dynamics in binary mixtures (figure 6.4). An additional factor comes in the form of the alcohol induced size variation of the protein. Recent MD simulation studies by Ghosh et al. report that the gyration radius (R_g) of a globular protein chicken villin headpiece (HP-36) exhibits an oscillating behaviour as a function of ethanol concentration.²⁵ A similar behaviour has experimentally been realized by Chatteraj et al. who reported on the oscillating size of lysozyme as a function of EtOH concentration.²⁴ The fluctuation in the protein size has been explained on the basis of a delicate balance between the alcohol-alcohol and alcohol-protein interactions. Interestingly we also notice an identical fluctuation on the hydration dynamics, with the oscillating pattern varying with the increased hydrophobicity of the alcohol. The periodic retardation and acceleration of hydration dynamics is perhaps caused by counter interactive interactions of the various factors described earlier. While the preferential alcohol accumulation at the protein surface and enhancement in the protein size decrease α , the water-alcohol or alcohol-alcohol aggregation and reduction in the protein size increase α .

To further investigate the effect of alcohol on protein hydration we study the protein concentration dependent THz absorption in EtOH-water and TBA-water mixtures keeping the alcohol concentration fixed at 5% (mol%). Concentration dependent α of BSA in these mixtures (averages in the 0.95-1.05 THz range, in this frequency window water does not

show any characteristic vibrational signature and α increases monotonically) are shown in figure 6.7.

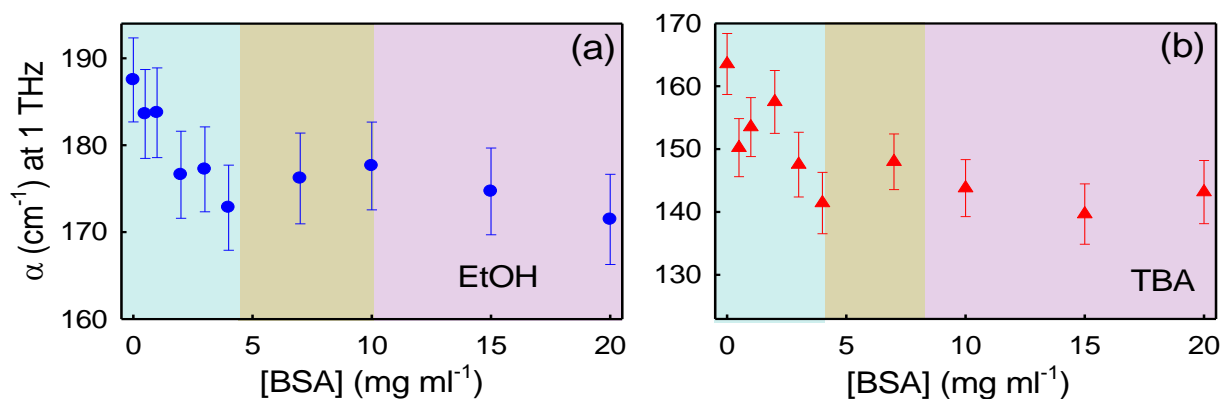


Figure 6.7. α measured at 1 THz as a function of BSA concentration at 5% mole of (a) EtOH and (b) TBA.

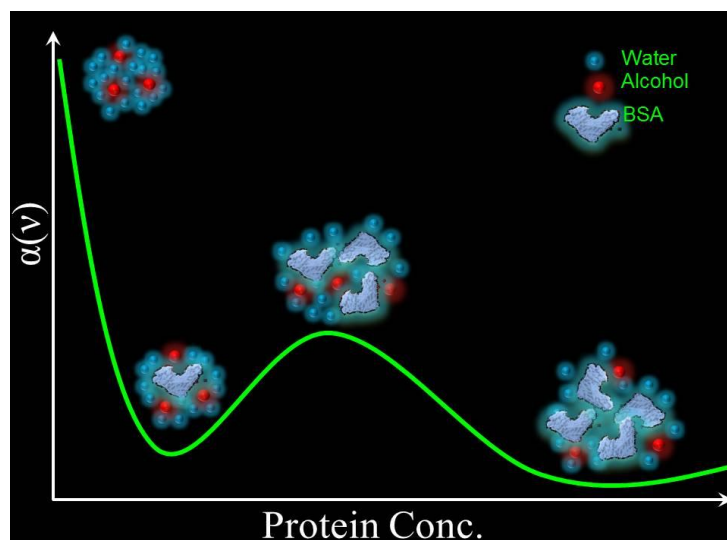
We observe an intriguing non-monotonous change in α as a function of alcohol concentration. It is important to note here that THz absorption of BSA in water has previously been carried out by Xu et al.⁶⁰ and Bye et al.,⁶¹ where in both these studies the authors reported a monotonous decrease in α with protein concentration. According to previous reports a three component model is better approach to explain protein hydration which takes into consideration the THz accessible extended hydration sheathe around biomolecules.^{62,63} However, in this present study, the system is more complex due to the presence of alcohol as a third component. The α vs. protein concentration profile can be divided into three distinct segments (figure 6.7): in the low alcohol concentration region α decreases rapidly (region 1), then it increases modestly (region 2) followed by a shallow decrease (region 3) after passing through a maximum. The profile in the high protein concentration regions resemble the concentration dependent THz profile reported earlier.⁶⁴ For TBA, the pattern remains almost the same, however, with a distinct rise at ~ 2 mg ml⁻¹ BSA concentration after a sharp fall (figure 6.7b). A simple replacement of polar solvents with protein molecules only provides with a linear decrease in α and is, therefore, not sufficient for explaining the complex nature of the curves. To describe the observed unusual non-monotonous nature of the profile we need to consider the various interactions involved between the different components. It should be noted here that α of water-alcohol mixture is lower than that of pure water, and the difference increases with increasing carbon chain length of the alcohols (figure 6.4). Also at this low alcohol concentration (5% mol), the protein is modestly unfolded with 55% and 47% α -helical content compared to that of 60% in

pure water, with a proportionate increase in the random coil content. This leads the protein to expose a fraction of its otherwise buried hydrophobic residues towards the solvent.

The initial steep decrease (region 1) is intuited to the replacement of high absorbing polar binary solvent with protein molecules. As protein is introduced into water-alcohol binary mixture the preferential binding of alcohols at the protein surface disrupts the apparently present water-alcohol or alcohol-alcohol clusters in the mixture. The effect is more prominent in TBA due to its higher affinity to bind the alcohol-induced exposed hydrophobic surface (higher content of random coil, figure 6.2 as well as the non-polar SASA of the protein.²⁵ An optimizing effect between these two opposing contributions brings about the increased α at $\sim 2 \text{ mg ml}^{-1}$ protein in TBA. Since the total alcohol concentration is low, beyond a certain protein concentration water starts predominantly solvating the protein surface over alcohol, and eventually α starts increasing⁴⁶ (region 2). This increase initiate at a slightly lower concentration of protein in TBA compared to that in EtOH. As protein concentration is increased sufficiently, the hydration layers of proteins start overlapping and α starts decreasing slowly⁶⁴ (region 3). The onset of this decrease occurs at a lower concentration in TBA than in EtOH as the protein molecule is more unfolded and enlarged compared to that in 5% EtOH (figure 6.2). At even higher protein concentration the protein molecules aggregate and precipitate out.

6.4. Summary

We report hydration behaviour of a model protein BSA in various alcohol-water binary mixtures. CD spectroscopic study indicates that the content of different secondary structures of BSA change as a function of alcohol concentration and carbon chain length. TTDS studies of the alcohol-water binary mixtures indicate a strong deviation of $\alpha(\nu)$ from ideality which is a manifestation of making and breaking of H-bonds, water-alcohol cluster formation and alcohol-alcohol aggregation. We observed a fluctuating change in the protein hydration as a function of alcohol. Concentration dependent study of protein solution in 5% mole EtOH- and TBA-water solutions indicated a non-monotonic behaviour of protein hydration. The experimentally observed non-monotonicity in the protein hydration is intriguing and the inherent complexity of the water-alcohol mixture makes an overall apprehension difficult. A detailed simulation considering all the pair-wise interactions is certainly of demand.



6.5. References

- (1) Spinozzi, F.; Mariani, P.; Ortore, M. G. *Biophysical Reviews* **2016**, *8*, 87-106.
- (2) Zhou, H.-X. *FEBS Lett.* **2013**, *587*, 1053-1061.
- (3) Timasheff, S. N. *Proceedings of the National Academy of Sciences* **2002**, *99*, 9721-9726.
- (4) Canchi, D. R.; García, A. E. *Annual Review of Physical Chemistry* **2013**, *64*, 273-293.
- (5) Franks, F.; Ives, D. J. G. *Quarterly Reviews, Chemical Society* **1966**, *20*, 1-44.
- (6) Benson, G. C.; Kiyohara, O. *Journal of Solution Chemistry* **1980**, *9*, 791-804.
- (7) Wensink, E. J. W.; Hoffmann, A. C.; van Maaren, P. J.; van der Spoel, D. J. *Chem. Phys.* **2003**, *119*, 7308-7317.
- (8) Požar, M.; Kerasidou, A.; Lovrinčević, B.; Zoranić, L.; Mijaković, M.; Primorac, T.; Sokolić, F.; Teboul, V.; Perera, A. *The Journal of Chemical Physics* **2016**, *145*, 144502.
- (9) Banik, D.; Roy, A.; Kundu, N.; Sarkar, N. *The Journal of Physical Chemistry B* **2015**, *119*, 9905-9919.
- (10) Wakisaka, A.; Abdoul-Carime, H.; Yamamoto, Y.; Kiyozumi, Y. *Journal of the Chemical Society, Faraday Transactions* **1998**, *94*, 369-374.
- (11) Takaizumi, K.; Wakabayashi, T. *Journal of Solution Chemistry* **1997**, *26*, 927-939.
- (12) Mizuno, K.; Miyashita, Y.; Shindo, Y.; Ogawa, H. *The Journal of Physical Chemistry* **1995**, *99*, 3225-3228.
- (13) Juurinen, I.; Nakahara, K.; Ando, N.; Nishiumi, T.; Seta, H.; Yoshida, N.; Morinaga, T.; Itou, M.; Ninomiya, T.; Sakurai, Y.; Salonen, E.; Nordlund, K.; Hämäläinen, K.; Hakala, M. *Physical Review Letters* **2011**, *107*, 197401.
- (14) Dolenko, T. A.; Burikov, S. A.; Dolenko, S. A.; Efitorov, A. O.; Plastinin, I. V.; Yuzhakov, V. I.; Patsaeva, S. V. *The Journal of Physical Chemistry A* **2015**, *119*, 10806-10815.
- (15) Ghoraiishi, M. S.; Hawk, J. E.; Phani, A.; Khan, M. F.; Thundat, T. *Scientific Reports* **2016**, *6*, 23966.
- (16) Gupta, R.; Patey, G. N. *The Journal of Chemical Physics* **2012**, *137*, 034509.

- (17) Banerjee, S.; Furtado, J.; Bagchi, B. *The Journal of Chemical Physics* **2014**, *140*, 194502.
- (18) Sciortino, F.; Geiger, A.; Stanley, H. E. *Nature* **1991**, *354*, 218-221.
- (19) Dixit, S.; Crain, J.; Poon, W. C. K.; Finney, J. L.; Soper, A. K. *Nature* **2002**, *416*, 829-832.
- (20) Li, R.; D'Agostino, C.; McGregor, J.; Mantle, M. D.; Zeitler, J. A.; Gladden, L. F. *The Journal of Physical Chemistry B* **2014**, *118*, 10156-10166.
- (21) Tan, N. Y.; Li, R.; Brauer, P.; D'Agostino, C.; Gladden, L. F.; Zeitler, J. A. *Physical Chemistry Chemical Physics* **2015**, *17*, 5999-6008.
- (22) McGregor, J.; Li, R.; Zeitler, J. A.; D'Agostino, C.; Collins, J. H. P.; Mantle, M. D.; Manyar, H.; Holbrey, J. D.; Falkowska, M.; Youngs, T. G. A.; Hardacre, C.; Stitt, E. H.; Gladden, L. F. *Physical Chemistry Chemical Physics* **2015**, *17*, 30481-30491.
- (23) Das Mahanta, D.; Patra, A.; Samanta, N.; Luong, T. Q.; Mukherjee, B.; Mitra, R. K. *The Journal of Chemical Physics* **2016**, *145*, 164501.
- (24) Chatteraj, S.; Mandal, A. K.; Bhattacharyya, K. *The Journal of Chemical Physics* **2014**, *140*, 115105.
- (25) Ghosh, R.; Roy, S.; Bagchi, B. *The Journal of Physical Chemistry B* **2013**, *117*, 15625-15638.
- (26) Asakura, T.; Adachi, K.; Schwartz, E. *Journal of Biological Chemistry* **1978**, *253*, 6423-6425.
- (27) Hamada, D.; Kuroda, Y.; Tanaka, T.; Goto, Y. *J. Mol. Biol.* **1995**, *254*, 737-746.
- (28) Hirota, N.; Mizuno, K.; Goto, Y. *J. Mol. Biol.* **1998**, *275*, 365-378.
- (29) Hirota-Nakaoka, N.; Goto, Y. *Bioorganic & Medicinal Chemistry* **1999**, *7*, 67-73.
- (30) Timasheff, S. N.; Inoue, H. *Biochemistry* **1968**, *7*, 2501-2513.
- (31) Deshpande, A.; Nimsadkar, S.; Mande, S. C. *Acta Crystallographica Section D* **2005**, *61*, 1005-1008.
- (32) Yoshikawa, H.; Hirano, A.; Arakawa, T.; Shiraki, K. *International Journal of Biological Macromolecules* **2012**, *50*, 865-871.
- (33) Wright, A. K.; Thompson, M. R. *Biophysical Journal* **1975**, *15*, 137-141.
- (34) Carrotta, R.; Manno, M.; Giordano, F. M.; Longo, A.; Portale, G.; Martorana, V.; Biagio, P. L. S. *Physical Chemistry Chemical Physics* **2009**, *11*, 4007-4018.
- (35) Guo, J.; Harn, N.; Robbins, A.; Dougherty, R.; Middaugh, C. R. *Biochemistry* **2006**, *45*, 8686-8696.
- (36) Yoshikawa, H.; Hirano, A.; Arakawa, T.; Shiraki, K. *International Journal of Biological Macromolecules* **2012**, *50*, 1286-1291.
- (37) Almagor, A.; Yedgar, S.; Gavish, B. *Biophysical Journal* **1992**, *61*, 480-486.
- (38) Pabbathi, A.; Patra, S.; Samanta, A. *ChemPhysChem* **2013**, *14*, 2441-2449.
- (39) Zeitler, J. A.; Taday, P. F.; Gordon, K. C.; Pepper, M.; Rades, T. *ChemPhysChem* **2007**, *8*, 1924-1927.
- (40) Schmuttenmaer, C. A. *Chemical Reviews* **2004**, *104*, 1759-1780.
- (41) Tonouchi, M. *Nat Photon* **2007**, *1*, 97-105.
- (42) Luong, T. Q.; Verma, P. K.; Mitra, R. K.; Havenith, M. *The Journal of Physical Chemistry A* **2011**, *115*, 14462-14469.
- (43) Leitner, D. M.; Gruebele, M.; Havenith, M. *HFSP Journal* **2008**, *2*, 314-323.
- (44) Samanta, N.; Das Mahanta, D.; Mitra, R. K. *Phys. Chem. Chem. Phys.* **2014**, *16*, 23308--23315.
- (45) Born, B.; Kim, S. J.; Ebbinghaus, S.; Gruebele, M.; Havenith, M. *Faraday Discussions* **2009**, *141*, 161-173.

- (46) Das, D. K.; Patra, A.; Mitra, R. K. *Biophysical Chemistry* **2016**, *216*, 31-36.
- (47) Polley, D.; Patra, A.; Mitra, R. K. *Chemical Physics Letters* **2013**, *586*, 143-147.
- (48) Sun, C.; Yang, J.; Wu, X.; Huang, X.; Wang, F.; Liu, S. *Biophysical Journal* **2005**, *88*, 3518-3524.
- (49) Samanta, N.; Mahanta, D. D.; Mitra, R. K. *Physical Chemistry Chemical Physics* **2014**, *16*, 23308-23315.
- (50) Xu, J.; Plaxco, K. W.; Allen, S. J. *The Journal of Physical Chemistry B* **2006**, *110*, 24255-24259.
- (51) Beard, M. C.; Turner, G. M.; Schmuttenmaer, C. A. *The Journal of Physical Chemistry B* **2002**, *106*, 7146-7159.
- (52) Das Mahanta, D.; Samanta, N.; Mitra, R. K. *Journal of Molecular Liquids* **2016**, *215*, 197-203.
- (53) Samanta, N.; Luong, T. Q.; Das Mahanta, D.; Mitra, R. K.; Havenith, M. *Langmuir* **2016**, *32*, 831-837.
- (54) Soper, A. K.; Dougan, L.; Crain, J.; Finney, J. L. *The Journal of Physical Chemistry B* **2006**, *110*, 3472-3476.
- (55) Khattab, I. S.; Bandarkar, F.; Fakhree, M. A. A.; Jouyban, A. *Korean Journal of Chemical Engineering* **2012**, *29*, 812-817.
- (56) Paez, S.; Contreras, M. *J. Chem. Eng. Data* **1989**, *34*, 455-459.
- (57) Kipkemboi, P. K.; Easteal, A. J. *Canadian Journal of Chemistry* **1994**, *72*, 1937-1945.
- (58) Tamura, K.; Osaki, A.; Koga, Y. *Physical Chemistry Chemical Physics* **1999**, *1*, 121-126.
- (59) Heugen, U.; Schwaab, G.; Bründermann, E.; Heyden, M.; Yu, X.; Leitner, D. M.; Havenith, M. *Proceedings of the National Academy of Sciences* **2006**, *103*, 12301-12306.
- (60) Xu, J.; Plaxco, K. W.; Allen, S. J. *Protein Science : A Publication of the Protein Society* **2006**, *15*, 1175-1181.
- (61) Bye, J. W.; Meliga, S.; Ferachou, D.; Cinque, G.; Zeitler, J. A.; Falconer, R. J. *The Journal of Physical Chemistry A* **2014**, *118*, 83-88.
- (62) Ebbinghaus, S.; Kim, S. J.; Heyden, M.; Yu, X.; Heugen, U.; Gruebele, M.; Leitner, D. M.; Havenith, M. *Proc. Natl. Acad. Sci. USA* **2007**, *104*, 20749-20752.
- (63) Niehues, G.; Heyden, M.; Schmidt, D. A.; Havenith, M. *Faraday Discussions* **2011**, *150*, 193-207.
- (64) Ebbinghaus, S.; Kim, S. J.; Heyden, M.; Yu, X.; Heugen, U.; Gruebele, M.; Leitner, D. M.; Havenith, M. *Proceedings of the National Academy of Sciences* **2007**, *104*, 20749-20752.

7. Contrasting Hydration Behaviour of DME and DMSO

Addition of cosolvents could introduce perturbation in the H-bond dynamics of water and the extent of perturbation is mostly dependent on the H-bond formation affinity of the respective cosolvent. We compare the H-bonding status and explore the contrasting hydration behaviours of two hydrophobic molecules DME and DMSO using two complementary experimental techniques to compare global (through dielectric relaxation study in the GHz-THz frequency domain) and local (through FTIR and degenerate pump-probe study) hydration environment and dynamics in the two binary mixtures. Due to the presence of an electronegative sulfur atom DMSO tends to form H-bonds with polar water molecules and subsequently forms various stable mDMSO:nH₂O H-bonded clusters. DME, owing to its higher carbon content and being a planer molecule, the steric obstacles screen the H-bond acceptor oxygen atoms and struggles to form H-bonds. Rather DME is more inclined to form hydrophobic aggregates resulting in a random orientation of water around those hydrophobic interfaces. The difference in the affinity of H-bond formation and self-aggregation is expected to modulate the hydration dynamics.

7.1. Introduction

Delicate balance between hydrophilic and hydrophobic interaction plays the central role in most of the bio-chemical and bio-physical processes such as protein folding/unfolding, membrane formations, molecular assembly recognition.¹⁻⁸ Such interactions could effectively be replicated in binary aqueous mixtures as the physical properties of such systems could easily be tuned by varying the nature of the non-aqueous solvent as well as their composition.⁹ There have been a plethora of efforts put forward by researchers to characterize various binary solvents. It has grossly been concluded that the interactions are non-specific in nature and depend on the solute type and dimension.¹⁰⁻¹² Small amphiphilic solutes can fit themselves in a slightly deformed cage of water whereas in large solutes water molecules fail to uphold its H-bonding network that results in a defect in the network. The H-bond strength of the percolating three dimensional tetrahedral networks of water is greater than 20 kJ mol⁻¹; about ten times larger than room temperature thermal energy (~ 2.5 kJ mol⁻¹) that constitute its robust liquid structure.¹³⁻¹⁵ These water networks are perturbed when some guest co-solvents are added in water. Depending on the nature (polarity and water affinity) of the co-solvents, they may or may not participate in the H-bonding with water. As a results there exist micro-heterogeneity in the solution, which is certainly control by the clusters of similar species with additional possibility of H-bond

formation with different species.¹⁶ Dynamics of water in such complex systems eventually differs from the bulk dynamics, and therefore it is important to investigate how the various physical properties of the mixture modulate the dynamics as the compositions are systematically altered.

The affinity of water to form H-bonds with polar segments is the key to induce hydrophobic phenomenon, as hydrophobic groups accumulate to form clusters to avoid interaction with polar water molecules.¹⁷⁻¹⁹ Such molecules force water molecules to reorient in a specific arrangement around them so as to minimize the surface contact area in comparison to bulk water where they are free to rotate and form H-bonds in all directions. This results in the formation of various sizes of clusters in the solution with an associated otherwise unusual entropy loss and high heat capacity gain.²⁰ Sometimes hydrophobic molecules create void space in water network by breaking the adjacent H-bonds to their surface.² A similar situation is apprehended for water molecules in confined environment or at the interface of large hydrophobic residues. Owing to the composition dependent heterogeneous nature and the tendency of self-association, small hydrophobic molecules are of interest as they can partly mimic the real extra cellular environment. To model such scenario we have considered aqueous mixtures of two amphiphilic, less polar cosolvents (compare to water), DME and DMSO. The difference in their structure is, DME is an in-plane molecule offer larger hydrophobicity (four carbon atoms) as compare to DMSO (two carbons) which is an out-of-plane molecule (trigonal bipyramidal shape).²¹ Thus the H-bond acceptor oxygen atoms in DME are more screened by its carbon molecules, whereas in DMSO the electronegative SO bond is open and accessible to water. That makes these two molecules to display different water affinity. In a previous study by Bakker et al.²¹ has concluded that acetone molecule has pronounced hydrophobic effect compare to DMSO molecule in their aqueous solutions, although they are very much similar in their molecular structure. It is also to note here that DME undergoes several conformational modifications with different polarity as one change the water content (X_w) in the solution.²²⁻²⁴ The preference and stability of those conformations depend solely on the urge of H-bonding.²⁵ The binary solutions of DME and DMSO with water often produce non-idealities and anomalous composition dependent behaviors in various physical parameters.^{21,24-32} The infinite miscibility of both of the cosolvents with water at room temperature makes these binary mixtures a beneficial candidate to compare the H-bonded interactions and dynamics as water changes from being a minor component (solute) to a major component (solvent). It is to note that water can act as both H-bond donor as well as acceptor whereas the cosolvents

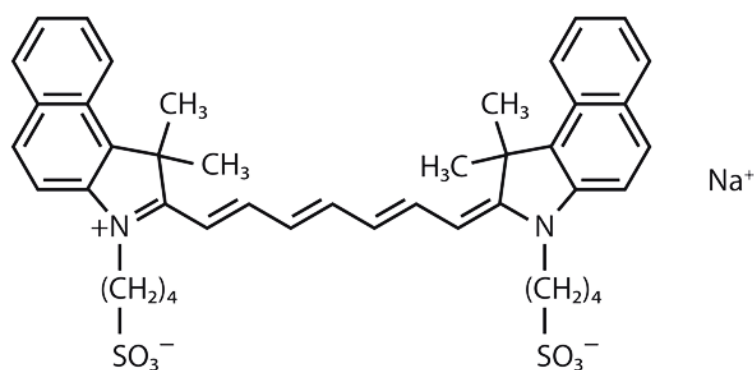
DMSO (polar aprotic solvent) and DME (non-polar solvent) are only H-bond acceptors. This difference gives rise to various non-linear properties in these two binary mixture solutions. In spite being comparable in size, the presence of S=O bond in DMSO ($\epsilon \sim 40$) makes this very molecule considerably polar compared to that of DME ($\epsilon \sim 7$). Thus one expects the hydration dynamics of water to vary accordingly in their aqueous mixtures. The intriguing question is that whether the polar-nonpolar interactions dominate over hydrophobic accumulation or not.^{1,33-37}

The deactivation of the ultrafast excited state dynamics in the form of the energy dissipation of that excited molecules strongly depend on the physical parameters such as viscosity, density, refractive index, thermal diffusivity, thermal conductivity etc of the local environment of the solutions.³⁸⁻⁴⁰ It certainly controls to choose the exact deactivation pathways and can infer the H-bonding status between the species.⁴¹ After excitation of any molecule with a short femtosecond (fs) light pulse, it can relax to the ground state in several pathways that includes vibrational as well as electronic relaxation.⁴² Pump-probe spectroscopy can accomplish to appraise the dynamics of a molecule in ground, excited, or both ground and excited states.^{43,44} It was also observed that the deactivation process also modulate as result of the formation of H-bonding between the species present in solution.⁴¹ A stronger H-bond tried to slow down the deactivation process relative to weaker one.⁴⁵ We measure the transient excited state deactivation dynamics of cyanine dye with single color pump-probe technique that is mainly governed by the ground state bleaching mechanisms.⁴³ The transient decay can exactly infer about the redistribution of the ground state population of the cyanine molecules. Besides probing the ultrafast transient decay dynamics, OD stretching mode and the combination band (liberation & bending) of the water in those binary mixtures in the mid-IR region are also explored to understand the local H-bond status of the mixtures.^{28,46} The associated fast and efficient couplings of water networks with solutes, which are very much collective in nature are difficult to realize in the conventional IR spectroscopy, is recoverable in the DR study. DR study has proven to be sensitive on the hydration dynamics. It can provide the rotational dynamics of the dipolar species. DR study can probe the ultrafast collective dynamics of the H-bond network in the extended hydration layers around the solute surface.^{47,48} The change in long range cooperative hydration in the surroundings of hydrophobic surfaces leave their imprints in the GHz frequency region. However, DR measurements in GHz region are unable to precisely probe the ultrafast component of the collective water relaxation. Thus we also extend our study to the elusive

THz frequency window. THz spectroscopy is a potential tool to label free determination of the collective hydration dynamics of water around complex systems.⁴⁹⁻⁵² One major advantage of this spectroscopic tool is that it measure both the amplitude and the phase of the transmitted THz radiation in a single experiment enabling one to estimate various optical parameters (e.g. absorption coefficient (α), complex refractive index (n), complex dielectric constant (ϵ) etc.).⁵³ This combined spectroscopic investigation brings forward the contrasting hydration behaviour in these two binary mixtures.

7.2. Materials and Methods

DME, DMSO and indocyanine dye (IR125) (scheme 7.1) were purchased from Sigma-Aldrich (~99% pure) and used without further purification. The aqueous solutions were prepared in deionized Milli-Q water. All the experiments were carried out in room temperature. We measured the FTIR spectra and DR measurement (0.2-50 GHz) with a JASCO FTIR-6300 spectrometer^{3,28,46} and PNA- L network analyzer (N5230C) with an open ended coaxial probe (85070E)⁵⁴, respectively. The coaxial dielectric probe measures the amplitude and the phase of the reflected power. The real and imaginary parts of the dielectric constants in this GHz frequency region were fitted with a single *Debye model*. The THz TDS experiments were carried out in a commercial THz spectrophotometer (TERA K8, Menlo System). The complex THz dielectric functions are fitted with a multiple *Debye dielectric relaxation* model. The transient absorption measurements with fs resolution were performed using a home built *optical pump optical probe* setup with a 1 mm cuvette kept exactly at the overlap region of the two beams. In order to avoid the dye aggregation its concentration was kept very low and fixed throughout. Further details about the instruments and the underline methods are provided in *chapter 2*.



Scheme 7.1: Molecular structure of the Indocyanine dye IR-125.

7.3. Results and Discussions

FTIR measurements: We measure the vibrational stretching mode of the OD oscillator (2% D₂O in the pure water/cosolvent mixtures), which appears in the 2400-2700 cm⁻¹ window, as a function of X_w in both the mixtures (figure 7.1).⁵⁵ As a water molecule form H-bond to its neighboring water molecules or cosolvents, the OH bonds of that water molecule get weaker as the H-bond gets stronger and vice-versa.^{28,46,56}

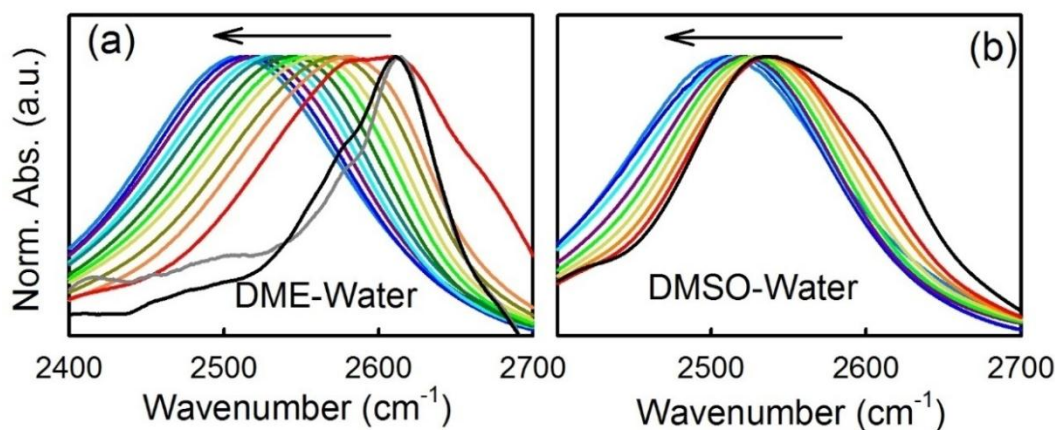


Figure 7.1. O-D stretching frequency of (a) HOD-DME and (b) HOD-DMSO mixtures at different mixing ratios. The arrow indicates increasing water mole fraction (X_w) in the mixture.

Keeping in mind this reciprocal relation, one can conclude the strengthening or weakening of inter-molecular H-bond strength by measuring the OD vibrational stretch of HOD molecules. Pure water has a broad spectrum (~ 175 cm⁻¹) with the frequency maximum at ~ 2505 cm⁻¹ (figure 7.1).^{46,57} We compare the H-bonding structure of water around DME and DMSO molecules through OD stretching modes that can probe the solute hydration and local H-bonding status. Both DME-water and DMSO-water binary mixtures display loss of intensity with blue shifted spectra with decreasing X_w . However, the extent of the shift is different; the effect being severe in DME compared to that in DMSO (figure 7.2). In general, such blue shift in the peak frequency characterizes an increasing force constant of the OD oscillator which in turn manifests weakening of the inter-molecular H-bond strength.^{9,58,59} In DMSO, the shift is small (from 2535 cm⁻¹ to 2506 cm⁻¹) and the spectral pattern suffers only modest alteration. In case of DME, however, the shift is considerable with an associated change in the spectral features. In pure DME, the spectrum is highly asymmetric (peak at 2600 cm⁻¹); addition of water produces ~ 40 cm⁻¹ red shift along with a gradual Gaussian like distribution of the spectrum. It is also observed that the DME-water IR spectrum gets deformed

asymmetrically, specially in the DME rich region, while such change is only subtle in DMSO-water mixtures. This identifies the dissimilar H-bonding mode of water with DME and DMSO; while water H-bonds to DME through the ether connected oxygen, it binds to DMSO through sulfur connected oxygen. The asymmetric distortions observed in the high frequency region are due to the redistribution of coordination numbers as well as H-bond strengths. The MIR results thus show that addition of co-solvents induces heterogeneity in the mixture, but in different ways.

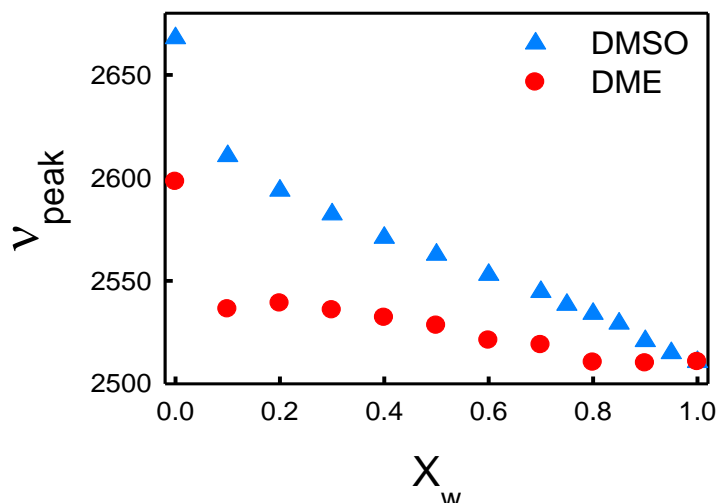


Figure 7.2. The peak frequency (ν_{peak}) of the mid-IR spectra of O-D stretch in HOD-DME and HOD-DMSO mixtures.

Dielectric Relaxation Study:

(a) *GHz frequency region:* The real permittivity and the dielectric loss for pure water and for the aqueous solutions of DMSO and DME are shown in figure 7.3 (a-d). Pure water produces a dielectric loss peak at ~ 20 GHz.^{60,61} In pure DMSO the peak appears at ~ 8 GHz with a reduced intensity compared to that of water while in DME it appears at ~ 38 GHz with a highly reduced intensity. In water-DMSO mixture, the dielectric loss peak suffers an initial decrease in the peak frequency with a progressive increase in the intensity with increasing X_w up to 0.8 (peak frequency ~ 35 GHz), beyond which a blue shift is observed (figure 7.4a). In DME-water mixture also we observe a similar trend. Similar observations have previously been observed for tetramethylurea-water mixtures.⁶²

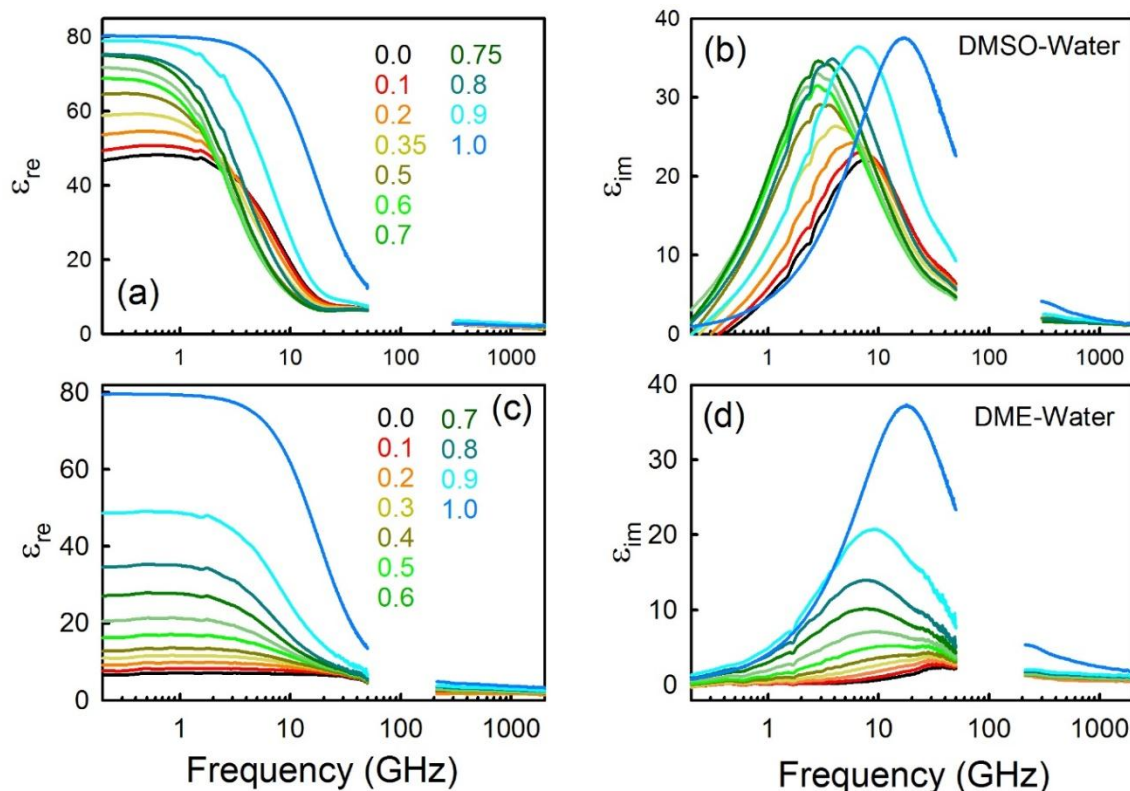


Figure 7.3. Real and imaginary parts of dielectric constant(s) of (a,b) water-DMSO and (c,d) water-DME mixtures at different X_w (mentioned in the corresponding figures). The frequency region extends from 0.2 - 50 GHz and 0.3 - 1.6 THz.

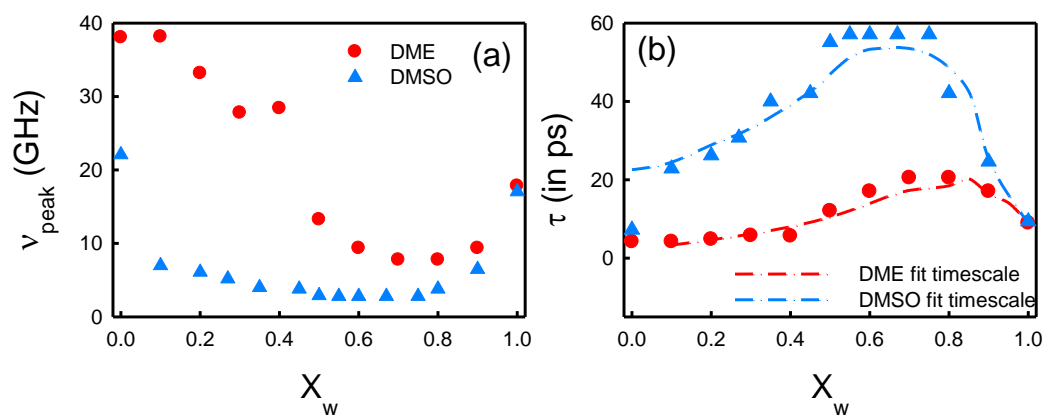


Figure 7.4. (a) The peak frequency of the imaginary dielectric constant, (b) $\tau = 1/\omega$ (symbol) and the single Debye fitted time constants (dotted lines) for water-DMSO and water-DME mixtures as a function of X_w .

Figure 7.5a shows the Cole-Cole plot of the imaginary and real permittivity for the three pure solvents. We obtain semi-circular curves for all the pure solvents which unambiguously confirms the single exponential decay pattern of the solvent relaxation.⁶³ The radiuses of these semi-circles manifest the overall polarity which decreases from water to DMSO to DME. The semi-circular symmetry is not conserved if we include the THz frequency region, and this region is, therefore, fitted using multiple exponential decay functions. We observe similar semi-circular curves in case of all the solvent mixtures

(figure 7.6). Being a non-polar aprotic solvent the area under the curve is very small in pure DME (radius ~ 3) while for DMSO it is moderate ~ 22 . We fit the real and imaginary dielectric function in the 0.2-50 GHz frequency region by single Debye relaxation model and the fitting parameters are presented in table 7.I and 7.II, respectively. It can be noted that the DR curves of water-DMSO system has previously been fitted by Lu et al⁶⁴ using stretched exponential function like Havriliak-Negami function which shows that in pure water DR fits perfectly in simple exponential while in pure DMSO it deviates by $\sim 15\%$ (the β parameter in the Havriliak-Negami equation). However, for the sake of comparison we prefer a Single Debye fit. To further strengthen our consideration of a single Debye relaxation, we calculate the reciprocal of the peak frequency of the imaginary part of the complex permittivity which is expected to correspond to the single relaxation time constant of a system. We observe that the time constants exactly match the time constants obtained by fitting the complex permittivity using Debye equation (figure 7.4b). We further try to fit the dielectric parameters using a double Debye relaxation model, however, the fit was not satisfactory, which exclude the possibility of the individual relaxation modes of water and DMSO to contribute separately to the overall relaxation process in the mixtures. We plot the relaxation time (τ) with X_w for both the solvent mixtures in figure 7.5b. For pure water we observe a time constant of 8.9 ps as reported earlier.⁵⁴ The time constant (τ) obtained for water-DMSO mixtures are in excellent agreement with those obtained by Lu et al.⁶⁴ For pure water we observe a time constant of 8.9 ps, which is in excellent agreement with previously reported values.⁵⁴ It is to be noted that DR study in this frequency region demonstrates the cooperative orientation of dipoles as a response of an external electric field. H-bond in water is cooperative in nature where formation of one bond can assist the formation of several other bonds and breakage of one bond can dissolve the whole cluster.⁶⁵ The ~ 9 ps time constant is the time taken by a water dipole to orient along the field. This time constant is expected to be longer in bulkier DMSO and we indeed observe a time constant of $\tau_{\text{DMSO}} \sim 22.5$ ps for pure DMSO relaxation.^{64,66} We observe a non-monotonic trend with the water content. The time constants are always slower than that expected considering an ideal mixing of the solvents ($\tau_{\text{ideal}} = \sum_i X_i \tau_i$), which perhaps follows the various micro-structures formed in the water-DMSO mixtures as evidenced by earlier MD simulation results.⁶⁷ At low concentrations ($X_w \sim 0.9$) DMSO forms micro-micelle type aggregates followed by the formation of different water-DMSO clusters (e.g. 2DMSO:H₂O, DMSO:2H₂O etc.) at

higher X_w . As we follow the change in τ , we observe an initial increase at $X_w \sim 0.9$, with a maximum at $X_w \sim 0.6$, which then linearly decreases to the value of τ_{DMSO} .

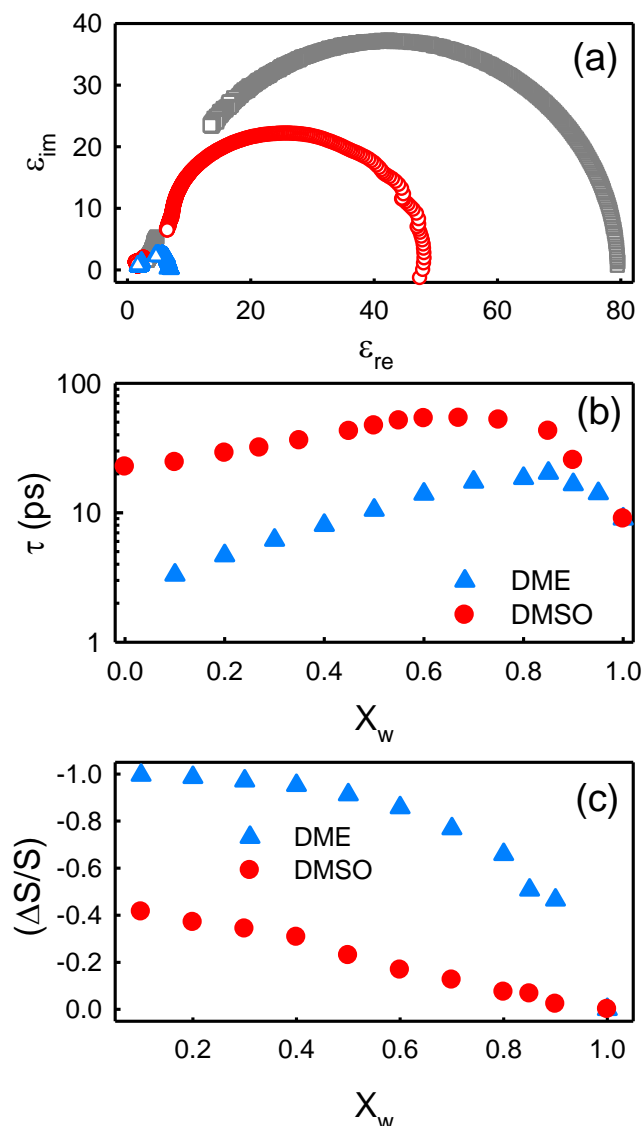


Figure 7.5. (a) Cole-Cole plot for the pure liquids: water (grey), DMSO (red) and DME (blue). (b) Cooperative relaxation dynamics time (τ) of water in presence of DME and DMSO as a function of X_w . (c) The depolarization ($\Delta S/S$) effect of water molecules in water-DME and water-DMSO mixtures as a function of X_w .

We observe a different trend in DME-water mixtures. Being a non-polar molecule we do not obtain any dipolar relaxation in pure DME within the studied frequency window. For the mixed systems we obtain the fitting parameters (see table 7.II). We observe that the relaxation is relatively fast (faster than pure water) in the low X_w region, while it is slower in the high X_w (0.7-0.8) region. This manifests that at low X_w , the cooperative binding of water is distracted by DME molecules while the formation of water-DME clusters at higher X_w makes the dynamics slower.

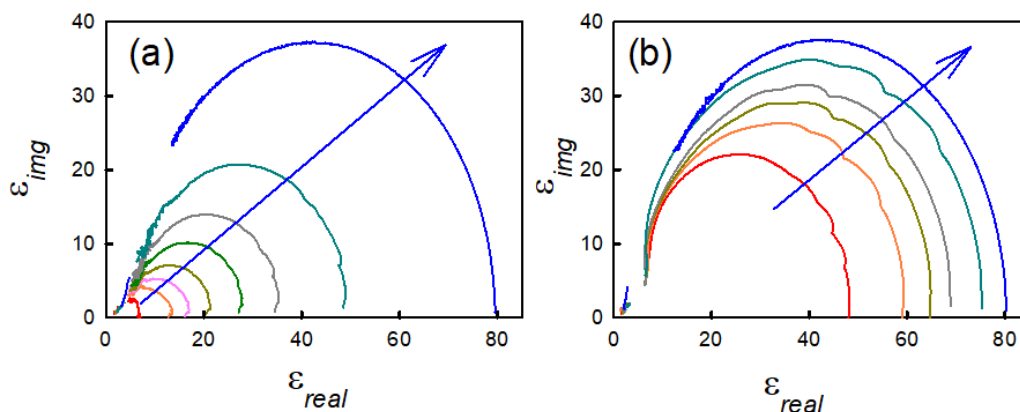


Figure 7.6. Cole-Cole plot of the complex dielectric constant of (a) water-DME and (b) water-DMSO mixtures.

(b) THz frequency region: THz (0.3-1.6 THz) absorption coefficient, $\alpha(\nu)$, is a useful parameter to provide with information on solute hydration.^{3,68-72} The value of $\alpha(\nu)$ correlates the population of water molecules undergoing collective vibrational modes in the corresponding frequency domain. We plot the $\alpha(\nu)$ profile of water-DMSO and water-DME mixtures at different X_w values in figures 7.7a,b respectively. We observe contrasting behaviors in these two liquid mixtures. Both DMSO and DME are low THz absorbing solvents compared to that of water, the difference being much prominent in DME compared to that in DMSO. It is expected that as water is replaced with the low absorbing cosolvents, the $\alpha(\nu)$ profile will lie below that of water. We found that indeed the curves lie below that of water, however, the decrease is regular in water-DME mixture (figure 7.7), while it is not so regular in water-DMSO mixtures. In fact, at certain X_w values, $\alpha(\nu)$ curves of water-DMSO mixtures lie below the $\alpha(\nu)$ curve of pure DMSO (figure 7.7a). Such a behavior is intriguing and not straightforward. It can be argued here that the observed $\alpha(\nu)$ profile is not always an algebraic sum of the contribution of the two pure solvents (i.e. $\alpha_{obs} \neq \varphi_w \alpha_w + \varphi_D \alpha_D$, where the subscripts W and D stand for water and DMSO, respectively, φ is the corresponding volume fraction), rather one needs to consider the individual contribution from the various water-DMSO complex structures which could offer altogether different $\alpha(\nu)$ values. The DR study in the GHz region has confirmed the abundance of these complex structures, which clearly is corroborated in the THz measurements. An MD simulation measurement by Heyden et al. has concluded that in the frequency domain <1.5 THz, the $\alpha(\nu)$ profile as well as the vibrational density of states (VDOS) of water oxygen changes abruptly as water molecules binds to the hydrophobic or hydrophilic surface of proteins. In DMSO-water mixtures also, the various

hetero-structures leads to such a situation as with change in X_w the interaction pattern changes. We have previously reported such changes in urea,⁶⁸ in GdmCl⁷³ and in glycine.⁵⁴

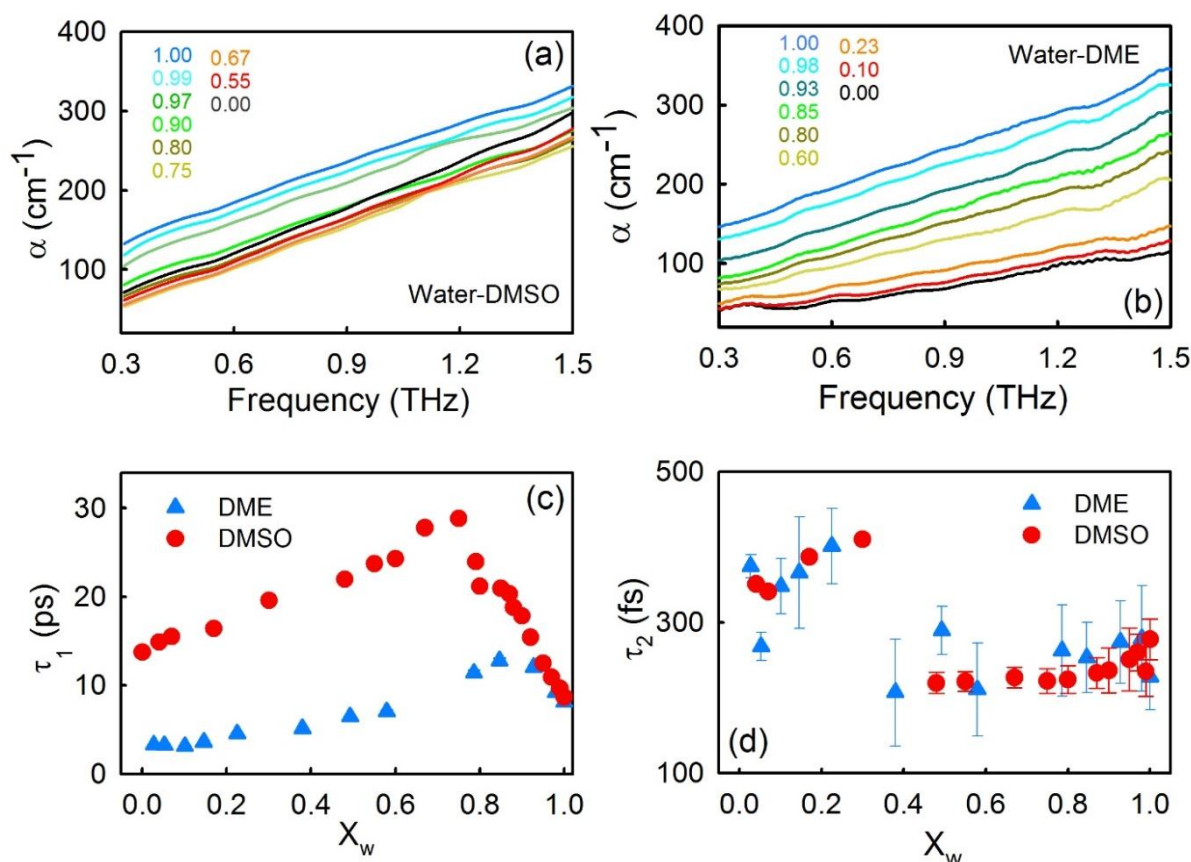


Figure 7.7. Absorption co-efficient (α) in the THz region as a function of frequency for (a) water-DMSO and (b) water-DME mixtures at different X_w (mentioned in the figure). Time constants (c) τ_1 and (d) τ_2 as a function of X_w for water-DME and water-DMSO mixtures.

To obtain the collective dynamics of water we fit the complex dielectric profiles of these solutions a triple *Debye relaxation model* (see table 7.III and 7.IV). DR of pure water in THz region produces three relaxation time constants of ~ 8 ps (τ_1), ~ 200 fs (τ_2) and ~ 90 fs (τ_3).^{46,68,74} The ~ 8 ps timescale of water corroborates the GHz measurement which explicitly associates with the spontaneous restructuring of the H-bond network.⁵⁴ The ~ 200 fs time constant, which is not recovered in the GHz measurements, emanates from either quick jumps of under-coordinated water or a small angular rotation preceding a large angle jump.⁷⁵ The ~ 80 fs timescale has its origin rooted to the 60 cm⁻¹ vibrational band due to the H-bond bending and the related transverse acoustic phonons which propagate in a direction normal to the H-bonds in between two neighbouring water molecules.⁶⁸ We plot the collective relaxation time constants (τ_1) in both the mixed

solvents as a function of X_w (figure 7.7c). The profiles more or less corroborate the GHz DR results. Accelerated τ_1 in the low X_w region in water-DME mixtures might emanate from confined water which unable to form large network in DME continuum. It could be noted here that water can form H-bond with the ether oxygen atoms of DME. Perhaps a close approach of water H-atom towards these ether O-atoms of DME is screened by its methoxy chain at low X_w and thus the inability to grow the network structure. At higher X_w , however, water-water and water-DME clusters predominate and the τ_1 value increases to ~ 12 ps and finally approaches that of pure water. In water-DMSO mixture, the collective dynamics is slow, and manifests the various complex aggregated structures formed at various X_w values. The faster time constant τ_2 , which mostly associates with the angular rotation of water molecules, behaves identically in both the solvent mixtures. At low X_w , it is a bit slow (~ 400 fs) and eventually converges to the ~ 200 fs time constant, which corresponds to the bulk water, at higher X_w (figure 7.7d). The apparent solvent indifference of this time constant is rooted in its very origin. τ_2 manifest the time taken by a water molecule to find its H-bond partner. At low X_w , this partner exchange processes are intuitively slower due to the low abundance as well as lack of water network structure in the solvent continuum that hinders the reorientational “jump motions”,^{75,76} which eventually eases as water is progressively added, and at $X_w \sim 0.4$, it resembles that of pure water. A recent 2D-IR study by Bagchi et al.⁷⁷ has shown an increase in the H-bond exchange rate with increase in the X_w in water-DMSO mixture. This study strongly corroborates our finding in τ_2 .

We measure depolarization, as calculated by the change in the dielectric relaxation strength (ΔS). It signifies the alteration in the cooperative H-bond structure of polar solvents. Typically dielectric response strength ($S = \epsilon_s - \epsilon_\infty$) decreases as compared to the bulk strength when one increases the concentration of the solute particles in the aqueous solution. The failure of the water dipoles to follow and reorient themselves with an applied oscillating electric field generates depolarization. It has grossly been believed that there exist three reasons behind such depolarization:⁷⁸ (a) *Dilution effect*: as one dissolve solute molecules in the solution the effective concentration of water decreases than bulk water, (b) *Kinetic depolarization*: if the solute particles contain charge, they move towards the external electric field and hence the water molecules are forced to reorient via another local electric field in the opposite direction to the external field, and (c) *Static depolarization*: if the water dipoles are H-bonded to the solute particles, they are

forced to orient and/or attached to the solute molecules. Such frozen water molecules fail to follow the external field and cannot participate in the DR processes. We measured the concentration of water in the mixtures (dilution effect) using densitometry and found that water concentration (C_w) decrease with decreasing X_w (data not shown here). This could be one of the reasons for the observed depolarization. However, the extent of decrement in C_w is comparable for both DME and DMSO; therefore, dilution cannot be the sole factor for depolarization. Also both the cosolvents do not contain any charge (no kinetic effect), and also the H-bonds are not so strong due to the presence of hydrophobic groups (no static effect). In DMSO the presence of polar SO bonds increase the affinity toward polar water molecules. It can act as a bridge between water clusters, and hence create a large and long lasting network of more aligned dipoles (less depolarization) than DME-water mixtures, where the presence of hydrophobic groups makes the orientation of water clusters random. Such randomized network leaves a positive contribution toward depolarization. Owing to the polar nature of DMSO molecules; it can fit themselves in the stretched water network whereas DME cannot. Presence of an electronegative SO bond makes DMSO molecule a more polar applicant than DME. The sulfur bonded oxygen of DMSO is more or less available to water specially at high X_w . But in DME the ether oxygens are screened by the carbon atoms resulting in the overwhelming effect of hydrophobicity.²⁸

Transient Absorption Study:

The pump-probe results, which involve the ultrafast de-activation dynamics of IR 125 is related to the immediate environment of the excited probe molecule and is, therefore informative of the micro-heterogeneity in the mixtures. To understand this micro-heterogeneity in further details we study the excited state lifetime dynamics of an NIR dye IR-125 in all the liquid mixtures. The results are depicted in figure 7.9. A representative UV-Vis absorption profile of IR-125 in DMSO-water mixtures with different X_w are shown in figure 7.9a. The corresponding absorption profiles for DME-water mixtures are shown in figure 7.8. We found with increasing X_w the absorption band (~790 nm in DMSO) suffers a slight blue shift with a moderate increment of the full width at half maxima (FWHM). We also found a comparatively broad shoulder in the blue end ~720 nm due to the vibronic side band coupling of the dye molecule. Increasing X_w also enhances the intensity of the vibronic band, which indicates that the increasing polarity of the solutions perhaps increases the

spacing of the ground vibrational states. Similar trends are also obtained in the DME-water mixtures (figure 7.8).

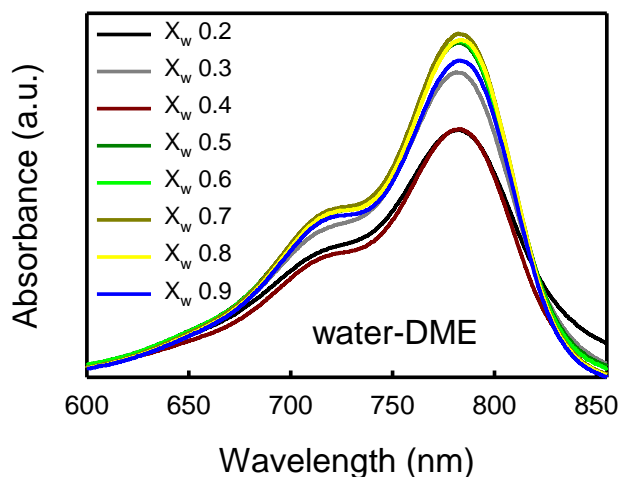


Figure 7.8. The absorption profile of IR-125 in water-DME binary mixtures.

In our experiment the laser pulse excites mainly the $|00\rangle$ and partially the $|01\rangle$ populations of the ground electronic states (see figure 7.10). The absorption decay transients of IR-125 in water-DMSO and water-DME solvent mixtures are shown in figures 7.9b,c respectively. We have fitted the transient intensity profiles, $I(t)$, with a triple exponential decay model as given by,

$$I(t) = \sum_{i=1}^3 a_i e^{-t/\tau_i}$$

where a_i and τ_i are the corresponding amplitude and time constant of the individual relaxation modes. We plot two representative fit of the pump-probe decay at $X_w \sim 0.5$ for water-DME and water-DMSO mixtures (see figure 7.11). The fitted parameters for the mixtures are listed in tables 7.V and 7.VI. We observe that the time constant of the dye in pure water are ~ 150 fs, 3.50 ps and 92 ps. The ~ 150 fs time constant can be assigned as due to vibrational relaxation, while the 3.5 and 92 ps time constants are due to the excited state relaxation process and ground state recovery/bleaching (GSB) or the population relaxation to the ground state respectively. Comparable decay pattern of the same dye in dichloromethane (DCM) was also reported previously by Goswami et al.⁷⁹ A previous magic angle pump-probe spectroscopy of cyanine dyes in neat solvents also showed a three exponential decay pattern⁴⁰ and it was further observed that solvent viscosity has a key role to play in determining the decay dynamics of the dye in neat solvents.⁴⁰ We notice that the

dynamics of the dye is very fast in pure water, whereas it is comparatively slower in pure DMSO and DME.

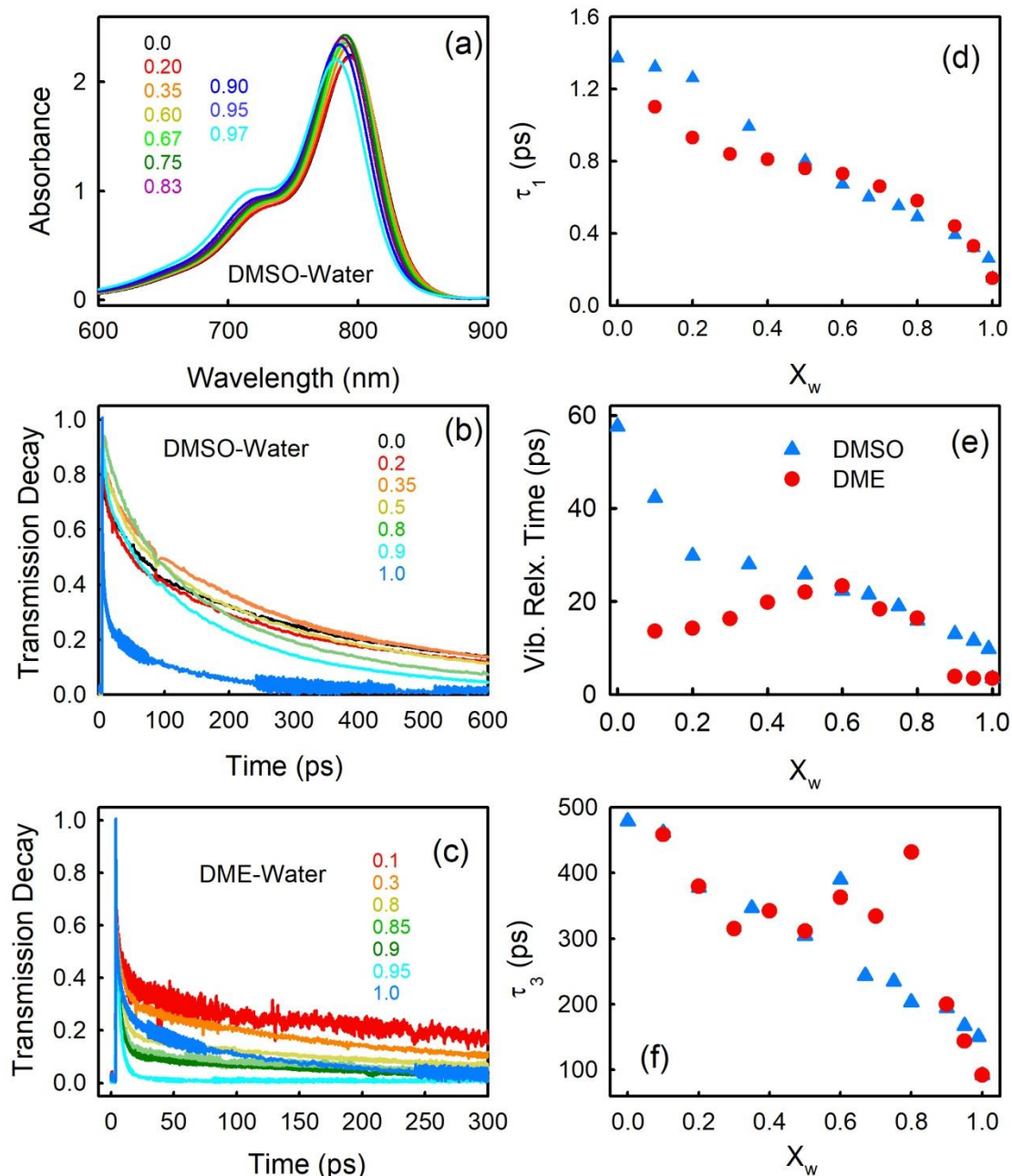


Figure 7.9. (a) Absorption spectra of IR-125 in water-DMSO mixtures at different X_w (mentioned in the figure). The probe is excited at 800 nm for the pump-probe experiments. (b and c) Transient decays of IR-125 absorption at different X_w values for DMSO-water and DME-water mixtures. Triple exponential fitting timescales (τ_1 , τ_2 and τ_3) IR-125 dye at different X_w in DMSO-water and DME-water mixtures.

The dynamics of the dye in water arises due to the low viscosity of water compared to the other two solvents. This is not straight forwardly intuitive in the binary mixtures, as the viscosity (η) and the refractive index (n) changes non-uniformly in the mixtures. Accordingly the absorption pattern of the dye as well as the overlap region of the laser spectrum and the

dye absorption spectra changes. As a result the transition in the different vibrational levels varies producing the non-linear variation in the τ_1 values (figure 7.9d). The changes in the τ_2 and τ_3 values are partly related to the viscosity of the mixtures. The slowest component (τ_3) is more or less of comparable magnitude for both the mixed solutions. A comparable appearance of maximum in dynamics is observed in methanol-chloroform mixtures of IR775 dye using pump-probe techniques.

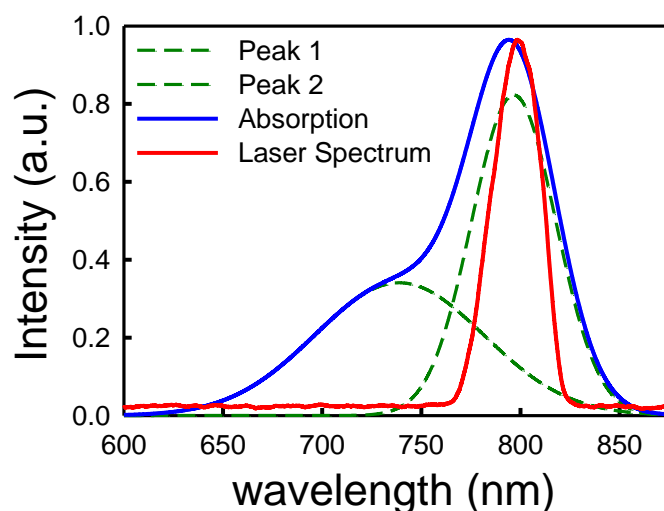


Figure 7.10. Absorption spectrum of IR-125 dye (blue solid line). The curve is deconvoluted into two Gaussian curves (dotted lines). The laser pulse is shown in red.

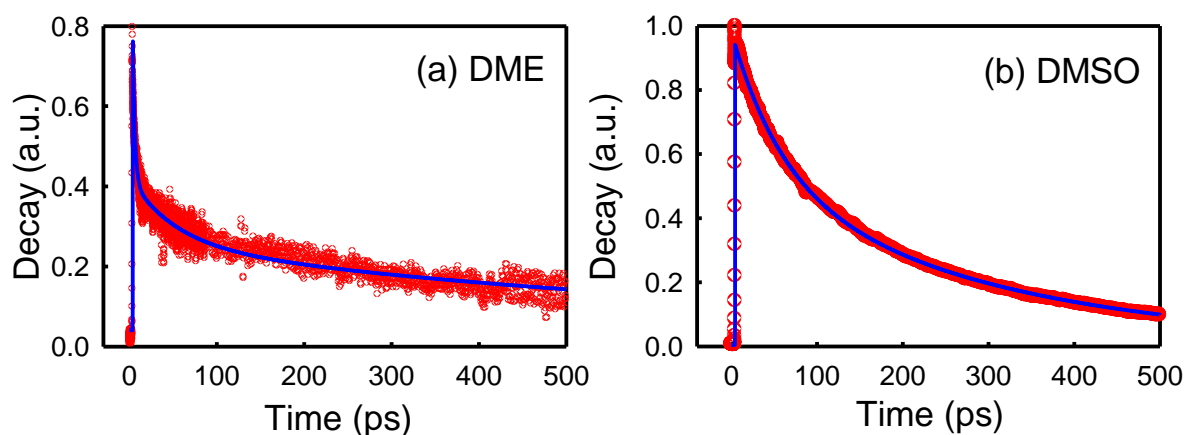


Figure 7.11. A representative plot for the transient decay with multiple exponential decay equation at $X_w = 0.5$ for (a) water-DME and (b) water-DMSO mixtures.

We prefer to focus our discussion on the time constant τ_2 , which eventually correlates the vibrational relaxation of the excited dye IR 125. In τ_2 , however, we observe a definite deviation in the magnitude, separately in the low X_w region. We found that this decay dynamics of the dye in pure water is very fast (~ 3.5 fs) while it is slower in pure DME (13.6 ps) and DMSO (57.6 ps). The magnitude of τ_2 is governed by the extent of collision between

the excited probe and solvent molecules. It could be noted that this is a non-radiative processes in which excited state molecular population relaxes through solvent medium and hence is defined by the local viscosity. The viscosity of water is almost half as that of DMSO, while that of DME is comparable. So a mere consideration of the microscopic viscosity is not sufficient to account for the observed slower relaxation. In the DMSO-water mixtures, increase in X_w decreases τ_2 sharply in the low X_w region, then gets more or less flat, and eventually decreases further at high X_w . In case of DME, however, it increases first to pass through a maxima at $X_w \sim 0.4$ and then decreases. In the low X_w region (from 0 to 0.1), DMSO-DMSO aggregation in the neighborhood of dye molecules could result in a slower decay of the dye molecules. In the intermediate region (from 0.1 to 0.4), due to the formation of DMSO-water H-bonded clusters, the collision with the dye and the other molecules decreases and hence the decay time constant remains slow compared to the water-DME mixtures. So, the micro-heterogeneous environments in those two liquid mixtures definitely differ and the extent of variation is rooted in the hydrophobic aggregation among the co-solvents as well as that extent of H-bond formation with water.

7.4. Summary

In this chapter we have studied the H-bond dynamics of water in presence of two cosolvents (DME and DMSO) which differ in their respective H-bond formation capacity with water. Due to the presence of an electronegative sulfur atom DMSO tends to form H-bonds with polar water molecules, which are also stronger than the H-bonds formed with water and DME molecules. Such polar-polar affinity results in various stable $m\text{DMSO}:n\text{H}_2\text{O}$ H-bonding clusters. DME, owing to its higher carbon content, and being a planer molecule the steric obstacles screened the H-bond acceptor oxygen atoms and struggle to form H-bonding. As a result it is more inclined towards the formation of hydrophobic aggregations, or a random orientation of water around those hydrophobic interfaces. The difference in the affinity of H-bond formation and self-aggregation is expected to get replicated in the hydration dynamics. We compare both global (through DR study) as well as local (through FTIR and pump-probe study) hydration environment and dynamics in the two binary mixtures.

Table 7.I. Dielectric relaxation fit parameters of the complex dielectric functions of water-DMSO mixtures in 0.2-50 GHz frequency region using single Debye relaxation model.

X_w	ϵ_s	t (in ps)	S_w (actual)	S_w (exp.)	μ_{eff} (D)
0.00	49.38	22.56	0.00	44.34	0
0.10	51.57	24.46	2.04	46.34	18.20
0.20	54.90	28.86	4.43	49.46	12.75
0.27	56.97	31.68	6.37	51.38	10.83
0.35	59.50	35.99	8.93	53.82	9.36
0.45	62.76	42.53	12.78	57.03	8.06
0.50	64.85	46.94	15.05	59.15	7.56
0.55	67.44	51.25	17.61	61.67	7.14
0.60	69.13	53.30	20.52	63.42	6.71
0.67	71.96	53.77	25.31	66.34	6.18
0.75	75.43	52.01	32.19	69.92	5.62
0.80	75.77	42.60	37.52	70.40	5.23
0.90	79.09	25.40	51.83	73.46	4.54
1.00	80.23	8.95	74.57	74.97	3.82

Table 7.II. Dielectric relaxation fit parameters of the complex dielectric functions of water-DME mixtures in 0.2-50 GHz frequency region using single Debye relaxation model.

X_w	ϵ_s	t (in ps)	S_w (actual)	S_w (exp.)	μ_{eff} (D)
0.10	8.00	3.30	1.32	5.63	7.84
0.20	9.36	4.65	2.92	6.32	5.58
0.30	10.92	6.14	4.89	7.33	4.64
0.40	12.61	7.99	7.37	8.63	4.10
0.50	15.95	10.47	10.60	11.38	3.93
0.60	20.23	13.93	14.90	15.18	3.83
0.70	26.82	17.28	20.92	21.35	3.83
0.80	34.42	18.47	29.87	28.89	3.73
0.85	45.65	20.25	36.28	39.31	3.94
0.90	48.24	16.50	44.65	42.26	3.69
0.95	67.07	14.10	56.37	58.56	3.86
1.00	79.48	8.95	73.59	74.35	3.81

Table 7.III. Debye relaxation fit parameters for water-DME mixtures at different compositions in 0.2-1.8 THz frequency region. We have fixed the value of ϵ_s from literature.

X_w	τ_1 (in ps)	τ_2 (in fs)
0.03	3.28±0.02	374.5±15.7
0.05	3.22±0.02	267.7±18.6
0.10	3.12±0.02	347.8±36.5
0.15	3.62±0.04	365.7±73.7
0.22	4.55±0.06	402.7±62.5
0.38	5.12±0.13	206.8±71.0
0.49	6.46±0.05	289.0±31.8
0.58	7.05±0.17	210.7±61.9
0.79	11.40±0.32	262.4±60.6
0.85	12.78±0.32	252.9±46.8
0.93	12.06±0.27	273.7±54.9
0.98	9.20±0.15	278.3±70.0
1.00	8.10±0.10	227.6±43.6

Table 7.IV. Debye relaxation fit parameters for water-DMSO mixtures at different compositions in 0.2-1.8 THz frequency region. We have fixed the value of ϵ_s from literature.

X_w	τ_1 (in ps)	τ_2 (in fs)
1.00	8.10±0.10	227.6 ±43.6
0.95	12.49 ±0.04	250.56 ±40.1
0.90	17.80 ±0.13	236.16 ±38.6
0.85	20.31 ±0.17	232.69 ±33.9
0.80	21.18 ±0.32	224.04 ±33.2
0.75	28.81 ±0.15	222.02±33.8
0.67	27.77 ±0.10	226.73 ±34.6
0.60	24.27 ±0.13	224.5 ±37.3
0.55	23.74±0.09	221.28 ±42.1
0.48	21.95 ±0.16	219.58 ±40.6
0.30	19.60 ±0.14	410.00±40.7
0.17	16.40 ±0.10	387.00 ±33.8
0.07	15.50 ±0.09	341.00 ±36.6
0.04	14.89 ±0.07	351.00 ±38.6

Table 7.V. The pump-probe decay fit parameters as fitted with a triple exponential relaxation equation for water-DMSO mixtures at different compositions.

X_w	a_1	τ_1 (in ps)	a_2	τ_2 (in ps)	a_3	τ_3 (in ps)
0.00	0.21	1.37±0.032	0.30	57.60±0.050	0.49	479.06±1.22
0.10	0.18	1.32±0.001	0.34	42.30±0.048	0.49	461.42±1.423
0.20	0.16	1.26±0.005	0.32	29.88±0.025	0.52	377.64±0.95
0.35	0.04	0.99±0.009	0.25	27.99±0.023	0.71	346.61±1.16
0.50	0.04	0.80±0.007	0.28	25.90±0.075	0.67	303.99±0.93
0.60	0.14	0.67±0.017	0.18	22.37±0.086	0.69	389.82±1.11
0.67	0.05	0.60±0.006	0.30	21.57±0.049	0.65	243.56±1.39
0.75	0.02	0.55±0.002	0.25	18.99±0.055	0.73	234.90±1.09
0.80	0.05	0.49±0.019	0.20	15.90±0.095	0.76	203.22±0.89
0.90	0.06	0.39±0.001	0.28	13.04±0.078	0.66	194.11±1.17
0.95	0.05	0.32±0.007	0.29	11.57±0.048	0.66	167.28±1.22
0.99	0.06	0.26±0.009	0.52	9.86±0.037	0.42	150.27±1.05
1.00	0.46	0.15±0.001	0.31	3.48±0.095	0.23	91.86±1.19

Table 7.VI. The pump-probe decay fit parameters as fitted with a triple exponential relaxation equation for water-DME mixtures at different compositions.

X_w	a_1	τ_1 (ps)	a_2	τ_2 (ps)	a_3	τ_3 (ps)
0.10	0.44	1.10±0.003	0.25	13.63±0.033	0.31	458.59±1.30
0.20	0.12	0.93±0.008	0.33	14.26±0.052	0.55	379.47±1.22
0.30	0.42	0.84±0.017	0.25	16.36±0.044	0.33	315.25±1.80
0.40	0.43	0.81±0.005	0.25	19.86±0.039	0.32	342.25±1.32
0.50	0.41	0.76±0.011	0.26	21.99±0.059	0.33	311.07±1.19
0.60	0.45	0.73±0.006	0.25	23.36±0.089	0.30	362.68±0.98
0.70	0.45	0.66±0.017	0.27	18.37±0.049	0.29	334.01±0.78
0.80	0.59	0.58±0.018	0.28	16.37±0.022	0.12	431.60±0.99
0.90	0.24	0.44±0.009	0.65	3.89±0.089	0.12	199.67±1.52
0.95	0.26	0.33±0.010	0.72	3.51±0.076	0.01	143.79±1.31
1.00	0.46	0.15±0.014	0.31	3.48±0.071	0.23	91.86±1.74

7.5. References

- (1) Tanford, C. *The Hydrophobic effect: formation of micellar and biological membranes*; 2nd ed.; Wiley Interscience: New York, **1980**.
- (2) Blokzijl, W.; Engberts, J. B. F. N. *Angewandte Chemie International Edition in English* **1993**, *32*, 1545-1579.
- (3) Das Mahanta, D.; Samanta, N.; Mitra, R. K. *The Journal of Physical Chemistry B* **2017**, *121*, 7777-7785.
- (4) Das, D. K.; Das Mahanta, D.; Mitra, R. K. *ChemPhysChem* **2017**, *18*, 749-754.
- (5) Ide, M.; Maeda, Y.; Kitano, H. *The Journal of Physical Chemistry B* **1997**, *101*, 7022-7026.
- (6) Wiggins, P. M. *Physica A: Statistical Mechanics and its Applications* **1997**, *238*, 113-128.
- (7) Southall, N. T.; Dill, K. A.; Haymet, A. D. J. *The Journal of Physical Chemistry B* **2002**, *106*, 521-533.
- (8) O'Brien, E. P.; Dima, R. I.; Brooks, B.; Thirumalai, D. *J. Am. Chem. Soc.* **2007**, *129*, 7346-7353.
- (9) Fenn, E. E.; Moilanen, D. E.; Levinger, N. E.; Fayer, M. D. *J. Am. Chem. Soc.* **2009**, *131*, 5530-5539.
- (10) Chandler, D. *Nature* **2005**, *437*, 640-647.
- (11) Buchner, R.; Holzl, C.; Stauber, J.; Barthel, J. *Physical Chemistry Chemical Physics* **2002**, *4*, 2169-2179.
- (12) Chandler, D. *Nature* **2002**, *417*, 491-491.
- (13) Thomas, S. *Angewandte Chemie International Edition* **2002**, *41*, 48-76.
- (14) Suresh, S. J.; Naik, V. M. *The Journal of Chemical Physics* **2000**, *113*, 9727-9732.
- (15) Chaplin, M. [Internet URL] <http://www1.lsbu.ac.uk/water/anmlies.html>. **April, 2010**.
- (16) Das Mahanta, D.; Rana, D.; Patra, A.; Mukherjee, B.; Mitra, R. K. *Chem. Phys. Lett.* **2018**, *700*, 50-56.
- (17) Pascal, T. A.; Goddard, W. A. *The Journal of Physical Chemistry B* **2012**, *116*, 13905-13912.
- (18) Bakker, H. J. *Nature* **2012**, *491*, 533-535.
- (19) Huang, N.; Schlesinger, D.; Nordlund, D.; Huang, C.; Tyliszczak, T.; Weiss, T. M.; Acremann, Y.; Pettersson, L. G. M.; Nilsson, A. *J. Chem. Phys.* **2012**, *136*, 074507.
- (20) Garde, S.; Hummer, G.; García, A. E.; Paulaitis, M. E.; Pratt, L. R. *Physical Review Letters* **1996**, *77*, 4966-4968.
- (21) Lotze, S.; Groot, C. C. M.; Vennehaug, C.; Bakker, H. J. *The Journal of Physical Chemistry B* **2015**, *119*, 5228-5239.
- (22) Bedrov, D.; Borodin, O.; Smith, G. D. *J. Phys. Chem. B* **1998**, *102*, 5683-5690.
- (23) Bedrov, D.; Pekny, M.; Smith, G. D. *J. Phys. Chem. B* **1998**, *102*, 996 - 1001.
- (24) Bedrov, D.; Smith, G. D. *J. Phys. Chem. B* **1999**, *103*, 3791-3796.
- (25) Goutev, N.; Ohno, K.; Matsuura, H. *The Journal of Physical Chemistry A* **2000**, *104*, 9226-9232.
- (26) Banik, D.; Kundu, N.; Kuchlyan, J.; Roy, A.; Banerjee, C.; Ghosh, S.; Sarkar, N. *J. Chem. Phys.* **2015**, *142* 054505.
- (27) Wong, D. B.; Sokolowsky, K. P.; El-Barghouthi, M. I.; Fenn, E. E.; Giammanco, C. H.; Sturlaugson, A. L.; Fayer, M. D. *The Journal of Physical Chemistry B* **2012**, *116*, 5479-5490.

- (28) Das Mahanta, D.; Patra, A.; Samanta, N.; Luong, T. Q.; Mukherjee, B.; Mitra, R. K. *The Journal of Chemical Physics* **2016**, *145*, 164501.
- (29) Rasmussen, D. H.; Mackenzie, A. P. *Nature* **1968**, *220*, 1315.
- (30) Havemeyer, R. N. *J. Pharm. Sci.* **1966**, *55*, 851-853.
- (31) Goutev, N.; Nickolov, Z. S.; Matsuura, H. *J. Mol. Liq.* **1998**, *76*, 117-126.
- (32) Jha, A. K.; Freed, K. F. *The Journal of Chemical Physics* **2008**, *128*, 034501.
- (33) Lee, S. H.; Rossky, P. J. *J. Chem. Phys.* **1994**, *100*, 3334-3345.
- (34) Yaminsky, V. V.; Voglerb, E. A. *Curr. Op. Colloid Interface Sci.* **2001**, *6*, 342-349.
- (35) TANFORD, C. *Proc. Natl. Acad. Sci. USA* **1979**, *76*, 4175-4176.
- (36) Scatena, L. F.; Brown, M. G.; Richmond, G. L. *Science* **2001**, *292*, 908-912.
- (37) Kropman, M. F.; Bakker, H. J. *Science* **2001**, *291*, 2118-2120.
- (38) Liu, J.-Y.; Fan, W.-H.; Han, K.-L.; Xu, D.-L.; Lou, N.-Q. *The Journal of Physical Chemistry A* **2003**, *107*, 1914-1917.
- (39) Nikowa, L.; Schwarzer, D.; Troe, J.; Schroeder, J. *The Journal of Chemical Physics* **1992**, *97*, 4827-4835.
- (40) Yu, A.; Tolbert, C. A.; Farrow, D. A.; Jonas, D. M. *The Journal of Physical Chemistry A* **2002**, *106*, 9407-9419.
- (41) Banno, M.; Ohta, K.; Yamaguchi, S.; Hirai, S.; Tominaga, K. *Accounts of Chemical Research* **2009**, *42*, 1259-1269.
- (42) Kumpulainen, T.; Lang, B.; Rosspeintner, A.; Vauthey, E. *Chemical Reviews* **2017**, *117*, 10826-10939.
- (43) Berera, R.; van Grondelle, R.; Kennis, J. T. M. *Photosynth. Res.* **2009**, *101*, 105-118.
- (44) Rosspeintner, A.; Lang, B.; Vauthey, E. *Annual Review of Physical Chemistry* **2013**, *64*, 247-271.
- (45) Mazur, K.; Heisler, I. A.; Meech, S. R. *The Journal of Physical Chemistry B* **2010**, *114*, 10684-10691.
- (46) Das Mahanta, D.; Samanta, N.; Mitra, R. K. *Journal of Molecular Liquids* **2016**, *215*, 197-203.
- (47) Agieienko, V.; Buchner, R. *Physical Chemistry Chemical Physics* **2016**, *18*, 2597-2607.
- (48) Tielrooij, K. J.; Paparo, D.; Piatkowski, L.; Bakker, H. J.; Bonn, M. *Biophys. J.* **2009**, *97*, 2484-2492.
- (49) Born, B.; Kim, S. J.; Ebbinghaus, S.; Gruebele, M.; Havenith, M. *Faraday Discuss.* **2009**, *141*, 161-173.
- (50) Plusquellic, D. F.; Siegrist, K.; Heilweil, E. J.; Esenturk, O. *ChemPhysChem* **2007**, *8*, 2412-2431.
- (51) Sajadi, M.; Berndt, F.; Richter, C.; Gerecke, M.; Mahrwald, R.; Ernsting, N. P. *The Journal of Physical Chemistry Letters* **2014**, *5*, 1845-1849.
- (52) Sibik, J.; Elliott, S. R.; Zeitler, J. A. *The Journal of Physical Chemistry Letters* **2014**, *5*, 1968-1972.
- (53) Beard, M. C.; Turner, G. M.; Schmuttenmaer, C. A. *J. Phys. Chem. B* **2002**, *106*, 7146-7159.
- (54) Samanta, N.; Mahanta, D. D.; Choudhury, S.; Barman, A.; Mitra, R. K. *The Journal of Chemical Physics* **2017**, *146*, 125101.
- (55) Ellis, J. W.; Sorge, B. W. *The Journal of Chemical Physics* **1934**, *2*, 559-564.
- (56) Śmiechowski, M.; Stangret, J. *Pure Appl. Chem.* **2010**, *82*, 1869-1887.
- (57) Verma, P. K.; Kundu, A.; Ha, J.-H.; Cho, M. *Journal of the American Chemical Society* **2016**, *138*, 16081-16088.

- (58) Kříž, J.; Dybal, J. *Chemical Physics* **2011**, 382, 104-112.
- (59) Smith, J. D.; Saykally, R. J.; Geissler, P. L. *J. Am. Chem. Soc.* **2007**, 129, 13847-13856.
- (60) Popov, I.; Ishai, P. B.; Khamzin, A.; Feldman, Y. *Physical Chemistry Chemical Physics* **2016**, 18, 13941-13953.
- (61) Hippel, A. R. v. *ITEI* **1988**, 23, 801-816.
- (62) Tielrooij, K.-J.; Hunger, J.; Buchner, R.; Bonn, M.; Bakker, H. J. *J. Am. Chem. Soc.* **2010**, 132, 15671-15678.
- (63) Yamada Pittini, Y.; Daneshvari, D.; Pittini, R.; Vaucher, S.; Rohr, L.; Leparoux, S.; Leuenberger, H. *Eur. Polym. J.* **2008**, 44, 1191-1199.
- (64) Lu, Z.; Manias, E.; Macdonald, D. D.; Lanagan, M. *The Journal of Physical Chemistry A* **2009**, 113, 12207-12214.
- (65) Ohno, K.; Okimura, M.; Akai, N.; Katsumoto, Y. *Physical Chemistry Chemical Physics* **2005**, 7, 3005-3014.
- (66) Kaatz, U.; Pottel, R.; Schaefer, M. *The Journal of Physical Chemistry* **1989**, 93, 5623-5627.
- (67) Roy, S.; Banerjee, S.; Biyani, N.; Jana, B.; Bagchi, B. *The Journal of Physical Chemistry B* **2011**, 115, 685-692.
- (68) Samanta, N.; Das Mahanta, D.; Kumar Mitra, R. *Chemistry – An Asian Journal* **2014**, 9, 3457-3463.
- (69) Bergner, A.; Heugen, U.; Bründermann, E.; Schwaab, G.; Havenith, M.; Chamberlin, D. R.; Haller, E. E. *Rev. Sci. Instr.* **2005**, 76, 063110.
- (70) Born, B.; Kim, S. J.; Ebbinghaus, S.; Gruebele, M.; Havenith, M. *Faraday Discussions* **2009**, 141, 161-173.
- (71) Leitner, D. M.; Gruebele, M.; Havenith, M. *HFSP journal* **2008**, 2, 314-323.
- (72) Schmidt, D. A.; Birer, Ö.; Funkner, S.; Born, B.; Gnanasekaran, R.; Schwaab, G.; Leitner, D. M.; Havenith, M. *J. Am. Chem. Soc.* **2009**, 131, 18512-18517.
- (73) Samanta, N.; Das Mahanta, D.; Mitra, R. K. *Physical Chemistry Chemical Physics* **2014**, 16, 23308-23315.
- (74) Samanta, N.; Das Mahanta, D.; Mitra, R. K. *Phys. Chem. Chem. Phys.* **2014**, 16, 23308--23315.
- (75) Laage, D.; Hynes, J. T. *Science* **2006**, 311, 832-835.
- (76) Laage, D.; Stirnemann, G.; Hynes, J. T. *J. Phys. Chem. B* **2009**, 113, 2428-2435.
- (77) Kashid, S. M.; Jin, G. Y.; Chakrabarty, S.; Kim, Y. S.; Bagchi, S. *The Journal of Physical Chemistry Letters* **2017**, 8, 1604-1609.
- (78) Tielrooij, K. J.; van der Post, S. T.; Hunger, J.; Bonn, M.; Bakker, H. J. *The Journal of Physical Chemistry B* **2011**, 115, 12638-12647.
- (79) Goswami, T.; Kumar, S. K. K.; Dutta, A.; Goswami, D. *The Journal of Physical Chemistry B* **2009**, 113, 16332-16336.

8. Decisive Role of Hydrophobicity over Electrolytes on Protein Stability

Many biological and chemical processes involve a subtle interplay between Columbic and hydrophobic interactions among molecular groups with water. A comprehensive understanding of such processes, specially while they are acting together in the same molecule is of practical importance. In this regard alkylammonium halides are the perfect candidate to study. Here we report the ultrafast (sub-ps to ps) collective hydrogen bond dynamics of water in the extended hydration layers of alkylammonium chloride salts using THz-TDS technique (0.3-1.6 THz ($10\text{-}55\text{ cm}^{-1}$)). We fit the frequency dependent dielectric constants with Debye dielectric relaxation model to obtain the hydrogen bond relaxation dynamics. We found these salts transform from being a water ‘structure breaker’ to ‘structure maker’ as we increase the carbon content. We further investigate their effect on the structure of a model protein BSA and observe a systematic trend towards disrupting the protein secondary structure. The associated changes in the protein hydration in presence of these salts have also been examined using TTDS.

8.1. Introduction

Non-polar hydrophobic molecules in water are supposed to increase disorder due to their inability to form H-bond with the polar water molecules.¹ The nature of such water phobia in hydrophobic molecules governs the structure and dynamics of water network that are very much different from the bulk. However, they can also enhance the ordering in their surrounding water network.² The notion of hydrophobic hydration, still a popular topic of research, is highly specific on the type and dimension of the solute. Small hydrophobic solutes either get arrested within the polyhedral cage formed by the under- or un-coordinated water molecules with dangling O-H bonds^{2,3} or, the solutes as well as the solvent separately aggregates to form clusters⁴ with enhanced H-bond network. Larger solutes can even disrupt the tetrahedral network of water. In both the cases there exist defects in the water H-bonded network,³ which is the key driving factor that directs most of the physicochemical and biological processes.⁵⁻⁹ Likewise, ion-water interaction also plays a vital role in biology and chemistry.^{10,11} The effect and the perturbation on the H-bonded structure and dynamics of liquid water provided by the electrolytes and the hydrophobic molecules are already

discussed in *chapter 4* and *chapter 5,6 & 7*. *Chapter 1* has broadly introduced the problem about the ion specific electrostatic interaction interactions and the hydrophobic interactions.¹²⁻¹⁷ Bakker et al. have found that the effect of some ions well extend beyond first hydration shell and the hydration dynamics of those ions is cooperative and also non-additive in nature. It depends on the hydration nature of the counter ions also.¹⁸ In another work Bakker et al. have found that the nature of perturbation of cations, anions and hydrophobic molecules are very much different in nature. The cations forced the water dipoles fixed in radially outwards direction with the OH dipoles are free to rotate, whereas anions holds one of the OH hand of the water molecules fixed and the water dipole can freely rotate within a cone. But in case of hydrophobic solutes the reorientation of water molecule is isotropic that is quite different from the anisotropic reorientation of water around ions.¹⁹ In comparison with the hydrophobic solutes, they observed that hydrophobic molecules perturb the water dynamics strongly than the ions, in which the Coulombic interactions are privilege.²⁰ THz spectroscopic investigation by another group Havenith et al.^{21,22} established the correlation between hydration dynamics and the ‘rattling’ motion of metal ions. However, a direct correlation between H-bonding and water structure making/breaking ability of ions is highly debatable. Generally ions perturb the structure and dynamics of water in its next adjacent layers, and hardly found to influence water in longer distances. However, for strongly hydrated ions such effect could be extended beyond the second or third solvation shell of the ions,^{12,23} that can be probed by DR spectroscopic study. There are lots of research regarding the structural information of ion hydration using various experimental and computer simulation techniques^{13,18-20,24-35}

Instead of understanding electrostatic and hydrophobic interactions discretely, it is a practical importance to investigate the two opposing effects while they are operating simultaneously. Such study can sketch a comparative outline among the two rivalry candidates. In this regard, cations consisting of water repelling moieties have recently attracted attention of the researchers owing to their unique hydration behaviour.^{20,33,36-39} Alkylammonium halides series are the most extensively studied salts that hold a rare combination of ionic and hydrophobic characters within the same molecule. The important fact is that one can compare the interaction patterns by tuning their hydrophobicity. Such molecules contain short chain alkanes and unlike amphiphilic molecules do not usually aggregate at moderate concentrations.³⁷ Several research groups investigate the physical nature of water around these hydrophobic ions using both experimental and simulation techniques.^{38,40-44} These studies have argued over the popular belief of enhancement of the H-

bonded 'ice-like' structure of water around these solutes^{45,46} concluding that in case of short chain alkylammonium halides the hydration structure is quite similar compared to that of bulk water. However, such effects are found to be prominent for larger ions having $n \geq 3$ ⁴¹ (n is the number of carbons in the alkylammonium cations). Previously some simulation studies have concluded about the enhancement of water structure around alkylammonium ions.^{47,48} Buchner et al. have made a detailed DR study in the GHz frequency region (0.2-89 GHz) in order to obtain both solute and solvent dynamics in a series of n -alkylammonium salts solutions.³⁸ They noticed that up to $n=2$, the effect of these ions on water dynamics is not significant, while for propyl and *t*-butyl salts the effect is noticeable. However in compare to the alkali monovalent metal cations, those hydrophobic cations display marked contrast in their nature of perturbation. A simple consideration of the increased size of the cations⁴⁹ does not suffice to explain this behavior.⁴² Beauchamp et al. have found that ions can as well influence hydrophobic effect also.⁵⁰ While most of the previous studies are rather concerned with the rigidly bound first solvation shell hydration, relatively less attention has been paid on the long-range semi-rigid H-bond cooperative relaxation dynamics. A recent simulation study has revealed the existence of strongly oriented water molecules in the first solvation shell of tetra-methylammonium cations, the effect being lost in the subsequent hydration shells.⁴³ Experimental validation of whether such effect is at all experienced beyond the first solvation shell, specially for larger carbon containing cations, definitely demands attention.

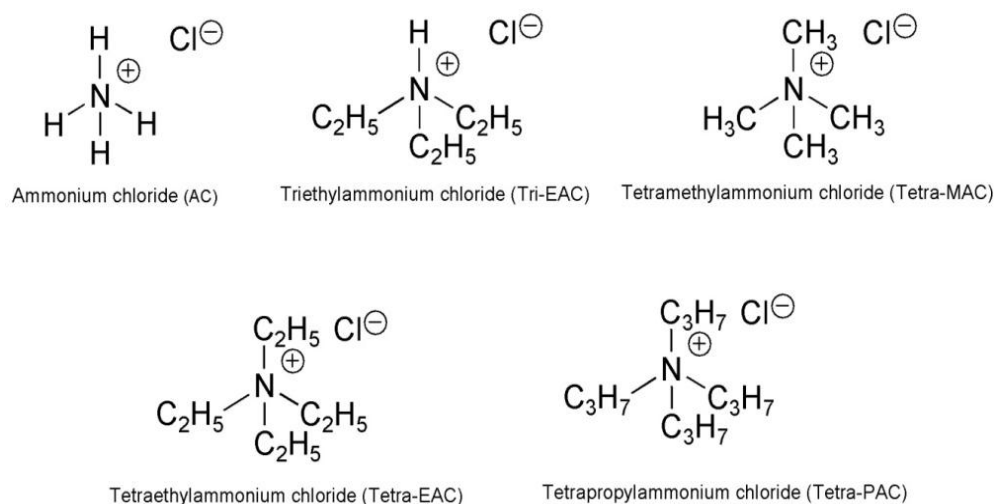
Intermolecular rotational and vibrational modes of water, which extend beyond the first solvation shell, produce their signature in the THz frequency region^{51,52} enabling to study collective hydration dynamics in complex systems.^{4,14,22,53-58} Due to its low energy (~ 4 meV at 1THz), THz radiation leaves biomolecules almost unperturbed and the extracted timescale can probe the ultrafast (ps to sub-ps) dynamics of their extended hydration shells water networks.^{56,59-61} Along with this, the advantage of measuring both the phase and the amplitude of the transmitted radiation in a single experiment by this technique can infer microscopic information about the cooperative H-bond dynamics of water around solutes and bio-molecules.^{56,59-62} Results achieved with this technique could often be found to be complementary to many other conventional techniques, specially to the low frequency Raman scattering technique, which extract pivotal information from biologically relevant molecules.⁶³ Recently we have studied H-bond relaxation dynamics around alkali metal monovalent ions and found these cations accelerate the water cooperative dynamics and the magnitude of such effect is not a mere linear manifestation of the cation radius only.^{14,56} We

also investigated such dynamics around amino acid aqueous solutions and evidenced the formation of more ordered water network around them depending upon the hydrophobic or hydrophilic nature of their side chains.⁵⁷ In this regards, it is more interesting to investigate how such dynamics is modified when hydrophobicity is introduced into the ions. We made an attempt to explicitly address the concern whether such ions exert any direct or indirect effect on proteins. Such interactions are important and yet highly debatable in chemical biology.^{64,65}

In this chapter, we choose a well-studied model protein BSA and a series of alkylammonium chlorides salts: tetra-methylammonium chloride (Tetra-MAC), tri-ethylammonium chloride (Tri-EAC), tetra-ethylammonium chloride (Tetra-EAC) and tetra-propylammonium chloride (Tetra-PAC). We measure the stability of the protein in presence of these monovalent hydrophobic salts using CD spectroscopy. We observed that salts with higher hydrocarbon content do perturb the stability of the native protein more intensely. This observation is intriguing that leads us to enquire whether this destabilization is associated with any change in the H-bond structure of water. We explore the water structure around these salts using FTIR and THz TDS (0.3-1.6 THz region). To obtain the co-operative H-bond dynamics of water in presence of these salts we fit the extracted real and imaginary part of the dielectric functions with a multiple *Debye DR model*. We fix Cl^- as the counter anion so as to compare the effect solely arising out of the cations only.¹⁴ We have already discussed in *chapter 4* that DR of water dipoles are mostly dominated by the cations while the dependency is only subtle for anions.²⁰ We observe contrasting cooperative water H-bond making or breaking behaviour. We also notice the proficient effect of tetra-EAC on the protein stability compared to that of tri-EAC, with the latter one differ only by one ethyl moiety. We estimate the effect of these two ions on the long range cooperative protein hydration dynamics using TTDS measurements. To get a comparative understanding, we also study the effect of electrolyte molecules NaCl, CsCl (as Cs^+ has comparable size to that of tetra-MA cation) and a well-known protein denaturant molecule, guanidinium hydrochloride (GdmCl).⁵⁶ These electrolytes samples also hold a unit charge itself that can exert purely electrostatic interactions into the solution. Our study is aimed to investigate the extent of hydrophobic hydration in alkylammonium chloride as a function of alkyl chain content and understand their effect on a model protein. The present study has unambiguously pointed out towards the decisive role of hydrophobicity over the electrostatic interaction in protein hydration.

8.2. Materials and Methods

All the chemicals (scheme 8.1) were of the highest available purity, purchased from Sigma-Aldrich and were used without further purification. We used deionized Milli-Q water to prepare the aqueous stock solutions of the salts. For protein solutions we used sodium phosphate buffer (10 mM) at pH 7.0.



Scheme 8.1: Chemical structures of the alkylammonium chloride salts.

FTIR spectroscopy measurements were carried out in a JASCO FTIR-6300 in the MIR region ($2200\text{-}2800\text{ cm}^{-1}$) with the HOD probes prepared by vigorous mixing of 4% D_2O in pure water. All the data represented in this study are difference absorbance spectrum with pure salt/water aqueous solutions used as the reference. THz-TDS measurements were carried out in the THz spectrophotometer (TERA K8, Menlo System). The relaxation dynamics of water dipoles in presence of those hydrophobic salts are obtained using *Debye DR model*. CD measurements were performed in a JASCO J-815 spectrometer.^{14,56} The protein concentration was fixed at $2\mu\text{M}$ for CD and 1mM for TTDS measurements. The native fraction of the BSA protein in buffer solution and in presence of salts solution are determined by this equation⁶⁶

$$\text{Native fraction} = \frac{\theta_T - \theta_U}{\theta_N - \theta_U} \quad (8.1)$$

where θ_T , θ_U , and θ_N are the CD signals at experimental temperature, when the protein is completely unfolded, and in its native state, respectively. Denaturation temperature (T_m) is the temperature at which the native fraction of the protein becomes 50% of its initial value. DLS measurements were carried out with *Nano S Malvern* instrument employing a 4mW He-

Ne LASER ($\lambda = 632.8$ nm) equipped with a thermostated sample chamber.^{66,67} According to Stokes-Einstein (SE) model, we calculate the hydrodynamic diameter d_H of BSA. The data for the viscosities of the solutions are taken from the literature.³⁸ *Further details about the instruments and the underline methods can be found in chapter 2.*

8.3. Results and Discussions

Effect of salts on protein: Far-UV (200-260 nm) CD measurements of BSA at room temperature with different alkylammonium salts are shown in figure 8.1. The native protein in buffer solution shows two characteristic negative peaks at 208 nm and 222 nm. These two peaks recognize the abundance of α -helical structure in BSA. The negative 222 nm band is due to the peptide $n-\pi^*$ transition, whereas 208 nm band results from the exciton splitting of the lowest peptide $\pi-\pi^*$ transition.^{66,68} We found that AC and tetra-MAC do not affect the CD spectra significantly, however, a noticeable perturbation is observed in case of higher alkyl chain salts. For tetra-PAC, the effect is intense even at low salt concentrations (figure 8.2).

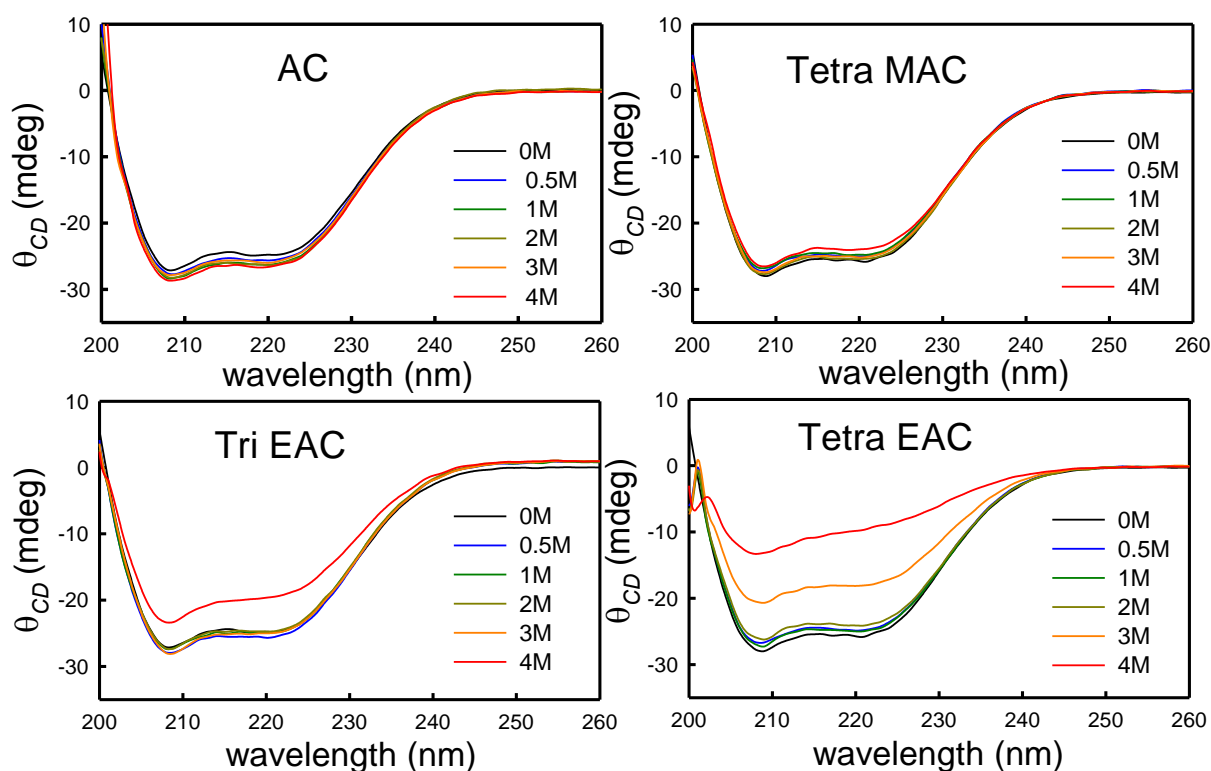


Figure 8.1. CD spectra of BSA protein at different concentrations of the various salts.

For a quantitative insight we plot the CD signal measured at 222 nm as a function of those hydrophobic salt concentrations (figure 8.3a). We observe a sharp change beyond 2M

tetra-EAC and at low concentration of tetra-PAC. A mild change is also observed at 4M concentration of tri-EAC. The native protein is rich in α -helix content (~70%) with smaller contributions of other secondary structures like random coils (~13%), β -turn (~12%) etc. We calculate the relative abundance of the secondary structures and plot the α -helical content with salt concentration (figure 8.3b). We found a striking contrast between tri- and tetra-EAC salts, while the latter one induces significant reduction (above 2M salt concentration) in the secondary structure the former one is rather mild towards it, at least up to a concentration of 3M. Such contrasting behaviour with a difference of only one ethyl group in their structure is salient. Tetra-PAC is known to unfold proteins and polypeptides,⁶⁹ however, such effect has rather been unexplored in smaller chain cations. At 1.5 M salt concentration, this effect follows the sequence of the increasing number of hydrocarbon chain (tetra-PAC>tetra-EAC>tri-EAC>tetra-MAC~AC). Earlier we observed that the content of α -helix in BSA did not change appreciably in presence of monovalent metal cations¹⁴ whereas with the same charge alkylammonium cations are found to behave differently, the reason being the added hydrophobicity.

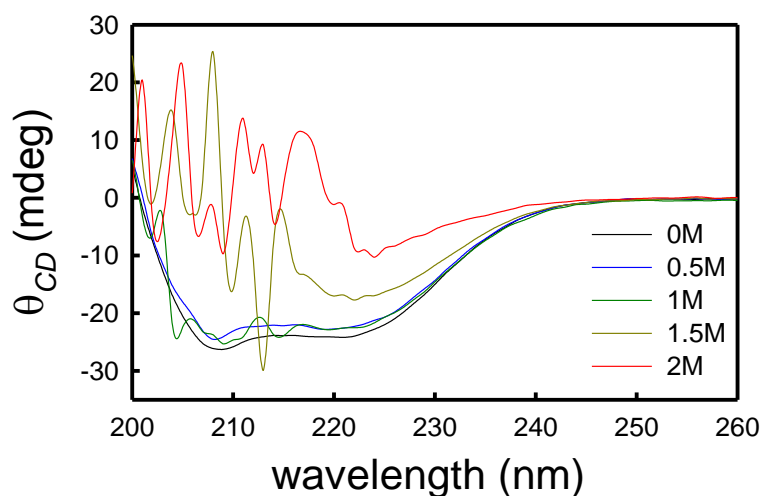


Figure 8.2. CD spectra of BSA in presence of tetra-PAC.

To examine the thermal stability of BSA in presence of these salts we measure the fraction of the native protein present at different temperatures (following the description given in the *chapter 2*). A representative profile for tetra-EAC is shown in figure 8.3c. We obtain the melting temperature (T_m) from the first derivative of those curves and plot it against salt concentration (figure 8.3d). Both tetra-MAC and AC modestly stabilize the protein by slightly increasing T_m compared to that in the buffer (~67⁰C), which is in good

agreement with a previous study using another globular protein ribonuclease.⁷⁰ On the other hand, tri- and tetra-EAC show marked thermal disability (lowering of T_m), the effect being more prominent in tetra-EAC compare to that in tri-EAC. Tetra-PAC shows drastic destabilization, as has already been evidenced in other proteins.⁶⁴

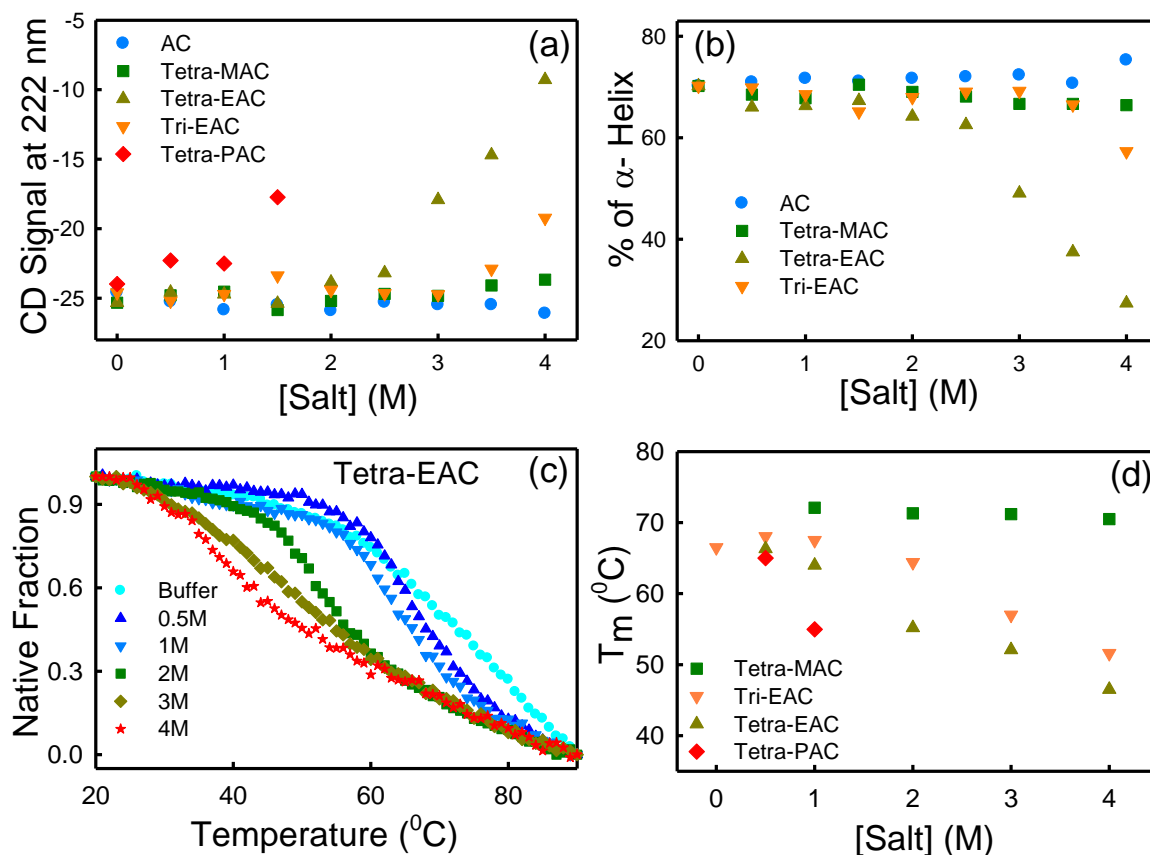


Figure 8.3. (a) CD signal at 222 nm of BSA solution in presence of different salts. (b) Relative population of α -helix content of BSA as a function of salt concentration. (c) Native fraction of BSA as a function of temperature of tetra-EAC at different salt concentrations. (d) Melting temperature (T_m) of BSA solutions as a function of salt concentration.

Size of the protein molecule in buffer and at different salt solutions is measured using DLS technique (figure 8.4). BSA is a globular protein with a hydrodynamic diameter of ~6-7 nm in aqueous solution.⁷¹ AC slightly reduces the size of BSA manifesting a modest compactness of the protein as has already been evidenced from the CD measurements (see figure 8.3). Tetra-MAC has only marginal effect and is comparable to that of an otherwise indifferent salt NaCl. On the other hand, the effect of tetra-EAC is intense compared to that of tri EAC. As a control, we measure the size of the protein in presence of GdmCl. We found that GdmCl increases the protein size moderately beyond 2M, which coincides with its protein unfolding threshold concentration.⁵⁶ Up to 1M concentration the effect of tetra-EAC and tri-EAC are comparable to that of GdmCl. At higher concentrations, both these salts

increase the protein size distinctly than GdmCl. As a control, we check the possibility of salt aggregation within the studied concentrations. We do not find any such signature from the DLS measurements inconclusive of the aggregation phenomenon. Our recent study on amino acids also confirmed no such aggregation behaviour irrespective of the solute's hydrophobicity.⁵⁷ The protein concentration was also kept low ($\sim 10 \mu\text{M}$) to avoid protein aggregation.

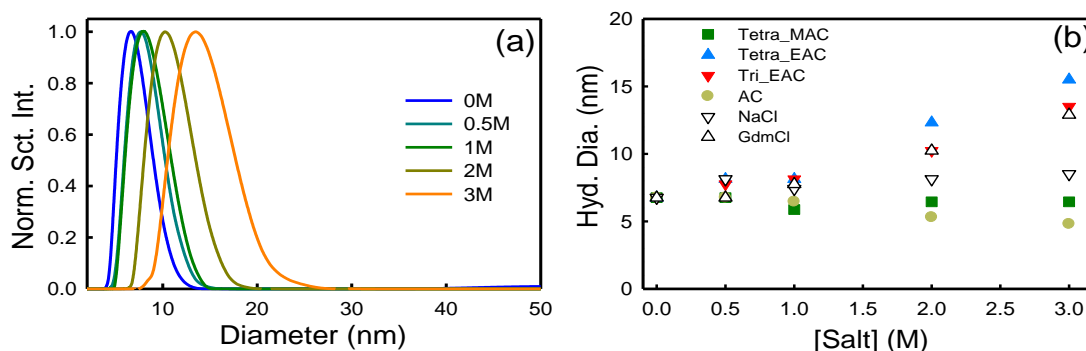


Figure 8.4. (a) Representative scattering profile of BSA in presence of Tri-EAC at different concentrations. (b) The hydrodynamic diameter of BSA in various salt solutions with increasing salt concentrations.

The above study shows that the presence of extra hydrocarbon group influences protein stability substantially (tetra-PAC>tetra-EAC>tri-EAC), moreover, the effect is contrasting when compared to a purely ionic salt NaCl. Cations with hydrophobic groups thus seem to preferentially interact with the hydrophobic milieu of BSA. This leads a priori to infer that it is the hydrophobic rather than the electrostatic interaction that plays the decisive role during interactions with proteins. In earlier studies^{55,56} we have observed that protein denaturant molecules (e.g. urea, GdmCl etc.) disrupt the cooperative water network, at least beyond a threshold concentration, which could in its turn render additional impetus towards protein denaturation. This suggests two possible independent pathways of protein denaturation: indirect (through perturbing the water network structure) and direct (preferentially interact with the hydrophobic core of the proteins), both occurring subsequently, the latter one having the predominant effect. In continuation with these findings, we now try to address the question whether the strong protein denaturing ability of tetra-EAC correlates H-bond modification of water. In the following section, we investigate the local and also the collective H-bond structure and dynamics of water in these salt solutions.

MIR study: The O-D vibrational stretch of isotopically diluted HOD (4% D₂O in pure water) in the 2300–2800 cm⁻¹ frequency window is an ideal tool to explore solute hydration and is

extremely sensitive to its local H-bond structure.^{4,72} It is important to remember here that MIR-FTIR explores the equilibrium water structure corresponding to individual O-D vibrational stretch only and does not correspond to the cooperative dynamics of water. Here we report the difference absorbance data where salt aqueous solutions are used as reference, the data is, therefore, bearing explicitly the signature of OD oscillators.

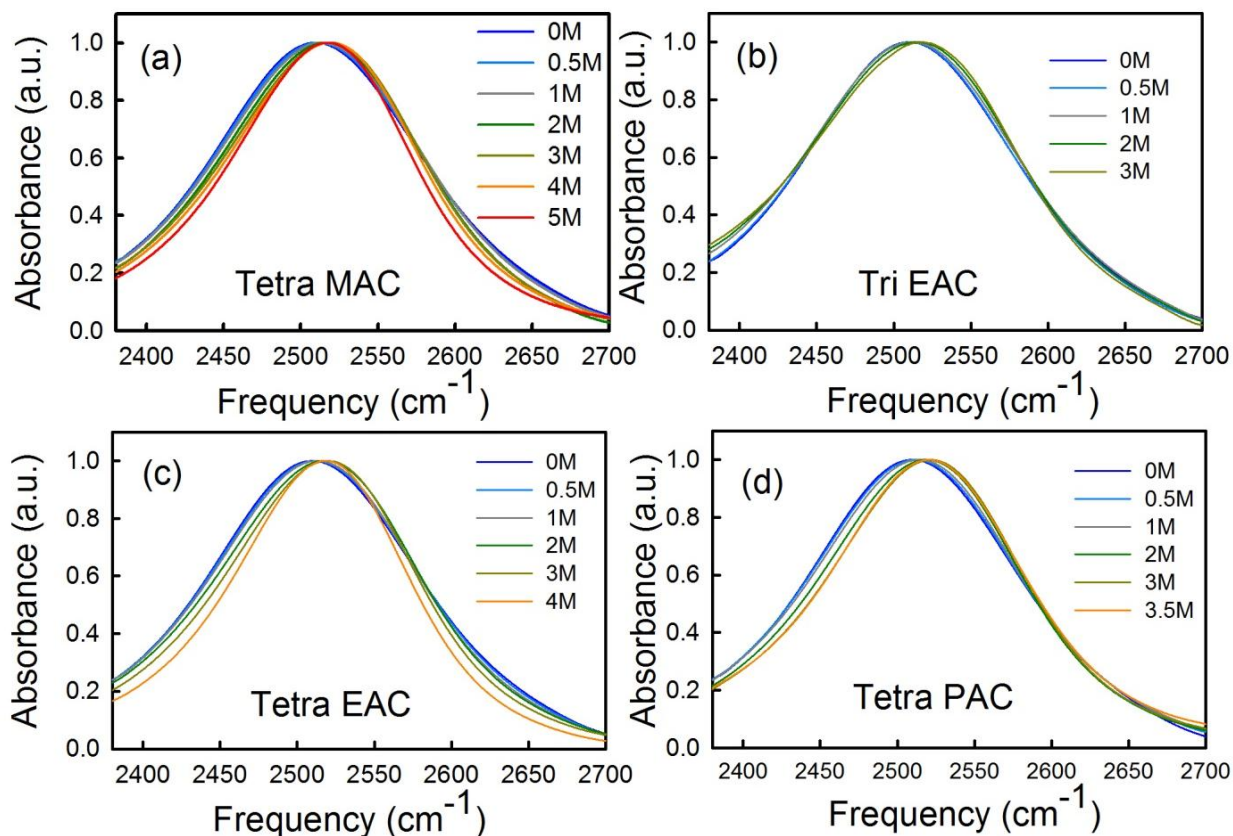


Figure 8.5. Normalized FTIR absorption spectra of HOD (4% D₂O in water) in presence of different salts.

The OD stretching band of pure water peaks at $\sim 2505 \text{ cm}^{-1}$, which gets progressively blue shifted in presence of these salts (figure 8.6). Similar trends had previously been observed for monovalent alkali salts¹⁴ and tetra-ethylammonium salts.³⁶ We plot the peak frequency (ν_{peak}) against salt concentration (figure 8.6b). The observed blue shift can be explained in terms of the reduction of the electric field along the hydroxyl stretch²⁶ coupled with the weakening of H-bond strength,^{73,74} the effect being most prominent in tetra-PAC. The extent of blue shift is found to be higher in case of the conventional univalent alkali metal ions (figure 8.6b); perhaps the larger size and lower charge density make the alkylammonium cations interacting weakly with water. For example, the radius of Na^+ (102 pm) and Cs^+ (170 pm) are smaller than those of tetra-EA (337 pm) and tetra-PA (379 pm)

ions, and the metal cations have the greater impact compared to the latter ones. In case of alkylammonium salts, the electrostatic interaction tries to reorient and hold strongly the nearby water molecules making them relatively less available to participate in the water network.

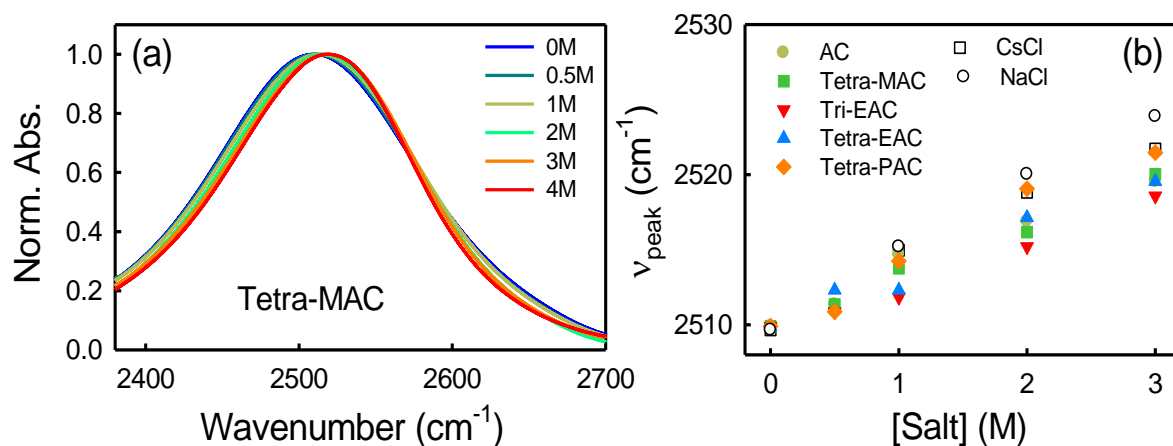


Figure 8.6. (a) Normalised FTIR absorption spectra of HOD in presence of tetra-MAC. (b) Peak frequency as a function of salt concentration.

On the other hand, due to the hydrophobic repulsion water molecules try to form enhanced ice-like structures.^{36,45,75} We investigate the existence of such ice-like water structure in presence of these salts and deconvolute each MIR spectra into two Gaussian peaks,⁷⁶⁻⁷⁸ keeping one band fixed at 2420 cm⁻¹ which corresponds to the ice like O-D stretch.^{36,79} We do not find any signature of ice-like water in NaCl and CsCl, however, a small but non-negligible abundance (3-8%) is observed in the alkylammonium salts (figure 8.7).

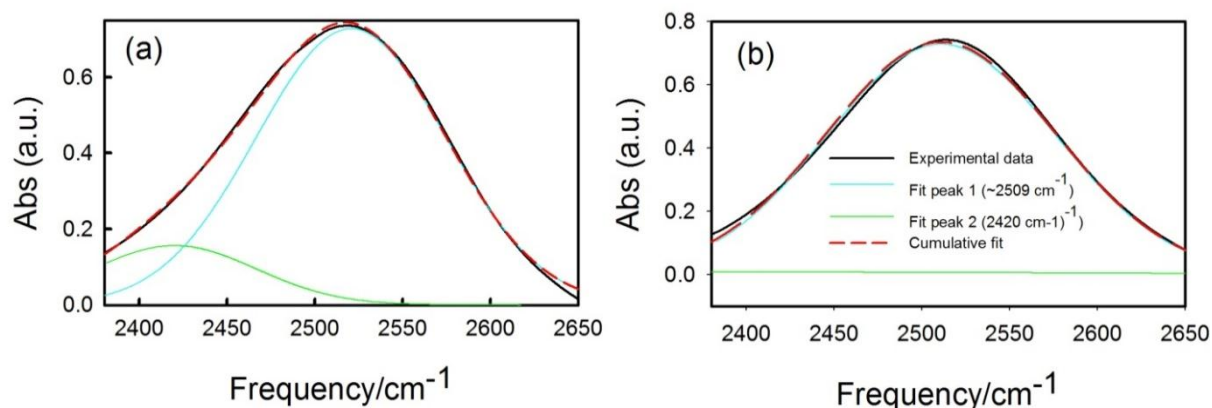


Figure 8.7. Representative deconvoluted FTIR absorption spectrum for (a) Tetra EAC and (b) NaCl.

THz TDS study: We obtain frequency dependent absorption coefficient $\alpha(\nu)$ of the solutions from TTDS measurements in the frequency range of 0.3 to 1.6 THz (figures 8.8). It is important to note here that α_{THz} is a direct manifestation of the cooperative dynamics of water.^{4,22,55,56,60,80} The absorption ($\alpha(\nu)$) profiles (figure 8.9a-b) are found to be contrasting for the salts containing hydrophobic groups compared to the purely ionic salts,¹⁴ in the former ones a THz defect (lower $\alpha(\nu)$ for solutions compared to bulk water) is observed while for the ionic salts we found THz excess. AC behaves identically to those of ionic salts exhibiting THz excess. As methyl group is introduced into it (tetra-MAC) the extent of THz excess decreases. Replacing highly absorbing water molecules with rather low absorbing hydrophobic groups induces “THz defect” in which $\alpha(\nu)$ lies below that of pure water as has previously been observed for alcohols,⁵⁸ sucrose, urea, tri-methylamine-N-oxide (TMAO),⁵⁵ tetra-methylguanidinium chloride (TMGdmCl)⁵⁶ and proteins.⁸¹ Interestingly, in glycine, urea and GdmCl solutions $\alpha(\nu)$ curves intersect that of pure water;⁵⁵⁻⁵⁷ this phenomenon, however, is not observed in these salts. This makes the hydration behaviour of alkylammonium salts somewhat intermediate between those of the conventional protein denaturants and alkali metals. For a comparative understanding we plot the α measured at 1 THz as a function of salt concentration (figure 8.9c). The dotted line represents $\alpha_{1\text{THz}}$ for pure water.

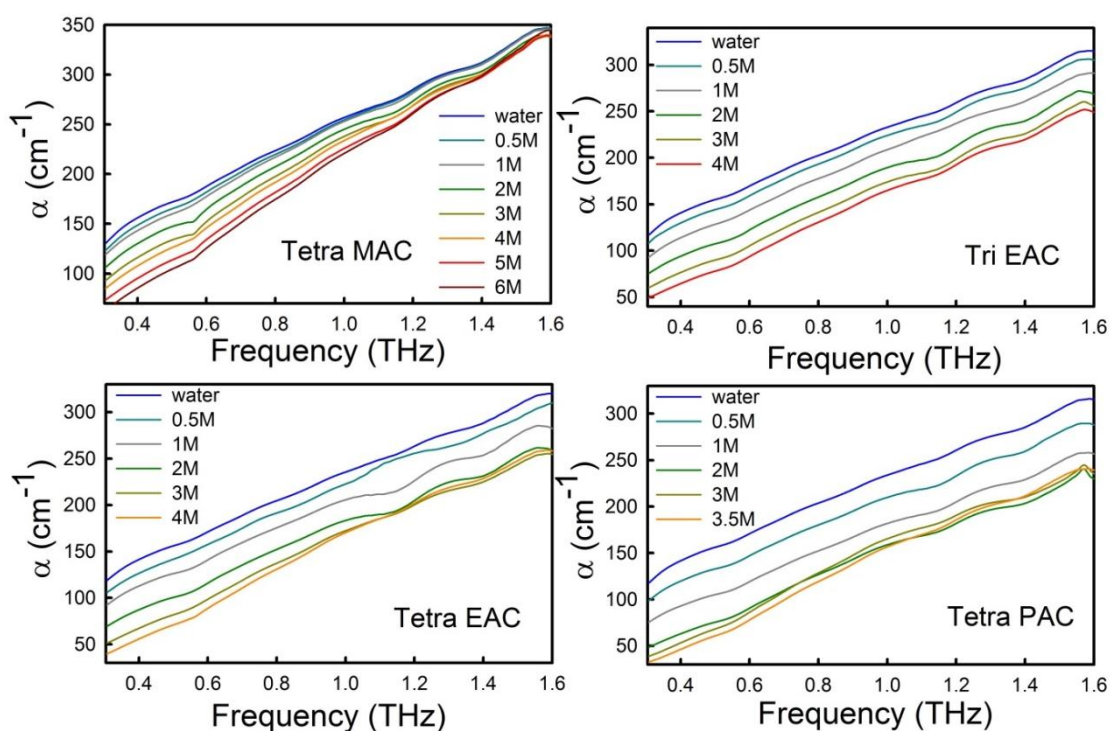


Figure 8.8. Absorption ($\alpha(\nu)$) profiles in the THz regime of the aqueous solutions of different alkylammonium chloride salts.

The figure distinctly defines two classes of ions on the either sides of the dotted line. It is important to note here that while explaining the behaviour of $\alpha(\nu_{\text{THz}})$, it should be taken into consideration that solutes associate a dynamic hydration shell with timescale ranging from ps to sub-ps, which might extend up to 5-7 Å and could offer optical properties markedly different from those of bulk water.⁸² Thus the overall change in α_{THz} is a collective contribution from the solvent, the solute and the hydration water, eventually introducing the observed non-linearity in the α -profile.⁸³ The maximum positive deviation is observed for Cs^+ while the maximum negative deviation is obtained for tetra-PAC. At low concentration (<1 M) tetra-MAC produces similar impact on water as that of Cs^+ , both having comparable sizes, however, at higher concentrations, the alkali metal is a prominent THz enhancer while tetra-MAC shows only low to moderate effect. The α_{THz} value of AC is found to be less than that of Cs^+ but higher than that of tetra-MAC. Metal cations exhibit pure electrostatic interactions to perturb the water network structure. A subtle interplay between the two counter interacting effects in alkylammonium salts gradually enhances water structure as depicted in the form of THz defect.

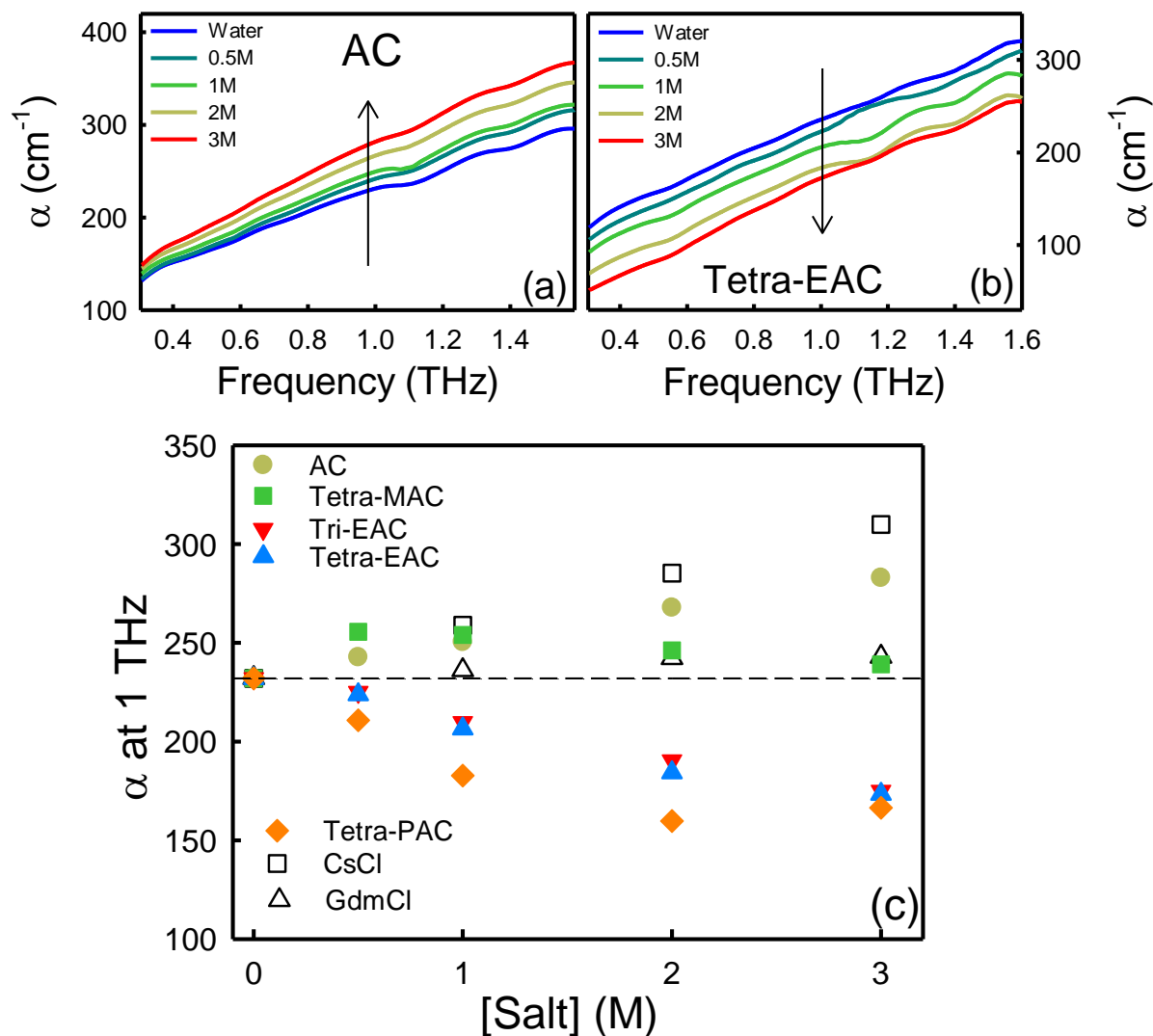


Figure 8.9. Frequency dependent absorption coefficient of water in presence of (a) ammonium chloride (AC) and (b) tetra-ethylammonium chloride (Tetra EAC) at different salt concentrations. The arrows indicate increasing salt concentration. (c) THz absorption (α) at 1 THz of different salt solutions as a function of salt concentration.

We obtain the collective H-bond dynamics of these salt solutions by fitting the complex permittivity into a triple *Debye DR model* (a representative fit is shown in figure 8.10a). DR directly probes macroscopic polarization of solution, which eventually gives the reorientation of the dipoles. The first mode describes the co-operative rearrangement of the bulk-like water with strength $S_1 = S_{\text{bulk}}$, and $\tau_1 = \tau_{\text{bulk}}$ (~ 9 ps). The second and the third terms correlate the large angular rotations of water molecules (~ 200 fs) and the H-bond bending mode (~ 80 fs).^{14,55} For pure water we obtain $\tau_{\text{bulk}} = 8.9$ ps (table 8.I). Monovalent metal ions act as water structure breakers, showing gradual decrease in τ_{bulk} .¹⁴ In the extended solvation shells the electro-restricted water molecules do not adhere to the network structure and consequently the collective dynamics gets faster.

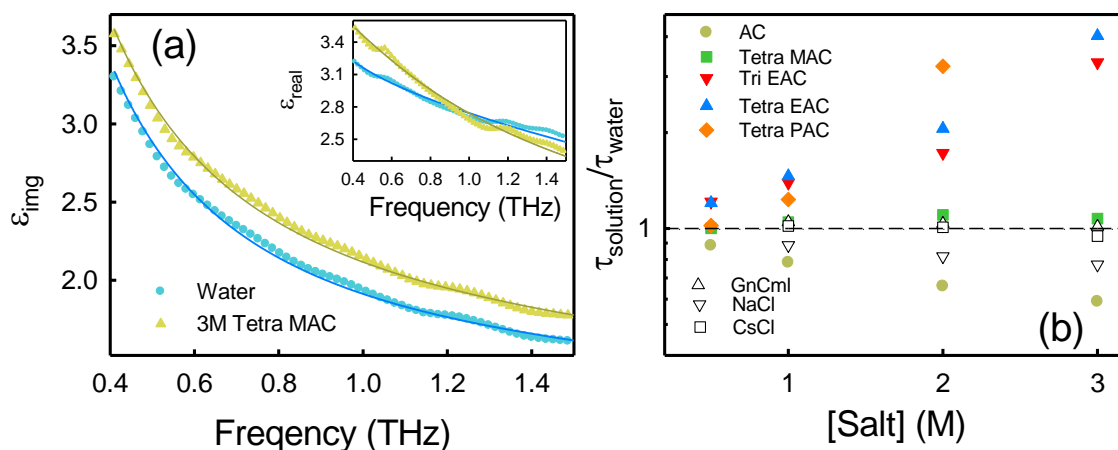


Figure 8.10. (a) Real (inset) and imaginary part of the dielectric constant (ϵ) of water and 3M tetra-MAC solution (symbol). The solid lines are multiple Debye fitted curves. (b) The ratio of $\tau_{\text{solution}}/\tau_{\text{water}}$ as a function of salt concentrations.

For the hydrophobic cations, however, the dynamics is observed to get retarded (table 8.I). Due to relatively low charge density and considerable hydrophobicity, the alkylammonium ions tend to repel water molecules, as has been evidenced by the existence of ice-like water structure formation (see figure 8.7). The exposure of these hydrophobic moieties forces water molecules to pack more tightly which perhaps induces the observed retardation in dynamics.^{38,84} An optimum interplay between these two opposing interactions causes only subtle changes in tetra-MAC (figure 8.10b, table 8.I). With increasing carbon content, the electrostatic effect weakens, and to avoid unfavourable interactions water network grows stronger resulting in a gradually retarding co-operative dynamics (table 8.1). Formation of such slow-mobile with enhanced H-bond configuration water molecules gains further support from the decreasing trend of bulk water relaxation strength, S_{bulk} (figure 8.11).

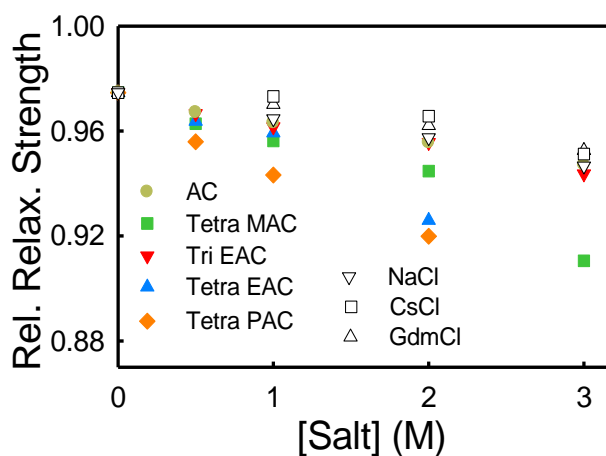


Figure 8.11. Cooperative relaxation strength ($\frac{S_1}{S_1+S_2+S_3}$) in presence of different salts.

Hydration of the protein: Our study unambiguously infers that introduction of alkyl groups considerably alters the associated hydration dynamics in alkylammonium ion. We also observe that tetra-EAC has prominent effect on protein stability compared to that of tri-EAC while their respective effects on water structure are comparable. We now investigate the effect of these two salts on the protein hydration itself. A representative frequency dependent absorption profile in presence and in absence of the salts is shown in figure 8.12a. The solid lines represent the spectra of aqueous solutions while the dotted lines stand for those in presence of 1 mM BSA. It is observed that the absorption profile of the protein solution lies below that of pure water. Such a decrease in the absorption coefficient is best explained on the basis of a three component model which takes care of the contributions from water (α_w), protein (α_{pr}) and the associated hydration sheathe (α_w^{hyd}) added together.^{58,81,83,85} The change in the THz absorption profile of proteins in presence of solutes is a direct consequence of the change in the cooperative dynamics of the protein hydration layer.⁵⁸ We calculate the values of $\Delta\Delta\alpha$ at 1 THz ($=\Delta\alpha_{salt}^{pr} - \Delta\alpha_w^{pr}$ where, $\Delta\alpha_{salt}^{pr} = \alpha_{pr-salt} - \alpha_{salt}$ and $\Delta\alpha_w^{pr} = \alpha_{pr-w} - \alpha_w$, while α for any multi-component system is defined as, $\alpha = \sum_i \phi_i \alpha_i$ with ϕ_i being the volume fraction of the i-th component)⁵⁸ which exemplifies the explicit change in the protein hydration due to the presence of the salts. We plot $\Delta\Delta\alpha$ as a function of salt concentration for the tri- and tetra-EAC in figure 8.12b. We found that the change in the hydrated water structure around the protein differs drastically in 3M tetra-EAC corroborating the protein disruption threshold concentration. It is interesting to note here that we did not observe noticeable change in $\Delta\Delta\alpha$ in alkali monovalent salts; however, the changes were severe in GdmCl.

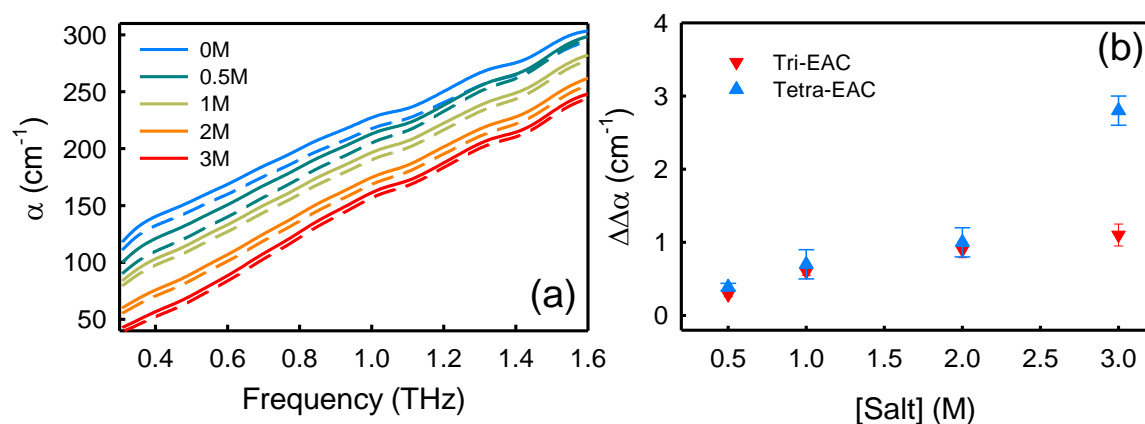


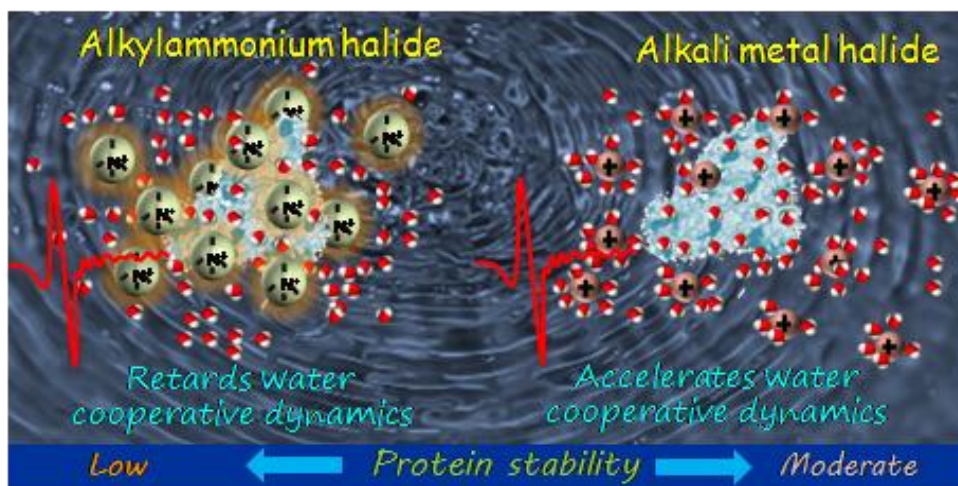
Figure 8.12. (a) Frequency dependent absorption coefficient (α) of tetra-EAC solutions of different concentrations in absence (solid line) and in presence (broken lines) of 1mM BSA. (b) Change in absorption coefficient ($\Delta\Delta\alpha$) of 1mM BSA solution as a function of salt concentration.

The CD study shows that at 3M tetra-EAC a significant fraction of α -helical structure of BSA opens up, c.f. from 70% it reduces to 49% at the expense of the formation of ~23% random coil structure. This, in turn, explores less structured hydrophobic residues towards the solvation layer⁸³ which eventually leads to the change in $\Delta\Delta\alpha$ at 3M. It is important to note here that the change in a protein hydration is not straightforward, rather is a juxtaposition of several factors that leads to change in $\Delta\Delta\alpha$. One such parameter is the change in the protein volume fraction (ϕ_{pr}); in DLS study we observed modest increase in protein size in presence of these two salts (see figure 8.4). However, the changes occur within a comparable range, and also α_{pr} is very small compared to α_w and α_w^{hyd} to produce significant effect in $\Delta\Delta\alpha$. This makes the difference in tri- and tetra-EAC even more interesting. Also interesting to note here that, GdmCl, which produces an equivalent change in protein dimension as of tri-EAC, has a pronounced destabilization of the protein's secondary structure. This suggests that these cations make specific interactions with the protein surface depending on their specific nature. Our previous studies have concluded that both urea and GdmCl act as water structure breaker, specially beyond a threshold concentration, which perhaps renders finite impetus on their respective protein denaturation ability. The present study shows that tetra-EAC, in spite of being an efficient water structure maker, beholds the property of disrupting protein structure through preferential hydrophobic interactions, whereas an efficient water structure breaker AC is rather naive towards proteins. This study strongly validates the predominating role of hydrophobic over electrostatic interaction to produce protein denaturation. The overwhelming effect of tetra-EAC on protein over tri-EAC is engaging; the difference of only one ethyl group does not bring about the drastic difference on their individual effect on water structure. A more systematic investigation in this direction both through experiment and simulation is much in need to unravel the delicate balance of real biological environments.

8.4. Summary

Our study was aimed to inquire the interplay between two apparently competing factors important in biological processes. We investigated the effect of a series of alkylammomium chlorides on BSA and found that these salts do perturb protein structure depending upon the hydrocarbon content. Striking difference in tetra-EAC and tri-EAC was observed. TTDS measurements reveal that AC acts as a water network structure breaker while tri-EAC and higher carbon containing salts are distinct water structure makers. The change in protein hydration is also found to trace its secondary structure rupture and the exposure of

hydrophobic moieties accordingly changes the protein hydration. Our study strongly concludes that it is the hydrophobic effect, at least in the case of this type of salts that plays the decisive role in determining their interaction with biomolecules.



Scheme 8.2: Contrasting interactions of alkali cations and hydrophobic cations with water and proteins.

Table 8.I. Multiple Debye fitting parameters of THz DR study in various salt solutions. The time constant τ_3 has been fixed constant at 0.06 ps.

Concentration (M)	ϵ_s	S_1	S_2	S_3	τ_1 (ps)	τ_2 (ps)
AC						
0.00	77	74.3	0.45	1.36	8.93±0.10	0.26±0.05
0.50	69	64.9	0.61	1.59	7.59±0.10	0.22±0.04
1.00	62	57.8	0.71	1.50	6.72±0.08	0.21±0.03
2.00	57	52.6	0.89	1.54	5.66±0.06	0.19±0.03
3.00	53	48.3	1.06	1.64	5.07±0.05	0.19±0.03
4.00	48	43.2	1.16	1.16	4.37±0.04	0.18±0.03
5.00	40	35.1	1.26	1.77	3.41±0.03	0.17±0.02
Tetra MAC						
1.00	67	64.1	0.83	1.11	9.87±0.10	0.31±0.03
2.00	60	56.8	1.25	1.17	14.8±0.60	0.27±0.03
3.00	57	53.7	1.25	1.16	14.9±0.60	0.27±0.03
4.00	48	44.6	1.42	1.21	17.3±0.90	0.25±0.03
5.00	40	36.5	1.53	1.35	22.9±2.70	0.27±0.03
6.00	30	26.3	1.66	1.40	25.5±1.90	0.25±0.03

Tri-EAC						
1.00	70.2	67.3	0.66	1.34	9.61±0.10	0.29±0.06
2.00	66	63.1	0.77	1.26	10.8±0.10	0.27±0.03
3.00	62	58.9	0.94	1.23	13.2±0.20	0.26±0.03
4.00	52	48.9	1.00	1.14	14.7±0.30	0.26±0.02
6.00	42	38.9	1.04	1.27	25.0±0.20	0.25±0.04
Tetra-EAC						
0.25	71	68.1	0.75	1.43	9.47±0.2	0.38±0.06
0.50	63.5	60.5	0.81	1.40	9.09±0.2	0.35±0.04
1.00	54.2	51.3	0.87	1.18	10.0±0.2	0.28±0.03
1.50	46	42.8	1.11	1.29	11.2±0.3	0.30±0.03
2.00	38	34.7	1.23	1.34	14.6±0.8	0.33±0.04
3.00	30	26.7	1.26	1.35	22.3±0.3	0.34±0.04
Tetra-PAC						
0.50	68.9	65.4	0.59	1.439	10.9±0.1	0.29±0.06
1.00	63.8	60.2	1.01	1.28	15.6±0.3	0.23±0.04
2.00	48	44.5	1.38	0.87	36.6±2	0.19±0.04

8.5. References

- (1) Bakker, H. J. *Nature* **2012**, *491*, 533-535.
- (2) Davis, J. G.; Gierszal, K. P.; Wang, P.; Ben-Amotz, D. *Nature* **2012**, *491*, 582-585.
- (3) Davis, J. G.; Rankin, B. M.; Gierszal, K. P.; Ben-Amotz, D. *Nat Chem* **2013**, *5*, 796-802.
- (4) Das Mahanta, D.; Patra, A.; Samanta, N.; Luong, T. Q.; Mukherjee, B.; Mitra, R. K. *The Journal of Chemical Physics* **2016**, *145*, 164501.
- (5) Chen, S.; Itoh, Y.; Masuda, T.; Shimizu, S.; Zhao, J.; Ma, J.; Nakamura, S.; Okuro, K.; Noguchi, H.; Uosaki, K.; Aida, T. *Science* **2015**, *348*, 555-559.
- (6) Wiggins, P. M. *Physica A: Statistical Mechanics and its Applications* **1997**, *238*, 113-128.
- (7) Luzar, A.; Chandler, D. *The Journal of Chemical Physics* **1993**, *98*, 8160-8173.
- (8) Zhou, R.; Huang, X.; Margulis, C. J.; Berne, B. J. *Science* **2004**, *305*, 1605-1609.
- (9) Estell, D.; Graycar, T.; Miller, J.; Powers, D.; Burnier, J.; Ng, P.; Wells, J. *Science* **1986**, *233*, 659-663.
- (10) Cacace, M. G.; Landau, E. M.; Ramsden, J. J. *Q. Rev. Biophys.* **1997**, *30*, 241-277.
- (11) Lo Nostro, P.; Ninham, B. W. *Chem. Rev.* **2012**, *112*, 2286-2322.
- (12) Marcus, Y. *Chem. Rev.* **2009**, *109*, 1346-1370.

- (13) Stirnemann, G.; Wernersson, E.; Jungwirth, P.; Laage, D. *J. Am. Chem. Soc.* **2013**, *135*, 11824-11831.
- (14) Das Mahanta, D.; Samanta, N.; Mitra, R. K. *Journal of Molecular Liquids* **2016**, *215*, 197-203.
- (15) Marcus, Y. *Ion solvation*; Wiley-Interscience: New York, **1985**.
- (16) Kunz, W. N. B.; Henle, J.; Ninham, B. W. *Curr. Opin. Colloid Interface Sci.* **2004**, *9*, 19-37.
- (17) Tobias, D. J.; Hemminger, J. C. *Science* **2008**, *319*, 1197-1198.
- (18) Tielrooij, K. J.; Garcia-Araez, N.; Bonn, M.; Bakker, H. J. *Science* **2010**, *328*, 1006-1009.
- (19) Tielrooij, K. J.; van der Post, S. T.; Hunger, J.; Bonn, M.; Bakker, H. J. *J. Phys. Chem. B* **2011**, *115*, 12638-12647.
- (20) van der Post, S. T.; Tielrooij, K.-J.; Hunger, J.; Backus, E. H. G.; Bakker, H. J. *Faraday Discussions* **2013**, *160*, 171-189.
- (21) Schmidt, D. A.; Birer, Ö.; Funkner, S.; Born, B.; Gnanasekaran, R.; Schwaab, G.; Leitner, D. M.; Havenith, M. *J. Am. Chem. Soc.* **2009**, *131*, 18512-18517.
- (22) Funkner, S.; Niehues, G.; Schmidt, D. A.; Heyden, M.; Schwaab, G.; Callahan, K. M.; Tobias, D. J.; Havenith, M. *J. Am. Chem. Soc.* **2012**, *134*, 1030-1035.
- (23) Mancinelli, R.; Botti, A.; Bruni, F.; Ricci, M. A.; Soper, A. K. *Phys. Chem. Chem. Phys.* **2007**, *9*, 2959-2967.
- (24) Mancinelli, R.; Botti, A.; Bruni, F.; Ricci, M. A.; Soper, A. K. *J. Phys. Chem. B* **2007**, *111*, 13570-13577.
- (25) Cappa, C. D.; Smith, J. D.; Messer, B. M.; Cohen, R. C.; Saykally, R. J. *J. Phys. Chem. B* **2006**, *110*, 5301-5309.
- (26) Smith, J. D.; Saykally, R. J.; Geissler, P. L. *J. Am. Chem. Soc.* **2007**, *129*, 13847-13856.
- (27) Buchner, R.; Hefter, G. *Phys. Chem. Chem. Phys.* **2009**, *11*, 8984-8999.
- (28) Chen, T.; Hefter, G.; Buchner, R. *J. Phys. Chem. A* **2003**, *107*, 4025-4031.
- (29) Moilanen, D. E.; Wong, D.; Rosenfeld, D. E.; Fenn, E. E.; Fayer, M. D. *Proc. Natl. Acad. Sci. U.S.A.* **2009**, *106*, 375-380.
- (30) Fayer, M. D. *Acc. Chem. Res.* **2012**, *45*, 3-14.
- (31) Turton, D. A.; Hunger, J.; Hefter, G.; Buchner, R.; Wynne, K. *J. Chem. Phys.* **2008**, *128*, 161102.
- (32) Levering, L. M.; Sierra-Hernández, M. R.; Allen, H. C. *The Journal of Physical Chemistry C* **2007**, *111*, 8814-8826.
- (33) Strazdaite, S.; Versluis, J.; Bakker, H. J. *The Journal of Physical Chemistry C* **2016**, *120*, 17290-17295.
- (34) Laage, D. L.; Hynes, J. T. *Proc. Natl. Acad. Sci. U.S.A.* **2007**, *104*, 11167-11172.
- (35) Gallo, P.; Corradini, D.; Rovere, M. *Phys. Chem. Chem. Phys.* **2011**, *13*, 19814-19822.
- (36) Pieniazek, P. A.; Stangret, J. *Vibrational Spectroscopy* **2005**, *39*, 81-87.
- (37) van der Post, S. T.; Scheidelaar, S.; Bakker, H. J. *The Journal of Physical Chemistry B* **2013**, *117*, 15101-15110.
- (38) Buchner, R.; Holzl, C.; Stauber, J.; Barthel, J. *Physical Chemistry Chemical Physics* **2002**, *4*, 2169-2179.
- (39) Turner, J. Z.; Soper, A. K.; Finney, J. L. *J. Chem. Phys.* **1995**, *102*, 5438-5443.
- (40) Shimizu, A.; Taniguchi, Y. *Bull. Chem. Soc. Jpn.* **1990**, *63*, 3255-3259.

- (41) Huang, N.; Schlesinger, D.; Nordlund, D.; Huang, C.; Tyliczszak, T.; Weiss, T. M.; Acremann, Y.; Pettersson, L. G. M.; Nilsson, A. *J. Chem. Phys.* **2012**, *136*, 074507.
- (42) Koga, Y.; Sebe, F.; Nishikawa, K. *J. Phys. Chem. B*, **2013**, (3), pp 117, 877-883.
- (43) Bhowmik, D.; Malikova, N.; Mériguet, G.; Bernard, O.; Teixeira, J.; P., T. *Phys. Chem. Chem. Phys.* **2014**, *16*, 13447-13457.
- (44) Ahmed, M.; Singh, A. K.; Mondal, J. A. *Phys. Chem. Chem. Phys.* **2016**, *18*, 2767-2775.
- (45) Frank, H. S.; Evans, M. W. *The Journal of Chemical Physics* **1945**, *13*, 507-532.
- (46) Wen, W.-Y. *J. Solution Chem.* **1973**, *2*, 253-276.
- (47) Garcí'a-Tarre's, L.; Gua`rdia, E. *J. Phys. Chem. B* **1998**, *102*, 7448-7454.
- (48) Slusher, J. T.; Cummings, P. T. *J. Phys. Chem. B* **1997**, *101*, 3818-3826.
- (49) Chandler, D. *Nature* **2005**, *437*, 640-647.
- (50) Beauchamp, D. L.; Khajehpour, M. *Biophys. Chem.* **2012**, *163-164*, 35-43.
- (51) Penkov, N.; Shvirst, N.; Yashin, V.; Fesenko, E.; Fesenko, E. *The Journal of Physical Chemistry B* **2015**, *119*, 12664-12670.
- (52) Heyden, M.; Sun, J.; Funkner, S.; Mathias, G.; Forbert, H.; Havenith, M.; Marx, D. *Proc. Natl. Acad. Sci. USA* **2010**, *107* 12068-12073.
- (53) Nibali, V. C.; Havenith, M. *J. Am. Chem. Soc.* **2014**, *136*, 12800-12807.
- (54) Heyden, M.; Ebbinghaus, S.; Havenith, M. In *Encyclopedia of Analytical Chemistry*; John Wiley & Sons, Ltd: **2006**.
- (55) Samanta, N.; Das Mahanta, D.; Kumar Mitra, R. *Chemistry – An Asian Journal* **2014**, *9*, 3457-3463.
- (56) Samanta, N.; Mahanta, D. D.; Mitra, R. K. *Physical Chemistry Chemical Physics* **2014**, *16*, 23308-23315.
- (57) Samanta, N.; Mahanta, D. D.; Choudhury, S.; Barman, A.; Mitra, R. K. *The Journal of Chemical Physics* **2017**, *146*, 125101.
- (58) Das, D. K.; Das Mahanta, D.; Mitra, R. K. *ChemPhysChem* **2017**, *18*, 749-754.
- (59) Born, B.; Kim, S. J.; Ebbinghaus, S.; Gruebele, M.; Havenith, M. *Faraday Discussions* **2009**, *141*, 161-173.
- (60) Bellissent-Funel, M.-C.; Hassanali, A.; Havenith, M.; Henchman, R.; Pohl, P.; Sterpone, F.; van der Spoel, D.; Xu, Y.; Garcia, A. E. *Chemical Reviews* **2016**, *116*, 7673-7697.
- (61) Ebbinghaus, S.; Kim, S. J.; Heyden, M.; Yu, X.; Gruebele, M.; Leitner, D. M.; Havenith, M. *J. Am. Chem. Soc.* **2008**, *130*, 2374-2375.
- (62) Plusquellic, D. F.; Siegrist, K.; Heilweil, E. J.; Esenturk, O. *ChemPhysChem* **2007**, *8*, 2412-2431.
- (63) Frontzek, A. V.; Embs, J. P.; Paccou, L.; Guinet, Y.; Hédoux, A. *The Journal of Physical Chemistry B* **2017**, *121*, 5125-5132.
- (64) Mason, P. E.; Dempsey, C. E.; Vrbka, L.; Heyda, J.; Brady, J. W.; Jungwirth, P. *The Journal of Physical Chemistry B* **2009**, *113*, 3227-3234.
- (65) Arakawa, T.; Timasheff, S. N. *Biochemistry* **1984**, *23*, 5924-5929.
- (66) Samanta, N.; Mahanta, D. D.; Hazra, S.; Kumar, G. S.; Mitra, R. K. *Biochimie* **2014**, *104*, 81-89.
- (67) Mitra, R. K.; Sinha, S. S.; Pal, S. K. *Langmuir* **2007**, *23*, 10224-10229.
- (68) Woody, R. W.; Tinoco, I. *The Journal of Chemical Physics* **1967**, *46*, 4927-4945.

- (69) Dempsey, C. E.; Mason, P. E.; Jungwirth, P. *J. Am. Chem. Soc.* **2011**, *133*, 7300-7303.
- (70) von Hippel, P. H.; Wong, K.-K. *J. Biol. Chem.* **1965**, *240*, 3909-3923.
- (71) Yu, M.; Ding, Z.; Jiang, F.; Ding, X.; Sun, J.; Chen, S.; Lv, G. *Spectrochimica Acta Part A: Molecular and Biomolecular Spectroscopy* **2011**, *83*, 453-460.
- (72) Śmiechowski, M.; Stangret, J. *Pure Appl. Chem.* **2010**, *82*, 1869-1887.
- (73) Fenn, E. E.; Moilanen, D. E.; Levinger, N. E.; Fayer, M. D. *J. Am. Chem. Soc.* **2009**, *131*, 5530-5539.
- (74) Kříž, J.; Dybal, J. *Chem. Phys.* **2011**, *382*, 104-112.
- (75) Wen, W.-Y. In *The Physical Chemistry of Aqueous System: A Symposium in Honor of Henry S. Frank on His Seventieth Birthday*; Kay, R. L., Ed.; Springer US: Boston, MA, **1973**, p 155-178.
- (76) Brubach, J.-B.; Mermet, A.; Filabozzi, A.; Gerschel, A.; Roy, P. *The Journal of Chemical Physics* **2005**, *122*, 184509.
- (77) Stangret, J.; Gampe, T. *J. Phys. Chem. B* **1999**, *103*, 3778-3783.
- (78) Stangret, J.; Gampe, T. *The Journal of Physical Chemistry A* **2002**, *106*, 5393-5402.
- (79) Falk, M. *Canadian Journal of Chemistry* **1971**, *49*, 1137-1139.
- (80) Ebbinghaus, S.; Kim, S. J.; Heyden, M.; Yu, X.; Heugen, U.; Gruebele, M.; Leitner, D. M.; Havenith, M. *Proc. Natl. Acad. Sci. USA* **2007**, *104*, 20749-20752.
- (81) Luong, T. Q.; Verma, P. K.; Mitra, R. K.; Havenith, H. *Biophys. J.* **2011**, *101*, 925-933.
- (82) Heyden, M.; Bründermann, E.; Heugen, U.; Niehues, G.; Leitner, D. M.; Havenith, M. *J. Am. Chem. Soc.* **2008**, *130*, 5773-5779.
- (83) Das, D. K.; Patra, A.; Mitra, R. K. *Biophysical Chemistry* **2016**, *216*, 31-36.
- (84) Barthel, J.; Buchner, R.; Bachhuber, K.; Hetzenauer, H.; Kleebauer, M.; Ortmaier, H. *Pure Appl. Chem.* **1990** *62*, 2287-2296.
- (85) Born, B.; Kim, S. J.; Ebbinghaus, S.; Gruebele, M.; Havenith, M. *Faraday Discussions* **2009**, *141*, 161-173.

Chapter 9

9. Reorientational Relaxation via Large Amplitude Angular Jumps and Its Connections to the Dynamic Heterogeneity

This chapter provides a complete microscopic picture of the reorientation mechanisms of water and DME molecules in their binary mixture solutions. We explore the jump reorientations of water and DME molecules with MD simulation techniques. It will briefly describe the coupling between rotational and translational motions and also about the inherent transient heterogeneity in aqueous solutions.

9.1. Introduction

Water, a prerequisite of life, plays important role in many chemical and biological processes. Most of the unique properties of water are related to the strong but disordered three dimensional H-bonded networks that interconnect themselves. The fluctuations of these disorder networks work as a driving force to reorient.^{1,2} The microscopic understanding and characterisation of the fluctuations is fundamentally important. The physical properties of water are quite different in presence of co-solutes or macromolecular fragment than its pure state.³ In such aqueous solutions viscosity become high as a result it offer sluggish relaxation. Associated with the viscosity rise, the dynamics also becomes strongly heterogeneous. Experiments have revealed that the water dynamics, which depends on the length scale and polarity of those macro-molecules, can vary up to five orders of magnitude than pure water. An intrinsic microscopic feature characterising liquids is that molecules constituting them can be temporarily caged (dynamically inactive) by their immediate neighbours. These molecules however can escape and thus transport when thermal density fluctuations break this temporary cage and it jumps (dynamical activity) to its next cage which constitutes the basic dynamical event. This sequence of “waits” and “jumps” continue to repeat, thus allowing molecules to be transported over macroscopic distances as observed in simple Lennard-Jones (LJ) fluids. It is also to note here that, the cage provided by the neighbours of the central water molecule are also in a dynamical cage formed by that central water with other surroundings. This defines the cooperative nature of the liquid water.

A description of this “caging” effect forms the bedrock for the mode coupling description, which is a fundamental theory for understanding relaxation phenomena in liquids.

Typically amorphous liquids which are computationally studied extensively are very generic in nature. They involve heterogeneities in translational dynamics. However, looking into real systems almost all are complicated than simple Lennard-Jones (LJ) fluids. Typically one studies binary mixtures of H-bonded liquids where, translational and rotational degrees of freedom are strongly coupled. However, before addressing the coupling, we wish to understand the details of the reorientational dynamics in the binary mixture as a function of concentrations of either the solute or the solvent. The microscopic dynamics of each molecule in liquid are manifest by periods during which the trajectory is temporarily localised (dynamical inactivity) and periods during which the particle jumps (dynamical activity) quickly (much faster than the average density relaxation time) from one localised cage to the next. Relaxation thus proceeds via the phenomena of “dynamic facilitation” whereby mobile and immobile molecules form separate spatial domains. The dynamic facilitation approach constitutes an alternative branch for describing the problem of glass transition where dynamics plays a central role, rather than thermodynamics.

Through MD simulations studies we monitor the periods of “waits” and “jumps” in microscopic trajectories of the molecules to understand the statistical properties of rotational and translational events.⁴⁻⁸ While the aspects of translational degrees of freedom have been explored in several amorphous systems, similar approach for monitoring microscopic rotation of single molecules in liquids is largely absent from the literature. The rotational dynamics of liquid water is essentially governed by the reorientation via a combination of diffusive processes and large amplitude angular jumps which are driven by the fluctuations in the H-bonding network. The periods of rotational “waiting” corresponds to the situation when the H-bond connectivity remains intact and a rotational jump occurs when the rotating water molecule exchanges the identity of its H-bond donor. This mechanism of rotation contradicts the traditional *Debye diffusion model*, which assumed that molecular rotation always occurred via small angular steps occurring in small time intervals. The extended jump model has further led to a reinterpretation of QENS spectra of liquid water, which also resolves the disparity between rotation timescales obtained via NMR and QENS measurements.

We study the statistics of these rotational jump events (mediated by H-bond partner exchange) within an aqueous binary mixture of DME at 300K in the whole concentrations range. DME is the simplest member of the poly-oxyethylene (POE) family and has an unlimited solubility in water. We explore the statistics of the rotational jump events in water-

DME binary mixture⁹⁻¹¹ where addition of guest hydrophobic molecules induces heterogeneities in dynamics. In *chapter 5* we have studied the evolution of the structure and dynamics of water in its binary mixture with DME, using experimental (the state of the art THz TDS, FTIR spectroscopy, TCSPC) and MD simulation over the entire concentration range and found that the H-bonded structures are highly heterogeneous and the dynamics has some non-monotonic trend with water concentration (X_w).^{12,13} The dynamical timescales obtained from TTDS shows a non-monotonic dependence with X_w , which is also captured by the MD simulations. We extend our simulation analysis further and found that the reorientation occurs via large amplitude angular jumps due to exchange of H-bond partners. We separately monitor and characterise these jumps of water as well as solute, including the distribution of trajectories. We characterized of the translational dynamics occurring with reorientational jump events (when H-bond breaks and formed with a different acceptor i.e, H-bond exchange) and the waiting periods between successive orientational jumps (when the H-bonds remain intact). DME-water mixture has been a subject of various experimental investigations including NMR relaxation, FTIR, Raman spectroscopy, volumetric and thermodynamic measurements as well as several simulation studies. It has been revealed that many macroscopic thermodynamic parameters of this binary mixture (viscosity, partial molar volume) including some microscopic parameters like diffusion coefficient pass through an inflation point in the composition profile, which clearly identifies the micro-heterogeneous environment of the mixtures. But the exact molecular pictures of the water reorientation around comparably less polar solvent molecule are still not clear.

9.2. Results and Discussions

MD simulation methodology and the analysis protocols are provided in *chapter 3*. The RDF between water oxygen and water oxygen (OW-OW), DME oxygen and DME oxygen (ODM-ODM) and water oxygen and DME oxygen (OW-ODM), provided in *chapter 3*, are important parameters that give an idea about the relative presence of other molecules in the neighbouring shell of a particular molecule. The RDF's do not show any change in the position of 1st peak. However, an appreciable change of the first peak height is observed with X_w . We plot the first peak value with water concentration (figure 9.1). In low X_w region, we found a greater structural order of water around water, whereas the cooperative structure for DME-DME is high in high X_w region. This indicates a clustering of similar particle. There exist water clusters and hydrophobic aggregations (DME clusters) in these mixtures, which is an indication of the hydrophobic hydration.

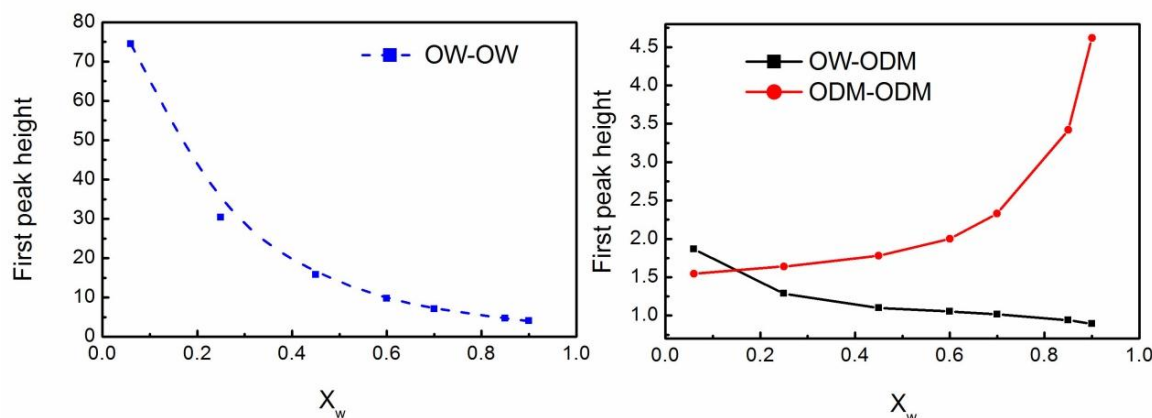


Figure 9.1. The height of the 1st peaks of water-water (left panel), water-DME and DME-DME RDFs (right panel).

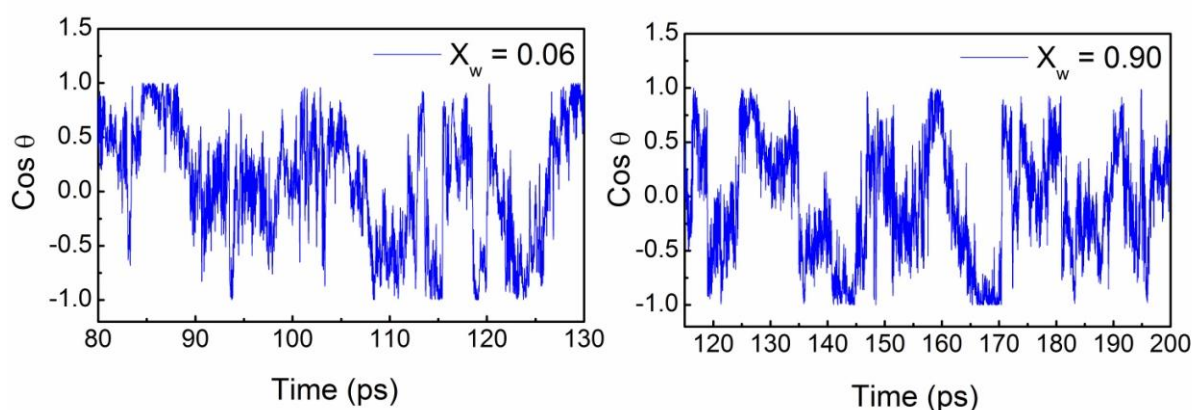


Figure 9.2. The time evolution of the cosine of the angle of the OH vector makes with the Z-axis of the simulation box of any randomly chosen water molecule.

The ratio of the characteristics time scales of the 1st and 2nd order reorientational time correlation functions deviates from the value 3 (see *chapter 5*); that signifies the deviation from the diffusive (Debye like) motion. In *Brownian motion*, the angular steps of the water rotations are very small. We characterise the non-diffusive motion of the water molecules that is governed by the large amplitude sudden angular jump rotation. At each time step we measure the cosine of the angle made by water OH vector with the z-axis of the simulation box, and found signature of the orientational jumps of water molecules in those mixtures. The time evolution of the cosine angle made by any OH vector of a water molecule with the z-axis of the simulation box (presented in figure 9.2), changes in small steps along with large fluctuation sometimes as large as $\sim 90^\circ$. This behaviour suggests that the water molecule executes diffusive reorientations with the presence of large amplitude angular jumps in the solutions. Here we only present the cosine angle value for two mixtures ($X_w \sim 0.06$ and 0.90), but signature of the large amplitude jumps are present in all water concentrations.

With this proof, we have analysed the microscopic features of those orientational jumps throughout the entire concentration range in details. For analysis protocols please see *chapter 3*. In figure 9.3 we present relative percentage of those different jump events in the mixtures. We add DME to water and water to DME jump populations as hetero-molecular jump events. As we increases water mole fraction from very low to very high, the water-water H-bond exchange events become more favourable with the reduction of the percentage of DME-DME jumps. Interestingly in the concentration region $X_w \sim 0.8$, where previously we found most retardation dynamics in collective H-bond dynamics as well as OH orientational dynamics, the population of water-water, DME-DME and also the hetero-partner events (DME-water and water-DME) become quite comparable. In the next section we discuss about the water–water jumps events in detail. We also try to characterise the other different type of jump events e.g. jump from water to DME, DME to water, and DME to DME. We found that these different types of microscopic jump events exhibit different properties.

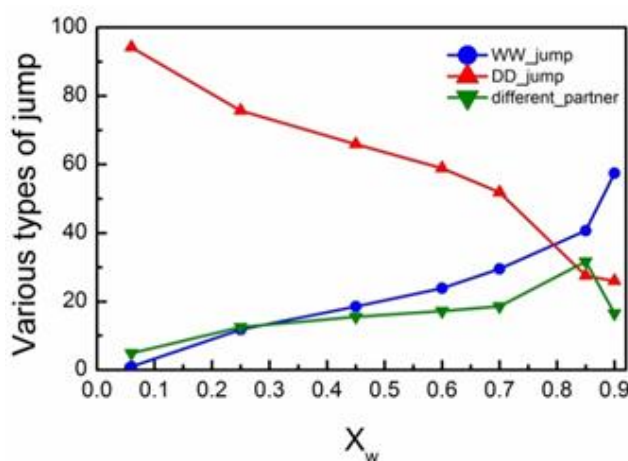


Figure 9.3. Relative populations (%) of different type of jump orientations events of water.

We compute the time evolution of the average path for the H-bond switching event (transition distances) and average jump angle during each jump events (see figure 9.4). The transition time is defined as the time when both the initial and final H-bond partners are at the same distances from the central water molecule which rotates by a large angle to exchange its partner. We select the jump events whose transition times differ by more than 4 ps. We ensure that within this 4 ps interval, that particular water molecule does not participate in any other jump event apart from the chosen one and carefully fix the instant when O^*H^* vector lies exactly on the $O^A O^* O^B$ bisector plane as a common origin (scheme 3.II.1 in *chapter 3*).

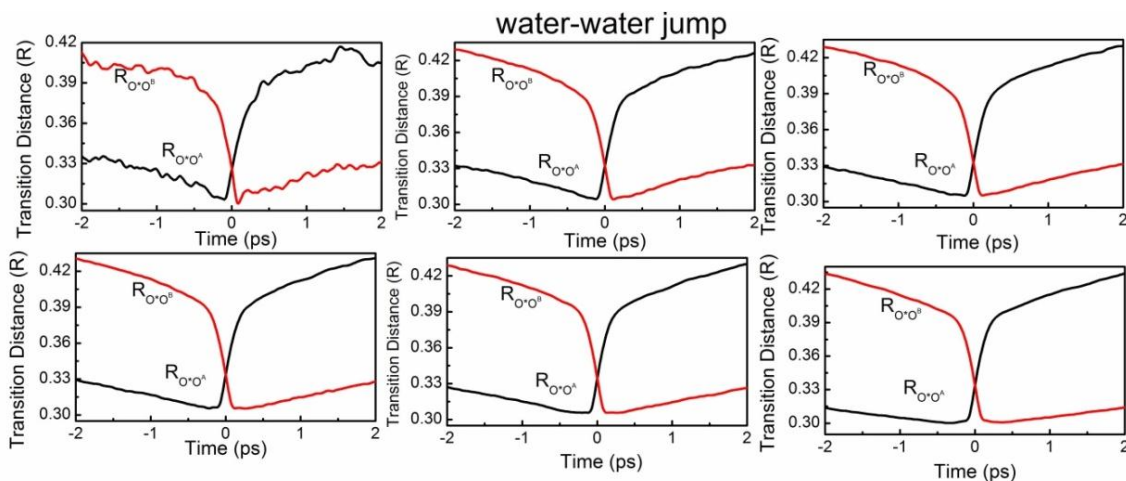


Figure 9.4. The distance between initial (black lines) and final (red lines) H-bond partners from the central water molecule at the instant of water to water H-bond switch (transition state) events for various concentration of water.

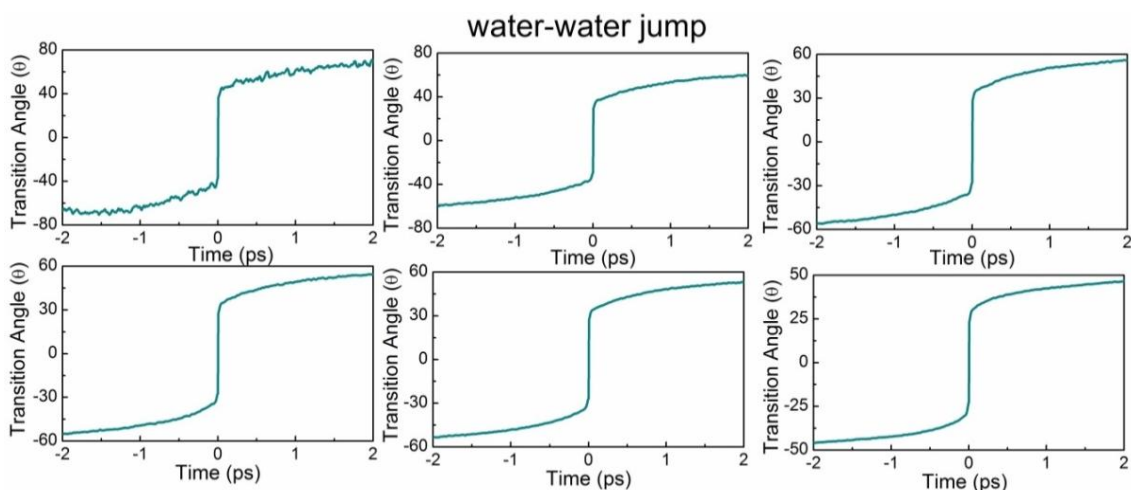


Figure 9.5. The angle between any water molecule and its two H-bond donor water molecules at the time of H-bond switch (transition state) for various concentration of water.

The transition distance and the transition angles are the result of the coherent averaging where we choose the transition states of the orientational jump events as origin and draw the figures with ± 2 ps time window. We follow the same procedure for all the water molecules for each successful jump event in the mixtures to average out. In figure 9.4 we provide the evolution of the average transition distances $R_{O^*O^A}$ between O^{central} (central water molecule) and O^{initial} (initial H-bond acceptor oxygen atom) and $R_{O^*O^B}$ between O^{central} and O^{final} (final H-bond acceptor oxygen atom). Just before the jump the initial H-bond partner was in the first solvation shell (connected via H-bond) of the central water molecule (black line) and the final partner was in the second solvation shell (not connected). Due to thermal and density fluctuation the final H-bond partner come closer to the central water molecule. At

the transition state, when the initial and the final partner are at equidistance from the central molecule, the central water performs a sudden large amplitude angular jump. Hence its initial H-bond break and final H-bond formed. That means during a successful jump processes the central water molecule exchange its H-bonded partner between the successive hydration shells. The translational displacement of the oxygen atom of initial and final acceptors is found to be ~ 2 Å. We found these transition distances are symmetric about the transition state (i.e., $R_{O^*OA} = R_{O^*OB}$) for the water-water jump. That is because the initial partner that was at first in first hydration shell goes to the second shell after jump, from where the final partner comes to the first shell. We also compute the average jump angle (see figure 9.5) which is the angle between the O^*H^* vector of the centre water molecule and the bisector plane of the $O^aO^*O^b$ (see scheme 3.II.1 in *chapter 3*) for all the mixtures. We found that the transition angles are very large in amplitude ($\sim 80^\circ$). Such microscopic study of the jump events signifies the coupling of the translational and rotational motions in liquid mixtures. In DME molecule there are two oxygen atoms which can act as H-bond donor and can form H-bond with other water molecules. We compute the other H-bond partner exchange events from water to DME, DME to water and DME to DME following the same mechanisms. The figures of transition distances and transition angles for those types of jumps are shown in figure 9.6 - figure 9.11. It is to note here that, the transition distances are very much symmetrical for homo-molecular jumps where both the initial and final partner molecules are of same type, whereas for hetero-molecular jumps (water-DME and DME water) the transition jumps are found to be asymmetrical.

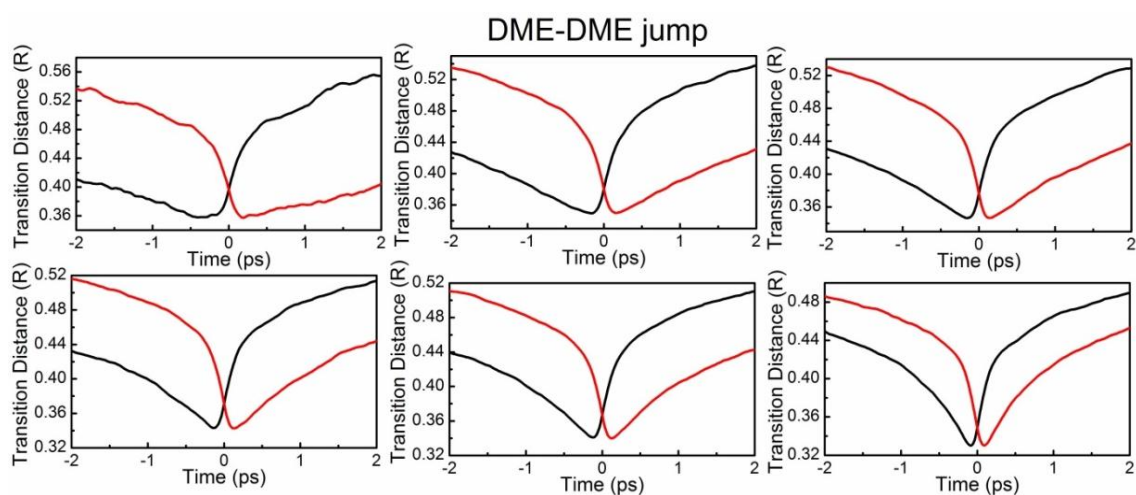


Figure 9.6. The distance between initial (black lines) and final (red lines) H-bond donor molecules at the time of H-bond switch (transition state) for various concentration of water.

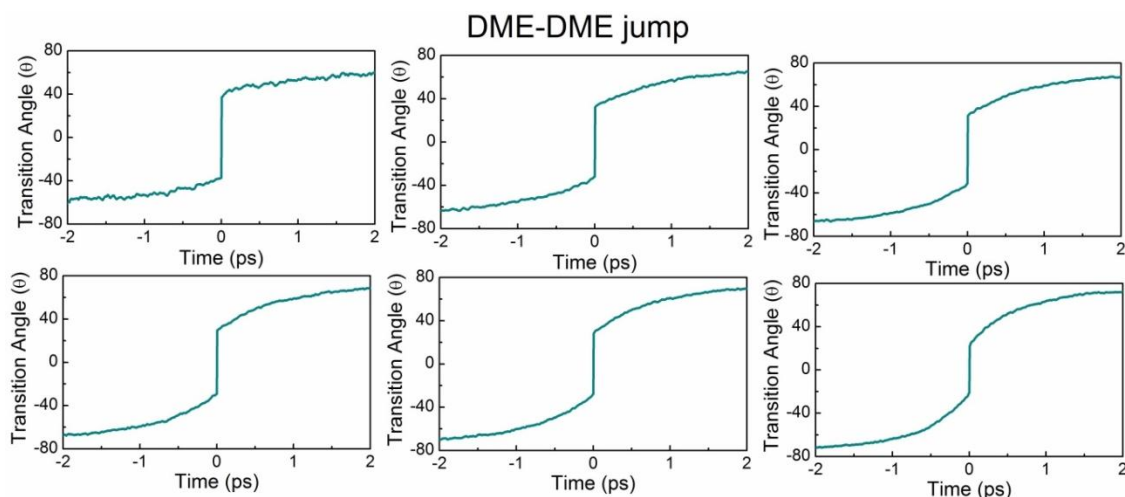


Figure 9.7. The angle between any water molecule and its two H-bond donor DME molecules at the time of H-bond switch (transition state) for various concentration of water.

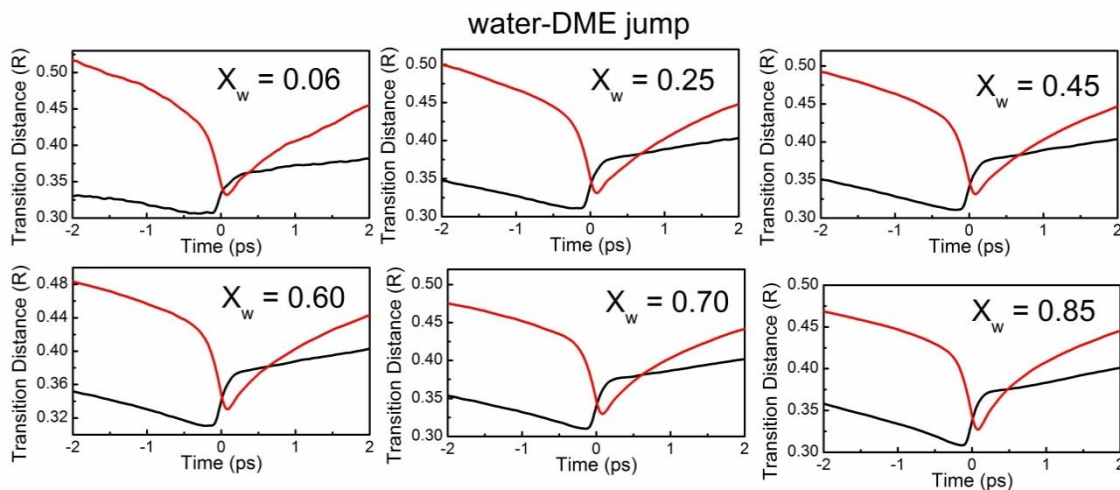


Figure 9.8. The distance between initial (black lines) and final (red lines) H-bond donor molecules at the time of H-bond switch (transition state) for various concentration of water.

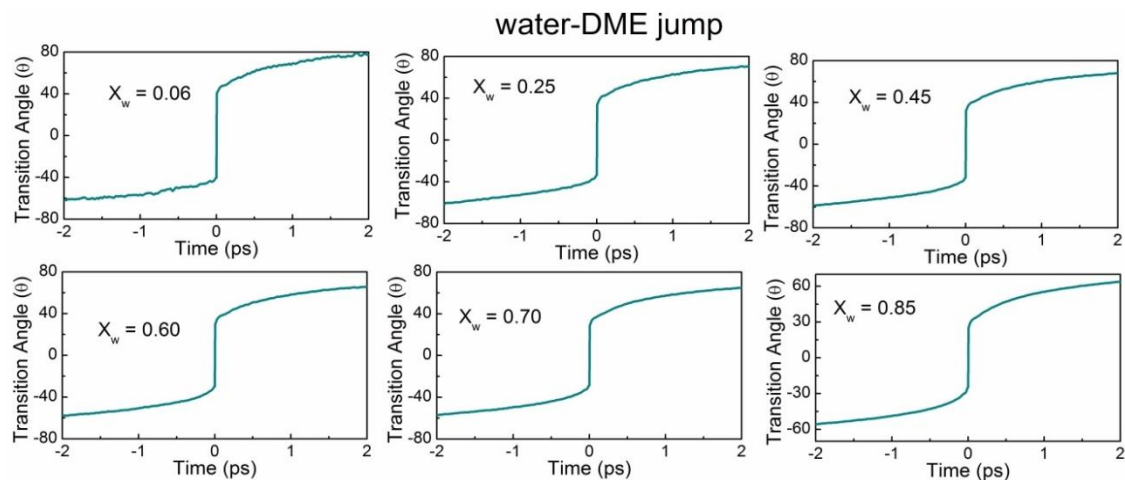


Figure 9.9. The angle between any water molecule and its two H-bond donor DME molecules at the time of H-bond switch (transition state) for various concentration of water.

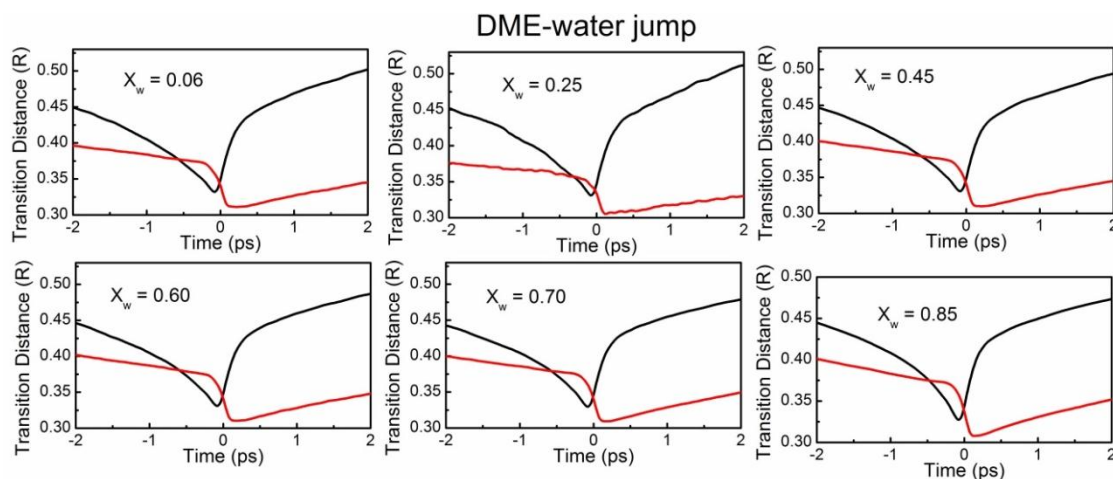


Figure 9.10. The distance between initial (black lines) and final (red lines) H-bond donor molecules at the time of H-bond switch (transition state) for various concentration of water.

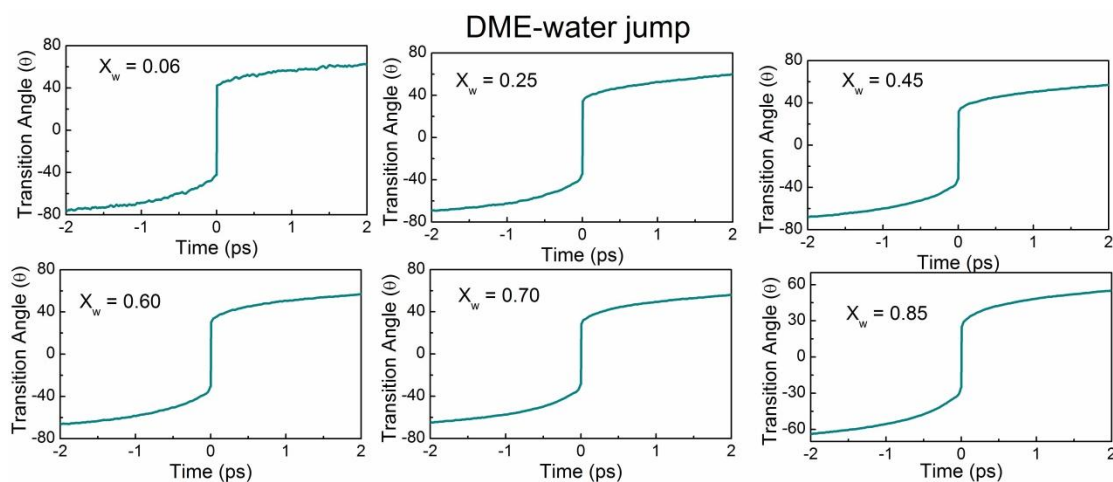


Figure 9.11. The angle between any water molecule and its two H-bond donor DME molecules at the time of H-bond switch (transition state) for various concentration of water.

In order to have a competitive description, we have shown two parameters, (i) the average jump angle of the angular rotation which is the angle swipes by the OH vector of the central molecule performing jump events as function of the water concentration (figure 9.12, left panel) and (ii) the partner separation. We found that the jump angle decreases from $\sim 90^{\circ}$ to $\sim 45^{\circ}$. The DME-DME jump angle also decreases with increasing X_w . We plot the distance between the two H-bond donor water molecule (initial and final) at 2 ps just after the jump happen in figure 9.12, right panel.

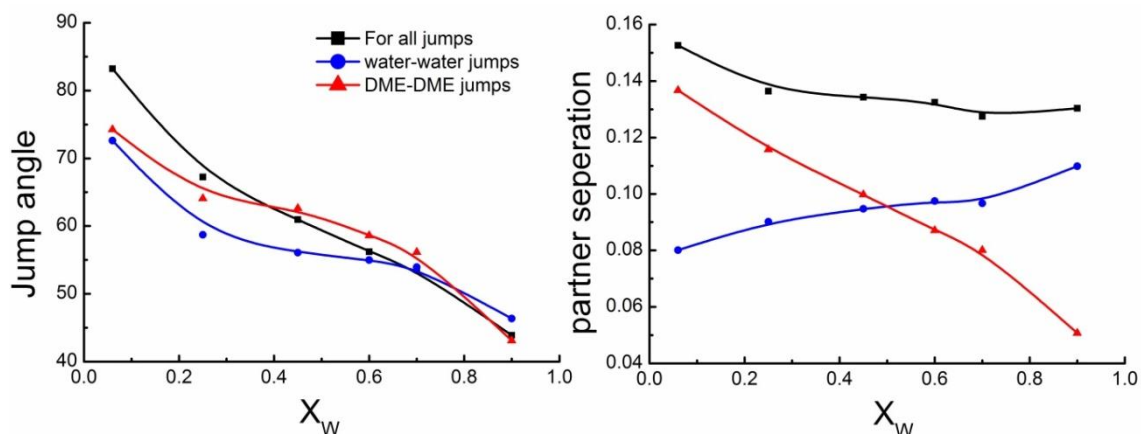


Figure 9.12. The jump angle and partner separation as function of water concentration for all types of orientational jump of water molecules.

In figure 9.13, left panel we compute the average H-bond coordination number of the central rotating water molecule for water-water jump event. For very low X_w ($X_w = 0.06$) coordination number is found to be ~ 2 , that indicates that the rotating water molecule finds almost two neighbour water molecule around it for H-bond. That corroborates our earlier findings that even at very low X_w , small confined water clusters exist in the vicinity of DME cage. With increasing X_w the number of average H-bond increases (figure 9.13, right panel). In low X_w region, coordination number increases linearly indicating polar-polar affinity. That is the driving force for hydrophobic hydration. In low X_w region, water can hardly hydrate the DME molecules, rather they aggregate among themselves. However in high X_w , DME molecules start to form extensive H-bond with the water molecules through their ether connected oxygen atoms. We also computed the average jump angle distributions (figure 9.14) and also for each type of jumps such as water-water, water-DME, DME-water and DME-DME (figure 9.15).

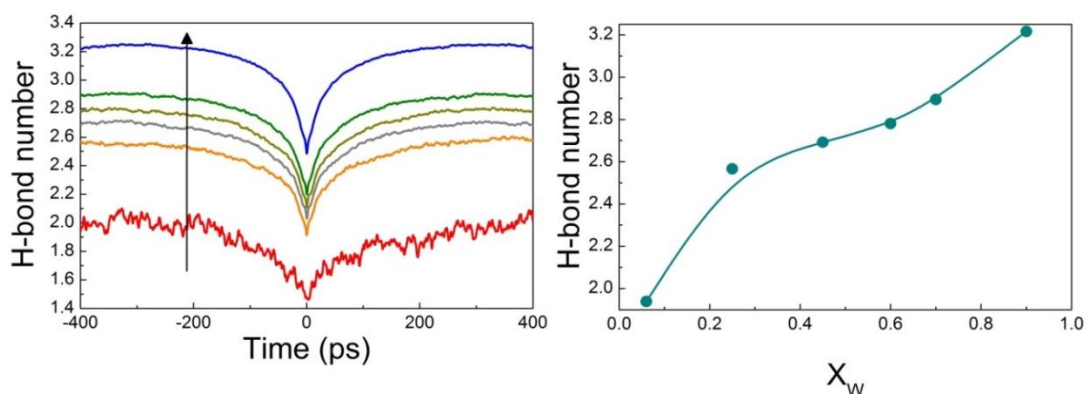


Figure 9.13. Coordination number of the rotating water molecule. Arrow indicates the increasing of water concentration. Arrow indicates the increasing of water concentration.

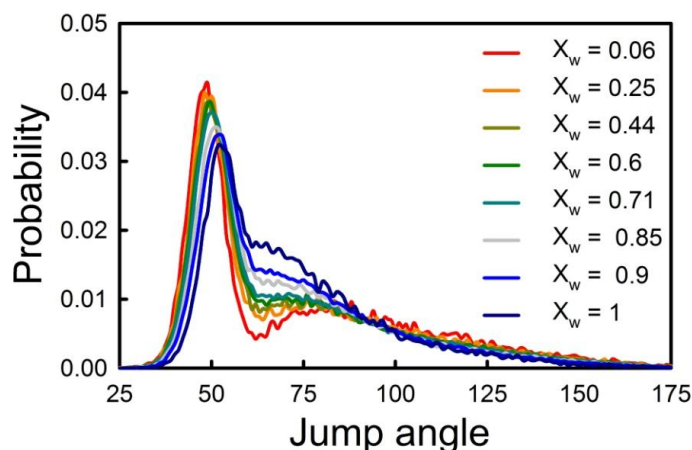


Figure 9.14. Average jump angle distributions for each simulated concentrations.

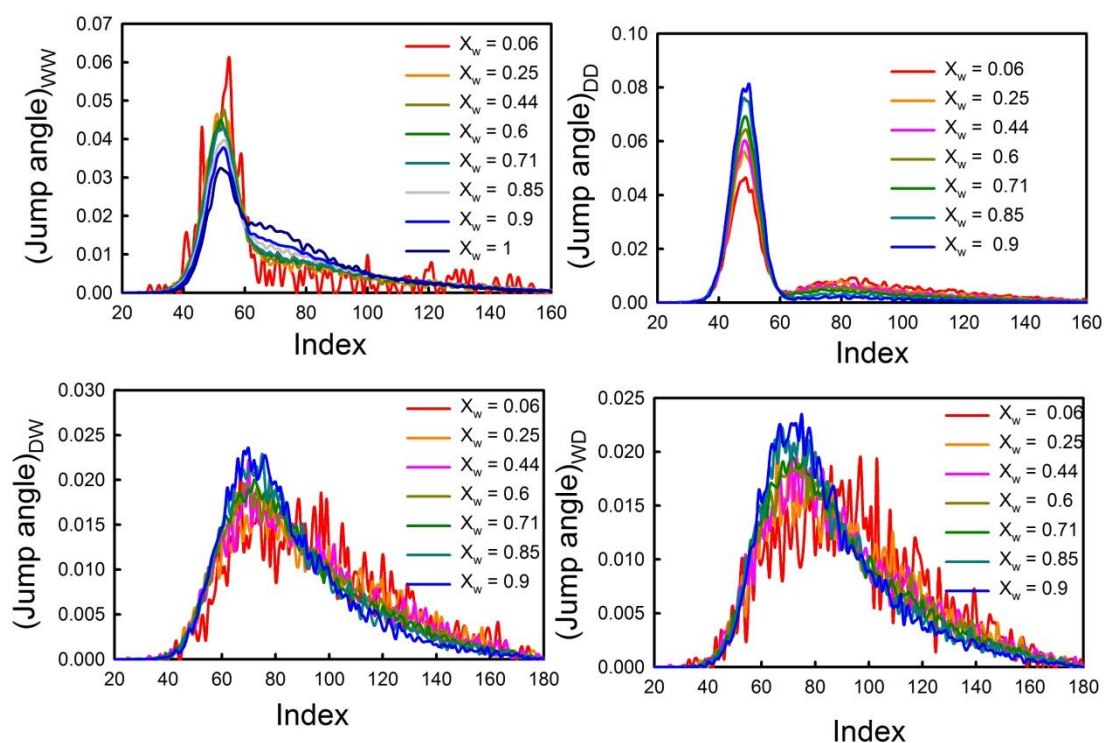


Figure 9.15. The jump angle distributions for various types of jump events (water-water (WW), DME-DME (DD), DME-water (DW) and water-DME (WD)) at each simulated concentrations.

Previously we found the existence of the water clusters with various structures that causes a micro-heterogeneous environment in the mixtures. Such heterogeneity shows a non-monotonic dynamics in translational and rotational motions. Here, from the trajectories of the water molecules, we calculate the transitional mean square displacements (TMSD) as well as the rotational mean square displacements (RMSD) of the OH vector as shown in figure 9.16(i) & (ii) according to the following relations,

$$TMSD = \langle \Delta r^2 \rangle = \langle (\vec{r}(t) - \vec{r}(0))^2 \rangle \quad (9.1)$$

$$RMSD = \langle \Delta \varphi^2 \rangle = \langle (\vec{\varphi}(t) - \vec{\varphi}(0))^2 \rangle \quad (9.2)$$

where, $\vec{r}(t)$ and $\vec{\varphi}(t)$ are the translational (spatial) and the orientational (angular rotation) vector of any OH vector in time t . While calculating the orientational MSD, we first unwrapped the orientational degrees of freedom as describe elsewhere.¹⁴

$$\varphi_i(t) = \int_0^t \delta\varphi_i(t') dt' \quad (9.3)$$

$$|\delta\varphi_i(t')| = \cos^{-1}[u_i^{OH}(t') \cdot u_i^{OH}(t' + \delta t')] \quad (9.4)$$

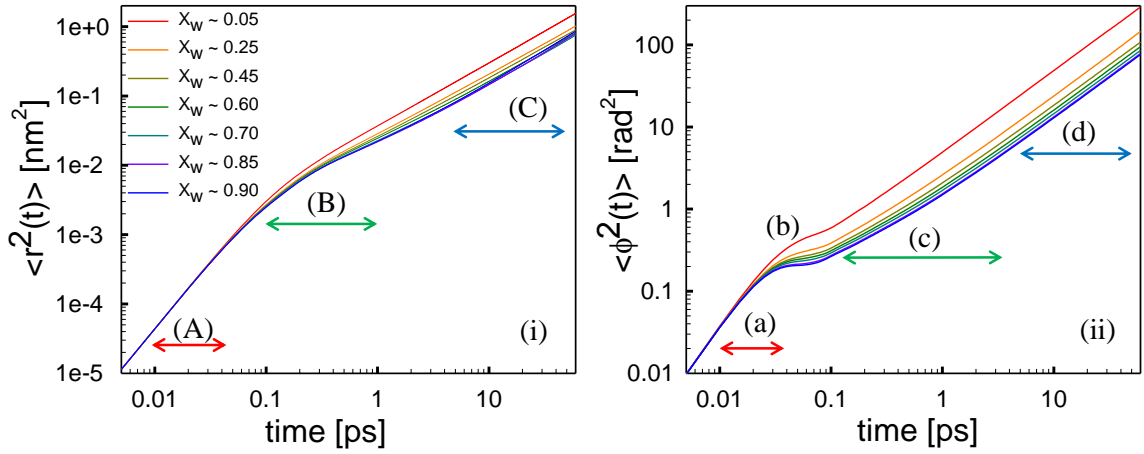


Figure 9.16. (i) Translational Mean Square Displacement (MSD) profile ($\langle r^2(t) \rangle$), with three different dynamical regimes (A) ballistic, (B) trapped, and (C) diffusive. (ii) Rotational MSD profile ($\langle \varphi^2(t) \rangle$), with (a) ballistic, (b) librational, (c) trapped, and (d) diffusive regimes of water-DME mixtures at different X_w .

We find that there are three different regime in the TMSD profile: (A) an initial ballistic regime where $\langle \Delta r^2 \rangle \sim t^2$, (B) after that TMSD exhibits a plateau or cage regime (molecules trapped in a cage formed by their neighbours), (C) and finally it reached in a diffusive regime where behaviour at long times $\langle \Delta r^2 \rangle \sim t$. In between these two regimes we also find a plateau region where the water molecules are caged in the vicinity of other water and DME molecules. In contrast to the TMSD, we found four regimes in RMSD profile. Here before the plateau cage region we observe a sharper curvature that is due to the librational motion (hindered rotation) of the water molecules.¹⁴ To explore the temporal dynamic heterogeneity in DME/water mixtures we calculate the orientational Van-Hove function (not shown here). The non-Gaussian shape of the Van-Hove distribution suggests the transient existence of the diffusivity distribution.¹⁵ To explore such dynamic heterogeneity we follow the relatively new prescription to systematically investigate the temporary coexistence of two

phases of high and low diffusivity that coexist for a time of the order of relaxation time and mix in subsequent times.^{16,17} Earlier such technique was used in glass forming liquids and supercooled liquids.^{16,18-20} Our aim is to explore the single particle diffusivity distribution through the relaxation dynamics of single particle large amplitude angular jump motion. The diffusivity distribution of each particle in any particular time is proportional to the number of successful jumps performed by the particle at that particular time frame.¹⁶ We try to describe the single particle reorientational dynamics through the *continuous time random walk* (CTRW) formalism and explore the heterogeneity coupled in the rotational and translational dynamics.²¹ Rather doing the standard ensemble average we are interested to characterise the dynamical events with the single particle transport that may explore the spatio-temporal correlations. We explicitly use the large amplitude angular jump events to construct the rotational CTRW. The exponential distribution of waiting times (we already discussed about the exponential fitted waiting times separately with a waiting partner as water and as DME in *chapter 5*) between two successive jumps signifies that the underline process might be Poissonian.²² We found that the average number of rotational jumps $\langle n \rangle$ per molecule during a time interval t is proportional to t ($\langle n(t) \rangle = t / \langle \tau_{wait} \rangle$). We also compute the time dependence of the probability distribution $P(n_j, t)$ of any arbitrary molecule undergoing “ n ” number of jumps during a time interval “ t ” (see figure 9.17) that is the single particle diffusivity distribution at different time window and relate this to the origin of heterogeneities in the rotational dynamics. We rescaled the x-axis by the average number of jumps $\langle n \rangle$. In small time window $P(n_j, t)$ is peaked at zero since most of the particles have not yet jumped. However, if one increase the time window (at very high enough time limit) the distribution shows a Gaussian shape with a maxima at $n_j = \langle n_j \rangle$. Interestingly, we notice that the distributions are broadened as we go to low X_w region. Such properties have been found earlier as temperature is increased. In between the transition of the distribution peak from $n_j = 0$ to $n_j = \langle n_j \rangle$ (Gaussian), the temporal diffusivities sometimes take a bimodal shape. Such transient bimodal shape of the diffusivity distribution indicates the coexistence of two phases of different mobility at the same instant. Two phases with different diffusivities coexist for a time of the order of relaxation times and mix afterwards. The microscopic origin of such temporal heterogeneity is the coupling of translational and rotational motion of water; translation dynamics become faster during the orientational jump events whereas it become slower at the periods of waiting.²³

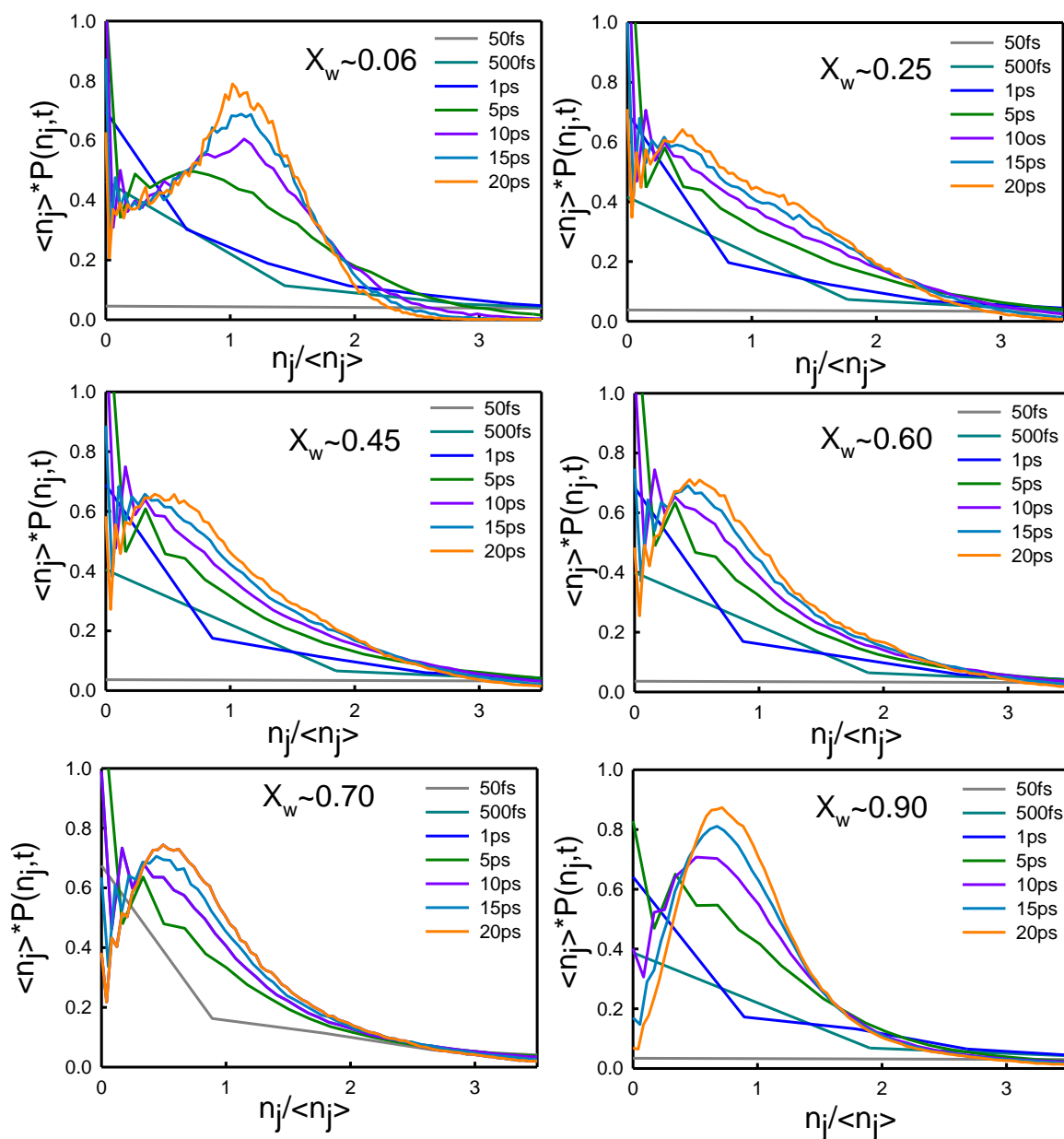


Figure 9.17. Probability distribution of the single particle diffusion coefficient at different time for various water concentrations.

9.3. Summary

In this chapter we have successfully shown a pictorial view of the large amplitude angular jump motions of water and DME molecules in their binary mixture systems. In liquid water the translational and the rotational motions are coupled. Such reorientational motions are not purely diffusive (small angular steps). Rather the movements are governed by sudden angular jump of large amplitude angles. Every successful jump is followed by a wait. It is known as “cage-jump model”. Due to density fluctuations the water molecule jump to exchange its partner with other and then it stay for some time with that partner and jump again. When this

wait and jump motions are going on a water molecule perform some translation and some amount of rotations. We have fully characterised the transition states. With the knowledge of all those microscopic jumps we then applied continuous time random walk model to probe the dynamic heterogeneity in their diffusivity. We found that in small time window the water molecules carry two types of diffusivity property ($n \sim 0$; along with $n = \langle n \rangle$). Such transient nature in the diffusivity distributions are previously found in the glassy systems, and it is not explored in liquid aqueous systems.

9.4. References

- (1) Chaplin, M. [Internet URL] <http://www1.lsbu.ac.uk/water/anmlies.html>. April, 2010.
- (2) Ball, P. *Chem. Rev.* **2008**, *108*, 74-108.
- (3) Levinger, N. E. *Science* **2002**, *298*, 1722-1723.
- (4) Laage, D.; Hynes, J. T. *Science* **2006**, *311*, 832-835.
- (5) Nigro, B.; Re, S.; Laage, D.; Rey, R.; Hynes, J. T. *J. Phys. Chem. A* **2006**, *110*, 11237-11243.
- (6) Laage, D. L.; Hynes, J. T. *Proc. Natl. Acad. Sci. U.S.A.* **2007**, *104*, 11167-11172.
- (7) Laage, D.; Hynes, J. T. *J. Phys. Chem. B* **2008**, *112*, 14230-14242.
- (8) Ciamarra, M. P.; Pastore, R.; Coniglio, A. *Soft Matter* **2016**, *12*, 358-366.
- (9) Bedrov, D.; Borodin, O.; Smith, G. D. *J. Phys. Chem. B* **1998**, *102*, 5683-5690.
- (10) Bedrov, D.; Pekny, M.; Smith, G. D. *J. Phys. Chem. B* **1998**, *102*, 996 - 1001.
- (11) Bedrov, D.; Smith, G. D. *J. Phys. Chem. B* **1999**, *103*, 3791-3796.
- (12) Das Mahanta, D.; Patra, A.; Samanta, N.; Luong, T. Q.; Mukherjee, B.; Mitra, R. K. *The Journal of Chemical Physics* **2016**, *145*, 164501.
- (13) Das Mahanta, D.; Rana, D.; Patra, A.; Mukherjee, B.; Mitra, R. K. *Chem. Phys. Lett.* **2018**, *700*, 50-56.
- (14) Mazza, M. G.; Giovambattista, N.; Starr, F. W.; Stanley, H. E. *Physical Review Letters* **2006**, *96*, 057803.
- (15) Giovambattista, N.; Mazza, M. G.; Buldyrev, S. V.; Starr, F. W.; Stanley, H. E. *The Journal of Physical Chemistry B* **2004**, *108*, 6655-6662.
- (16) Pastore, R.; Coniglio, A.; Ciamarra, M. P. *Scientific Reports* **2015**, *5*, 11770.
- (17) Pastore, R.; Coniglio, A.; Candia, A. d.; Fierro, A.; Ciamarra, M. P. *Journal of Statistical Mechanics: Theory and Experiment* **2016**, *2016*, 054050.
- (18) Kob, W.; Donati, C.; Plimpton, S. J.; Poole, P. H.; Glotzer, S. C. *Physical Review Letters* **1997**, *79*, 2827-2830.
- (19) Rubner, O.; Heuer, A. *PhRvE* **2008**, *78*, 011504.
- (20) Pastore, R.; Coniglio, A.; Pica Ciamarra, M. *Soft Matter* **2014**, *10*, 5724-5728.
- (21) Le Vot, F.; Abad, E.; Yuste, S. B. *PhRvE* **2017**, *96*, 032117.
- (22) Ross, S. M.; Mehdi, J. *Stochastic Processes*; Wiley, **1996**.
- (23) Mukherjee, B. *The Journal of Chemical Physics* **2015**, *143*, 054503.

10. Summary and Future Perspective

10.1. Summary

In this thesis we have systematically investigated the structure and hydration behaviour of protein molecules in presence of some guest crowding agents through in-vitro studies. Up to 60% of the human body contains water. With respect to this polar candidate water, there are only three kinds of interactions that govern the real extracellular processes. They are ionic (electrostatic interaction), polar (hydrophilic interaction) and non-polar (hydrophobic interaction). We examine the effect of electrolytes and amphiphilic molecules on protein structure and hydration when they act individually as well as simultaneously. Besides interacting directly with protein molecules, these molecules may also perturb the water networks in the hydration layers around the bio-molecules. This also can modulate the native structures of proteins. It therefore stands pertaining to study how these molecules perturb the structure and dynamics of bulk water. We choose some monovalent salts; LiCl, NaCl, KCl, CsCl (as electrolytes), DME, DMSO, methyl alcohol, ethyl alcohol, isopropanol (as amphiphilic molecules) and a series of alkylammonium chloride salts; tetra MAC, tetra EAC, tri EAC, tetra PAC (as a combination of hydrophobic and electrostatic effects). We used BSA as a model protein.

With a combination of experimental investigation and computer simulation studies, we explored various physical properties (both local and global environments) related to the structure and dynamics of water network. The ultrafast dynamics of water was measured using some complementary experimental techniques: (i) DR study (in GHz to THz frequency region) with time resolution of ps to few hundreds of fs, (ii) time-resolved fluorescence spectroscopy with time resolution of ns to few hundreds of ps, (iii) degenerate (central wavelength of 800 nm) pump-probe spectroscopy with time resolution of ps to few hundreds of fs, and also with all-atom MD simulation study (resolution of 5fs). To explore the H-bonded structure of water in a pure and altered environment we have used FTIR spectroscopy. We also explored MD simulation investigation to understand the water reorientation behaviour (both structure and dynamics) around a single water or DME

molecule microscopically. Secondary and tertiary structures and their stability of the protein molecule were detected using CD spectroscopy. The size of the protein has measured using DLS technique. THz TD spectroscopy has used to monitor the collective hydration around the protein molecules.

For bulk water, the timescales we obtain from the fitting of the real and imaginary dielectric constants with a *Debye relaxation model* are ~ 9 ps, 200 fs and 80 fs. The ~ 9 ps timescale is due to the cooperative rearrangement of the H-bonded network of water, whereas the ~ 200 fs timescale corresponds to the small angular rotational modes of polar water molecules. The ~ 80 fs timescale has its origin rooted to the 1.8 THz (60 cm^{-1}) vibrational band owing to the H-bond bending and the related transverse acoustic phonons, which propagate in the direction normal to the H-bonds between two neighbouring water molecules. We found that the monovalent metal chloride ions unambiguously accelerate the cooperative reorientational dynamics (~ 9 ps) of water dipoles which confirms the fact that these ions do act as “*water structure breakers*”. Due to the strong electrostatic interactions, ions hold the water dipoles around themselves and make a semi-rigid hydration structure around them. As a result, such water molecules cannot participate in the dielectric relaxation processes further. However, the extent of this effect is ion specific. A simple consideration of the sizes and/or charge densities is not enough to account for the observed changes. K^+ is found to be the most effective ion. In case of amphiphilic DME molecules we found the existence of under coordinated water molecules in DME continuum with dangling OH bonds. We found a signature of “*hydrophobic hydration*”, where to minimize the surface contact area the hydrophobic molecules aggregates. The water molecules also prefer to remain H-bonded with other water molecules. Water molecule just near to the water repelling carbon atoms of the DME molecule cannot form H-bond. As a result, it remains dangling that create defect or void in the H-bonding network. We therefore conclude that the solutions are not ideal mixtures. Similar non-ideal mixing behaviour is also found for other non-polar hydrophobic aqueous mixture (water-DMSO and water-alcohol binary mixtures). The size of DMSO is quite similar to that of DME molecule which also contains hydrophobic and hydrophilic atoms, but the total polarity of the molecules are different. The cooperative H-bond dynamics of water obtained from TTDS measurement show a non-monotonic behaviour as a function of X_w , in which collective dynamics is much faster in low X_w region, whereas in $X_w \sim 0.8$ region, the dynamics get slower than that of pure water. For water-DMSO binary mixtures also we found non-monotonic behaviour in the collective dynamics of water; we observed slower dynamics around $X_w \sim 0.6$. This observation is in stark contrast to that of electrolytes

samples, in which we do not observed any slower dynamics. We also studied the solvation dynamics of C500 molecules in water-DME mixtures and found that up to $X_w \sim 0.6$, the water molecules are confined within the cage formed by the hydrophobic DME molecules. From MD simulation study, we capture such non-monotonic character in the single molecule water reorientation times. We found that there exist quite stable H-bonded water clusters in all simulated water concentration mixtures (even in very low water concentration). We identified the local structures of water clusters that appear in various concentration regions. The water reorientations are found to occur via a combination of large amplitude angular jumps and diffusive reorientations. We have modelled those jump reorientations with the “*jump and wait model*”. We observed that the orientational dynamics is dominated by water-DME waiting time, which is much less than water-water waiting time. The abundance of water-DME H-bond leads to an acceleration of the rotational dynamics. The polar water molecules prefer to form H-bond with the neighbouring polar water molecules only. The different affinity of amphiphilic molecules towards polar water molecules causes the formation of clusters of similar molecules in the mixture and also the defect in H-bonding network. Different waiting time of water with another water and DME molecules also proves that it is not only the different H-bonding ability, the H-bonding stability also makes the mixtures heterogeneous. Such heterogeneity is also not specific for all types of amphiphilic molecules rather it depends on the polarity, viscosity and density of the mixtures.

Although the monovalent ions accelerate the collective reorientation of water network, they induce negligible perturbation on the protein (BSA) secondary structure and hydration. We found that the salt hydration and the BSA hydration act independently of each other. This finding does not support the idea of indirect protein denaturation processes. The presence of water at protein surface plays a pivotal role during a conformational makeover. This interaction is contrasting with the interaction pattern of amphiphilic molecules that supports the direct denaturation mechanisms. We examine the interaction patterns of BSA with the amphiphilic alcohol molecules and observed that the collective hydration of BSA in presence of alcohols of varying carbon chain lengths changes non-monotonically. The THz absorption coefficient (α) of protein solutions fluctuates periodically with alcohol concentrations at a fixed BSA concentration. We also increased the protein concentrations and monitored BSA hydration at a fixed alcohol concentration, and found a similar non-monotonic fluctuating trend. The α value first decreased rapidly then increased which was followed by a shallow decrease. This anomalous change in the hydration structures is a

delicate balance between various interactions (water-water, water-solute, solute-solute, water-protein and solute-protein) present in the systems. In aqueous solutions, protein molecules fold to hide its non-polar hydrophobic part from water, and the hydrophilic amino acid residues stay on the interface to interact with the polar water molecules. Owing to the hydrophobic non-polar nature, such molecule prefers to interact with the core of the protein molecules which is hydrophobic in nature. Hence the protein is forced to unfold to permit the hydrophobic molecules to access the hydrophobic core of the protein. This preferential hydrophobic interaction accelerates protein denaturation processes. With this knowledge that electrostatic effect has negligible perturbation (at least for monovalent ions) and hydrophobic molecules have an intense effect on protein structure and hydration, we include cations that contain hydrophobic moieties (e.g. alkylammonium halides) and investigate their effect on the structure and hydration of BSA molecules. We conclude that it is the hydrophobic effect that takes the decisive role in protein stability rather the electrostatic effect.

10.2. Future Perspective

With this perspective, we plan to extend our study using some other important amphiphilic molecules with a complex structure (such as Tetrahydrofuran, 1,4-Dioxane, 2,2,2-Trifluoroethanol) to investigate the perturbation on water structure and dynamics. The hydrophobicity of any molecule and its effect depend on the structure and conformations of the molecules. Hence it is also important to study the isomeric effect of the hydrophobic molecules. In this regard, we plan to take various isomers of the alcohol molecules “*Butyl alcohol* (C_4H_9OH)”, and molecules with replacing their hydrogen with deuterium (H_2O & D_2O , $(CH_3)_2SO$ & $(CD_3)_2SO$). Here we have studied the direct and indirect denaturation mechanisms, but there are some cosolutes such as TMAO, Trifluoroethanol, they can stabilize the protein molecules. We will explore this stabilization mechanisms microscopically by both experimental and simulation techniques.